WELL-TESTING METHODOLOGIES FOR CHARACTERIZING HETEROGENEITIES IN ALLUVIAL-AQUIFER SYSTEMS: FINAL TECHNICAL REPORT

A research project of the
Water Resources Research Program
United States Department of the Interior
Geological Survey

by

James J. Butler, Jr. and Carl D. McElwee
Kansas Geological Survey
The University of Kansas

with

Geoffrey C. Bohling, Wenzhi Liu, Zafar Hyder,
Christine M. Mennicke, Michael D. Orcutt, Matthias Zenner,
and Meredith L. Beilfuss
Kansas Geological Survey
The University of Kansas

Kansas Geological Survey
Open-File Report 95-75

February, 1996

Research supported by the U.S. Geological Survey (USGS), Department of the Interior, under USGS award number 14-08-0001-G2093. The views and conclusions contained in this document are those of the authors and should not be interpreted as necessarily representing the official policies, either expressed or implied, of the U.S. Government.

Kansas Geological Survey
Open-file Report

Disclaimer

The Kansas Geological Survey does not guarantee this document to be free from errors or inaccuracies and disclaims any responsibility or liability for interpretations based on data used in the production of this document or decisions based thereon. This report is intended to make results of research available at the earliest possible date, but is not intended to constitute final or formal publication.

ABSTRACT

A considerable amount of research on the mechanisms of large-scale solute transport has identified the spatial distribution of hydraulic conductivity as a significant factor in determining how a plume of a conservative constituent will move in the subsurface. This report summarizes the work of a three-year research project whose focus was on the use of well-testing technology to describe spatial variations in hydraulic conductivity. Theoretical and field investigations of the potential of various types of well tests to provide information about lateral and vertical variations in hydraulic conductivity comprise the majority of the work performed during the period covered by this report. The theoretical components of this effort included the development of a time-continuous numerical model for the analysis of well-test data, an evaluation of the viability of multilevel slug tests in layered aquifers, a sensitivity analysis of slug tests with observation wells, a study of the effective properties obtained from the analysis of slug tests performed in wells with skins, an assessment of the Nguyen and Pinder method for the analysis of slug tests performed in partially penetrating wells, and an investigation of hydraulic tomography in a planar steady-state flow field. The field components of this work emphasized slug tests. A prototype multilevel slug-test system was tested. Results indicated that test responses were being affected by mechanisms not accounted for in the conventional theory. A new nonlinear slug-test model was developed in an attempt to account for these mechanisms. This model served as the basis of a new approximate approach for the analysis of slug tests in high-conductivity media. A field program of multiwell slug tests (slug tests with observation wells) led to the development of a new model for the analysis of data from multiwell slug tests. As a result of these field investigations, a series of practical guidelines were proposed that should allow the quality of parameter estimates obtained from a program of slug tests to be considerably improved. In the final phases of the project, a new approach for the identification of low-permeability well skins using slug tests was investigated. Additional work performed during the period of this research included drilling and sampling activities, and laboratory analysis of sampled cores.

TABLE OF CONTENTS

I. INTRODUCTION

A. RESEARCH OBJECTIVES

Over the last decade, a considerable amount of theoretical, laboratory, and field research on the mechanisms of large-scale solute transport has identified the spatial distribution of hydraulic conductivity as a significant factor in determining how a plume of a conservative tracer will move in the subsurface (e.g., Freyberg, 1986; Gelhar, 1986; Dagan, 1986; Moltyaner and Killey, 1988; Hess et al., 1992). Many researchers now recognize (e.g., Molz et al., 1989a) that if we are to improve our predictive capabilities for subsurface transport, we must first improve our capabilities for measuring and describing conditions in the subsurface. The estimation of hydraulic conductivity in the subsurface on a scale of relevance for contaminant transport investigations, however, has proven to be a rather difficult task. Recent work at the Kansas Geological Survey (KGS) and elsewhere (e.g., Streltsova, 1988; Butler and Liu, 1993) has shown that conventional pumping tests provide large-scale volumetric averages of hydraulic conductivity that may be of rather limited use in transport investigations. Although multiwell tracer tests can provide information on the average interwell conductivity, these tests are rather expensive in terms of time, money, and effort. Other techniques are needed if information on conductivity variations is to be used by practicing hydrogeologists outside of the research community. The specific objective of the research described in this report is to assess the potential of well-testing technology for providing more accurate estimates of spatial variations in the physical properties that control contaminant plume movement in saturated porous media. Although effective porosity is clearly an important consideration, the major emphasis of this work is on characterizing spatial variations (heterogeneities) in hydraulic conductivity.

Ideally, heterogeneities in hydraulic conductivity must be studied and characterized at several different scales in order to understand their influence on the movement of a contaminant plume. Although theoretical modeling work is an important element of any study of the influence of spatial variations in hydraulic conductivity on contaminant movement, a rigorous study of this subject must have a major field component. A field site, the Geohydrologic Experimental and Monitoring Site (GEMS), has been established in order to allow researchers at the University of Kansas to pursue work on characterizing spatial variations in flow and transport properties. GEMS is located in the floodplain of the Kansas River, just north of Lawrence, Kansas on land owned by the University of Kansas Endowment Association. Figure I.1 is a map showing the general location of GEMS and some of the major features at the site. GEMS

overlies approximately 21.3 meters (70 ft) of Kansas River valley alluvium. These recent unconsolidated sediments overlie and are adjacent to materials of Pleistocene and Pennsylvanian age. A cross-sectional view of the subsurface at one of the well nests at GEMS is shown in Figure I.2. The alluvial facies assemblage at this site consists of approximately 10.6 meters (35 ft) of clay and silt overlying 10.6 meters (35 ft) of sand and gravel. The stratigraphy is a complex system of stream-channel sand and overbank deposits. The general nature of the stratigraphy would lead one to expect that a considerable degree of lateral and vertical heterogeneity in hydraulic conductivity would be found in the subsurface at GEMS. Although analyses of sampled cores do indicate considerable variability in hydraulic conductivity within the sand and gravel interval at GEMS, it is unclear how the variability at the small scale of a core translates into variability at larger scales.

The primary focus of this project was on the use of well tests to describe spatial variations in hydraulic conductivity. Theoretical and field investigations of the potential of various types of well tests to provide information about lateral and vertical variations in hydraulic conductivity comprise the majority of the work performed during the period covered by this report. Since the slug test has become the most common technique for estimation of hydraulic conductivity at sites of suspected groundwater contamination, a large component of this work was directed at improving slug-test methodology. In addition to the focus on well tests, a considerable amount of work was also directed at increasing our knowledge of the subsurface at GEMS. This effort involved continued drilling and sampling of the alluvium, and laboratory analysis of sampled cores. These characterization efforts were directed at providing the detailed information that will allow us to better assess the quality of the estimates provided by the various well-testing approaches evaluated in this work. The ultimate goal of these characterization efforts is to describe the site in so much detail that it effectively becomes an underground laboratory at which new technology can be evaluated.

B. BRIEF OUTLINE OF REPORT

The remainder of this report is divided into four major chapters, each of which is essentially a self-contained unit consisting of one or more sections. Although pages are numbered consecutively throughout the report, figures, tables, and equations are labelled by section for the convenience of the reader. Note that four sections of this report have been or will shortly be published in peer-reviewed scientific journals. For this final report, reprints of these articles replace the corresponding sections of the earlier yearly reports. Manuscripts describing the work of several other sections are

currently in the review or preparation process.

The first of the four major chapters of this report describes theoretical work directed at developing a better understanding of the information that can be obtained from well tests performed under non-ideal conditions. A continuous-in-time numerical model, which has proven quite useful for the analysis of well-test data under non-ideal conditions, is described in the first section. In the second section, this model is employed in a detailed study of multilevel slug tests in layered aquifers. The primary purpose of this work was to assess the potential of multilevel slug tests to provide information about vertical variations in hydraulic conductivity under conditions commonly faced in field settings. Sensitivity analysis is a formalism that allows relationships between model responses and model parameters to be examined in considerable detail. The next two sections describe the use of the principles of sensitivity analysis to investigate the type of information that can be obtained from slug tests with observation wells and from slug tests performed in the presence of a well skin. Since many of the wells at GEMS are screened for only a portion of the sand and gravel interval, the partially penetrating nature of the wells must be considered when slug-test data from these wells are analyzed. One approach for the analysis of slug-test data from partially penetrating wells is the method of Nguyen and Pinder. In the fifth section of this chapter, a theoretical examination of this method is described. The original proposal for this research project discussed the possibility of hydraulic tomography, i.e. the utilization of data from multiple well tests in a tomographic inversion procedure. An initial investigation of this topic in a steady-state flow field is presented in the final section of this chapter. Note that three sections of this chapter have already been published in the peer-reviewed literature, and a manuscript based on an additional section is currently under review.

The second chapter primarily describes field investigations of slug tests at GEMS. A prototype multilevel slug test system, which has been developed at the KGS, is described and its use at GEMS is detailed in the first section. An extensive series of field experiments that were undertaken in order to explain the causes of anomalous behavior observed during multilevel slug tests in wells in the sand and gravel section at GEMS are then described in the second section. The third section describes the development and field application of a new unified slug-test model that accounts for the major mechanisms thought to be affecting the GEMS slug-test data. The original proposal presented pulse testing as a promising well-testing methodology for use in hydrogeologic investigations. The fourth section of this chapter deals with the simplest type of pulse test: slug tests with observation wells (multiwell slug tests). The results of

a program of field testing at GEMS and a subsequent theoretical analysis motivated by those tests are described. The fifth section summarizes many of the conclusions of our field and theoretical research on slug tests. A series of field guidelines are proposed that should help improve the quality of parameter estimates obtained from slug tests. Based on our experience, the failure to recognize the existence of a low-permeability well skin is the largest source of error in parameter estimates obtained from slug tests. The sensitivity analysis of slug tests in the presence of well skins described earlier clearly demonstrates the dominating influence of low-permeability well skins on slug-test responses. In the sixth section of this chapter, a new approach for the identification of a low-permeability well skin through repeat slug tests is described. An example field application demonstrates the potential of this approach. Note that one section of this chapter is currently in press at a peer-reviewed journal, while manuscripts based on two more sections are in the review/preparation phase.

The third chapter primarily describes activities directed at increasing our knowledge of the subsurface at GEMS. Drilling and sampling activities that occurred during the project at GEM are briefly summarized in the second section. The analysis of the core samples obtained during drilling is then described in the third section. Modifications to the procedures employed in the KGS core properties laboratory are discussed and the results of the analyses performed during this project are presented.

The fourth chapter summarizes the report and briefly outlines the major accomplishments of this project.

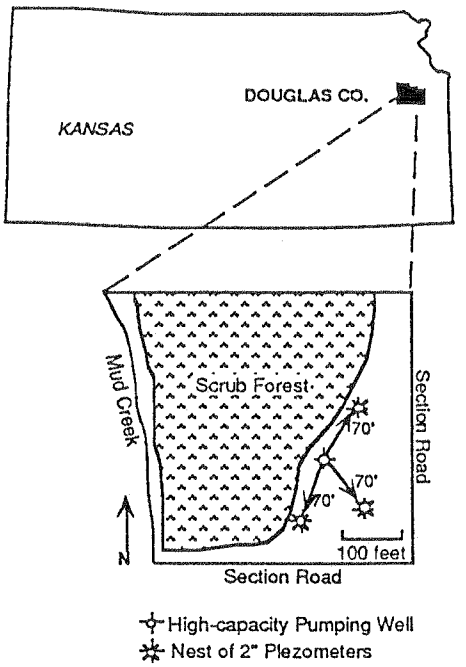

Figure I.1. - Location map for the Geohydrologic Experimental and Monitoring Site (GEMS).

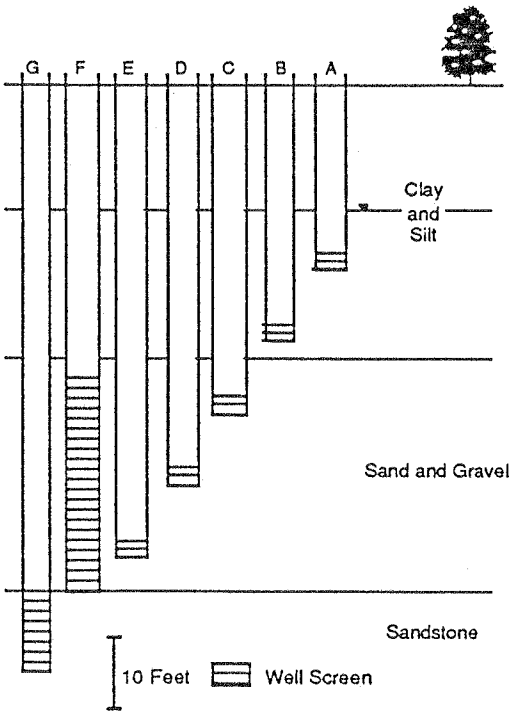

Figure I.2. Cross-sectional view of a well nestt at GEMS. Wells A-E are screened for .8 meters (2.5 ft.), well F is screened for 9.1 meters (30 ft.), and well G is screened for 1.5 meters (5 ft.).

II. THEORETICAL INVESTIGATIONS OF WELL TESTS IN HETEROGENEOUS MEDIA

A. A CONTINUOUS-IN-TIME NUMERICAL MODEL FOR THE ANALYSIS OF WELL TESTS IN THREE-DIMENSIONAL NONUNIFORM AQUIFERS

Introduction

Analytical solutions for drawdown in response to a pressure disturbance induced at a central well are the basis of conventional well-test analysis methodology. For the most part, these solutions consider hydraulic behavior in an idealized aquifer in which flow properties are invariant in space. Aquifers in nature, however, are characterized by a considerable degree of spatial variation (heterogeneity) in flow properties. Not surprisingly, analyses based on solutions to flow in idealized uniform systems may be of limited use in assessing the effect of heterogeneities in the vicinity of the stressed well. A better understanding of these near-well heterogeneities, however, is critical if we are to improve our ability to predict the transport of contaminants in the subsurface. A small component of the research of this project was therefore directed at further exploration of a numerical modeling approach that would allow the actual complexity of the geological system to be incorporated into the analysis of well-test data. This approach could be useful as a tool for both the development of insight into the role of heterogeneity in controlling well-test responses and the analysis of well tests in complex natural systems.

A general model for well-test analysis must allow the actual complexity of the geologic formation to be represented in the full three dimensions. Analytical solutions for well tests in simplified three-dimensional settings have been developed by a number of authors using traditional integral transform techniques (e.g., Russell and Prats, 1962; Papadopulos, 1966; Prijambodo et al., 1985; Hayashi et al., 1987; Raghavan, 1989; McElwee et al., 1990). However, an exact analytical solution has yet to be derived for the general case of transient flow in a three-dimensional nonuniform system. Given the limitations of the traditional analytical solution methodology, a new approach for the analysis of well-test data is considered in this work. The approach considered here is based on the idea of combining the spatial discretization used in a conventional numerical model with the Laplace transform in time used in conventional analytical models. A solution to this hybrid numerical model is obtained in Laplace space using standard techniques of matrix algebra. A set of solutions in Laplace space is then back transformed to real space, producing

a solution in real space that can be formulated in a continuous manner over a range of times. In this section, the theoretical basis of this approach is explored and its implementation for this project is described.

A Time-Continuous Numerical Method

Approximate numerical methods such as the finite-difference or finite-element approaches have been widely used in groundwater studies for applications where analytical solutions are not feasible. These numerical approaches involve both spatial and temporal discretization of the governing equations, with the quality of the approximation dependent on the discretization strategy. The size of the time increment is often varied during the course of a simulation in order to improve computational efficiency. However, limitations on the magnitude of the initial time step and the size of the time-step acceleration factor can result in a large number of time steps being required, even in cases when model output is only desired at a few points in time. In addition, if the rate of pumpage changes significantly, as in a simulation of a step-drawdown test, the time-stepping scheme must be reset to its initial values with the change in pumping rate in order to accurately simulate the system response to the new stress. Selection of the proper time increment may also present difficulties when model output is required for comparison with measured data at particular points in time.

In order to avoid some of the problems associated with temporal discretization, a hybrid method, which combines spatial discretization with a Laplace transform in time, is employed here. The spatial discretization scheme is the same as that in a conventional finite-difference model. The resultant spatially discretized system of algebraic equations in complex space is solved using complex arithmetic for the matrix inversion. The Laplace-space solution is then inverted back into real space using an appropriate numerical inversion scheme. This procedure yields a solution that is continuous over a range of times, with the only approximation in the temporal domain being that introduced by the numerical inversion scheme.

This time-continuous method has been employed by a number of workers during the past two decades (e.g., Gurtin, 1965; Javandel and Witherspoon, 1968; Chen and Chen, 1988; Sudicky, 1989; Moridis and Reddell, 1991; Sudicky and McLaren, 1992; Li et al., 1992). The most difficult problem associated with this method has been the inversion of the Laplace-space solution back into real space. Various methods for approximate numerical inversion, all of which involve the evaluation and summation of the transform-space function, have been developed by

a number of authors (e.g., Stehfest, 1970; Crump, 1976; Talbot, 1979). One focus of this work is the development of a more efficient inversion algorithm. As noted by Sudicky (1989), De Hoog et al. (1982) propose a quotient difference algorithm for increasing the rate of convergence of the summation-series approach of Crump (1976). This quotient-difference algorithm has been shown to have a significant computational advantage over other algorithms for the analysis of well-test data (Liu and Butler, 1991). The computational savings are such that this method appears to hold considerable promise for use as a practical tool for analysis of well tests in fully three-dimensional systems. The following subsection describes an implementation of this method in a discrete-in-space, continuous-in-time model that has been developed for the analysis of well tests in systems where conventional analytical approaches are not viable.

The Three-Dimensional Finite-Difference Time-Continuous Model (3DFDTC)

The time-continuous approach can be used only if Laplace transforms exist for the governing equation together with all boundary and initial conditions. Thus, the approach described here only strictly applies to confined flow systems. The cylindrical-coordinate form of the governing equation for three-dimensional flow in a confined system is

$$\frac{1}{r}\frac{\partial}{\partial r}\left(rK_r\frac{\partial h}{\partial r}\right) + \frac{1}{r^2}\frac{\partial}{\partial \theta}\left(K_\theta\frac{\partial h}{\partial \theta}\right) + \frac{\partial}{\partial z}\left(K_z\frac{\partial h}{\partial z}\right) = S_s\frac{\partial h}{\partial t} \qquad \text{(II.A.1)}$$

where

h = drawdown, [L];
S_s = specific yield, [1/L];
K_r, K_θ, K_z = hydraulic conductivity in the radial, angular, and vertical direction, respectively, [L/T];
t = time, [T];
r = radial direction, [L];
θ = angular position, in radians;
z = vertical depth from the top of the aquifer, [L].

For the case of a pumping test in a layered aquifer, the initial and boundary conditions are defined as

$$h(r,0) = h_a,\ r < \infty \qquad \text{(II.A.2)}$$

$$h(\infty,t) = h_a,\ t \geq 0 \qquad \text{(II.A.3)}$$

$$2\pi \sum_{j=1}^{J} K_{rj} m_j \left(r \frac{\partial h}{\partial r} \right)_{r \to r_w} = -\sum_{i=1}^{NP} q_i \square_i(t) \qquad \text{(II.A.4)}$$

where

$$\square_i(t) = \text{box car function} = \begin{cases} 1, & \text{if } t_{1i} \leq t \leq t_{2i},\ i = 1, 2, \cdots, NP \\ 0, & \text{elsewhere} \end{cases}$$

h_a = initial head in the aquifer, [L];
NP = number of pumping periods;
t_{1i} = starting time for pumping period i, [T];
t_{2i} = ending time for pumping period i, [T];
r_w = radius of pumping well, [L];
q_i = pumpage for pumping period i, [L^3/T];
J = total number of layers intersecting the well screen;
K_{rj} = conductivity in radial direction for layer j;
m_j = thickness of layer j.

The application of the Laplace transformation to equations (II.A.1) and (II.A.4), in conjunction with (II.A.2), results in:

$$\frac{1}{r} \frac{\partial}{\partial r} \left(r K_r \frac{\partial \bar{h}}{\partial r} \right) + \frac{1}{r^2} \frac{\partial}{\partial \theta} \left(K_\theta \frac{\partial \bar{h}}{\partial \theta} \right) + \frac{\partial}{\partial z} \left(K_z \frac{\partial \bar{h}}{\partial z} \right) = S_s (\bar{h} p - h_a) \qquad \text{(II.A.5)}$$

$$2\pi \sum_{j=1}^{J} K_{rj} m_j \left(r \frac{\partial \bar{h}}{\partial r} \right)_{r \to r_w} = -\sum_{i=1}^{NP} q_i \frac{e^{-t_{1i}p} - e^{-t_{2i}p}}{p} \qquad \text{(II.A.6)}$$

where

p = Laplace transform variable;

$\bar{h}$ = head in Laplace space.

In order to improve the ease of radial discretization, the derivatives in the radial direction can be rewritten in a logarithmic form using the transformation $\tilde{r}=\log_e(r/r_w)$. This approach allows a discretization in the radial direction that increases exponentially when using a constant $\Delta\tilde{r}$. Equations (II.A.5) and (II.A.6) can be rewritten using this transformation as

$$\frac{1}{r^2}\frac{\partial}{\partial\tilde{r}}\left(K_r\frac{\partial\bar{h}}{\partial\tilde{r}}\right) + \frac{1}{r^2}\frac{\partial}{\partial\theta}\left(K_\theta\frac{\partial\bar{h}}{\partial\theta}\right) + \frac{\partial}{\partial z}\left(K_z\frac{\partial\bar{h}}{\partial z}\right) = S_s(\bar{h}p-h_a) \qquad \text{(II.A.7)}$$

$$2\pi\sum_{j=1}^{J}K_{rj}m_j\left(\frac{\partial\bar{h}}{\partial\tilde{r}}\right)_{\tilde{r}\to 0} = -\sum_{i=1}^{NP}q_i\frac{e^{-t_{1i}p}-e^{-t_{2i}p}}{p} \qquad \text{(II.A.8)}$$

Unlike many analytical and numerical models, which assume the radius of the well to be infinitely small, the model developed here allows the influence of well-bore storage to be taken into consideration. As noted by Papadopulos and Cooper (1967), effects of well-bore storage on drawdown can be significant during early times when the majority of the water is being removed from storage inside the well bore. As time increases during a constant-rate pumping test, the influence of well-bore storage will gradually diminish, eventually reaching a point at which the infinitely small well-bore assumption is viable.

The implementation of the well-bore storage option in the three-dimensional, finite-difference, time-continuous model (3DFDTC) is based on earlier work of Settari and Aziz (1974), Rushton and Chan (1977), and Butler (1986). As described by Butler (1986), the approach is based on rewriting the classical pipe flow equation (Vennard and Street, 1975) in a Darcy Law-like formulation and defining a term (involving the friction factor, the cross-sectional area of the well bore, and distance along the well bore) analogous to hydraulic conductivity. This approach allows flow inside the well bore to be governed by the porous media flow equation given by (II.A.7). Note that the implementation of this approach for this project produces an approximation of well-bore behavior that is equivalent to the hydrostatic head assumption employed in most analytical representations of the well bore (e.g., Papadopulos and Cooper, 1967; Cooper et al., 1967).

In the three-dimensional representation employed here, the portion of the well bore passing through the modelled unit consists of several grid cells in the vertical.

The storage coefficient is assumed to be one for the top cell of the well bore, while the storage coefficients for the remaining nodes in the well bore are set equal to the compressibility of water or zero (assuming water is incompressible). Since the radial-discretization scheme employed in the model uses logarithmic increments, the radial location (r_{min}) of the first node inside the well bore must be larger than zero (i.e. 0.0 < r_{min} < r_w). This produces a well bore whose projection in the (r,θ) plane is in the shape of an annular ring rather than a circle. The storage coefficient of the well-bore cells must therefore be adjusted (by a factor of $r_w^2/(r_w^2-r_{min}^2)$) to account for the decrease in well-bore cross-sectional area produced by the annular-ring representation. In addition, the traditional boundary condition at the well bore (II.A.8), which is based on the definition of radial flow along the well screen, is not used in this approach. Instead, a boundary condition in which the total flow out of the screened portion of the well is defined is used for the top grid cell. This flow boundary condition is written as

$$2\pi K_{rJ} m_J \left(\frac{\partial h}{\partial \tilde{r}}\right)_{\tilde{r}=\log_e\left(\frac{r_{min}}{r_w}\right)} = -\sum_{i=1}^{NP} q_i \frac{e^{-t_{1i}p} - e^{t_{2i}p}}{p} \qquad \text{(II.A.9)}$$

where m_J is the thickness of the top grid cell. Note that no-flow conditions in the radial direction are assumed at $r=r_{min}$ for the remaining nodes in the well bore. The use of (II.A.9) as a boundary condition makes this approach very appropriate for analyzing well tests in layered systems, where the test well may be screened in more than one layer (as in (II.A.4) with J>1). Instead of having to define in advance the amount of water withdrawn from each layer, the model will implicitly calculate the flow out of each layer given the total flow out of the system defined by (II.A.9).

Since the representation of the well bore employed here is equivalent to the conventional hydrostatic head assumption, the "hydraulic conductivity" of the well bore must be defined such that the heads for all the nodes in the well bore are approximately equal. All three components of well-bore "hydraulic conductivity" must be at least four orders of magnitude larger than the formation conductivity in order to ensure negligible head loss within the well bore. In order to ensure that the majority of water will be drawn from the well bore at early times, the ratio of vertical well-bore "hydraulic conductivity" over its angular and radial counterparts must be large. An extensive set of experiments indicates that a ratio larger than 100 will ensure that all water will initially be drawn out of well-bore storage.

The 3DFDTC model is developed by applying a conventional central-

difference scheme to (II.A.7), which now represents conditions within both the formation and the well bore. After incorporating (II.A.9) and the Laplace transform of (II.A.3) into the finite-difference scheme, the system of algebraic equations for 3DFDTC can be expressed in matrix form as

$$([A] + p[B])[\bar{h}] = -[C]h_a + \sum_{i=1}^{NP} q_i \frac{e^{-t_{1i}p} - e^{-t_{2i}p}}{p}[D] \qquad \text{(II.A.10)}$$

where A, B, C, and D are matrices of constant coefficients and $\bar{h}$ is a vector of unknown heads. For the sake of conciseness, (II.A.10) is rewritten in the following form:

$$[G][\bar{h}] = [W] \qquad \text{(II.A.11)}$$

Both the left-hand side coefficient matrix G and the right-hand side matrix W of (II.A.11) involve the Laplace variable p, for which a value must be given before a solution in Laplace space can be obtained. The resultant solution in Laplace space can then be inverted back into real space using numerical inversion schemes such as those of Stehfest (1970) or Crump (1976). A detailed discussion of inversion algorithms with an emphasis on the method of Crump (1976) can be found in Appendix A.

The Crump algorithm approximates the inversion of a Laplace-space function by means of a Fourier series that involves both sine and cosine functions. This method has a smaller error than that of a similar method presented by Dubner and Abate (1968). If the value of h at node j is desired, h_j is found using the following equation developed by Crump [1976]:

$$h_j(t) \approx \frac{e^{p_0 t}}{Tmax}\left\{\frac{\overline{h_j}(p_0)}{2} + \sum_{k=1}^{2N+1}\left[RE(\overline{h_j}(p_k))\cos\left(\frac{k\pi t}{Tmax}\right) - IM(\overline{h_j}(p_k))\sin\left(\frac{k\pi t}{Tmax}\right)\right]\right\} \qquad \text{(II.A.12)}$$

where

$\bar{h}_j(p_k)$ = solution from (II.A.11) at node j for $p = p_k$;

2Tmax = the period of the Fourier series approximating the inverse function on

the interval [0, 2Tmax];

RE($\bar{h}$) = real part of $\bar{h}$;

IM($\bar{h}$) = imaginary part of $\bar{h}$;

Er = minimum relative error;

$p_k = p_0 + ik\pi/Tmax$;

$p_0 = \mu$ - ln(Er/2Tmax), the real part of p_k;

μ = maximum real value of all the singularity points of the function in Laplace space;

$i = (-1)^{1/2}$.

Equation (II.A.12) shows that the time variable t appears only in the sine, cosine, and exponential functions. Since p_k is independent of time, we can perform the inversion over a range of times based on one set of solutions of $\bar{h}$ for one specific Tmax. The solution is thus continuous in time because once a set of $\bar{h}$ values is calculated from (II.A.11), (II.A.12) will give the desired result at any time within the range of [0, 2Tmax].

If the summation is performed as in (II.A.12), hundreds of terms (i.e. solutions of (II.A.11)) may be needed in order to obtain a solution that satisfies a given convergence criterion. Since the computational effort required for the calculation of each p-space solution of (II.A.11) is at least equal to that required for one time step in a conventional numerical model, considerable attention is paid to the convergence of the summation series given in (II.A.12). An algorithm developed by De Hoog et al. (1982) has been found to significantly accelerate the convergence of the summation series and has therefore been incorporated into the 3DFDTC model. The acceleration of the summation series is great enough that the continuous-in-time approach may often be the most computationally efficient approach for the analysis of well tests in heterogeneous formations. A detailed explanation of the De Hoog algorithm is given in Appendix A. Note that each of the solutions of (II.A.11) is independent of all the others. Thus, this approach has considerable potential for use with parallel-processing computer systems.

Discussion and Model Validation

The 3DFDTC model is considerably more flexible than its conventional analytical or numerical counterparts. Since no time-discretization scheme is employed, stability issues related to the time-stepping scheme can be ignored and a solution can be obtained directly for any specific time. Boundary conditions can also

be changed easily to adapt to different patterns of stress being placed on the test well. For example, by simply setting q_i=0.0 and changing h_a to H_0 in (II.A.10) for nodes located inside the well bore, 3DFDTC can be used to simulate a slug test with an initial head of H_0. If necessary, partial penetration and well skin effects can be accounted for by specifying the vertical position of the well screen and the radius of the skin, respectively. If there exists a symmetry in heads in either the angular or vertical direction, 3DFDTC will simulate only part of the flow system by assuming a no-flow condition along the plane of symmetry. Note also that 3DFDTC can be used in a one- or two-dimensional mode if heads can be assumed equal in the angular and/or vertical directions. In such cases, only one node should be used in the direction of equal heads.

In order to validate the implementation of the time-continuous approach and the well-bore approximation, 3DFDTC has been checked against many analytical solutions for both pumping and slug tests. In all cases, a comparison between the analytical results and those of 3DFDTC revealed very small differences. Four typical examples are chosen here to demonstrate the viability of the 3DFDTC model.
The first example was designed to assess the viability of the well-bore approximation employed in the model. Drawdown produced by pumping at a constant rate from a well of finite radius in a uniform aquifer is simulated. In Figure II.A.1, the simulated results for drawdown within the pumping well are compared with the analytical results of Papadopulos and Cooper (1967) for the same case. The results produced by the two approaches essentially fall on top of one another throughout the duration of the simulation. The small difference in the computed drawdown is attributed mainly to the error caused by the spatial discretization scheme employed in 3DFDTC. Further simulations have shown that by increasing the number of nodes in the radial direction, the difference between the analytical and 3DFDTC results will gradually disappear. Note that in addition to the two curves depicting well-bore storage effects, a third curve, depicting drawdown calculated by 3DFDTC when well-bore storage effects are not included, is plotted on Figure II.A.1 to illustrate the period when well-bore storage effects are important.

In the initial phases of this project, there was considerable concern about numerical problems that might accompany the well-bore approximation as a result of the dramatic change in hydraulic conductivity between the formation and the well bore that is required by the approach. The second example is thus chosen to illustrate the performance of 3DFDTC when adjacent hydraulic conductivities differ by many orders of magnitude. A slug test in a well surrounded by a low-permeability

well skin of finite radius was simulated in order to assess model performance when a permeability contrast of ten orders of magnitude is employed. The configuration consisted of three distinct zones of differing properties: a very-high-permeability well bore ($K=10^7$), a low-permeability skin ($K=10^{-3}$), and an aquifer of moderate permeability ($K=1$). The well was assumed screened throughout the aquifer. Figure II.A.2 illustrates a comparison of the heads simulated by 3DFDTC with the results from the analytical solution of Moench and Hsieh (1985) for a slug test in a well with a skin of finite radius. The solid line in Figure II.A.2 depicts the head at the slugged well simulated by 3DFDTC, while the dashed line displays the results of the analytical solution. As with Figure II.A.1, the two lines essentially fall on top of one another. The differences between the two curves are again mainly due to the error introduced by spatial discretization.

The third example is selected to illustrate model performance when there is a strong component of vertical flow, such as might occur in multilevel slug tests. A slug test is simulated in a well that is screened for only a portion of the aquifer thickness. The aquifer is assumed to be homogeneous and isotropic with respect to flow properties. Figure II.A.3 displays a comparison of the normalized head (H/H_0) simulated by 3DFDTC with the results of the analytical solution of McElwee et al. (1990) for a slug test in a well partially penetrating an aquifer. The solid line in Figure II.A.3 depicts the head at the slugged well simulated by 3DFDTC, while the dashed line displays the results of the analytical solution. The inset provides details of the specific configuration employed for this example. As with the previous examples, 3DFDTC yields results that are essentially indistinguishable from those of the analytical solution.

The final example is selected to illustrate the advantages of this model when dealing with variable pumping rates. Figure II.A.4 includes a plot of pumping rate versus time for a well test performed by the Kansas Geological Survey in 1992 in Stanton County, Kansas. This test, which was plagued by malfunctioning generators, would be rather difficult to analyze using a conventional numerical model because of the need to refine the time-stepping scheme each time the pumping rate changed. The continuous-in-time approach is very convenient in this case, however, since the full detail of the rate variations can easily be incorporated in (II.A.9). In order to demonstrate the viability of this approach for the variable-rate pumping case, a comparison was performed between a variable-rate form of the solution of Theis (1935) and 3DFDTC. Figure II.A.4 includes the results of this comparison. 3DFDTC yields results that are quite close to those of the analytical solution. The

reasons for the differences that are observed are presently the focus of additional study. Note that 17,755 different pumping rates were used in 3DFDTC for this example, allowing the pumping-rate history in all of its detail to be incorporated into the model. The inclusion of a very detailed pumping-rate history into the model may not greatly add to the total time of computation. In principle, only an increased number of terms in the summation of (II.A.10) is required. However, these initial results indicate that if the rate variations are particularly dramatic, additional terms may also be required in the summation of (II.A.12). In order to be computationally competitive with the time-continuous approach, a conventional numerical model would have to approximate the variable-rate pumping rate with a small number of constant-rate steps, thereby introducing considerable error into the analysis.

Given the closeness of the match between the simulation results from 3DFDTC and those from the analytical solutions, it appears that 3DFDTC can be a useful tool for the design and analysis of well tests performed under conditions not readily represented by conventional analytical approaches. Therefore, in the following section of this report, 3DFDTC is used to examine the viability of multilevel slug tests in layered systems. The purpose of this numerical examination of multilevel slug tests in layered systems is to gain insight into how such tests might be designed in order to get more accurate information concerning vertical variations in hydraulic conductivity.

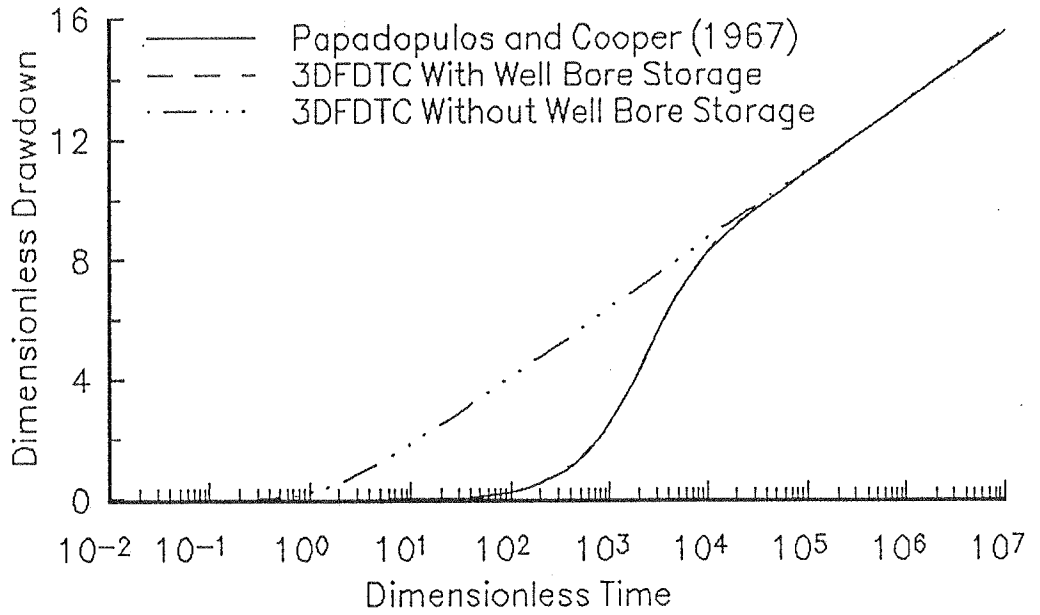

Figure II.A.1 Dimensionless drawdown ($4\pi Ts/Q$) versus time ($4Tt/Sr^2$) plot comparing the Papadopulos and Cooper (1967) solution with 3DFDTC results. (Observation well is located at r=4.6; r_w=0.167, T=1 and S=10^{-5}; 3DFDTC discretization: 3 radial nodes inside well bore, 39 nodes in the radial from r_w to 37364.15 meters and 5 nodes in vertical).

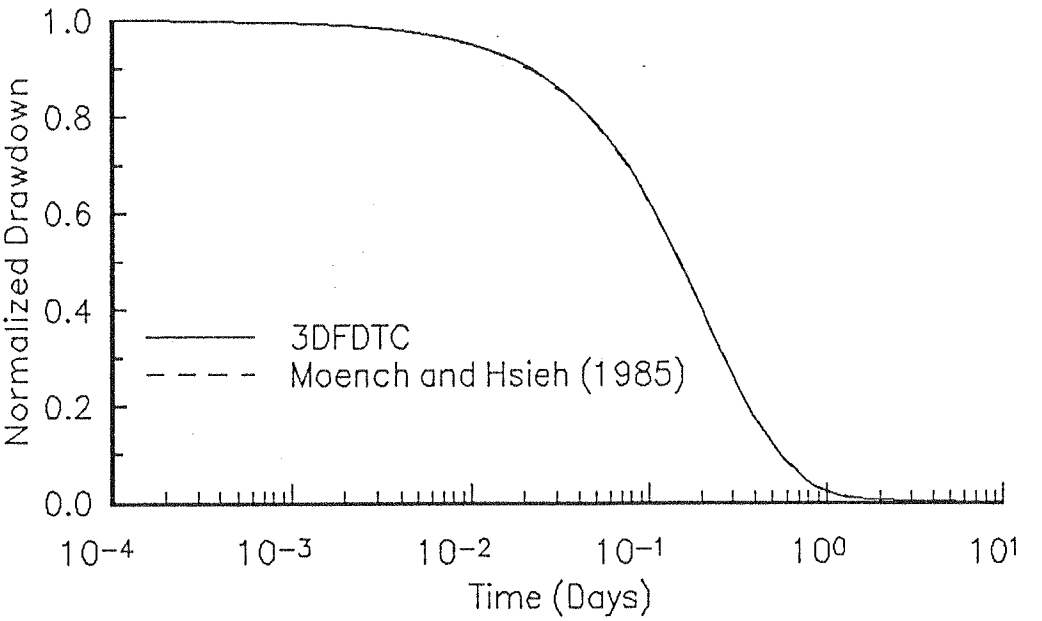

Figure II.A.2 Normalized drawdown (H/H_0) versus time plot comparing Moench and Hsieh (1985) solution with 3DFDTC results. (r_w=0.167, r_{skin}=0.333, T_{skin}=10^{-3}, S_{skin}=10^{-3}, $T_{aquifer}$=1, $S_{aquifer}$=10^{-5}; discretization as in Figure II.A.1 except that 3 of the 39 radial nodes are placed between r_w and r_{skin}).

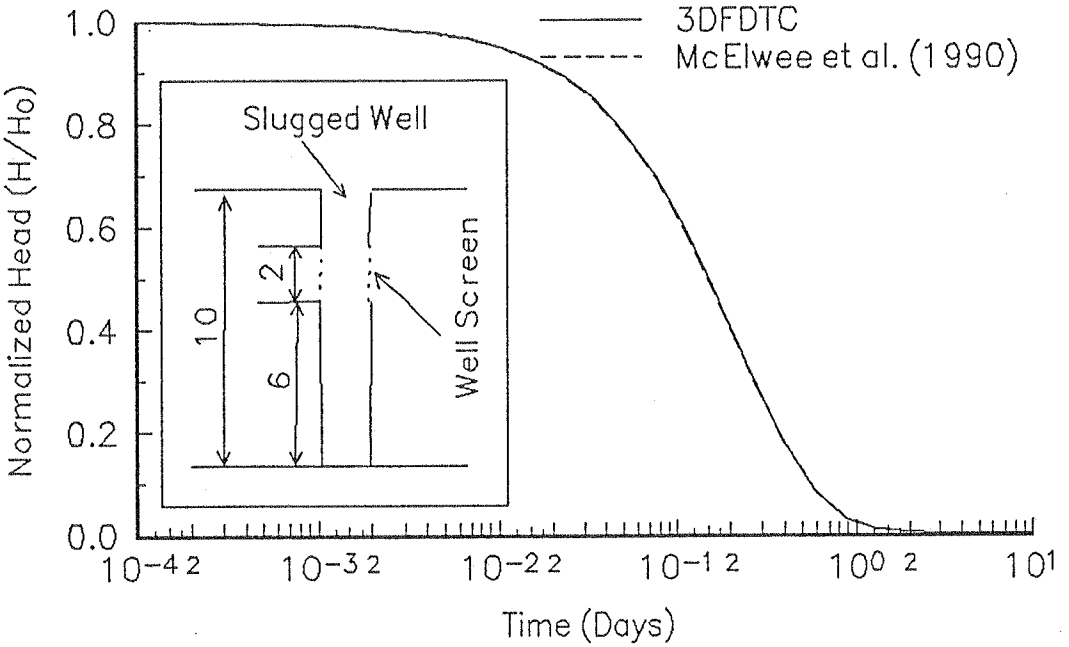

Figure II.A.3 Normalized head (H/H_0) versus time plot comparing McElwee et al. (1990) solution with 3DFDTC results. (r_w=0.167, K=0.1, S_s=10^{-6}; discretization as in Figure II.A.1).

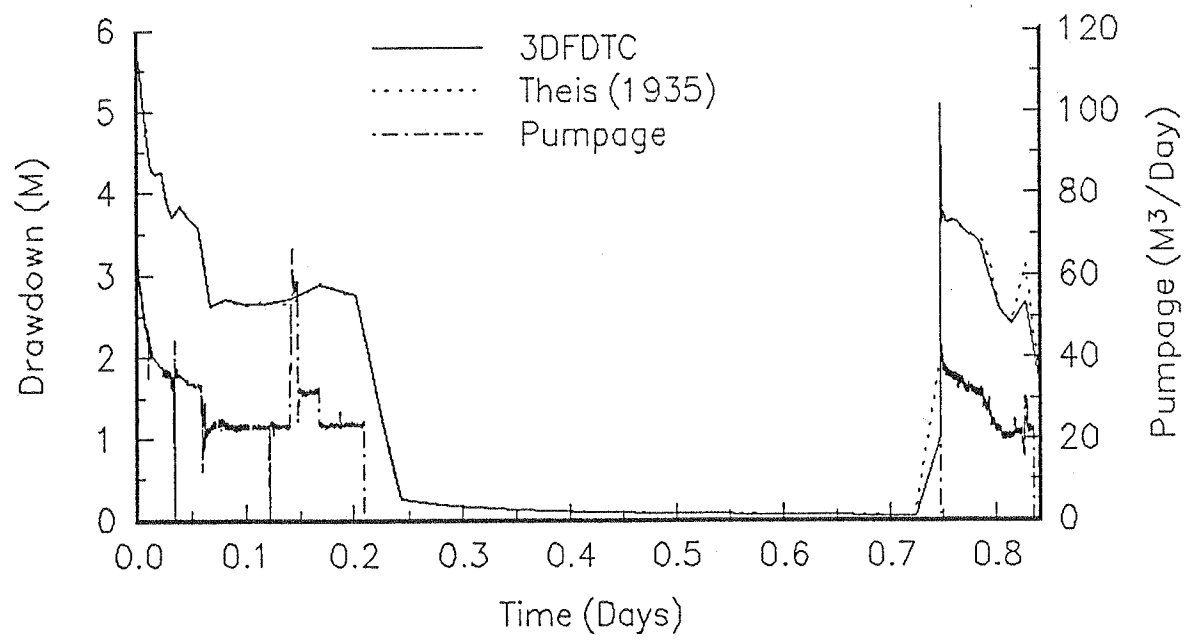

Figure II.A.4 Pumpage versus time and drawdown versus time plots comparing Theis (1935) solution with 3DFDTC results. (r=.208, T=1, S=10^{-6}, r_w=0.005; Discretization: 100 nodes from .005 to 836500 meters)

B. THE USE OF SLUG TESTS TO DESCRIBE VERTICAL VARIATIONS IN HYDRAULIC CONDUCTIVITY

A manuscript describing the work of this section was submitted to the Journal of Hydrology in April of 1993. A revised version of the manuscript was accepted in September of 1993, and the article was published in volume 156 of the Journal of Hydrology in 1994. The remainder of this section consists of a reprint of that article.

ELSEVIER

Journal of Hydrology 156 (1994) 137–162

Journal of Hydrology

[2]

The use of slug tests to describe vertical variations in hydraulic conductivity

James J. Butler, Jr.*, Geoffrey C. Bohling, Zafar Hyder, Carl D. McElwee

Kansas Geological Survey, 1930 Constant Avenue, Campus West, Lawrence, KS 66046-2598, USA

(Received 17 April 1993; revision accepted 28 September 1993)

Abstract

Multilevel slug tests provide one means of obtaining estimates of hydraulic conductivity on a scale of relevance for contaminant transport investigations. A numerical model is employed here to assess the potential of multilevel slug tests to provide information about vertical variations in hydraulic conductivity under conditions commonly faced in field settings. The results of the numerical simulations raise several important issues concerning the effectiveness of this technique. If the length of the test interval is of the order of the average layer thickness, considerable error may be introduced into the conductivity estimates owing to the effects of adjoining layers. The influence of adjoining layers is dependent on the aspect ratio (length of test interval/well radius) of the test interval and the flow properties of the individual layers. If a low-permeability skin is present at the well, the measured vertical variations will be much less than the actual variations, owing to the influence of the skin conductivity on the parameter estimates. A high-permeability skin can also produce apparent vertical variations that are much less than the actual, owing to water flowing vertically along the conductive skin. In cases where the test interval spans a number of layers, a slug test will yield an approximate thickness-weighted average of the hydraulic conductivities of the intersected layers. In most cases, packer circumvention should not be a major concern when packers of 0.75 m or longer are employed. Results of this study are substantiated by recently reported field tests that demonstrate the importance of well emplacement and development activities for obtaining meaningful estimates from a program of multilevel slug tests.

1. Introduction

Over the last decade, a considerable amount of theoretical, laboratory, and field research on the mechanisms of large-scale solute transport has identified the spatial

* Corresponding author.

SSDI 0022-1694(93)02399-I

distribution of hydraulic conductivity as a significant factor in determining how a plume of a conservative tracer will move in the subsurface (e.g. Dagan, 1986; Freyberg, 1986; Gelhar, 1986; Moltyaner and Killey, 1988; Hess et al., 1992). The measurement of hydraulic conductivity in the subsurface on a scale of relevance for contaminant transport investigations, however, has proven to be a rather difficult task. Conventional pumping tests will provide large-scale volumetric averages of hydraulic conductivity, which may be of rather limited use in transport investigations (e.g. Butler and Liu, 1993). Multi-well tracer tests, which can provide information on the average inter-well conductivity, are expensive in terms of time, money and effort. Other techniques are needed if information on conductivity variations is to be used by practicing hydrogeologists outside the research community.

Techniques that have been reported in the literature include multilevel (straddle-packer) slug tests, borehole flowmeter surveys, laboratory core analyses, correlation with geophysical logs, and a variety of single-well tracer tests. Melville et al. (1991) described a program of multilevel slug tests at a research site, and showed that the results compare favorably with the information obtained from a large-scale multi-well tracer test. A number of workers in both the petroleum and groundwater fields (e.g. Hufschmied, 1986; Ehlig-Economides and Joseph, 1987; Morin et al., 1988; Molz et al., 1989; Rehfeldt et al., 1989; Hess et al., 1992) have shown that borehole flowmeters have the potential to provide detailed information about the vertical variations in hydraulic conductivity at a well. Laboratory analysis of sampled cores is undoubtedly the most common method of assessing vertical variations in hydraulic conductivity. However, the collection of reasonably intact cores in permeable unconsolidated materials, the geologic media in many contaminant transport investigations, can be difficult (e.g. Zapico et al., 1987; McElwee et al., 1991). In addition, the time and expense of performing permeameter analyses on a complete set of cores can be considerable. Taylor et al. (1990) described several recently developed techniques for characterizing vertical variations in hydraulic conductivity. One particularly interesting approach is the single-well electrical tracer test (Taylor and Molz, 1990), which involves using a focused induction downhole probe to measure changes in electrical conductivity as an electrically conductive tracer moves away from the borehole.

The focus of this paper is the evaluation of multilevel slug tests as a source of information on vertical variations in the radial component of hydraulic conductivity. Slug tests have both economic and logistical advantages over the other techniques described above. A logistical advantage that cannot be overemphasized for waste-site investigations is that a slug test can be configured so that water is neither added nor removed from the test well. Such a slug test can be initiated by introducing (or removing) an object of known volume to (or from) the water column, or by pneumatic means (e.g. Orient et al., 1987; McLane et al., 1990). Problems arising as a result of the injection of waters of different compositions or the disposal of potentially contaminated waters can thus be avoided.

A number of workers have examined multilevel slug tests or the related multilevel constant-head injection test, using both analytical and numerical approaches. In terms of analytical approaches, Dagan (1978) employed Green's functions and a steady-state approximation to simulate tests in partially penetrating wells in uncon-

fined flow systems. Dougherty and Babu (1984) presented a fully transient analytical solution for slug tests performed in partially penetrating wells in isotropic confined systems. Hayashi et al. (1987) developed an analytical solution for multilevel slug tests in vertically unbounded, isotropic confined systems that explicitly includes the effects of packers above and below the test zone. Butler et al. (1990; see also McElwee et al., 1990) presented a solution for slug tests in partially penetrating wells in vertically bounded, anisotropic confined units that includes the effect of a finite-radius well skin. None of the above contributions, however, considered the effects of formation layering, owing to the difficulty of incorporating a general representation of formation layering into an analytical solution. Karasaki (1986) looked at the effect of layering on a slug test performed in a well that is fully screened across a layered aquifer, in which flow is only in the radial direction. An extension to the general case of unrestricted flow in the vertical direction has apparently not been attempted.

In terms of numerical approaches, Braester and Thunvik (1984) presented the results of a series of transient numerical simulations of multilevel constant-head injection tests. In a somewhat similar study, Bliss and Rushton (1984) used a steady-state model to simulate constant-head injection tests in a fractured aquifer. More recently, Widdowson et al. (1990) used a steady-state numerical model to develop an approach for analyzing multilevel slug tests based on a method similar to that of Dagan (1978). Melville et al. (1991) employed this approach to analyze multilevel slug tests from an experimental field site.

Although several of the studies cited above have touched upon important aspects of the issue of the viability of multilevel slug tests, there are still many unanswered questions about the usefulness of the information provided from such tests under conditions commonly faced in the field, where anisotropy, layering, and well skins of either higher or lower permeability than the undamaged formation may influence the measured response data. The purpose of this paper is to address many of these questions in the context of a theoretical assessment of the potential of multilevel slug tests to provide information about vertical variations in hydraulic conductivity in the vicinity of the well bore. As no general analytical solution has been developed for the case of slug tests in layered aquifers, this assessment will be performed through numerical simulation. The major objectives of this work are: (1) to assess possible techniques for the analysis of slug tests in layered systems; (2) to evaluate the effects of various geologic features (e.g. density of layering, anisotropy within layers, distance from boundaries, etc.) and well-construction features (e.g. well skins, length of the test interval, etc.) on the parameters estimated from slug-test data; (3) to explore the nature of vertical averaging in slug tests in layered aquifers; (4) to assess the effects of packer length and determine under what conditions packer circumvention may be an important mechanism; (5) to make recommendations on the performance of multilevel slug tests in layered systems that can be utilized by the field practitioner.

2. Problem statement

The problem of interest here is that of the head response, as a function of r, z, and t,

produced by the instantaneous introduction of a slug of water into a portion of the screened interval of a well. As shown in Fig. 1, the portion of the screened interval into which the slug is introduced is isolated from adjacent screened sections of the well by a pair of inflatable packers (straddle packer). Different intervals of the screen can be tested by moving the string of packers and pipes up and down in the well. A third packer is set above the top of the screen, isolating the well casing from the screened sections of the well outside the test interval. It should be noted that this configuration is in keeping with that commonly used in the field for multilevel slug tests (e.g. Melville et al., 1991; Butler and McElwee, 1992). In this analysis, flow properties are assumed to be invariant in the angular direction, and radial variations are limited to changes between a well skin created during drilling and development and the adjacent formation. Variations in flow properties of any magnitude are allowed between layers in the vertical direction.

The partial differential equation representing the flow of groundwater in response to the instantaneous introduction of a slug of water at a central well is:

$$\frac{\partial}{\partial r}\left(K_r \frac{\partial h}{\partial r}\right) + \frac{K_r}{r}\frac{\partial h}{\partial r} + \frac{\partial}{\partial z}\left(K_z \frac{\partial h}{\partial z}\right) = S_s \frac{\partial h}{\partial t} \tag{1}$$

where h is the hydraulic head (L), K_r is the component of hydraulic conductivity in the radial direction (L/T), K_z is the component of hydraulic conductivity in the vertical direction (L/T), S_s is the specific storage (1/L), t is the time (T), r is the radial direction (L), and z is the vertical direction (L).

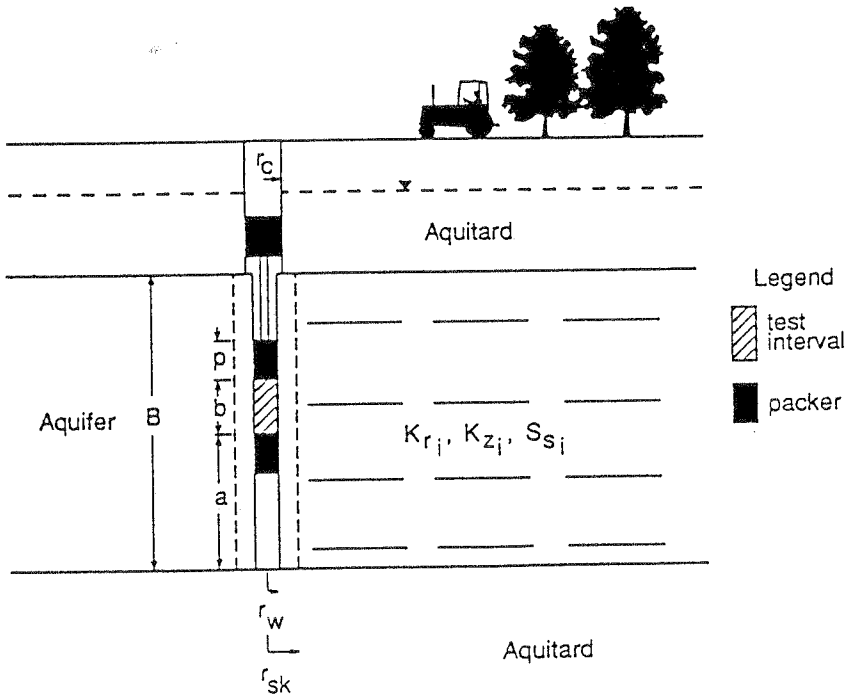

Fig. 1. Cross-sectional view of multilevel slug-test configuration (r_w, radius of test interval; r_c, radius of well casing above screen; r_{sk}, radius of skin; B, thickness of aquifer; a, distance of the bottom of the test interval above the base of the aquifer; b, width of the test interval; p, packer length; K_{r_i}, K_{z_i}, S_{s_i}, radial component of conductivity, vertical component of conductivity, and specific storage, respectively, of layer i). Layering is assumed to extend throughout the cross-section.

The initial conditions can be written as

$$h(r, z, 0) = 0, \qquad r_w < r < \infty, \qquad 0 \leqslant z \leqslant B \tag{2}$$

$$h(r_w, z, 0) = \begin{cases} H_0, & a \leqslant z \leqslant a + b \\ 0, & \text{elsewhere} \end{cases} \tag{3}$$

where r_w is the radius of the screen in the test interval (L), B is the thickness of the aquifer (L), H_0 is the height of the initial slug (L), a is the distance of the bottom of the test interval above the base of the aquifer (L), and b is the width of the test interval (L).

The boundary conditions are as follows:

$$h(\infty, z, t) = 0, \qquad t > 0, \qquad 0 \leqslant z \leqslant B \tag{4}$$

$$\frac{\partial h(r, 0, t)}{\partial z} = \frac{\partial h(r, B, t)}{\partial z} = 0, \qquad r_w < r < \infty, \qquad t > 0 \tag{5}$$

$$h(r_w, z, t) = H(t), \qquad t > 0, \qquad a \leqslant z \leqslant a + b \tag{6}$$

$$2\pi r_w \int_a^{a+b} K_r \frac{\partial h(r_w, z, t)}{\partial r} \, dz = \pi r_c^2 \frac{dH(t)}{dt}, \qquad t > 0 \tag{7}$$

$$\frac{\partial h(r_w, z, t)}{\partial r} = 0, \qquad t > 0, \qquad a - p \leqslant z < a, \qquad a + b < z \leqslant a + b + p \tag{8}$$

$$\frac{\partial h(0, z, t)}{\partial r} = 0, \qquad t > 0, \qquad 0 \leqslant z < a - p \tag{9}$$

$$\frac{\partial h(r_p, z, t)}{\partial r} = 0, \qquad t > 0, \qquad a + b + p < z \leqslant B \tag{10}$$

where $H(t)$ is the head within the well in the test interval (L), r_c is the radius of the cased portion of the well above the upper packer (L), r_p is the radius of the pipe through which the slug has been introduced to the test interval (L), and p is the length of the straddle packer (L). It should be noted that the conditions (8), (9), and (10) are a no-flow condition for the portion of the screen sealed by the packers, a symmetry boundary below the packers, and a no-flow condition along the pipe connecting the straddle packers to the upper packer, respectively.

Eqs. (1)–(10) describe the flow conditions of interest here. Given the generality of the property variations allowed in the vertical direction, analytical approaches are not feasible. Thus, for this work, a numerical model was employed to obtain approximate solutions to the mathematical model represented by the above equations.

3. Numerical model

In this work, a cylindrical-coordinate, three-dimensional, finite-difference model

(3DFDTC), developed at the Kansas Geological Survey (Butler and McElwee, 1992), was employed to simulate multilevel slug tests. The model was centered on the well in which the slug tests were being performed. The influence of well bore storage is taken into consideration using an approach based on earlier work of Settari and Aziz (1974), Rushton and Chan (1977), and Butler (1986). As described by Butler (1986), the approach is based on rewriting the classical pipe flow equation (Vennard and Street, 1975) in a formulation similar to Darcy's Law and defining a term (involving the friction factor, the cross-sectional area of the well bore, and distance along the well bore) analogous to hydraulic conductivity. This approach allows flow

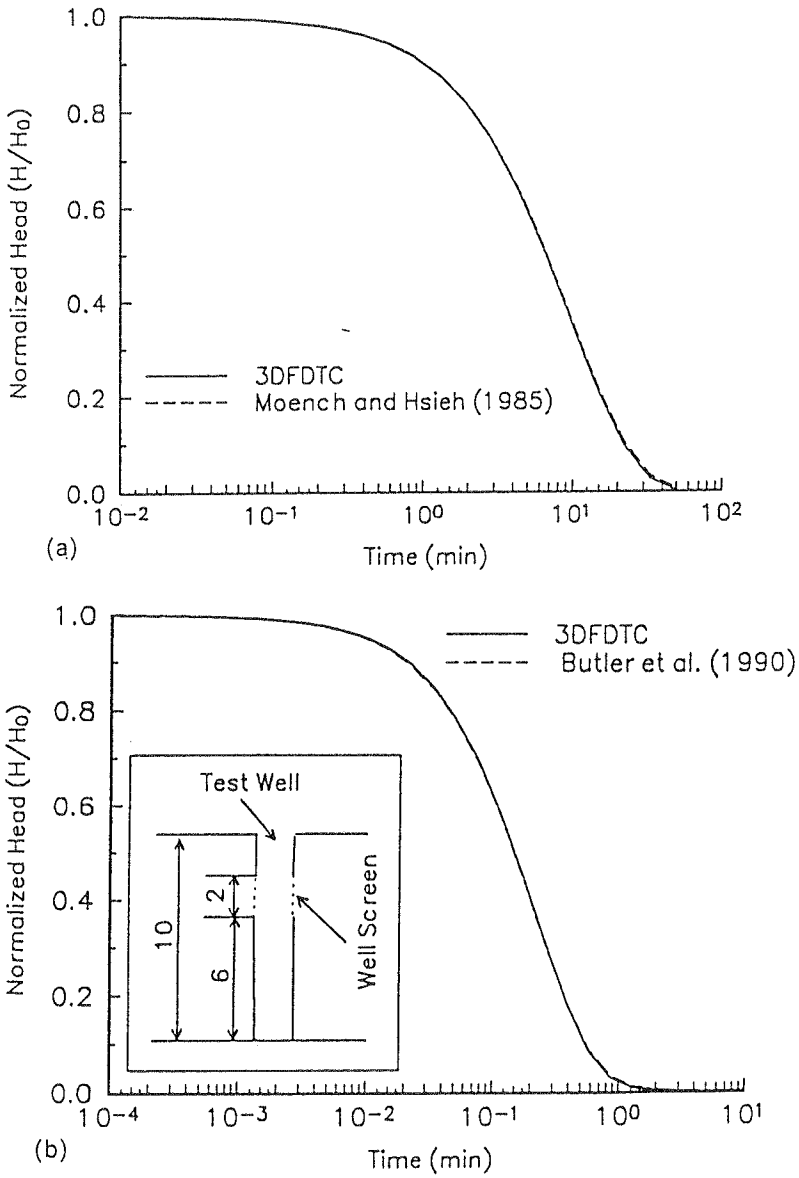

Fig. 2. Plots of normalized head ($H(t)/H_0$) vs. time comparing analytical solutions with 3DFDTC results. (a) Comparison of Moench and Hsieh (1985) solution with 3DFDTC results ($r_w = 0.167$ m, $r_{sk} = 0.33$ m, $T_{sk} = 0.001$ m^2 min^{-1}, $S_{sk} = 0.001$, $T_{aq} = 1$ m^2 min^{-1}, $S_{aq} = 0.00001$). (b) Comparison of Butler et al. (1990; see also McElwee et al., 1990) solution with 3DFDTC results ($r_w = 0.167$ m, $K = 0.1$ m min^{-1}, $S_s = 0.000001$ m^{-1}).

inside the well bore to be governed by the porous media flow equation (Eq. (1)). It should be noted that the implementation of this approach for this study produces an approximation of well-bore behavior that is equivalent to the hydrostatic head assumption employed in most analytical representations of the well bore (e.g. Papadopulos and Cooper, 1967; Cooper et al., 1967).

To demonstrate the validity of the well-bore approximation, the model has been checked against many analytical solutions for both pumping and slug tests. Two examples of such comparisons are presented here. The first example illustrates model performance when the hydraulic conductivity of adjacent grid cells differs by several orders of magnitude. A slug test in a well surrounded by a low-permeability well skin of finite radius was simulated. The well was assumed to be screened throughout the aquifer. Fig. 2(a) illustrates a comparison of the heads simulated by 3DFDTC with the results from the analytical solution of Moench and Hsieh (1985) for a slug test in a well with a skin of finite radius. The plots of the results are essentially the same. The small differences that do exist are attributed mainly to the error caused by the spatial discretization scheme employed in 3DFDTC (20 nodes in the radial direction from 0.1 to 37 364 m using equal log spacing). Further simulations have shown that, on increasing the number of nodes in the radial direction, the difference between the analytical solution and 3DFDTC results will gradually disappear.

The second example is selected to illustrate model performance when there is a strong component of vertical flow, such as might occur in multilevel slug tests. A slug test is simulated in a well that is screened for only a portion of the aquifer thickness. The aquifer is assumed to be homogeneous and isotropic with respect to flow properties. Fig. 2(b) displays a comparison of the heads simulated by 3DFDTC with the results of the analytical solution of Butler et al. (1990; see also McElwee et al., 1990) for a slug test in a well partially penetrating a confined aquifer. As with the previous example, 3DFDTC yields results that are essentially indistinguishable from those of the analytical solution. It should be noted that the error introduced by the radial discretization scheme employed in these examples was considered acceptable for the purposes of this work. Further issues concerning the vertical discretization scheme are discussed in a later section.

4. Techniques for analysis of slug tests in layered systems

The approach employed in this research was to simulate a series of multilevel slug tests using the 3DFDTC model, and then estimate the hydraulic conductivity of the portion of the formation opposite the screened interval from the simulated results. Several methods were considered for the analysis of the simulated slug-test responses. The most commonly used methods for the analysis of slug-test data in confined aquifers are the approaches of Cooper et al. (1967), henceforth designated as the CBP model, and Hvorslev (1951). As the CBP model was developed for slug tests performed in wells fully screened across an aquifer, the method of Hvorslev was the major focus of this work.

Hvorslev (1951) developed a series of models for the analysis of slug tests

performed in confined aquifers. A major assumption of the Hvorslev approach is that the specific storage of the aquifer can be neglected. As the head response at the test well is relatively insensitive to specific storage (Cooper et al., 1967), this assumption may be acceptable in many cases. Each of the well–aquifer configurations that Hvorslev considered requires the use of a 'shape factor', which is related to the geometry of the well intake region. The shape factor used here is that of Case 8 described by Hvorslev (1951), which is for a configuration consisting of a well with a screened interval of finite length located in a uniform, vertically unbounded, aquifer with a horizontal to vertical anisotropy in hydraulic conductivity. The Hvorslev model for this case is in the form of a two-parameter (K_r and anisotropy ratio) function:

$$h(t) = H_0 \exp(-t/T_0) \tag{11}$$

where

$$T_0 = (\pi r_c^2)/FK_r$$

$$F = (2\pi b)/(\ln\{mb/2r_w + [1 + (mb/2r_w)^2]^{1/2}\})$$

$$m = (K_r/K_z)^{1/2}$$

Unfortunately, the two parameters in (11) are perfectly correlated, so they cannot be estimated independently. Eq. (11) can be rearranged to produce the following expression for the estimated hydraulic conductivity:

$$K_{HV} = \frac{r_c^2 \ln\{mb/2r_w + [1 + (mb/2r_w)^2]^{1/2}\}}{2bt_0} \tag{12}$$

where K_{HV} is the hydraulic conductivity estimated using the Hvorslev model and t_0 is the time at which a normalized head of 0.37 is reached. Clearly, an anisotropy ratio must be assumed to estimate K_{HV}.

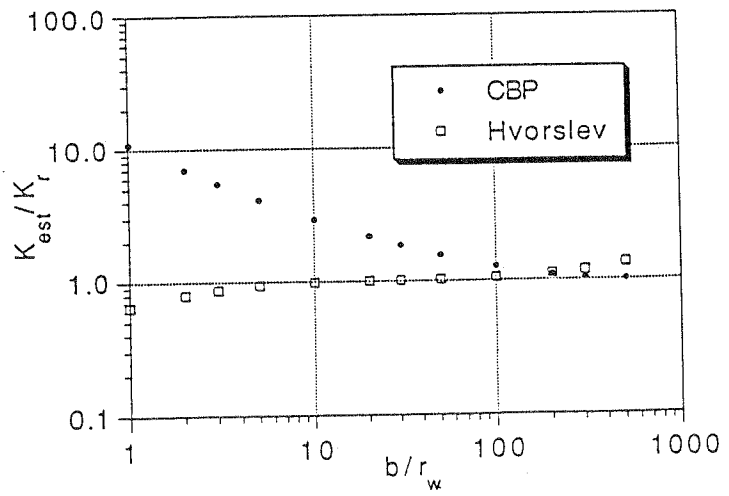

Fig. 3. Plot of aspect ratio (b/r_w) vs. conductivity ratio (K_{est}/K_r) for the case of boundaries at a large distance from the test interval.

An initial series of simulations was performed using 3DFDTC to assess the viability of the Hvorslev model for the estimation of hydraulic conductivity from multilevel slug-test data. Fig. 3 presents the results of a set of simulations in which the effects of the magnitude of the aspect ratio (b/r_w) on conductivity estimates, obtained from slug tests in a uniform aquifer, are investigated. Aspect ratios extending over two orders of magnitude were employed to evaluate parameter estimates over the range of conditions expected in multilevel slug tests. It should be noted that conductivity estimates obtained using both the Hvorslev and CBP models are included on this plot to illustrate the dependence of both models on aspect ratio. Fig. 3 indicates that the Hvorslev model should provide acceptable parameter estimates (within 20% of the actual conductivity) for aspect ratios between 3 and 300. The CBP model provides better estimates than the Hvorslev model at large aspect ratios (200 or higher) as a result of the slug-test responses becoming increasingly similar to those from a fully screened well at large aspect ratios.

The results presented in Fig. 3 are for the case of the test interval being at a large distance from a formation boundary (infinite aquifer case). Fig. 4 depicts the results of a further set of simulations in which the effects of an impermeable boundary on parameter estimates are examined. In these simulations, the test interval, which has an aspect ratio of five, is progressively moved from the center of the aquifer to the upper impermeable boundary. A test interval with a small aspect ratio and an isotropic aquifer were employed to emphasize the effects of vertical flow. The boundary effects are straightforward. As the test interval approaches the boundary, the vertical flow out of the interval is constrained, resulting in a decrease in the K_{HV} estimate. It should be noted that the effect of an impermeable horizontal boundary is less dramatic with larger aspect ratios and/or the presence of a pronounced anisotropy ($K_r > K_z$). Thus, Figs. 3 and 4 indicate that for the aspect ratios commonly employed in programs of

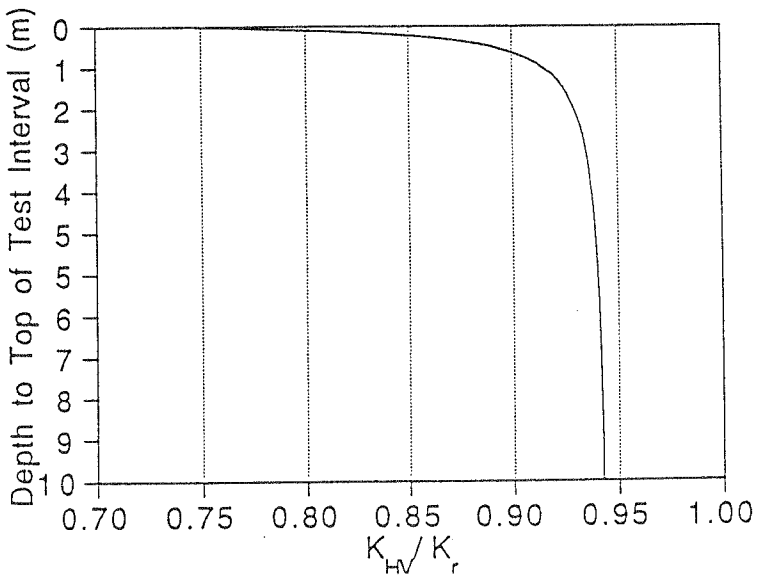

Fig. 4. Plot of conductivity ratio (K_{HV}/K_r) vs. depth to top of test interval (aspect ratio (b/r_w) = 5, impermeable boundary assumed at zero). (Note that in Fig. 3 (infinite aquifer case) $K_{HV}/K_r = 0.94$ for this aspect ratio.)

multilevel slug tests, the Hvorslev model should provide acceptable estimates as long as the test interval is several meters below an impermeable boundary.

Although the focus of this discussion has been on the Hvorslev model, several additional models were considered for the analysis of the simulated slug tests. As discussed in the Introduction, Butler et al. (1990; see also McElwee et al., 1990) have developed an analytical solution for slug tests in partially penetrating wells with skins, which can be readily configured to analyze data from multilevel slug tests in homogeneous, anisotropic aquifers. Although this solution avoids the simplifying approximations of the Hvorslev approach, the calculated parameters are not significantly different from those of Hvorslev for the range of aspect ratios commonly employed in multilevel slug tests. A major drawback of this model is that it is computationally intensive as a result of the use of both Fourier and Laplace integral transforms to obtain the solution.

Dagan (1978) and Widdowson et al. (1990) have developed techniques for the analysis of multilevel slug tests that are based on a series of graphs or charts developed from simulation of slug tests under conditions similar to those considered by Hvorslev (1951). A major drawback of these techniques is that new simulations are required for each well–aquifer configuration that is examined.

The Hvorslev model was considered the most appropriate model for use here, given the results of the simulations presented in Figs. 3 and 4 and its advantages in terms of computational efficiency. Thus, in the remainder of this paper, the Hvorslev model is employed for the analysis of simulated slug-test responses. The analyses were performed using the implementation of the Hvorslev model found in the SUPRPUMP automated well-test analysis package of the Kansas Geological Survey (Bohling and McElwee, 1992). This use of the Hvorslev model, however, should not be considered a blanket endorsement of the approach, as the model must be used with caution when analyzing actual field data, owing to its neglect of storage effects on slug-test responses (Chirlin, 1989), its poor performance in the presence of a well skin (Butler et al., 1990), and its increasing error in wells with very small aspect ratios (Hvorslev, 1951).

5. Dependence of multilevel slug-test results on density of layering

The simulations discussed in the previous section illustrate the performance of multilevel slug tests in ideal homogeneous systems. Many aquifers in nature, however, consist of layers of differing flow properties. To address the effects of layering on multilevel slug tests, a hypothetical aquifer, made up of alternating layers of constant thickness consisting of two distinct materials (denoted here as A and B), was constructed. Although layering in natural systems is clearly more complex than this configuration, the use of an alternating two-component system will allow the major effects of layering on a program of multilevel slug tests to be assessed.

The base set of parameters for this layered aquifer model are given in Table 1. A grid of 20 nodes in the radial direction (the same discretization scheme as used in simulations of Fig. 2) and 48–96 nodes in the vertical direction was employed. The

Table 1
Parameters for layered aquifer model

$H_0 = 1.0\,\text{m}$
$r_w = 0.05\,\text{m}$
$K_A = 2.0 \times 10^{-5}\,\text{m s}^{-1}$
$K_B = 2.0 \times 10^{-4}\,\text{m s}^{-1}$
$S_{SA} = S_{SB} = 1.0 \times 10^{-5}\,\text{m}^{-1}$
B = aquifer thickness = 30 m
r_{bnd} = radial distance to outer boundary = 37 364 m

number of nodes in the vertical varied depending on the layering and test interval length used in a particular scenario. To assess the error introduced by the various vertical discretization schemes, a number of additional simulations were performed using increasingly finer vertical discretization. In all cases, the discretization schemes used here were found to introduce an error of less than 2% to the calculated parameters. These errors were considered acceptable for the purposes of this work. It should be noted that in simulations using very small test intervals (0.156 m), the thickness of the aquifer (B) was decreased from the base case of 30 m to 15 m. In all cases, however, the results reported here were for test intervals far enough away from a boundary for boundary effects to be negligible.

The results of the simulations of slug tests in layered aquifers are presented using the range of conductivities estimated from a series of slug tests performed as the

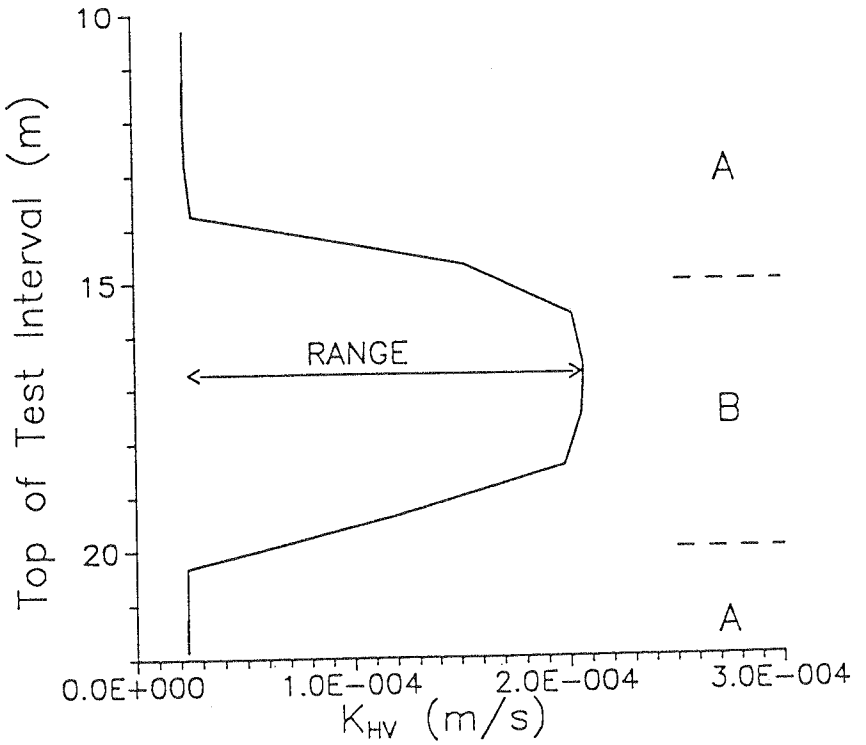

Fig. 5. Plot of estimated conductivity vs. depth to top of test interval for multilevel slug tests simulated in a layered aquifer consisting of alternating layers of material A and B (see Table 1; L (layer thickness) is 5 m, and b (length of test interval) is 1.25 m). Range is defined as distance between the maximum and minimum estimated conductivity.

packer string was moved in small increments up the well bore. Fig. 5 displays a plot of hydraulic conductivity values estimated from such a series of multilevel slug-test simulations in which the packer string is moved in 0.94 m increments up the well bore. The results are shown for only a portion of the series of alternating high- and low-conductivity layers to clarify the definition of the range as the distance between the peak and trough of the conductivity vs. depth plot. The range of estimated conductivities was considered a succinct way to display the manner in which the actual conductivity variations are being distorted in the results of a program of multilevel slug tests. In addition to the range, however, the estimated maximum and minimum conductivity values are also considered, so that the degree of over- or underestimation of layer conductivities is clear. It should be noted that the slight overestimation of K_A and K_B shown in Fig. 5 is in keeping with the results displayed in Fig. 3 for a test interval of the same aspect ratio ($b/r_w = 25$).

The first set of layered-aquifer simulations was designed to investigate the effect of layering density on multilevel slug tests. For these simulations, the test interval length was constrained to be less than or equal to the layer thickness, which was assumed to be constant for any particular simulation. In a later section, simulations using test intervals of lengths greater than the layer thickness are described. Fig. 6 displays the results of a series of simulations in which the test interval length was assumed to equal layer thickness. In these simulations, the test interval length (and thus the layer

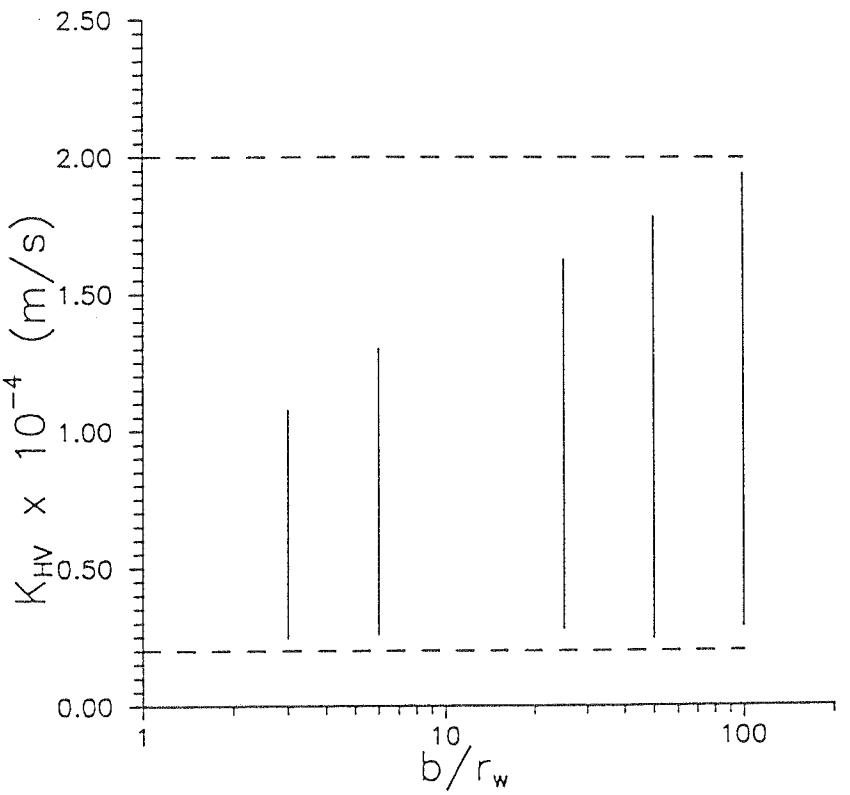

Fig. 6. Plot of range of estimated conductivities vs. aspect ratio (b/r_w). (Note that layer thickness changes in the same manner as b.) Lower and upper dashed lines indicate the conductivities of Layers A and B, respectively.

thickness) was gradually decreased from 5 m (aspect ratio of 100) to 0.156 m (aspect ratio approximately three). The results are displayed in the form of a plot of the range of the estimated conductivities vs. aspect ratio. Clearly, the range of estimated conductivities decreases significantly with decreases in aspect ratio. It should be noted that most of this decrease is a result of the conductivity estimated for layer B becoming increasingly smaller than the actual conductivity owing to suppression of vertical flow by the adjoining layers of material A. Hayashi et al. (1987) described how a decrease in aspect ratio promotes partial penetration effects, i.e. vertical flow from either end of the test interval. Thus, adjoining lower-conductivity layers will have a greater impact on slug-test responses as the aspect ratio decreases and the importance of vertical flow increases.

The general result of these simulations is that the effect of adjoining layers on multilevel slug tests becomes increasingly important as the layers decrease in thickness. Fig. 6, however, should only be considered as an example of these effects. The exact nature of the influence of adjoining layers will depend on a number of additional factors, including the specific storage of the layers and the degree of anisotropy in layer conductivity. The above simulations were performed assuming a specific storage of 1×10^{-5} m^{-1}. Additional simulations have shown that use of a lower specific storage value results in the pressure disturbance induced by the slug test spreading out more rapidly in all directions, causing the effect of adjoining lower-conductivity layers to be accentuated. The increased influence of adjoining lower-conductivity layers produces considerably lower values for the estimated layer B conductivities. Likewise, a specific storage greater than that used in Fig. 6 lessens the influence of adjoining layers on conductivity estimates. Thus, the specific storage can have a considerable influence on the estimated conductivity in layered systems. This is in contrast to slug tests in homogeneous systems, where specific storage has relatively little influence on conductivity estimates obtained from heads at the test well (Cooper et al., 1967).

The addition of anisotropy ($K_r > K_z$) into the configuration does not produce results significantly different from those shown in Fig. 6. The influence of adjoining layers is clearly diminished by the addition of anisotropy as a result of the suppression of vertical flow. The suppression of vertical flow itself, however, causes a decrease in the estimated conductivities. The net result is a decrease in the conductivities estimated for both layers and estimated conductivity ranges slightly narrower than those displayed in Fig. 6. It should be noted that the analyses described in this section were performed with the Hvorslev model, assuming an isotropic aquifer. This is a reasonable assumption, because one will not normally know what degree of anisotropy is appropriate. As discussed above, the anisotropy ratio and the horizontal conductivity are perfectly correlated in the Hvorslev model. Thus, some error will always be introduced into the parameter estimates as a result of the uncertainty concerning anisotropy.

The results displayed in Fig. 6 were obtained assuming that the test interval length was equal to layer thickness. If the test interval length is less than the layer thickness, adjoining layers will have less of an impact on the estimated conductivity. Fig. 7 shows the results of a series of simulations in which the layer thickness was

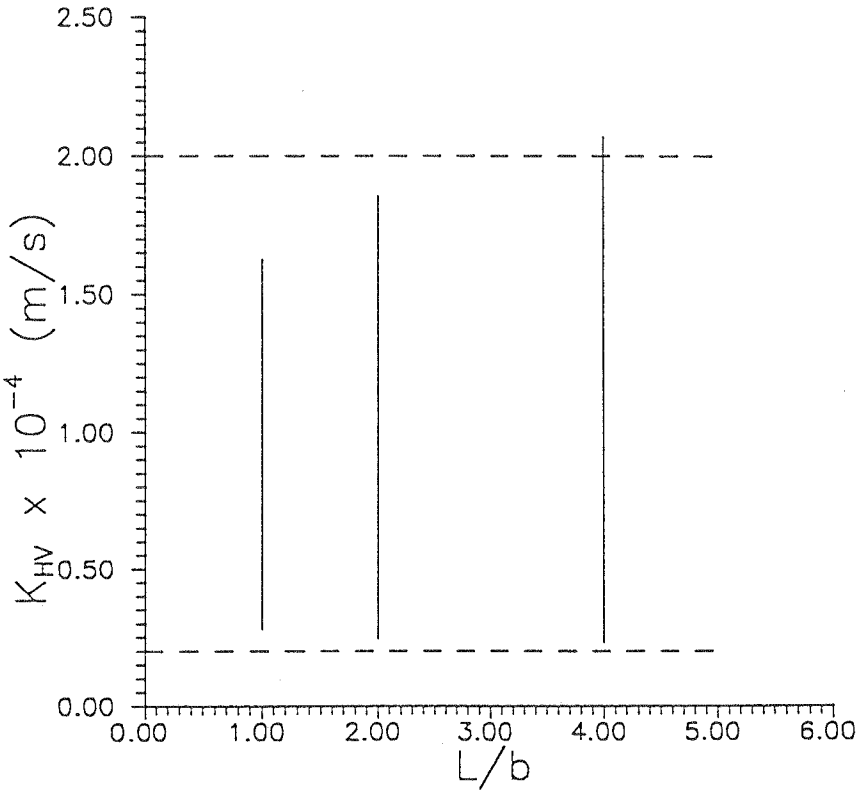

Fig. 7. Plot of range of estimated conductivities vs. L/b. (Note that b remains constant (1.25 m) for the cases displayed in this plot.) Lower and upper dashed lines indicate the conductivities of Layers A and B, respectively.

progressively increased, while the test interval, which was centered within the layer, was not changed (constant aspect ratio of 25). As expected, increases in the ratio of layer thickness to test interval length decrease the impact of adjoining layers. In Fig. 7, the effects of adjoining layers are essentially negligible for ratios of four or greater (overestimation of K_r seen at $L/b = 4$ is in keeping with Fig. 3). It should be noted that the exact nature of the decrease in the effects of adjacent layers will depend on the aspect ratio (the larger the aspect ratio, the more rapid the decrease). Clearly, however, the use of a test interval length considerably smaller than the average layer thickness will greatly improve the information obtained from a program of multilevel slug tests. When the results of Figs. 6 and 7 are considered together, it is also clear that r_w should be kept as small as practically possible to decrease the impact of the effects of small aspect ratios.

6. Dependence on well skins

The results depicted in Figs. 6 and 7 were determined for the ideal case, in which formation layering extends to the well screen. Often, however, as illustrated in Fig. 1, well drilling and development creates a near-well zone (well skin) of properties differing from those of the formation in which the well is screened. An additional

series of simulations was performed here to assess the effects of well skins on multi-level slug-test results.

Fig. 8 shows the results from a set of simulations in which a low-permeability well skin was employed. The results are displayed in the form of a plot of the range of estimated conductivities vs. simulation case. These results show that the addition of a low-permeability skin produces a near-complete suppression of the vertical variations in conductivity (calculated conductivity ranges are 2.9% and 1.7% of actual for Cases A and B, respectively). In addition to the suppression of the conductivity variations, the estimated conductivities are much lower than in the case with no skin, as a result of the heavy weighting of the low-permeability skin in the parameter estimates. Butler et al. (1990; see also McElwee et al., 1990) discussed the nature of the weighting of a low-permeability well skin in conductivity estimates obtained using the Hvorslev model. It should be noted that the estimated conductivities are lower in Case B as a result of the greater importance of vertical flow with smaller aspect ratios. In this case, the vertical flow is being suppressed by the low-permeability well skin, resulting in lower calculated conductivities.

A well skin may be of higher permeability than the formation as a result of voids forming along the well screen during well emplacement activities or a high-permeability sand pack. A high-conductivity skin can serve as a conduit for additional

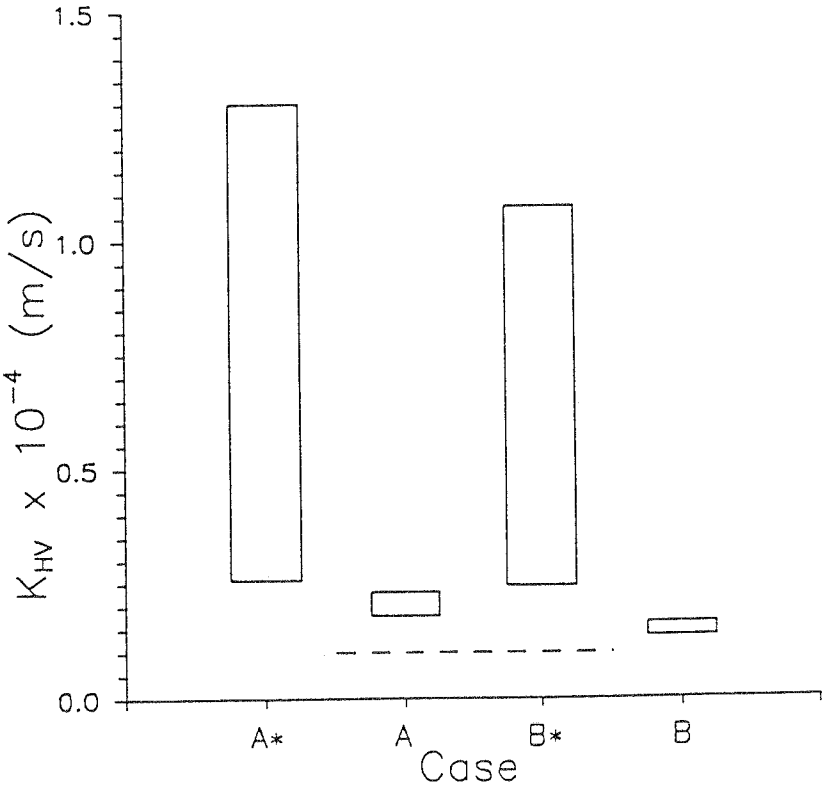

Fig. 8. Plot of range of estimated conductivities vs. simulation case for the low-permeability (K_{sk} = 0.00001 m s^{-1}) skin scenario (Case A*, case with no skin, $L = b = 0.312$ m; Case A, $L = b = 0.312$ m, $r_{sk} = 0.11$ m; Case B*, case with no skin, $L = b = 0.156$ m; Case B, $L = b = 0.156$ m, $r_{sk} = 0.11$ m). Dashed line indicates the skin conductivity.

vertical flow. Fig. 9 shows the results of a series of simulations in which a high-permeability skin of 0.11 m in radius was employed for most cases. Once again, the results are given in the form of a plot of the range of estimated conductivities vs. simulation case. It should be noted that, in relatively thick layers, the width of the calculated conductivity range does not change greatly from that in the case with no skin (compare Cases C* and C), although the estimated conductivities themselves increase significantly. As the thickness of the layers decreases, the layers become thin enough that, when the test interval is opposite a layer of material A, substantial amounts of water flow vertically along the well skin and into the layers of material B. This results in a great increase in the conductivity estimated for layers of material A and a dramatic decrease in the calculated conductivity range. As shown by Case G, this effect increases with the thickness of the skin. Clearly, a highly conductive skin in an aquifer consisting of thin layers can cause multilevel slug tests to be of rather limited effectiveness for describing vertical variations in hydraulic conductivity.

Given that a highly conductive skin can greatly limit the effectiveness of multilevel slug tests, a series of additional simulations was performed to assess whether measures could be taken during well construction to reduce the effect of a conductive skin. One possibility suitable for wells where the sand pack is the high-conductivity

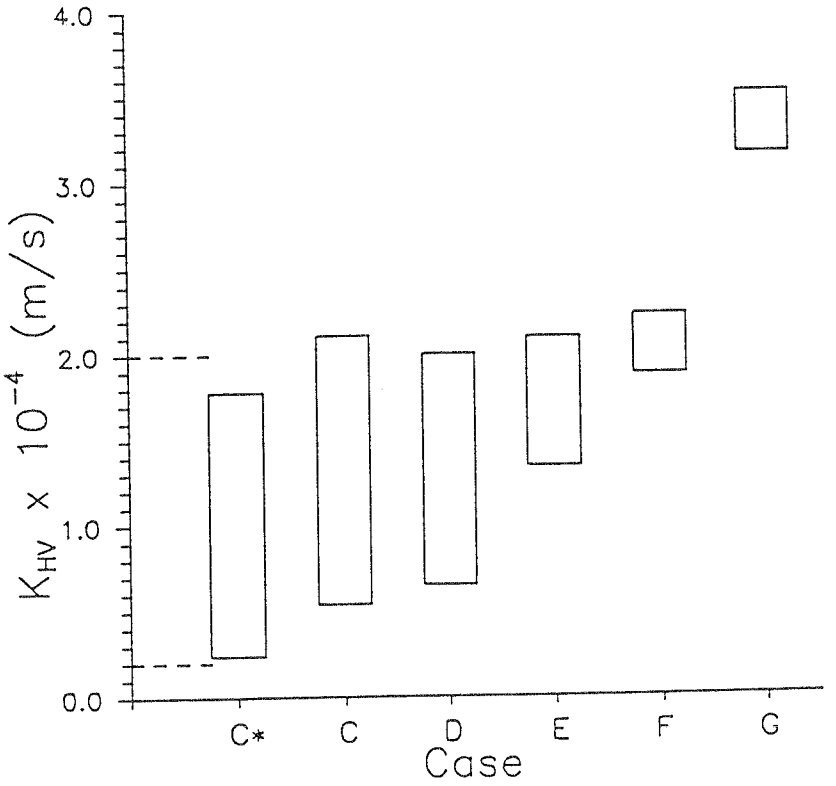

Fig. 9. Plot of range of estimated conductivities vs. simulation case for the high-permeability ($K_{sk} = 0.001$ m s^{-1}) skin scenario (Case C*, case with no skin, $L = b = 2.5$ m; Case C, $L = b = 2.5$ m, $r_{sk} = 0.11$ m; Case D, $L = b = 1.25$ m, $r_{sk} = 0.11$ m; Case E, $L = b = 0.312$ m, $r_{sk} = 0.11$ m; Case F, $L = b = 0.156$ m, $r_{sk} = 0.11$ m; Case G, $L = b = 0.312$ m, $r_{sk} = 0.22$ m). Lower and upper dashed lines indicate the conductivities of Layers A and B, respectively.

skin would be to place very thin layers (1–2 cm) of low-conductivity material (e.g. bentonite pellets) in the sand pack at an interval similar to the length of the planned test interval. These layers would serve to decrease the vertical movement of water in the sand pack, but would have very little impact on horizontal flow. This scheme was evaluated here by simulating slug tests in wells with high-conductivity skins in which an anisotropy in conductivity was assumed for the skin. Fig. 10 presents the results of a series of simulations in which anisotropy ratios (K_r/K_z) of one, two, and 10 were employed (K_r remaining constant and K_z decreased). As shown in the figure, increases in the anisotropy ratio cause the calculated conductivity range to increase and the estimated conductivities to decrease towards the value for the case with no skin. These results indicate that if a well is to be used for multilevel slug tests, the emplacement of periodic thin layers of low-conductivity material in the sand pack would be useful in partially mitigating the effect of a high-conductivity skin. Unfortunately, in cases where the high-conductivity skin is not the sand pack (e.g. uncased wells in consolidated rock), such an approach would not be possible, thereby making it difficult to remove the effect of a high-conductivity skin in those situations. It should be noted that the successful emplacement of periodic layers of bentonite in the sandpack should produce much greater anisotropy ratios (more than 1000) than those employed here. However, practically speaking, it will be difficult to insure that unbroken layers of bentonite have been placed at the desired locations. Lower

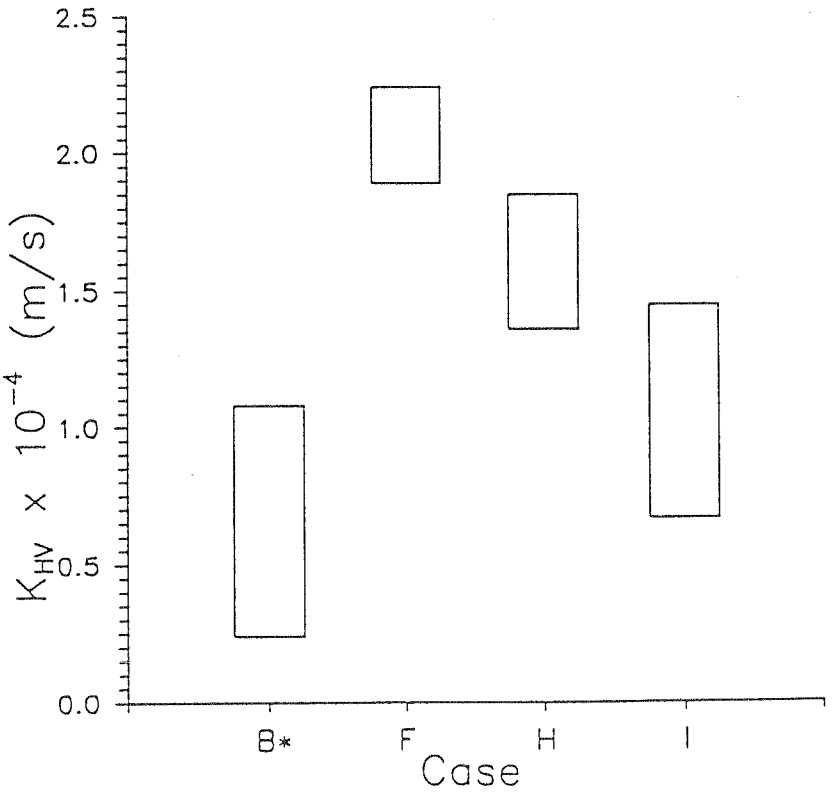

Fig. 10. Plot of range of estimated conductivities vs. simulation case for the high-permeability skin with anisotropy scenario (Case B*, case with no skin, $L = b = 0.156$ m; Case F, same as in Fig. 9; Case H, same as Case F except $K_{r(skin)}/K_{z(skin)} = 2$; Case I, same as Case F except $K_{r(skin)}/K_{z(skin)} = 10$).

anisotropy ratios were therefore employed here to yield conservative estimates of the expected behavior.

7. Vertical averaging in slug tests in layered aquifers

One issue of considerable interest to hydrogeologists is the way in which flow properties are averaged in various types of hydraulic tests in heterogeneous systems (e.g. Desbarats, 1992; Harvey, 1992). As a number of layers may be spanned by the test interval in a multilevel slug test, the issue of the manner in which the properties of those layers are averaged to form the effective parameter estimated from the response data is of some importance. In this work, the nature of this vertical averaging was explored empirically through numerical simulation.

The initial step of this investigation was to assess the manner in which hydraulic

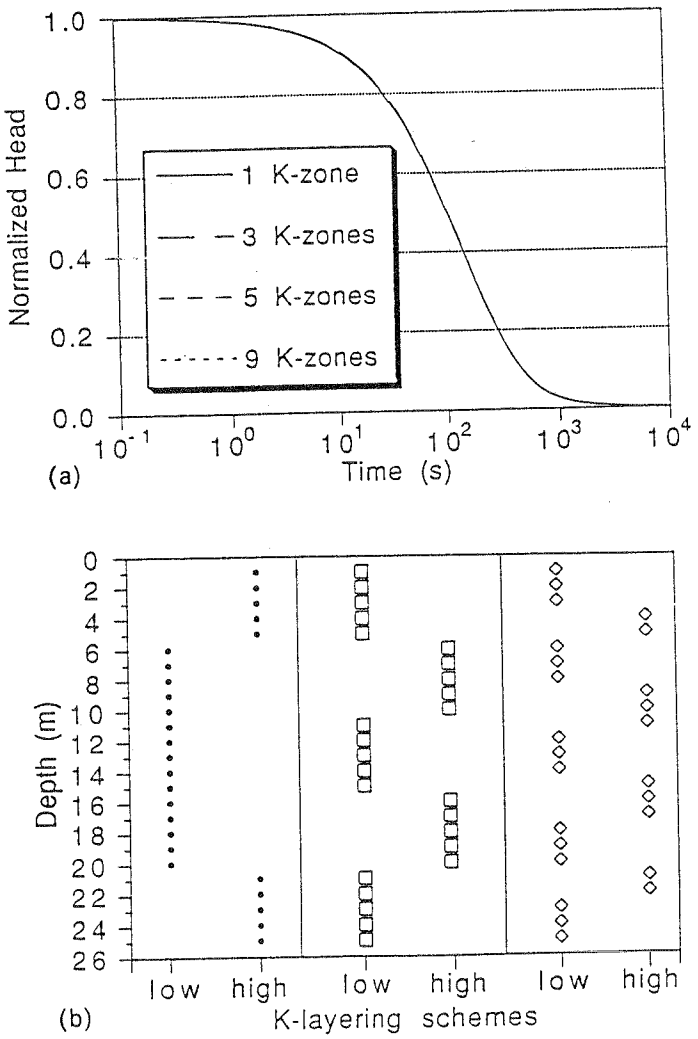

Fig. 11. Effects of variable layering on fully penetrating slug-test results. (a) Plot of normalized head $(H(t)/H_0)$ at the test well vs. time. (b) Layering schemes employed in the simulations shown in (a) (low and high conductivities defined in Table 2).

conductivity values that vary in the vertical direction are averaged in a slug test performed over the entire screened interval of a well fully penetrating the aquifer (fully penetrating slug test). A set of four simulations were performed. These simulations consisted of a uniform, anisotropic aquifer case, and three layered-aquifer cases with alternating layers of high and low conductivity. The layering schemes are shown in Fig. 11(b) and the parameter values used in each case are given in Table 2. It should be noted that all three layering schemes have a thickness-weighted average K_r of 9.2×10^{-5}, which is the same value for K_r as used in the uniform aquifer case.

Fig. 11(a) shows the results of the simulations for the case of head in the test well. As shown in this figure, the simulated heads at the test well are essentially identical in the uniform and all three layered cases. Clearly, slug tests over the entire screened interval in fully penetrating wells can provide little information about vertical variations in conductivity when the test well is the measurement location. In all cases, the estimated conductivity will be a thickness-weighted arithmetic average of the horizontal conductivities of the individual layers. It should be noted that this result is an extension of the work of Karasaki (1986), who found the same result using an analytical solution for slug tests in layered aquifers in which there is no vertical flow between layers. Thus, the vertical averaging in fully penetrating slug tests appears to be independent of the degree of vertical flow between layers. It is important to stress that there is vertical flow in the layered simulations of Fig. 11. These and additional simulations have shown that there will be considerable differences in head in the vertical direction outside of the test well ($r > r_w$) during a fully penetrating slug test in a layered aquifer (Butler and McElwee, 1992). Apparently, the flow between layers is in some sort of hydraulic balance dependent on the thickness of layers, the density of layering, layer flow properties, etc., such that the response at the central test well is independent of the degree of vertical flow.

As Fig. 11(a) shows that no indication of layering will be evident from the head response at the test well in a fully penetrating slug test, an obvious question of importance for multilevel slug tests is how much will layering be suppressed as the test interval becomes larger than the average layer thickness. Additional simulations have shown that the degree of suppression will depend on vertical variations in the arithmetic average of the conductivities of the test interval and the aspect ratio. In all cases, when the aspect ratio is much greater than 200, the estimated conductivity can be assumed to be a thickness-weighted average of the conductivities of the layers intersected by the test interval. It should be noted that this statement is based on

Table 2
Parameters for analysis of vertical averaging

Uniform, anisotropic case
$K_r = 9.2 \times 10^{-5}\,\mathrm{m\,s^{-1}}$, $K_z = 9.2 \times 10^{-6}\,\mathrm{m\,s^{-1}}$
Layered cases
Low-conductivity layer: $K_r = 2.0 \times 10^{-5}\,\mathrm{m\,s^{-1}}$, $K_z = 2.0 \times 10^{-6}\,\mathrm{m\,s^{-1}}$
High-conductivity layer: $K_r = 2.0 \times 10^{-4}\,\mathrm{m\,s^{-1}}$, $K_z = 2.0 \times 10^{-5}\,\mathrm{m\,s^{-1}}$

the assumption that the slug-test responses will be analyzed with the model of Cooper et al. (1967) for aspect ratios greater than 200, in keeping with the results displayed in Fig. 3.

8. Effect of packer length

All the multilevel slug-test simulations described above were performed assuming that the well was cased everywhere in the aquifer except at the test interval (infinite packer) in order to remove any effects related to the circumvention of the packers from the results. In field applications, however, packer circumvention is a very real concern. Increased vertical flow owing to packer circumvention can result in an overestimation of layer conductivities and an underestimation of the degree of vertical variations.

A series of additional simulations was performed to assess the effect of packer length on parameters estimated from multilevel slug tests. In the 3DFDTC model, packers are simulated as no-flow boundaries in the well bore, so there is no restriction on the length of the modelled packers. Four configurations were employed in this analysis to allow the effects of packer length to be evaluated in homogeneous and layered situations, both with and without a high-conductivity skin (see Table 3 for the

Table 3
Parameter sets for packer simulations

Case 1
$K_A = K_B = 2 \times 10^{-5}\ m\ s^{-1}$
$S_{SA} = S_{SB} = 1 \times 10^{-5}\ m^{-1}$
$b = 0.15\ m$

Case 2
$K_A = 2 \times 10^{-5}\ m\ s^{-1}$
$K_B = 2 \times 10^{-4}\ m\ s^{-1}$
$S_{SA} = S_{SB} = 1 \times 10^{-5}\ m^{-1}$
$b = 0.15\ m$
$L = 0.15\ m$

Case 3
$K_A = K_B = 2 \times 10^{-5}\ m\ s^{-1}$
$S_{SA} = S_{SB} = 1 \times 10^{-5}\ m^{-1}$
$K_{sk} = 0.001\ m\ s^{-1}$
$b = 0.15\ m$
$r_{sk} = 0.11\ m$

Case 4
$K_A = 2 \times 10^{-5}\ m\ s^{-1}$
$K_B = 2 \times 10^{-4}\ m\ s^{-1}$
$S_{SA} = S_{SB} = 1 \times 10^{-5}\ m^{-1}$
$K_{sk} = 0.001\ m\ s^{-1}$
$b = 0.15\ m$
$L = 0.15\ m$
$r_{sk} = 0.11\ m$

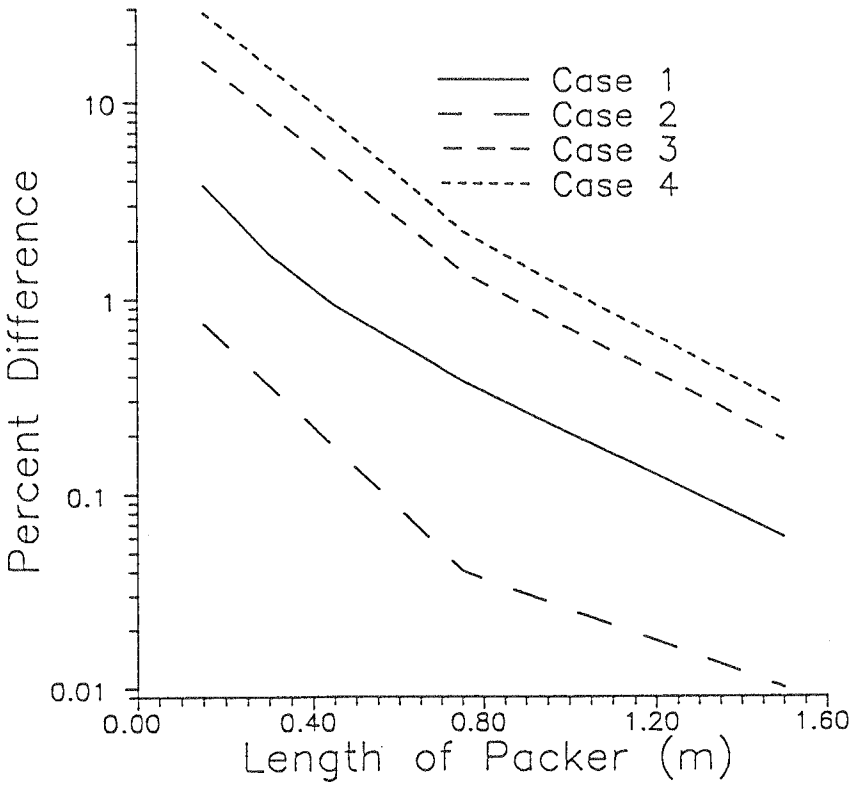

Fig. 12. Plot of packer length vs. normalized difference $((K_{packer} - K_{\infty\ packer})/K_{\infty\ packer} \times 100)$ for Cases 1–4 of Table 3. Plotted results are for case of test interval opposite layer A.

parameters used in each configuration). Cases 1 and 2 were designed to assess behavior in homogeneous and layered situations, respectively, in the absence of a high-conductivity skin, and Cases 3 and 4 were designed to assess behavior in the same systems in the presence of a high-conductivity skin.

Fig. 12 presents the results of these simulations in the form of a plot of packer length against the difference between the estimated conductivity using a packer of that length (K_{packer}) and the estimated conductivity using an infinite packer ($K_{\infty\ packer}$) normalized by the infinite packer estimate. It should be noted that a dramatic decrease in this difference is seen in all cases with an increase in packer length. This plot clearly indicates that a highly conductive skin will exacerbate packer circumvention problems. In all cases, however, these results demonstrate that the relationships derived in this work are essentially the same as would be obtained using packers of 0.75–1.5 m in length, which is the length range of many commercially available packers. Given that the skin is 50 times more permeable than layer A, these results should be considered conservative, worst-case estimates. Thus, packers greater than 0.75 m in length should prevent packer circumvention in the vast majority of field applications. Bliss and Rushton (1984) found similar results for the effect of packer length on constant-head injection tests. It should be noted that the results reported here are dependent on the thickness of the high-conductivity skin. In cases where very thick skins are suspected, longer packers or a number of packers in series should be employed. However, as demonstrated in an earlier section, a thick high-conductivity

skin will hinder the effectiveness of multilevel slug tests even without packer circumvention.

9. Recent field experiences

Recently reported field experiences with multilevel slug tests in unconsolidated aquifers support some of the findings of this study. Melville et al. (1991) reported on a program of multilevel slug tests for which the results compared favorably with information obtained from tracer tests. Butler and McElwee (1992), on the other hand, described a program of multilevel slug tests for which the results indicated essentially no vertical variations in flow properties, a finding that was not in agreement with existing core data. Although the test procedures followed in both studies were similar, the well drilling and emplacement procedures were not. Melville et al. (1991) described a procedure of well emplacement using mud rotary drilling followed by forcing a slotted pipe of slightly smaller diameter into the drilled hole. The small annular space between the slotted pipe and the drilled hole was filled by collapsing material from the borehole wall. The wells were then extensively developed to remove as much of the drilling mud as possible from the formation. Butler and McElwee (1992) described a procedure of well emplacement using hollow-stem auger drilling followed by placing a slotted pipe down the center of the augers and withdrawing the auger flights from about the pipe. In this case, a much larger annular space was formed, which was then filled by a natural sand pack consisting of material collapsing inward from the borehole wall. Permeameter analyses of cores from this same formation (Jiang, 1991; Butler and McElwee, 1992) have shown that repacked cores have considerably higher conductivities than the original sampled cores, indicating that the collapsed zone would probably form a skin of higher conductivity than the formation as a whole. The poor results of the tests reported by Butler and McElwee (1992) may well be due to preferential water movement along this thick high-conductivity skin. The success of the Melville et al. (1991) program appears to be largely due to the thin well skin coupled with unremoved drilling muds that are apparently preferentially impeding vertical flow. Although their approach seems to have met with success, the results of Melville and coworkers could have suffered from the same effects as illustrated in Fig. 8 without a very extensive program of well development. Thus, it is clear that well drilling and development procedures cannot be overemphasized in the planning of multilevel slug tests.

An approach for multilevel slug testing in unconsolidated formations that appears to minimize many of the problems arising as a result of well emplacement was described by Hinsby et al. (1992). This approach is based on progressively driving a well point and short screen into the formation. At any level desired, well driving can be stopped and a slug test performed. Although the results of the slug tests will still be a function of layering density, etc., as outlined here, this approach appears to have less potential for producing a thick high-conductivity skin along the driven pipe. Work currently under way at the Kansas Geological Survey and elsewhere is evaluating this approach in more detail.

10. Summary and conclusions

This paper reports the results of a series of numerical experiments designed to assess the potential of slug tests for the purpose of describing vertical variations in the radial component of hydraulic conductivity. Although most natural systems will not consist of the ideal two-component system of repetitive layers considered here, such a conceptual model allows considerable insight to be gained concerning behavior in more complex systems. Five general conclusions, which are independent of the particular parameter values employed here, can be drawn from this work:

(1) when the length of the test interval is of the order of the average layer thickness, considerable error can be introduced into the description of vertical variations in hydraulic conductivity as a result of the influence of layers adjoining the test interval. The magnitude of the influence of the adjoining layers will strongly depend on the aspect ratio (test interval length/r_w). The specific storage of the tested interval will also be an important factor.

(2) Regardless of layering density, a low-conductivity skin will make it difficult to describe vertical variations in hydraulic conductivity because the estimated conductivity will be strongly influenced by the conductivity of the skin.

(3) A high-conductivity skin will make it difficult to describe vertical variations in hydraulic conductivity when the test interval and the average layer thickness are both small. In this case, a large amount of vertical flow can occur along the skin, making it difficult to detect the existence of layers of low conductivity. Periodic emplacement of thin, low-conductivity layers in the sand pack can help decrease vertical flow and allow a more accurate description of the conductivity variations to be obtained.

(4) When the aspect ratio is large (more than 200), a slug test will yield an approximate thickness-weighted average of the hydraulic conductivities of the layers intersecting the test interval if the data are analyzed with the model of Cooper et al. (1967) (exact average in the case of a fully penetrating slug test). As the aspect ratio decreases, the properties of layers outside of the test interval will influence the calculated conductivity owing to the increased vertical flow.

(5) Packer circumvention should not be a major problem in most field applications when packers of 0.75 m or longer are employed. Packer circumvention is of greatest concern in the case of a thick, high-conductivity skin.

In summary, multilevel slug tests can provide considerable information about vertical variations in hydraulic conductivity under the right conditions. The best conditions would be thick layers, with test intervals considerably smaller than the average layer thickness. Even under these conditions, however, well skins can dramatically decrease the effectiveness of the approach. Considerable attention must therefore be given to well construction and development, to minimize the impact of a well skin on test results. Results from recently reported field tests demonstrate the importance of well construction and development procedures.

It should be noted that the findings of this study must be considered in the light of two major assumptions employed here. First, the simulated responses from each slug

test were analyzed using a homogeneous-aquifer model, an approach in keeping with standard field practices. Analysis of each test in isolation from the others in the same series of multilevel tests, however, led to the strong dependence of test results on layering density and, in many cases, to a significant underestimation of the actual conductivity variations. A more rigorous approach would be to analyze all the test results together using a numerical model coupled to an optimization routine. An initial attempt at such an approach for a series of drill-stem tests has been given by Yu and Lloyd (1992). Even if such a technique was used, however, it would not remove the effects of well skins or vertical averaging from test results. Given the nature of current field practices, the approach employed here was considered appropriate.

Second, the findings discussed in this paper were based on a series of simulations performed in perfectly stratified aquifers, i.e. layering is continuous throughout the entire model domain. Although many natural systems consist of a series of discontinuous layers, the rate of variation in flow properties in the direction perpendicular to the plane of layering would be expected to be considerably larger than that in the direction parallel to layering (Butler, 1986; Hess et al., 1992). Thus, the results presented here should be applicable to most field situations. Further work, however, is required to assess fully the effect of layer discontinuity on slug tests.

Acknowledgments

This research was sponsored in part by the Air Force Office of Scientific Research, Air Force Systems Command, USAF, under grant or cooperative agreement AFOSR 91-0298, and by the US Geological Survey (USGS), Department of the Interior, under USGS award 14-08-0001-G2093. The views and conclusions contained in this document are those of the authors and should not be interpreted as necessarily representing the official policies, either expressed or implied, of the US Government.

References

Bliss, J.C. and Rushton, K.R., 1984. The reliability of packer tests for estimating the hydraulic conductivity of aquifers. Q. J. Eng. Geol., 17: 81–91.

Bohling, G.C. and McElwee, C.D., 1992. SUPRPUMP: an interactive program for well test analysis and design. Ground Water, 30(2): 262–268.

Braester, C. and Thunvik, R., 1984. Determination of formation permeability by double-packer tests. J. Hydrol., 72: 375–389.

Butler, Jr., J.J., 1986. Pumping tests in nonuniform aquifers: a deterministic and stochastic analysis. Ph.D. dissertation, Stanford University, Stanford, CA, 220 pp.

Butler, Jr., J.J. and Liu, W.Z., 1993. Pumping tests in nonuniform aquifers: the radially asymmetric case. Water Resour. Res., 29(2): 259–269.

Butler, Jr., J.J. and McElwee, C.D., 1992. Well-testing methodologies for characterizing heterogeneities in alluvial-aquifer systems: first year report. Kans. Geol. Surv. Open-File Rep., 92-53, 152 pp.

Butler, Jr., J.J., McElwee, C.D., Bohling, G.C. and Healey, J.M., 1990. Hydrogeologic characterization of hazardous waste sites. Kansas Water Resources Research Inst., Manhattan, KS, Contrib. 283, 114 pp.

Chirlin, G.R., 1989. A critique of the Hvorslev method for slug test analysis: the fully penetrating well. Ground Water Monit. Rev., 9(2): 130–138.

Cooper, Jr., H.H., Bredehoeft, J.D. and Papadopulos, I.S., 1967. Response of a finite-diameter well to an instantaneous charge of water. Water Resour. Res., 3(1): 263–269.

Dagan, G., 1978. A note on packer, slug, and recovery tests in unconfined aquifers. Water Resour. Res., 14(5): 929–934.

Dagan, G., 1986. Statistical theory of groundwater flow and transport: pore to laboratory, laboratory to formation, and formation to regional scale. Water Resour. Res., 22(9): 120S–134S.

Desbarats, A.J., 1992. Spatial averaging of transmissivity in heterogeneous fields with flow toward a well. Water Resour. Res., 28(3): 757–767.

Dougherty, D.E. and Babu, D.K., 1984. Flow to a partially penetrating well in a double-porosity reservoir. Water Resour. Res., 20(8): 1116–1122.

Ehlig-Economides, C.A. and Joseph, J.A., 1987. A new test for determination of individual layer properties in a multilayered reservoir. SPE Formation Eval., 2(3): 261–283.

Freyberg, D.L., 1986. A natural gradient experiment on solute transport in a sand aquifer, 2. Spatial moments and the advection and dispersion of nonreactive tracers. Water Resour. Res., 22(13): 2031–2046.

Gelhar, L.W., 1986. Stochastic subsurface hydrology from theory to applications. Water Resour. Res., 22(9): 135S–145S.

Harvey, C.F., 1992. Interpreting parameter estimates obtained from slug tests in heterogeneous aquifers. M.S. Thesis, Stanford University, Stanford, CA, 99 pp.

Hayashi, K., Ito, T. and Abe, H., 1987. A new method for the determination of in situ hydraulic properties by pressure pulse tests and application to the Higashi Hachimantai geothermal field. J. Geophys. Res., 92(B9): 9168–9174.

Hess, K.M., Wolf, S.H. and Celia, M.A., 1992. Large-scale natural gradient tracer test in sand and gravel, Cape Cod, Massachusetts, 3. Hydraulic conductivity variability and calculated macrodispersivities. Water Resour. Res., 28(8): 2011–2027.

Hinsby, K., Bjerg, P.L., Andersen, L.J., Skov, B. and Clausen, E.V., 1992. A mini slug test method for determination of a local hydraulic conductivity of an unconfined sandy aquifer. J. Hydrol., 136: 87–106.

Hufschmied, P., 1986. Estimation of three-dimensional anisotropic hydraulic conductivity field by means of single well pumping tests combined with flowmeter measurements. Hydrogeologie, 2: 163–174.

Hvorslev, M.J., 1951. Time lag and soil permeability in ground-water observations. US Army Corps Eng. Waterways Exp. Sta. Bull. 36, 50 pp.

Jiang, X., 1991. A field and laboratory study of scale dependence of hydraulic conductivity. M.S. Thesis, University of Kansas, Lawrence, 149 pp.

Karasaki, K., 1986. Well test analysis in fractured media. Ph.D. Dissertation, University of California, Berkeley, 239 pp.

McElwee, C.D., Butler, Jr., J.J., Liu, W.Z. and Bohling, G.C., 1990. Effects of partial penetration, anisotropy, boundaries and well skin on slug tests (abstract). EOS, 71(17): 505.

McElwee, C.D., Butler, Jr., J.J., and Healey, J.M., 1991. A new sampling system for obtaining relatively undisturbed samples of unconsolidated coarse sand and gravel. Ground Water Monit. Rev., 11(3): 182–191.

McLane, G.A., Harrity, D.A. and Thomsen, K.O., 1990. A pneumatic method for conducting rising and falling head tests in highly permeable aquifers. Proc. 1990 NWWA Outdoor Action Conf.

Melville, J.G., Molz, F.J., Guven, O. and Widdowson, M.A., 1991. Multilevel slug tests with comparisons to tracer data. Ground Water, 29(6): 897–907.

Moench, A.F. and Hsieh, P.A., 1985. Analysis of slug test data in a well with finite-thickness skin. In: Mem. 17th Int. Congr. on Hydrogeology of Rocks of Low Permeability, Int. Assoc. Hydrogeo. pp. 17–29.

Moltyaner, G.L. and Killey, R.W.D., 1988. Twin Lake tracer tests: longitudinal dispersion. Water Resour. Res., 24(10): 1613–1627.

Molz, F.J., Morin, R.H., Hess, A.E., Melville, J.G. and Guven, O., 1989. The impeller meter for measuring aquifer permeability variations: evaluation and comparison with other tests. Water Resour. Res., 25(7): 1677–1686.

Morin, R.H., Hess, A.E. and Paillet, F.L., 1988. Determining the distribution of hydraulic conductivity in a fractured limestone aquifer by simultaneous injection and geophysical logging. Ground Water, 26(5): 587–595.

Orient, J.P., Nazar, A. and Rice, R.C., 1987. Vacuum and pressure test methods for estimating hydraulic conductivity. Ground Water Monit. Rev., 7(1): 49–50.

Papadopulos, I.S. and Cooper, Jr., H.H., 1967. Drawdown in a well of large diameter. Water Resour. Res., 3(1): 241–244.

Rehfeldt, K.R., Hufschmied, P., Gelhar, L.W. and Schaefer, M.E., 1989. Measuring hydraulic conductivity with the borehole flowmeter. Rep. EN-6511, Electric Power Res. Inst., Palo Alto, CA.

Rushton, K.R. and Chan, Y.K., 1977. Numerical pumping test analysis in unconfined aquifers. J. Irrig. Drainage Div., 103(IR1): 1–12.

Settari, A. and Aziz, K., 1974. A computer model for two-phase coning simulation. Soc. Pet. Eng. J., 14(3): 221–236.

Taylor, K. and Molz, F., 1990. Determination of hydraulic conductivity and porosity logs in wells with a disturbed annulus. J. Contaminant Hydrol., 5: 317–332.

Taylor, K., Wheatcraft, S., Hess, J., Hayworth, J. and Molz, F., 1990. Evaluation of methods for determining the vertical distribution of hydraulic conductivity. Ground Water, 28(1): 88–98.

Vennard, J.K. and Street, R.L., 1975. Elementary Fluid Mechanics. Wiley, New York, 740 pp.

Widdowson, M.A., Molz, F.J. and Melville, J.G., 1990. An analysis technique for multilevel and partially penetrating slug test data. Ground Water, 28(6): 937–945.

Yu, Y.H. and Lloyd, J.W., 1992. A multi-layered radial flow model interpretation of drill stem test data. J. Hydrol., 136: 73–86.

Zapico, M., Vales, S. and Cherry, J., 1987. A wireline piston core barrel for sampling cohesionless sand and gravel below the water table. Ground Water Monit. Rev., 7(3): 74–82.

C. SENSITIVITY ANALYSIS OF SLUG TESTS WITH OBSERVATION WELLS

A manuscript describing the work of this section was submitted to the Journal of Hydrology in September of 1993. A revised version of the manuscript was accepted in June of 1994, and the article was published in volume 164 of the Journal of Hydrology in 1995. The remainder of this section consists of a reprint of that article.

ELSEVIER

Journal of Hydrology 164 (1995) 69–87

Journal of Hydrology

[2]

Sensitivity analysis of slug tests Part 2. Observation wells

C.D. McElwee*, J.J. Butler, Jr., G.C. Bohling, W. Liu

Kansas Geological Survey, 1930 Constant Ave., Lawrence, KS 66047, USA

Received 30 September 1993; revision accepted 25 June 1994

Abstract

An earlier paper (Part 1, this issue) dealt with the use of sensitivity analysis for the design of a slug test that would give reasonably accurate estimates of the aquifer parameters by an informed choice of the number and times of measurements. An investigation of the radial dependence of the Cooper et al. analytical solution for a slug test in a confined aquifer shows that the use of one or more observation wells can vastly improve the parameter estimates, particularly the estimate of the storage parameter. Generally, the observation well must be fairly close (about 10 m or less) to the slugged well to be effective. The storage coefficient must be small in order to see the effect of the slug at greater distances from the stressed well. Since the temporal and spatial dependence of the sensitivities for transmissivity and storage are considerably different, the addition of one or more observation wells will substantially reduce the correlation between these two parameters, which will result in much better estimates than are usually obtained in slug tests. These ideas are illustrated using typical data representative of our research sites.

1. Introduction

Slug tests are commonly used for site characterization because they are relatively easy and inexpensive to perform. Although a great deal of information about the aquifer hydraulic parameters in the vicinity of the stressed well is contained in slug test data, it is unclear if current practices are actually yielding accurate estimates of those parameters. At the Kansas Geological Survey (KGS), we have been studying the capabilities and limitations of the slug test as a tool for site characterization. This is the second paper in a series detailing our findings. An earlier paper (McElwee et al., 1995) dealt with the use of sensitivity analysis to design a slug test that would give

* Corresponding author.

SSDI 0022-1694(94)02569-W

reasonable estimates of homogeneous aquifer parameters by an informed choice of the number and times of measurements.

Most practitioners know that slug tests are not very sensitive to the storage coefficient; the reasons for this are explained in the earlier paper (McElwee et al., 1995). The complete analytical solution of Cooper et al. (1967, henceforth designated the CBP solution) includes the time-varying radial dependence of head away from the slugged well. Most researchers use the form restricted to the slugged well itself and simply measure head data in the slugged well. In this paper we investigate the use of observation wells with slug tests. Since slug tests are often used as a rapid, inexpensive, and sometimes first attempt at characterizing a site, many times observation wells are not available. However, we also know from experience that sometimes other wells, which were installed for other purposes, are available nearby. It is probably not economically feasible most times to install observation wells specifically for use with slug tests. On the other hand, if nearby wells are available we advocate that the field investigator consider using them as observation wells. The objective of this paper is to show that the use of one or more observation wells can vastly improve the parameter estimates, particularly the estimate for storage. The tools we use for this study are sensitivity analysis (McElwee, 1987) and an automated well test analysis package, SUPRPUMP (Bohling and McElwee, 1992), developed at the KGS.

A number of other researchers have considered the radial dependence of slug tests and/or the use of observation wells with slug tests, although, not in the quantitative manner presented here. Ramey et al. (1975) were perhaps the first to investigate the radius of influence of a slug test. They showed that a measurable response in an observation well could be observed at a distance of 100 well radii or more from the stressed well under favorable conditions. However, they did not advocate the routine use of observation wells. They simply wanted to refute arguments that slug tests were affecting only a small volume of the aquifer. Walter and Thompson (1982) advocated using repeated slug test pulses with observation wells in tight formations. However, they used the Ferris and Knowles (1954) solution with its assumption of vanishing stressed well radius (i.e. no well bore storage). The advantages of using observation wells with slug tests that Walter and Thompson saw were that a larger volume was tested, that storativity can be determined from the observation well response, and that anisotropy may be determined. Barker and Black (1983) and Black (1985) also considered the concept of the radius of influence of a slug test, which they defined as the radius where a given fraction of the initial slug input (H_0) can be measured in an observation well. Sageev (1986) presented a good discussion of radius of influence and showed some detailed curves for head in observation wells. He pointed out that wellbore storage in observation wells can dramatically reduce the response there, and suggested that packers be used in observation wells to reduce the effect of observation wellbore storage. Karasaki et al. (1988) presented slug-test solutions for various geometries that may be encountered in heterogeneous systems, including head (interference) responses at observation wells for slug tests. They graphed head response at some radial distances and came to the conclusions that: (1) fairly large responses can be observed at wells a considerable distance away under the right conditions; (2) curves characterizing different storativities are uniquely different at

the observation well; and (3) transmissivity and storativity can be estimated independently. Novakowski (1989) also considered pulse interference tests (observing slug test responses at observation wells). He developed solutions including wellbore storage effects at the observation well, thus extending the earlier work of Sageev (1986). (He also recommended isolating the observation interval with packers to minimize observation wellbore storage effects.) Novakowski gave his solutions in Laplace space and used the Talbot algorithm for inversion. He presented the radial response of a slug test for some cases and defined a graphical analysis procedure to overcome borehole storage effects at the observation well. Chirlin (1989) realized that the head distribution as a function of radius around a slugged well was different for the Hvorslev (1951) and CBP solutions, but he did not suggest the use of observation wells to determine the storage coefficient. He did show some contours of head versus radius for the CBP model. Chirlin (1990) later commented on the radius of influence of a slug test and noted that "it would not be unusual to have a radius of investigation equal to hundreds of well radii". However, the use of observation wells for parameter estimation was not addressed. Recently, Guyonnet et al. (1993) have analyzed the volume of investigation for a slug test. They considered the effect of various boundaries on the slugged well response, but they did not explicitly consider the use of measurements from an observation well.

In this paper we attempt to quantify the use of observation well data along with slugged well data to determine aquifer parameters. Generic plots of relative head show the radius of influence of a slug test as a function of α (storage coefficient and well radii), β (transmissivity and time), and r (observation radius). Plots of sensitivity coefficients versus α, β, and r are used to illustrate the regions where time and space measurements give the greatest sensitivity to the aquifer parameters. The issue of correlation between parameters, in particular T and S, is addressed. Graphically, the sensitivity coefficients show why measurements in the slugged well are relatively insensitive to S and why the addition of an observation well reduces the correlation and provides better estimates of S. The paper concludes with applications to data typical of our research sites.

2. Analytical solution for slug tests

The complete CBP analytical solution for the radial dependence of head around a slugged well having a finite radius is given by

$$H\left(\alpha,\beta,H_0,\frac{r}{r_s}\right)=\frac{2H_0}{\pi}\int_0^\infty \frac{\exp(-\beta x^2/\alpha)}{\Delta(x)}F\left(x,\alpha,\frac{r}{r_s}\right)\mathrm{d}x \tag{1}$$

where

$$F\left(x,\alpha,\frac{r}{r_s}\right)=\left\{J_0\left(x\frac{r}{r_s}\right)[xY_0(x)-2\alpha Y_1(x)]-Y_0\left(x\frac{r}{r_s}\right)[xJ_0(x)-2\alpha J_1(x)]\right\} \tag{2}$$

and

$$\Delta(x) = [xJ_0(x) - 2\alpha J_1(x)]^2 + [xY_0(x) - 2\alpha Y_1(x)]^2 \tag{3}$$

x is the variable of integration, J and Y are Bessel functions, and r_s and r_c are the screen and casing radii, respectively. The variables α and β are defined as

$$\beta = \frac{Tt}{r_c^2} \tag{4}$$

$$\alpha = \frac{r_s^2}{r_c^2} S \tag{5}$$

This analytical solution shows that slug-test responses can be expressed as a function of four parameters: α, a parameter related to screen and casing radii and the storage coefficient; β, a dimensionless time involving transmissivity and the casing radius; H_0, the initial head displacement; and r/r_s, the distance to an observation well divided by the screen radius. It is often convenient to use relative head (h), which is defined as

$$h = \frac{H}{H_0} \tag{6}$$

It should be stressed that in many complex geologic environments the CBP model may not be adequate. However, this study should give valuable specific insight when the CBP model is applicable and perhaps general insight to more complex situations. It should be emphasized at this point that these analytically predicted responses, Eq. (1), are assuming no observation wellbore storage. If indeed open boreholes of substantial radii are used as observation wells, the response obtained will be much smaller owing to wellbore storage effects. For this reason, we will assume from here on that a packer has been placed in the observation well to minimize wellbore storage effects. The effectiveness of the packer will depend on the elastic properties of the gland material under the given inflation pressures. If packers in good condition of nearly the same diameter as the hole are used with inflation pressures of 50 psi or more, they should be adequate in shallow wells.

3. Sensitivity analysis

Sensitivity analysis (McElwee, 1987) can be used to look at the effect of a small parameter change on the head. Background material is presented in some detail in the first paper (McElwee et al., 1994) and will only be briefly summarized here for completeness. A first-order Taylor series expansion can be performed and used to define normalized sensitivity coefficients of relative head to the parameters, in this case T, S, and H_0. These sensitivity coefficients

$$u'_T = T\frac{\partial h}{\partial T} = \beta\frac{\partial h}{\partial \beta} \tag{7}$$

$$u'_S = S\frac{\partial h}{\partial S} = \alpha\frac{\partial h}{\partial \alpha} \tag{8}$$

$$u'_{H_0} = \frac{\partial H}{\partial H_0} = h \tag{9}$$

are simply derivatives of the head with respect to the parameter and may be evaluated analytically or numerically. Sensitivity coefficients are a measure of how much the head changes when a parameter is changed by a small amount; therefore, they are very useful to examine in some detail. The sensitivity coefficients defined by Eqs. (7)–(9) are normalized sensitivities to relative head (dimensionless) and may be compared on a single plot to infer the relative sensitivity of the three parameters. Sensitivity coefficients may be positive or negative, the sign merely indicating the direction of change in head caused by a change in the parameter. These sensitivity functions are only functions of α, β and r/r_s. For given values of α and r/r_s a generic sensitivity curve can be plotted versus β, which is valid for any value of transmissivity; differing transmissivity values simply scale the time differently. In a similar manner, given values for α and β, a plot can be made showing the radial dependence of the sensitivity coefficient. The fact that may vary over a wide range gives rise to a family of curves in each of these plots. All normalized sensitivity plots in the following sections are of Eqs. (7)–(9) and are dimensionless.

4. Relative head or sensitivity to H_0

Figs. 1–4 display the dependence of the relative head (h), or the sensitivity to H_0 (u'_{H_0}, Eq. (9)), on the parameters α, β, and the normalized radius (r/r_s). Fig. 1 shows the response that would be expected at several observation well distances, each response in time being a bell-shaped curve whose maximum amplitude decays with distance from the slugged well. At about $175r_s$ the response has fallen to about 0.01 H_0 at a dimensionless time of 10 for $\alpha = 10^{-3}$. Fig. 2 shows the radial dependence for various dimensionless times. From Figs. 1 and 2 it is clear that responses from the stressed (slugged) well can propagate significant distances (50–100 r_s) in the radial direction. Fig. 2 shows that the area of influence spreads with time, but that the response decays and becomes diffuse at later times. Figs. 3 and 4 are designed to show the effect of α (related to storage coefficient and the ratio of screen radius to casing radius squared) on the response in time and space. Clearly, smaller α's result in larger responses in space and time. For $\alpha = 10^{-5}$ it is clear that significant responses can be propagated to distances of over 200 screen radii. It would clearly be beneficial to construct a well with a casing radius several times the screen radius if that did not create an economical or logistic problem. A factor of just over 3 increase in the ratio of casing radius to screen radius will decrease α by an order of magnitude, thereby increasing the response at observation wells, whatever the naturally occurring storage coefficient.

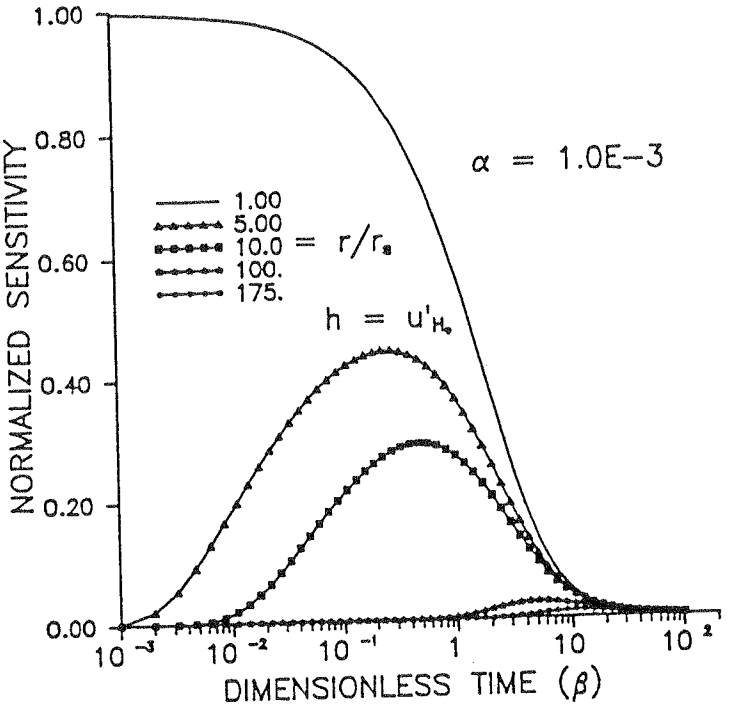

Fig. 1. Variation of u'_{H_0} with time for various r/r_s.

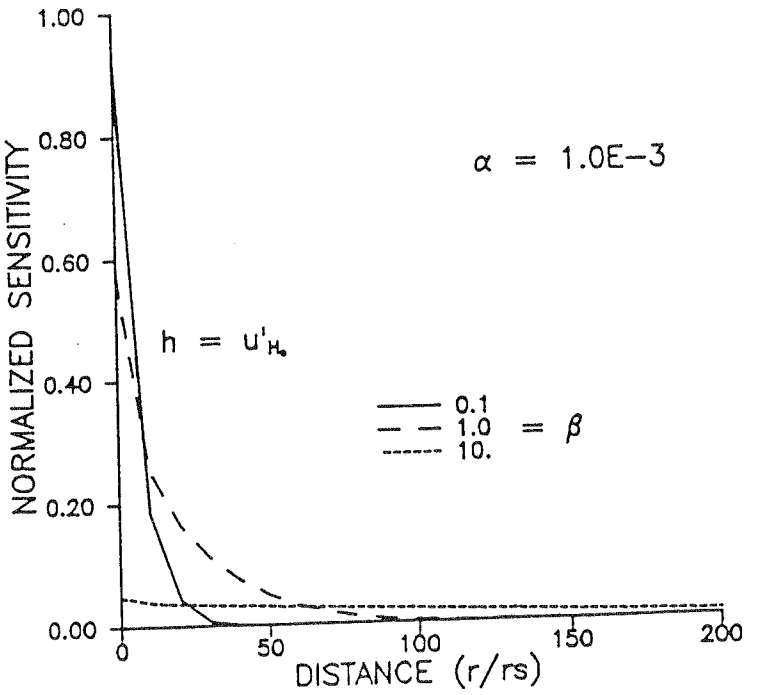

Fig. 2. Variation of u'_{H_0} with distance for various times.

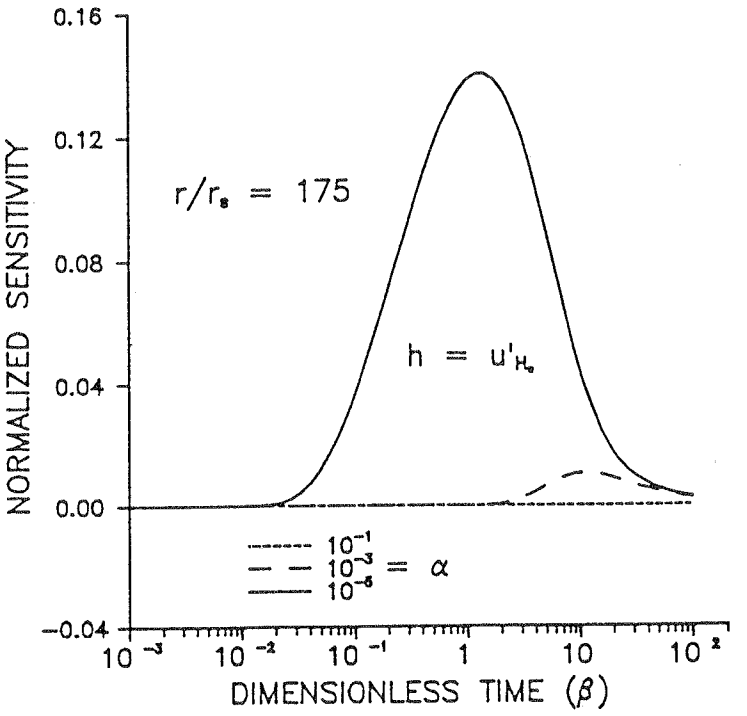

Fig. 3. Variation of u'_{H_0} with time for various α.

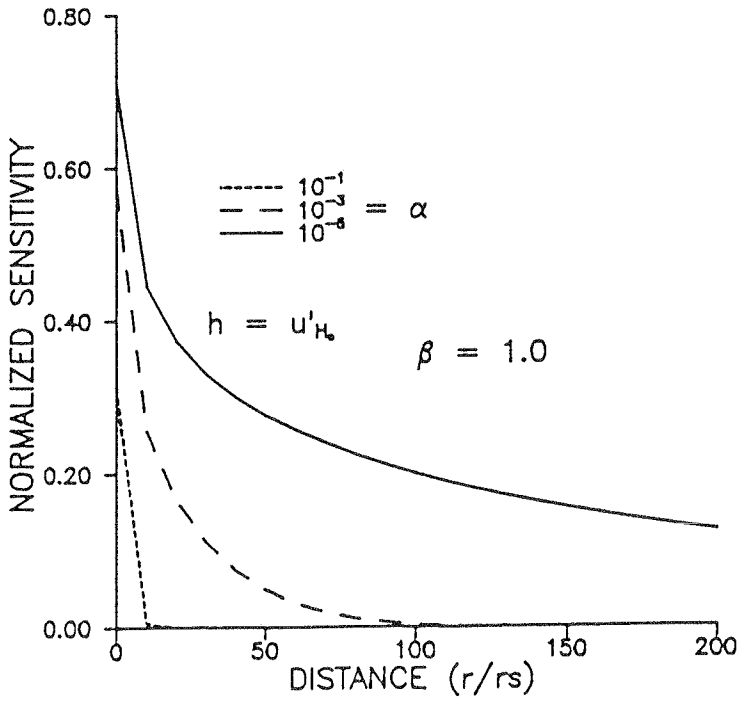

Fig. 4. Variation of u'_{H_0} with distance for various α.

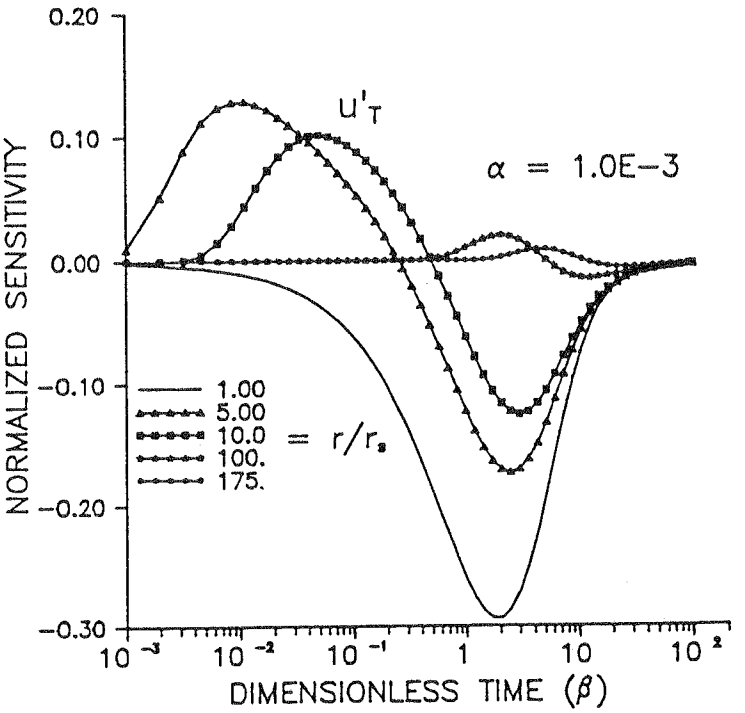

Fig. 5. Variation of u'_T with time for various r/r_s.

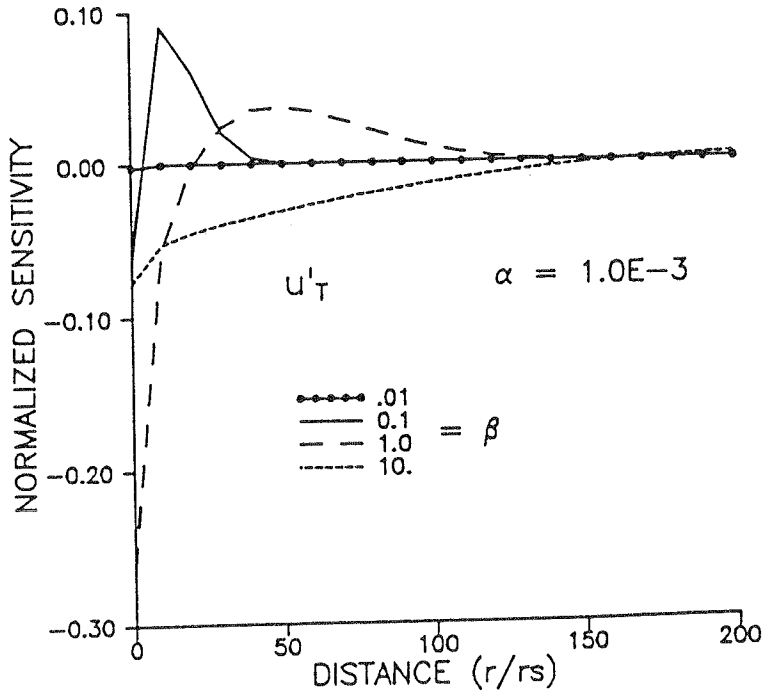

Fig. 6. Variation of u'_T with distance for various times.

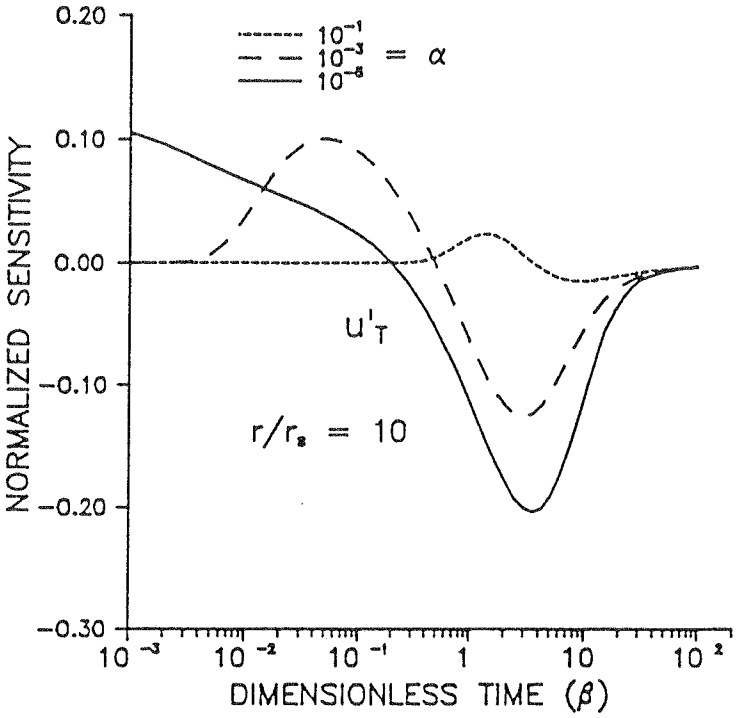

Fig. 7. Variation of u'_T with time for various α.

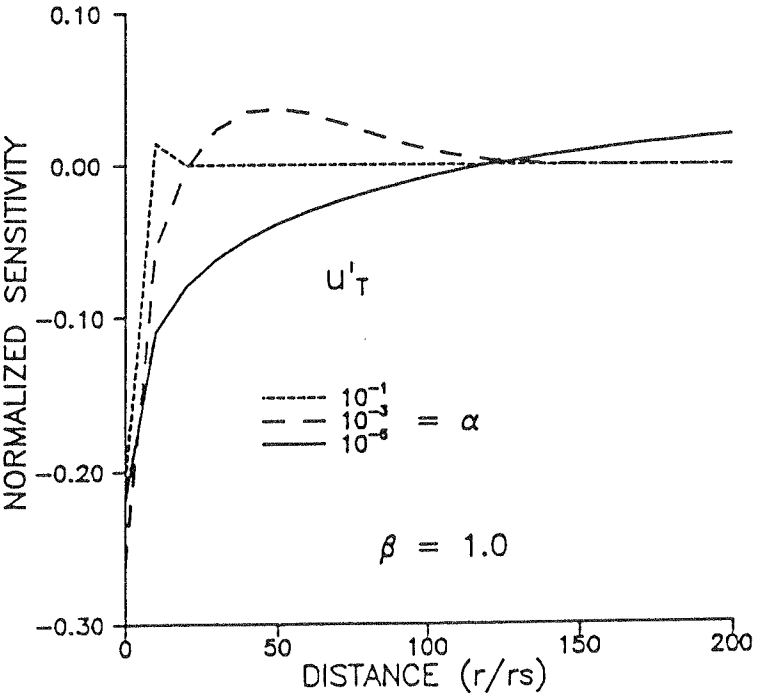

Fig. 8. Variation of u'_T with distance for various α.

5. Sensitivity to transmissivity

Figs. 5–8 illustrate the dependence of the sensitivity to transmissivity (u'_T) on time, distance, and α. As shown on Figs. 5 and 6, the sensitivity to transmissivity has positive and negative lobes in time and space except for $r = r_s$. These figures (5 and 6) indicate that the maximum sensitivity to transmissivity occurs near the slugged well. Somewhat surprising is the fact that for early times the maximum sensitivity to transmissivity is near but not at r_s. A given observation well will be sensitive to the transmissivity over a definite time interval (Fig. 5), with the magnitude of the sensitivity decaying rapidly with increasing r. Figs. 7 and 8 illustrate the dependence of the sensitivity to transmissivity on α. The maximum amplitude of the sensitivity seems to vary inversely with α (Fig. 7), while the amplitude at $r = r_s$ does not seem to have a strong dependence on α (Fig. 8). As noted previously, a small α is required for sensitivities to propagate a considerable distance from the slugged well (Fig. 8).

6. Sensitivity to storage

Figs. 9–12 illustrate the dependence of the sensitivity to storage (u'_S) on α, β, and r. Figs. 9 and 10 indicate that the maximum sensitivity does not occur at $r = r_s$, but rather at a distance which increases with time. Fig. 10 shows that the pulse of sensitivity to storage moves out to larger distances while widening and decaying with increasing time. Fig. 11 shows that, for a chosen r, the maximum amplitude

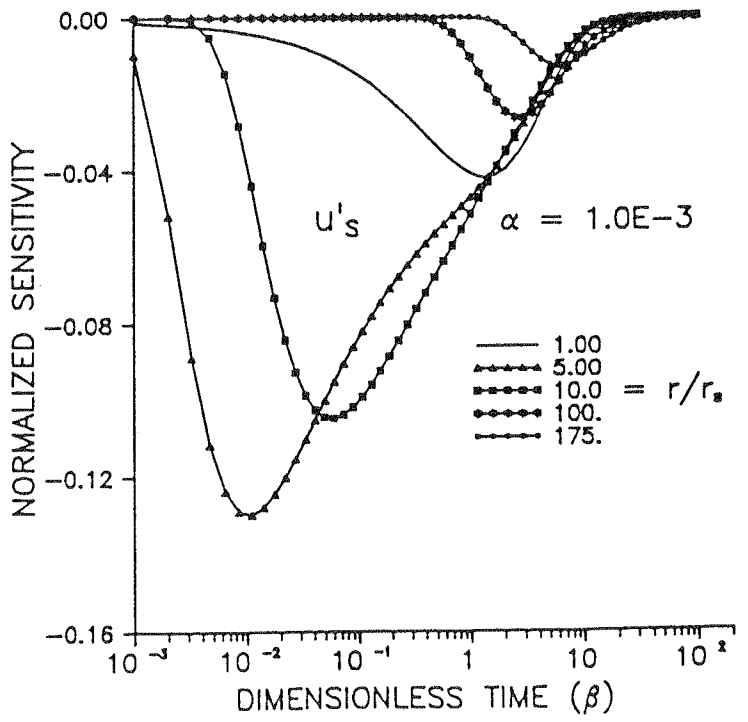

Fig. 9. Variation of u'_S with time for various r/r_s

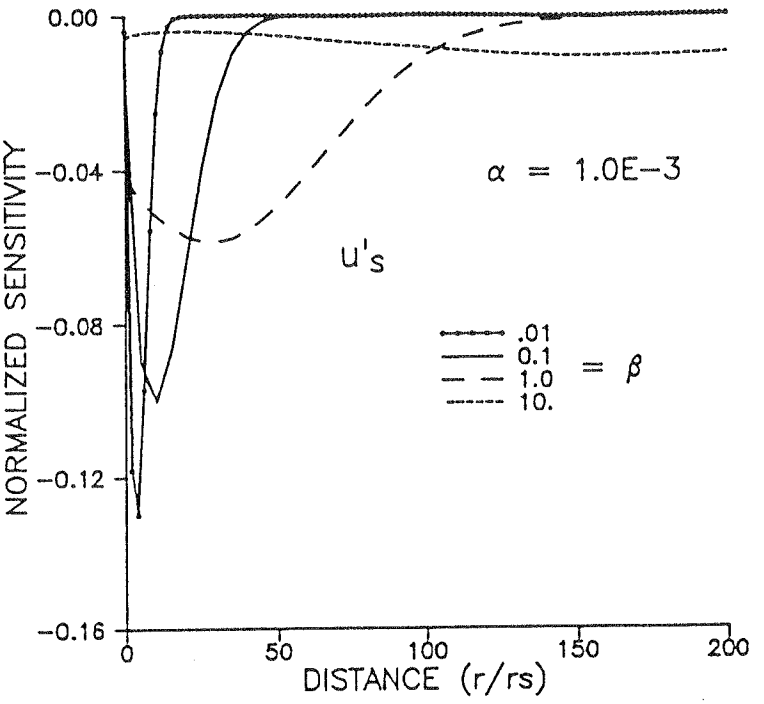

Fig. 10. Variation of u_S' with distance for various times.

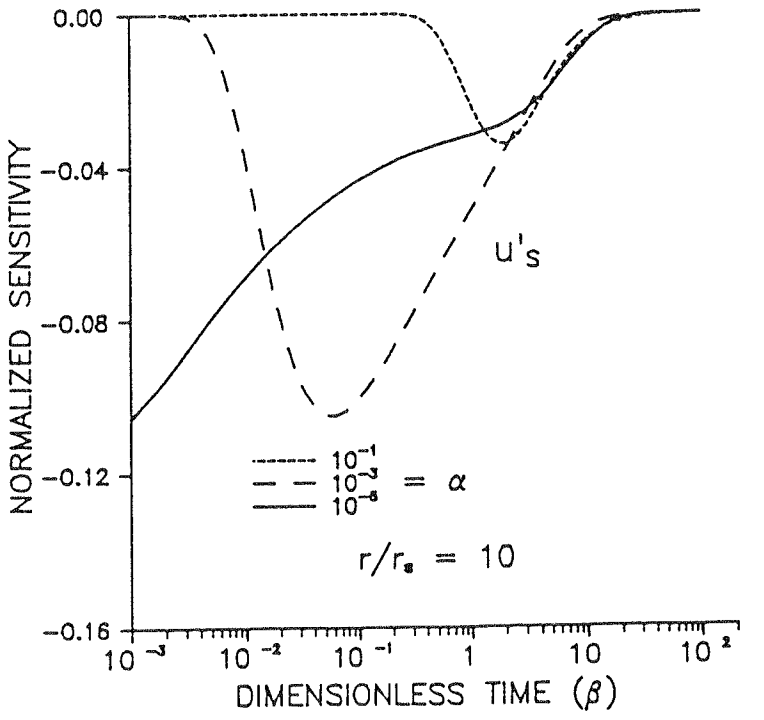

Fig. 11. Variation of u_S' with time for various α.

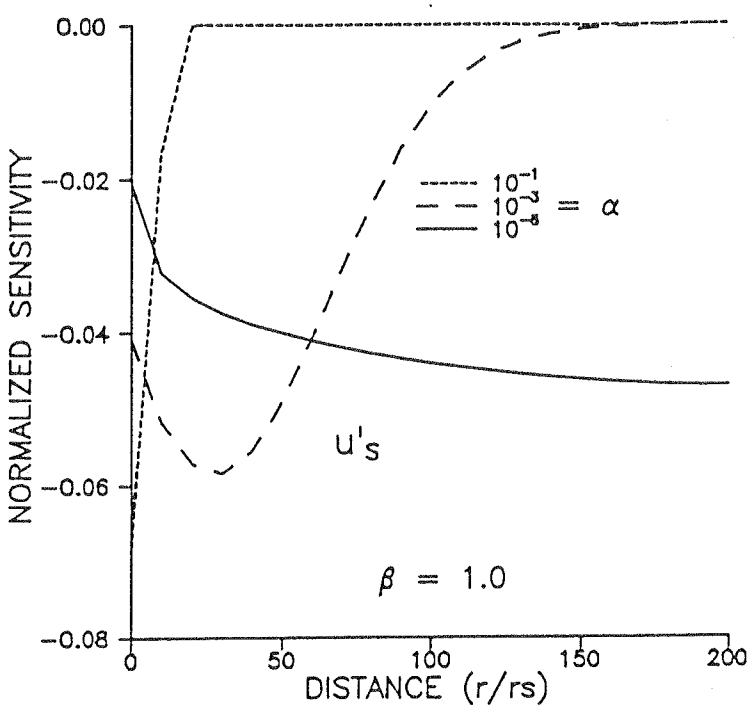

Fig. 12. Variation of u'_S with distance for various α.

of the sensitivity is inversely proportional to α and occurs at earlier times for smaller α's. The dependence on α shown in Fig. 12 reveals that the signal for the sensitivity with respect to storage propagates much farther from the well for smaller values of α.

7. Parameter estimation and error analysis

The first paper of this series (Part 1, McElwee et al., 1995) and other papers (McElwee, 1987; Butler and McElwee, 1990) present a detailed discussion of the relationship of parameter estimation and error analysis to sensitivity coefficients, so that material will only be briefly summarized here. A common method of performing parameter estimation involves minimizing a squared error functional which can be written in terms of sensitivity coefficients (Eq. (14), Part 1). The sensitivity design matrix [A] (Eq. (15), Part 1) arises naturally out of the process of minimizing the error functional. In general, the solution is well behaved if the diagonal elements are large and nearly equal and the off-diagonal elements are small. This will be the case if the sensitivity coefficients are large and do not have similar shapes over the chosen measurement times and locations. One way to measure the similarity of the sensitivity coefficients is to define the sensitivity correlation matrix (Eq. (16), Part 1). The reliability of the parameter estimates can be assessed by looking at the parameter covariance matrix (Eq. (17), Part 1). Usually some simplifying assumptions about the errors in head such as additive, zero mean, uncorrelated and constant variance (Beck and Arnold, 1977) are made. With these assumptions, the estimated standard errors

(ESE) of the parameters and confidence intervals can be related to the square root of the diagonal elements of the parameter covariance matrix (Eq. (18), Part 1). A computer program for automated least squares analysis of well-test data using sensitivity analysis, SUPRPUMP (Bohling and McElwee, 1992), has been used in this work to do the parameter estimation and to compute sensitivity correlations and confidence intervals.

8. Correlation of u'_T and u'_S

Fig. 13 is from our earlier paper (Part 1, McElwee et al., 1995) showing that the shape of the sensitivities with respect to transmissivity and storage at $r = r_s$ are extremely similar except for amplitude. This means that responses in a slugged well are much more sensitive to T than S and that there will be high correlation between these two parameters. Consequently, rarely can one determine both T and S with only data from the slugged well (Part 1, McElwee et al., 1995). On the other hand, Fig. 14 shows the same two sensitivities for an observation well at $r = 10r_s$. The sensitivity coefficient plots have considerably different shapes and nearly the same maximum amplitude. This means that the observation well is much more sensitive to storage than the slugged well and that the correlation between T and S will be dramatically reduced by the use of an observation well. In the next two sections these ideas of using one or more observation well with a slug test are illustrated for some cases of practical interest.

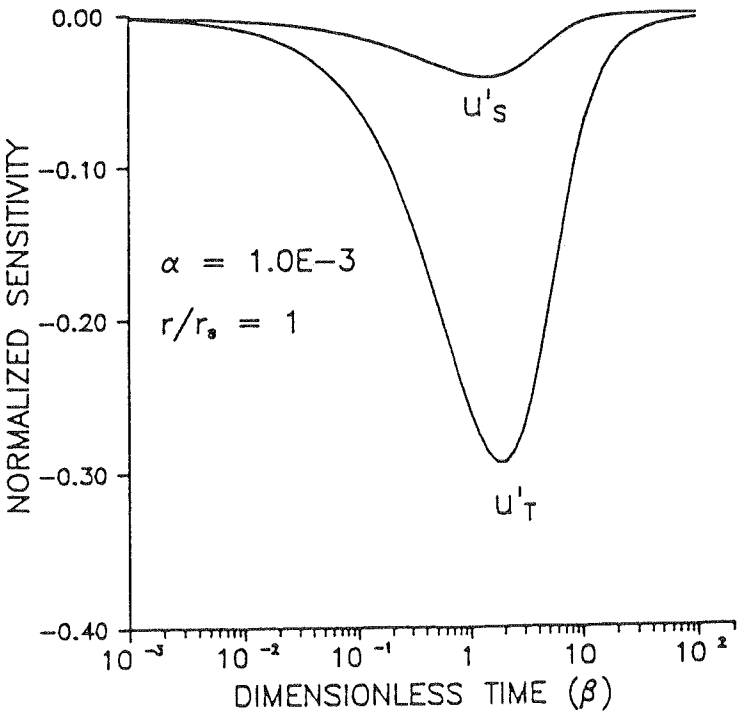

Fig. 13. A comparison of sensitivities (u'_T and u'_S) at the screen radius.

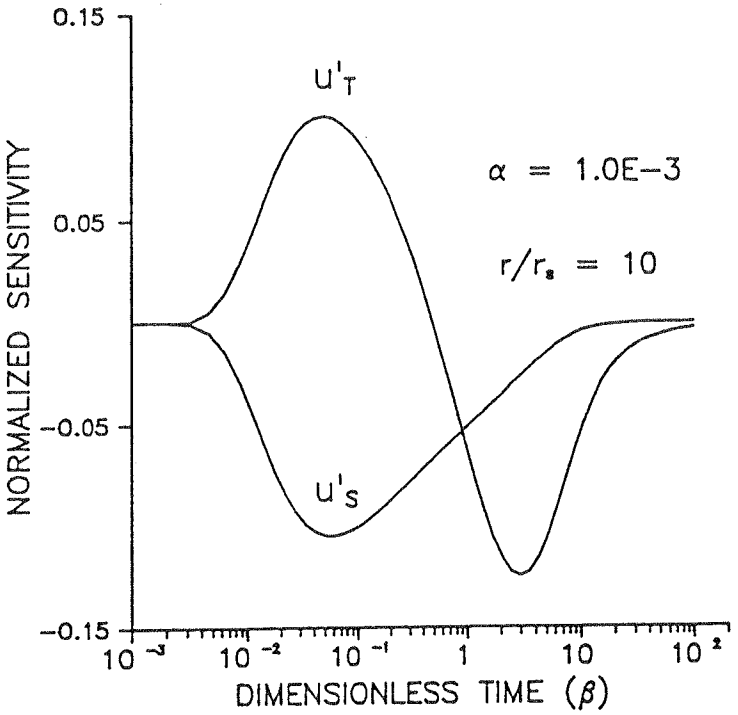

Fig. 14. A comparison of sensitivities (u'_T and u'_S) at a distance of 10 screen radii from the slugged well.

9. Simulation for a field site in an alluvial aquifer

At the KGS, we have developed a field site in the Kansas River alluvium for carrying out research on hydraulic testing. The shallow subsurface at this site consists of about 10.7 m (35 ft) of coarse sand and gravel overlain by about 10.7 m (35 ft) of silt and clay. The following is a simulation of expected results at this site in the very conductive lower sand and gravel zone. From earlier laboratory work and aquifer tests we know some average values for K, T and S. $K \approx 91.3$ m day^{-1} (300 ft day^{-1} or 0.208 ft min^{-1}); $T \approx 91.3$ m day^{-1} × 10.7 m = 974 m^2 day^{-1} (7.28 ft^2 min^{-1}); $S \approx 0.00063$.

We simulate the results for a slugged well and two observation wells at 1.5 m (5 ft) and 3.0 m (10 ft) away, taking data with a high sample rate over a 3 min interval (slug tests have a very short duration in this media). The initial slug height is taken as 3 m (10 ft). It is assumed the slugged well is 0.10 m (4 in) in diameter and all wells are fully screened. The simulated data are rounded to the nearest 0.03 m (0.1 ft) and then analyzed with the SUPRPUMP program (Bohling and McElwee, 1992). The results are shown in Table 1 for three different data sets: (1) data from the slugged well only; (2) data from the slugged well and one observation well; and (3) data from the slugged well and both observation wells.

The ranges of T and S shown in Table 1 are the approximate 95% confidence limits calculated by SUPRPUMP. The correlation between the two parameters (Corr.) is also shown. The root mean squared deviation (rms Dev.) is an indication of the average level of noise present or the degree of lack of fit to the theoretical model.

Table 1
Simulated alluvial results

	Slugged well only	Slugged well + obs. well	Slugged well + 2 obs. wells
Range of T ($m^2\,day^{-1}$)	951–1070	966–986	969–987
Range of S ($\times 10^{-3}$)	0.178–0.722	0.616–0.666	0.609–0.648
Corr.	0.98	0.54	0.44
rms Dev. (m)	0.0079	0.0079	0.0076
Remarks	Trouble converging	Converging rapidly	

The rms deviation of near 0.0076 m (0.025 ft) is consistent with data rounded to the nearest 0.03 m (0.1 ft). Table 1 shows that when only slugged well data are analyzed, the calculated ranges for T and S are relatively broad and there is an extremely high correlation of 0.98 between T and S. As a result, the SUPRPUMP program sometimes has trouble converging to a unique solution, depending on the starting values. Note that although the addition of one or two observation wells does not greatly improve the model fit (rms deviation), the width of the parameter ranges and the magnitude of the correlation are significantly decreased. As a result, the SUPRPUMP program converges rapidly to a unique solution in most cases, being much less sensitive to starting values. The reason for this can be seen by plotting contours of

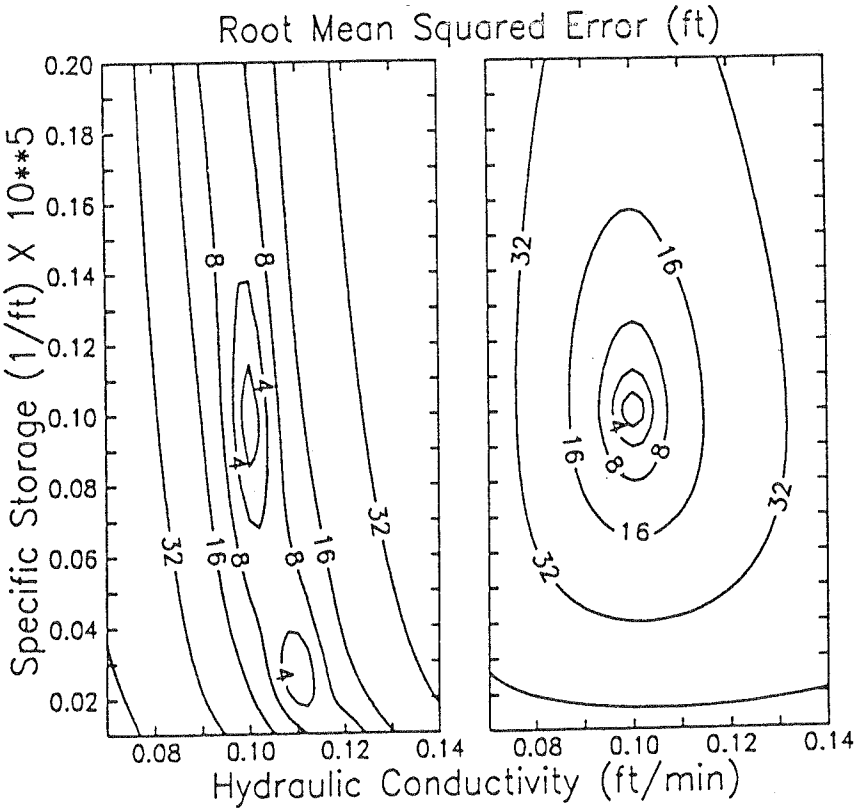

Fig. 15. Error functional contours plotted vs. specific storage and hydraulic conductivity when only the slugged well data are used (left side) and when both slugged well and observation well data are used (right side).

the error functional (Eq. (13), Part 1, McElwee et al., 1995) versus trial parameter values (T and S) for two cases: (1) for slugged well data alone, and (2) for data from both the slugged well and the observation well. Fig. 15 illustrates this point for a slightly different aquifer configuration but similar to that used in this section. In the case of Fig. 15 we are plotting the error functional versus two parameters, specific storage and hydraulic conductivity. The plot on the left in Fig. 15 displays the error functional when only data from the slugged well are used. It is easy to see that the minimum is elongated along the y-axis and that a potential false local minimum exists at smaller values of specific storage. In contrast, the plot on the right in Fig. 15 includes data from the slugged well and an observation well. Including observation well data makes the error functional contours more nearly circular and the minimum much more clearly defined. There is no indication of a possible false local minimum. Therefore, it is easier to arrive at good fitted values with a fitting program.

Actually, we have had trouble observing the expected level of response at the alluvial field site described; a number of things may be contributing to that problem. Until recently only 2 in wells were available for testing; we expect that larger diameter wells will increase the magnitude of the signal at observation wells. Other possible problems include partial penetration in some wells and the effect of leakage by the overlying aquitard. Additional work at this site indicates that partial penetration of some wells may be our main problem in observing the expected level of response. McElwee and Butler (1993) show that partial penetration effects can reduce the expected response from the CBP model by an order of magnitude. However, for a nearly ideal confined system with a fairly small storage coefficient and a long screen, the use of observation wells with slug tests should produce good results as seen in the next section.

10. Results from Dakota aquifer, Lincoln County, Kansas

A program of well testing is being carried out by the KGS as part of a regional study of the Dakota aquifer (a sandstone aquifer of Cretaceous age) in Kansas. At one site in Lincoln County, Kansas, two wells (0.102 m (4 in) and 0.051 m (2 in) in diameter and about 30 m (100 ft) deep), screened over similar intervals (24–30 m (80–100 ft)), are located 6.46 m (21.2 ft) apart. A number of slug tests were carried out at this site and they illustrate some of the concepts discussed in this paper. These tests consisted of introducing a slug at the larger of the two wells and measuring the responses both at the stressed well and at the observation well. Measurements from the observation well were taken using a transducer placed below a packer located just above the top of the screen. The packer enabled effects associated with wellbore storage at the observation well to be kept very small. Three different data sets were used in the analysis of the test responses: (1) data from the stressed well only; (2) data from the observation well only; and (3) data from both the stressed well and the observation well. The results of these three analyses are shown in Table 2.

Fig. 16 shows the field measurements and fitted model results for the analysis using the third data set. The model seems to fit the field data extremely well. Although the

Table 2
Dakota aquifer results

	Slugged well	Obs. well	Slugged well + obs. well
T ($m^2 day^{-1}$)	7.20	8.03	8.26
S ($\times 10^{-4}$)	2.0	0.51	0.52
Corr.	0.99	0.27	0.49
rms Dev (m)	0.0067	0.0084	0.0112

actual parameter values for this site are not known, the results of the sensitivity analysis and the previous theoretical example indicate that the parameters in Table 2 from the second and third data sets are probably more representative of conditions at the site than the parameters from the first data set. Note that the dramatic decrease in correlation is seen when data from an observation well are employed making the [A] matrix (Eq. (15), Part 1) much better conditioned. Additional work on the analysis of this data has shown that it is important to make a critical analysis of the best effective screen radius to use in the definition of α (Eq. 5). This choice will usually lie somewhere between the actual screen radius and the radius of the gravel pack. The choice of best effective screen radius is much more important if only data from the slugged well are used in the analysis. The analysis of observation well data is much less sensitive to effective screen radius. In the case of Table 2, it is possible to make the estimate for S obtained by analyzing only slugged well data agree with the other two analyses by the appropriate choice of effective screen radius. However, if one does not have observation well data, it is not possible to go through this procedure to obtain consistency of all the analyses.

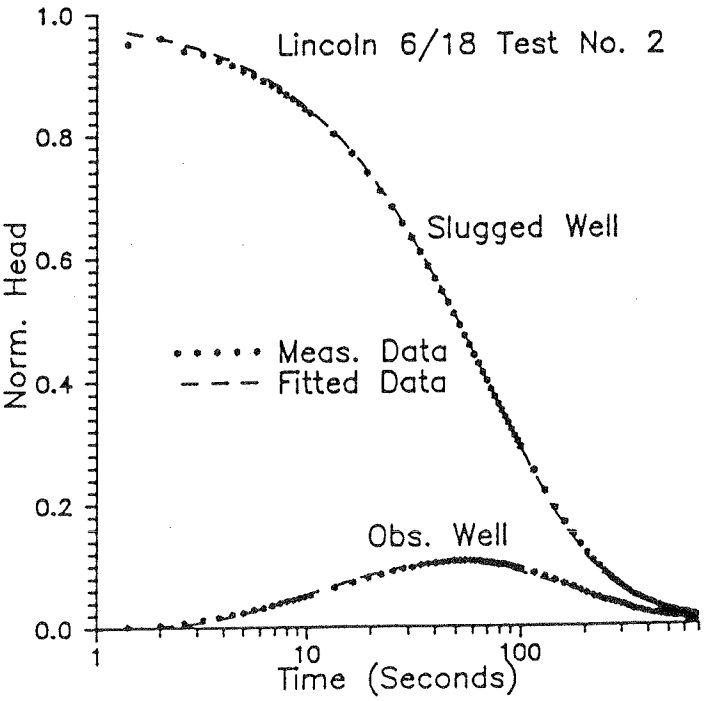

Fig. 16. Experimental and fitted results for the Dakota aquifer test, Lincoln County Kansas.

11. Conclusion

An investigation of the radial dependence of the Cooper et al. (1967) analytical solution for a slug test in a confined aquifer has shown that the use of one or more observation wells can vastly improve fitted parameter estimates, particularly the estimate of the storage parameter. It is usually not practical to install an observation well solely for use in a slug test, however, many times nearby wells are available. Generally, the observation well must be fairly close (about 10 m or less) to the slugged well to be effective. Other mitigating factors such as leakage and partial penetration should be minimal for optimum results. The storage coefficient and the ratio of screen radius to casing radius must be small in order to see the effect of the slug at greater distances from the slugged well. The observation well should be packed off in order to remove or minimize the lagging and damping effect on the signal that occurs due to wellbore storage at the observation well. Since the temporal and spatial dependence of the sensitivities to transmissivity and storage are considerably different, the addition of one or more observation wells will substantially reduce the correlation between these two parameters, which will result in estimates of greater reliability than normally obtained from slug tests.

These ideas have been illustrated using typical data from our research sites. Theoretically, both field examples could benefit from using observation wells with the slug test. However, in practice it has been difficult to see a significant response in observation wells in the leaky alluvial case; several potential problems have been identified. However, observation wells should be most useful in nearly ideal confined systems with a low storage coefficient or α. From a practical standpoint, α can be lowered by about an order of magnitude when using a casing radius a little over three times the screen radius. The other example, from a consolidated sandstone aquifer, bears out this conclusion and shows good agreement with the theory presented here. In this case, the use of an observation well has greatly aided in the determination of the storage coefficient. In conclusion, the use of observation wells with slug tests can significantly improve the reliability of the aquifer parameter estimates where suitable conditions exist.

Acknowledgment

This research was sponsored in part by the Air Force Office of Scientific Research, Air Force Systems Command, USAF, under grant or cooperative agreement number, AFOSR 91-0298. This research was also supported in part by the US Geological Survey (USGS), Department of the Interior, under USGS award number 14-08-0001-G2093. The views and conclusions contained in this document are those of the authors and should not be interpreted as necessarily representing the official policies, either expressed or implied, of the Air Force Office of Scientific Research, of the US Geological Survey, or of the US Government. The US Government is authorized to reproduce and distribute reprints for Governmental purposes notwithstanding any copyright notation thereon.

References

Barker, J.A. and Black, J.H., 1983. Slug tests in fissured aquifers. Water Resour. Res., 19: 1558–1564.

Beck, J.V. and Arnold, K.J., 1977. Parameter Estimation in Engineering and Science. John Wiley, New York.

Black, J.H., 1985. The interpretation of slug tests in fissured rocks. Q. J. Eng. Geol., 18: 161–171.

Bohling, G.C. and McElwee, C.D., 1992. SUPRPUMP: An interactive program for well test analysis and design. Ground Water, 30: 262–268.

Butler, Jr. and McElwee, C.D., 1990. Variable-rate pumping tests for nonuniform aquifers. Water Resour. Res., 26: 291–306.

Chirlin, G.R., 1989. A critique of the Hvorslev method for slug test analysis: The fully penetrating well. Ground Water Mon. Rev., 9: 130–138.

Chirlin, G.R., 1990. The slug test: The first four decades. In: Proc. NWWA 1990 Cluster of Conferences, 20–21 February 1990, Groundwater Management and Wellhead Protection, NWWA. pp. 365–381.

Cooper, H.H., Bredehoeft, J.D. and Papadopulos, I.S., 1967. Response of a finite-diameter well to an instantaneous charge of water. Water Resour. Res., 3: 263–269.

Ferris, J.G. and Knowles, D.B., 1954. The slug test for estimating transmissibility. U.S., Geol. Surv., Ground Water Note 26.

Guyonnet, D., Mishra, S. and McCord, J., 1993. Evaluating the volume of porous medium investigated during slug tests. Ground Water, 31: 627–633.

Hvorslev, M.J., 1951. Time lag and soil permeability in ground-water observations. U.S. Army, Corps Eng., Waterways Exp. Stn, Bull. No. 36.

Karasaki, K., Long, J.C.S. and Witherspoon, P.A., 1988. Analytical models of slug tests. Water Resour. Res., 24: 115–126.

McElwee, C.D., 1987. Sensitivity analysis of ground-water models. In: J. Bear and M. Yavuz Corapcioglu (Editors), Proc. 1985 NATO Advanced Study Institute on Fundamentals of Transport Phenomena in Porous Media. Martinus Nijhoff, Dordrecht, pp. 751–817.

McElwee, C.D. and Butler, Jr., J.J., 1993. Characterization of heterogeneities controlling transport and fate of pollutants in unconsolidated sand and gravel aquifers: Second year report. Open File Rep. 93-21, Kansas Geological Survey.

McElwee, C.D., Bohling, G.C. and Butler, Jr., J.J., 1995. Sensitivity analysis of slug tests. Part 1. The slugged well. J. Hydrol., 164: 53–67.

Novakowski, K.S., 1989. Analysis of pulse inteference tests. Water Resour. Res., 25: 2377–2387.

Ramey, Jr., H.J., Agarwal, R.G. and Martin, I., 1975. Analysis of 'slug test' or DST flow period data. J. Can. Pet. Technol., 14: 37–47.

Sageev, A., 1986. Slug test analysis. Water Resour. Res., 22: 1323–1333.

Walter, G.R. and Thompson, G.M., 1982. A repeated pulse technique for determining the hydraulic properties of tight formations. Ground Water, 20: 186–193.

D. SLUG TESTS IN THE PRESENCE OF A WELL SKIN

Introduction

Conventional methods for the analysis of slug-test data are based on a series of assumptions about the formation being tested. One of the more important of these assumptions is that the formation is homogeneous in the vicinity of the stressed well. In natural systems, however, there is often a near-well zone of disturbance (well skin), created during well drilling or development activities, which has flow properties that may differ from those of the formation as a whole. The issue of how to analyze slug-test data from a well with a skin is one of considerable importance. In this section, an initial investigation of various approaches for analyzing data from a slug test in a well with a skin is described. The results of this investigation show that it may be very difficult to accurately estimate formation properties from a slug test performed at a well with a low-permeability skin. This situation is especially worrisome when the existence of a low-permeability skin is not recognized and skin-influenced estimates from a slug test are inadvertently assigned to the formation. In Sections III.E and III.F, approaches for the identification of a low-permeability well skin through repeat slug tests are described.

Model for Slug Tests in the Presence of a Well Skin

Figure II.D.1 depicts the configuration of interest here. A slug test is being performed in a well that is screened over the full thickness (b) of a perfectly confined aquifer. In the immediate vicinity of the well, there is a well skin of radius R_S. The well skin extends through the full thickness of the aquifer and has transmissive (T_1) and storage (S_1) properties that may be different from those of the aquifer (T_2 and S_2). The well has a screen of radius r_w that may be different from the radius of the casing (r_c). The initial change in water level due to the introduction of the slug is denoted by H_0.

Moench and Hsieh (1985) have proposed a mathematical model to describe head responses to a slug test in this configuration. The mathematical model is defined by the following partial differential equations and auxiliary conditions:

Governing equations:

$$\frac{\partial^2 H_1}{\partial r^2} + \frac{1}{r}\frac{\partial H_1}{\partial r} = \frac{S_1}{T_1}\frac{\partial H_1}{\partial t}, \quad r \le R_s \qquad \textbf{(II.D.1)}$$

$$\frac{\partial^2 H_2}{\partial r^2} + \frac{1}{r}\frac{\partial H_2}{\partial r} = \frac{S_2}{T_2}\frac{\partial H_2}{\partial t}, \quad r \ge R_s \qquad \textbf{(II.D.2)}$$

Initial conditions:

$$H_1(r,0) = H_2(r,0) = 0, \quad r > r_w \qquad \textbf{(II.D.3)}$$

$$H_1(r_w,0) = H_0 \qquad \textbf{(II.D.4)}$$

Boundary conditions:

$$\pi r_c^2 \left(\frac{\partial H_1}{\partial t}\right)_{r_w} = \left(2\pi T_1 r \frac{\partial H_1}{\partial r}\right)_{r_w} \qquad \textbf{(II.D.5)}$$

$$H_1(R_s,t) = H_2(R_s,t) \qquad \textbf{(II.D.6)}$$

$$T_1\left(\frac{\partial H_1}{\partial r}\right)_{R_s} = T_2\left(\frac{\partial H_2}{\partial r}\right)_{R_s} \qquad \textbf{(II.D.7)}$$

$$H_2(\infty,t) = 0 \qquad \textbf{(II.D.8)}$$

Note that two conditions (equations (II.D.6) and (II.D.7)) are required in order to

ensure continuity across the boundary between the well skin and the aquifer.

Equations (II.D.1)-(II.D.8) describe the flow conditions of interest here. Moench and Hsieh (1985) present a semianalytical solution for the functions H_1 and H_2 that satisfy these conditions. Their solution is used here to assess the sensitivity of head responses to various model parameters.

Sensitivity to T_1 and T_2

Figures II.D.2 and II.D.3 depict the sensitivity of head at the stressed well to the transmissivity of the skin and the aquifer (R_s equals $10r_w$ for both figures). Figure II.D.2 shows the sensitivity coefficients (see Appendix B for further discussion of sensitivity coefficients) for the case when the transmissivities of the skin and aquifer are equal, while Figure II.D.3 illustrates conditions when the skin transmissivity is an order of magnitude smaller than that of the aquifer. In both cases, the plots of the sensitivity coefficients for T_1 and T_2 are very similar in shape, although the plot for T_2 is slightly shifted towards larger times. Note that the maximum amplitude of the sensitivity plots is inversely proportional to the transmissivity. The lower sensitivity for T_2 displayed in Figure II.D.3, coupled with the similarity in the shape of the two sensitivity plots (correlation between the two sensitivity coefficients is large), indicates that it will be very difficult to accurately estimate T_2 using measurements from the stressed well. The small sensitivity to T_2 and the large correlation with T_1 will result in the sensitivity summation matrix being poorly conditioned and, consequently, an unreliable T_2 estimate (see Appendix B). Note that at observation points other than the stressed well there is some difference in shape between plots of the sensitivity coefficients for T_1 and T_2. The amplitude of the sensitivities, however, decays rapidly with distance from the stressed well, making it difficult to utilize these differences. Although not shown here, the head response at the test well is rather insensitive to the storage properties of both the skin and the aquifer. Section II.C of this report discusses the sensitivity of slug-test responses to the storage coefficient in more detail. As discussed in that section, it is very difficult to obtain a reliable estimate of the storage properties of the formation using only measurements from the stressed well.

Effect of Varying the Skin Radius

Figures II.D.4 and II.D.5 show how slug-test responses change with variations in the skin radius. Regardless of the location of the observation point, increasing the skin radius shifts head responses to larger dimensionless times when $T_1 < T_2$. Figure

II.D.4 shows the normalized head in the test well for various skin radii, while Figure II.D.5 is a similar plot for an observation well located at a distance of 100 r_w from the test well. Note that, as expected, the response in the observation well declines with increasing skin radius for $T_1 < T_2$.

Correlation Between T_1 and R_s

Figure II.D.6 depicts sensitivity of head at the stressed well to the transmissivity of the skin and to the skin radius. Note that the sensitivity to the skin radius is smaller than that to the skin transmissivity and of an opposite sign. The shape of the two sensitivity plots is very similar, however, so the absolute magnitude of the correlation between the two sensitivity coefficients is very large. As discussed in Appendix B, a large correlation between two sensitivity coefficients can make it very difficult to reliably estimate one or both of the two parameters, as there may be many pairs of parameter values (in this case, T_1 and R_s) that give equally good results. In some instances, the approximate value of the skin radius may be known based on the diameter of the hole created by the drilling equipment, etc. In such cases, the skin radius can be assumed known for the parameter-estimation process.

Analyzing a Slug Test at a Well With a Skin Using a Uniform-Aquifer Model

Since one may not know whether the well being tested has a skin, slug-test data are normally initially analyzed using a uniform-aquifer model. A commonly used uniform-aquifer model for slug tests is that of Cooper et al. (1967) (henceforth designated the C-B-P model). An important issue to consider is the nature of the effective transmissivity estimated using this model when a well skin is present. Figure II.D.7 displays a plot of simulated data computed using the Moench and Hsieh (1985) model and the best-fit curve to the data obtained with the C-B-P model, assuming that the storage coefficient is known. Note that the fitting was performed using SUPRPUMP, a well-test analysis package developed at the Kansas Geological Survey (Bohling and McElwee, 1992). This figure shows a systematic deviation between the simulated data and the model fit for the case of $T_1 < T_2$. This deviation consists of the simulated data lying above the C-B-P model curve at early times and below the C-B-P model curve at late times.

The effective transmissivity calculated from the C-B-P model must be some sort of average of the skin and aquifer transmissivities. As shown in the next subsection, we have developed the following equation for effective transmissivity based on a quasi-steady-state analysis:

$$\frac{1}{T_{eff}} = \left[\frac{\ln\left(\frac{R_s}{r_w}\right)}{T_1} + \frac{\ln\left(\frac{r_{eff}}{r_w}\right) - \ln\left(\frac{R_s}{r_w}\right)}{T_2}\right]\left[\ln\left(\frac{r_{eff}}{r_w}\right)\right]^{-1} \qquad \text{(II.D.9)}$$

where

$r_{eff}/r_w = [C/S]^{.5}$, $1 \le C \le 2$;

r_{eff} = effective radius of influence of the slug test;

C = empirical coefficient;

S = storage coefficient.

Although the effective parameter obtained from this equation is biased somewhat towards T_1, the lowest value of transmissivity (whether it is in the aquifer or the skin) will be the dominant factor in determining T_{eff} in equation (II.D.9). Note that, as expected, the effective transmissivity is independent of the height of the initial slug.

We have found that equation (II.D.9) can provide reasonable estimates of the effective transmissivity obtained from a C-B-P analysis. In order to demonstrate this, a series of slug-test simulations were run using the model of Moench and Hsieh (1985) and the simulated data were analyzed using the C-B-P model. The effective transmissivities estimated from the C-B-P model were then compared to the effective transmissivities calculated using equation (II.D.9). Table II.D.1 lists the results of this exercise, which demonstrate the viability of equation (II.D.9). Note that a constant storage coefficient of 0.001 was used in all of the simulations and the head data were assumed to come from an observation well at a distance of 100 r_w from the stressed well.

Derivation of Equation (II.D.9)

Consider steady-state flow in the aquifer of Figure II.D.1. It can be readily shown that the steady-state solution for heads in this system is of the following form:

$$H_2 = -\frac{Q}{2\pi T_2}\ln\left(\frac{r}{R_s}\right) + H_2(R_s), \quad R_s \le r \le r_{eff} \qquad \textbf{(II.D.10b)}$$

where

Q = rate of flow into/out of the test well.

If we apply the conditions that H_2 is zero at the effective radius (r_{eff}) and that H_1 and H_2 are equal at R_s, then the above two equations can be rewritten as:

$$H_1 = -\frac{Q}{2\pi T_1}\ln\left(\frac{r}{r_w}\right) - \frac{Q}{2\pi}\left[\frac{\ln\left(\frac{R_s}{r_{eff}}\right)}{T_2} + \frac{\ln\left(\frac{r_w}{R_s}\right)}{T_1}\right], \quad r_w \le r \le R_s \qquad \textbf{(II.D.11a)}$$

$$H_2 = -\frac{Q}{2\pi T_2}\ln\left(\frac{r}{r_{eff}}\right), \quad R_s \le r \le r_{eff} \qquad \textbf{(II.D.11b)}$$

The underlying assumption of the concept of effective parameters is that the actual heterogeneous system can be replaced by a hypothetical homogeneous system characterized by a set of effective parameters. This hypothetical system must honor the boundary conditions of the actual system and reproduce the expected "average" behavior of that system. An equation employing an effective transmissivity can be written for the system described by equations (II.D.11):

$$H_{eff} = -\frac{Q}{2\pi T_{eff}}\ln\left(\frac{r}{r_w}\right) + H_1(r_w), \quad r_w \le r \le r_{eff} \qquad \textbf{(II.D.12)}$$

Since the head must be zero at r_{eff}, equation (II.D.12) can be solved for the effective transmissivity:

$$\frac{1}{T_{eff}} = \frac{2\pi}{Q}\left[\ln\left(\frac{r_{eff}}{r_w}\right)\right]^{-1} H_1(r_w)$$

$$\frac{1}{T_{eff}} = \left[\frac{\ln\left(\frac{R_s}{r_w}\right)}{T_1} + \frac{\ln\left(\frac{r_{eff}}{R_s}\right)}{T_2}\right]\left[\ln\left(\frac{r_{eff}}{r_w}\right)\right]^{-1} \qquad \textbf{(II.D.13)}$$

The final form of this equation was obtained by substituting for $H_1(r_w)$ using equations (II.D.10a) and (II.D.11a). Note that after some minor algebraic manipulations, equation (II.D.13) will be identical to equation (II.D.9).

The above derivation assumes that steady-state hydraulic conditions will exist during a slug test. Obviously, this is not correct. However, a considerable amount of work (e.g., Chirlin, 1989; Hyder and Butler, 1995) has shown that a quasi-steady-state assumption (e.g., Hvorslev, 1951; Bouwer and Rice, 1976) is reasonable for most slug tests. Therefore, the above derivation needs to be extended to quasi-steady-state conditions. This extension is done here using the notation of Hvorslev (1951).

The Hvorslev model for slug tests assumes that equations (II.D.10) and (II.D.11) hold at any instant in time, but that Q varies with time. The Q term for a slug test can be written as

$$Q = -\frac{dH_1(r_w,t)}{dt}\pi r_w^2 \qquad \textbf{(II.D.14)}$$

Substituting this expression for Q into equation (II.D.11a) and evaluating at $r=r_w$ yields the following:

$$H_1(r_w,t) = \frac{dH_1(r_w,t)}{dt} r_w^2 \frac{A}{2} \qquad \textbf{(II.D.15)}$$

where

$$A = \left[\frac{\ln\left(\frac{r_w}{R_s}\right)}{T_1} + \frac{\ln\left(\frac{R_s}{r_{eff}}\right)}{T_2}\right]$$

Integrating this equation gives a quasi-steady-state expression similar to that

employed by Hvorslev:

$$\ln(H_1(r_w,t)) = \frac{2t}{Ar_w^2} + B \qquad \text{(II.D.16)}$$

where

B = integration constant.

Using the expression for Q given in equation (II.D.14), equation (II.D.12) can be evaluated at r_{eff} and solved for head at the test well to yield

$$H_1(r_w,t) = \frac{dH_1(r_w,t)}{dt} r_w^2 \frac{\ln(\frac{r_w}{r_{eff}})}{2T_{eff}} \qquad \text{(II.D.17)}$$

This expression can also be integrated to give an equation that is analogous to (II.D.16):

$$\ln(H_1(r_w,t)) = \frac{2T_{eff}t}{r_w^2 \ln(\frac{r_w}{r_{eff}})} + B \qquad \text{(II.D.18)}$$

Setting equations (II.D.16) and (II.D.18) equal to one another will yield an expression for T_{eff} that is identical to equation (II.D.9).

Equation (II.D.9) appears to be a quite general expression for the effective transmissivity estimated from a slug test in the presence of a well skin. The expression can be theoretically derived for the quasi-steady-state model of Hvorslev and others, which has been shown to be reasonable for many slug tests. In addition, simulation experiments have shown that the expression is quite reasonable for the fully transient case represented by the C-B-P model. Although a viable expression for the effective transmissivity has apparently been obtained, a uniform-aquifer model may still be of limited use for estimation of the transmissive properties of the aquifer. An alternative approach would be to recognize the existence of a skin and analyze the response data using a model that explicitly incorporates a well skin. The earlier-

described model of Moench and Hsieh is an example of such a model.

Analyzing a Slug Test at a Well With a Skin Using the Moench and Hsieh Model

If there is a systematic deviation between the measured data from a slug test and the best-fit C-B-P curve such as shown in Figure II.D.7, one possible explanation would be the existence of a low-permeability well skin (see Section III.E for discussion of another possible explanation). The Moench and Hsieh (1985) model could be employed to analyze the test data in this situation. However, the results of the previously discussed sensitivity analysis indicate that there is considerable correlation between several of the parameters of this model. Thus, it is unclear how effective the model will be in estimating formation parameters.

A theoretical investigation of the viability of the Moench and Hsieh model for the analysis of slug-test data was undertaken as part of this work. A slug test in a well with a low-permeability skin was simulated with the Moench and Hsieh model assuming four observation wells at varying distances from the stressed well (r/r_w = 1, 25, 50, 100). Fifty-six measurements between .01 and 1000. units of dimensionless time ($\beta = T_2 t / r_w^2$) were simulated. The data from all four wells were analyzed simultaneously with the Moench and Hsieh model assuming three unknowns (the skin and aquifer transmissivities, and the skin radius). The analysis was performed using the SUPRPUMP well-test analysis package (Bohling and McElwee, 1992). Table II.D.2 displays the result of the analysis and additional diagnostic output from SUPRPUMP. Note that the approximate 95% confidence intervals indicate that T_1 and T_2 can be determined to within 40%, while the skin radius estimate is very unreliable (a physically unrealistic negative skin radius arises from the use of approximate confidence intervals). The underlying reasons for these results are revealed by looking at the diagnostic output from SUPRPUMP displayed in Table II.D.2. The sensitivity summation matrix (designated as the crossproducts matrix in Table II.D.2) indicates that the simulated data are much more sensitive to T_1 than the other parameters. Note the large correlation between T_1 and R_s shown by the sensitivity correlation matrix. The high degree of correlation between these two parameters and the large difference in the sensitivity of the simulated data to the model parameters results in very broad confidence intervals for the skin radius and a very large parameter correlation between the skin transmissivity and the skin radius. Note that the correlation between the two transmissivities is smaller than might have been expected from Figures II.D.2 and II.D.3 because of the use of data from observation points other than at the stressed well. Also note that these results

are based on simulated data that have been truncated to the nearest 0.025 H_0. One would expect considerably worse results when the noise characteristic of actual applications is added to the truncated measurements employed here.

Summary

The analyses of this section indicate that it can be very difficult to estimate aquifer parameters using data from a slug test performed at a well with a low-permeability skin. Although the form of the effective transmissivity obtained with a uniform-aquifer model has been clarified, it still may be quite difficult to translate the effective parameter estimate into components characterizing skin and aquifer properties, respectively. An important related issue is how to recognize the existence of a low-permeability skin, so that the skin-biased effective transmissivity from a uniform-aquifer model is not mistakenly applied to the formation as a whole. Sections III.E and III.F discuss field approaches that should enable low-permeability well skins to be recognized from the results of a series of repeat slug tests performed at a single well.

Table II.D.1

Effective Transmissivities in the Presence of a Skin

T_1	T_2	R_s/r_w	T_{CBP}	C (emp.)	T_{eff}
0.1	1.0	5	.205	2	.208
0.1	1.0	10	.155	2	.155
0.1	1.0	20	.126	2	.124
1.0	0.1	5	.175	1	.172
1.0	0.1	10	.260	1	.250
1.0	0.1	20	.456	1	.456

TABLE II.D.2
SUPRPUMP OUTPUT
THREE PARAMETER FIT

The estimated root-mean-squared residual is .2500E-01

The parameter values with approximate 95% confidence intervals are:

Parameter	Value	Lower Bound	Upper Bound
TRANSMISS. OF AQUIFER	1.000	.6227	1.377
TRANSMISS. OF SKIN	.1000	.5668E-01	.1433
SKIN RADIUS	10.00	-1.459	21.46

For the following arrays:
Col-Row 1 represents TRANSMISSIVITY OF AQUIFER (T2)
Col-Row 2 represents TRANSMISSIVITY OF SKIN (T1)
Col-Row 3 represents SKIN RADIUS (Rs)

Raw crossproducts matrix of normalized sensitivities:

	1	2	3	
1	.2357E-01	.8306E-01	-.3155E-01	This matrix shows that
2	.8306E-01	1.093	-.4113	T1 has the highest
3	-.3155E-01	-.4113	.1566	sensitivity by far.

The reciprocal condition number of the
sensitivity crossproducts matrix is .1079E-02

Sensitivity correlation matrix:

	1	2	3	
1	1.000	.5174	-.5192	
2	.5174	1.000	-.9940	-------Very high correlation
3	-.5192	-.9940	1.000	between T1 and Rs.

Covariance matrix of normalized parameter variations:

	1	2	3
1	.3630E-01	-.6035E-03	.5727E-02
2	-.6035E-03	.4787E-01	.1256
3	.5727E-02	.1256	.3349

Parameter correlation matrix:

	1	2	3	
1	1.000	-.1448E-01	.5194E-01	
2	-.1448E-01	1.000	.9918	--------Very high correlation
3	.5194E-01	.9918	1.000	between T1 and Rs.

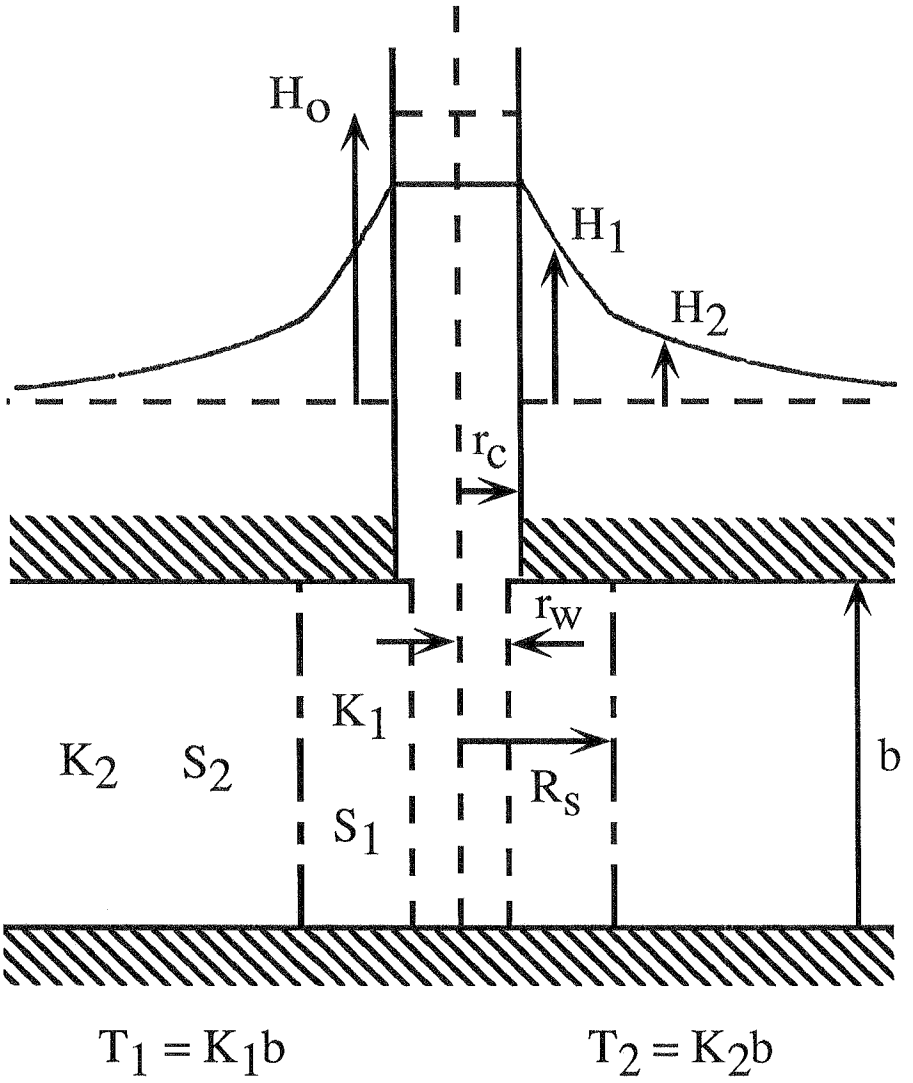

Figure II.D.1 Schematic of a slug test in a well with a skin.

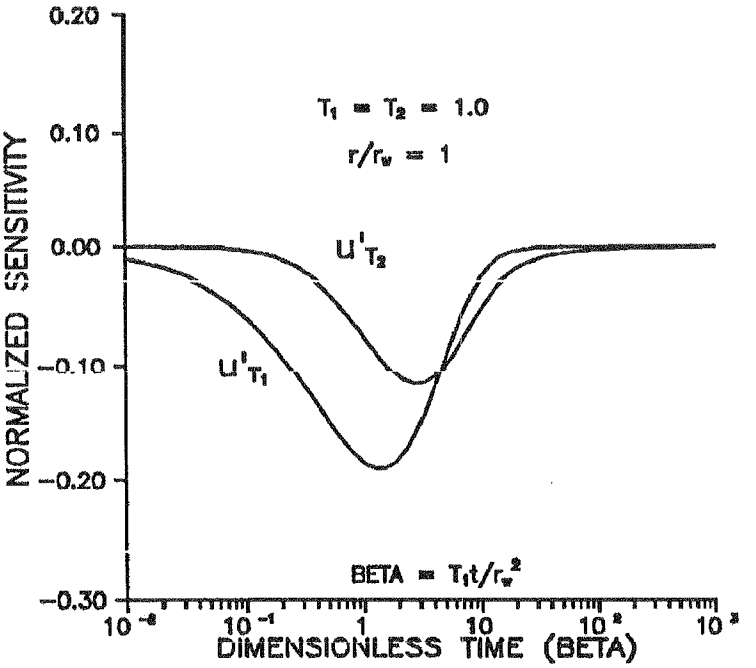

Figure II.D.2 Variation of u'_T with time at the slugged well.

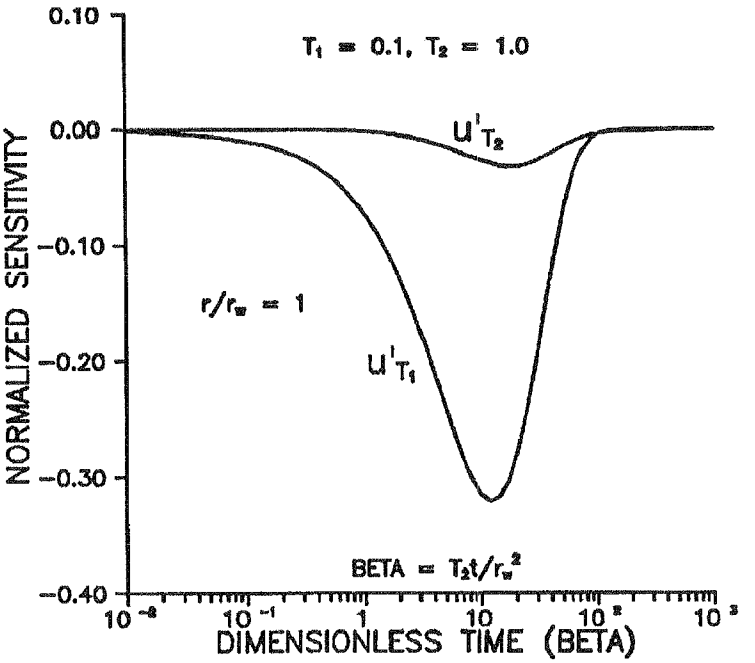

Figure II.D.3 Variation of u'_T with time at the slugged well.

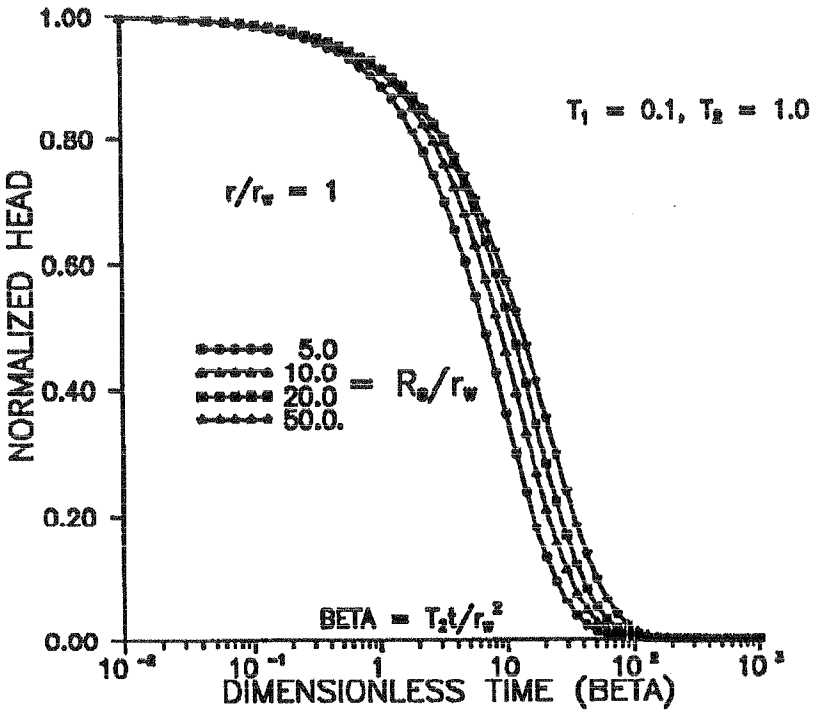

Figure II.D.4 Variation of head in slugged well with skin radius.

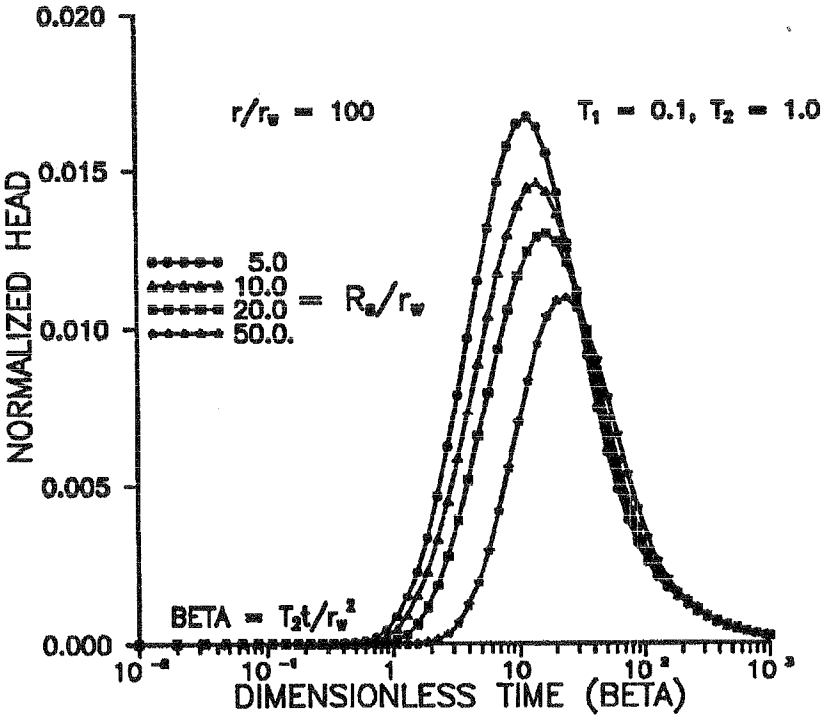

Figure II.D.5 Variation of head in observation well with skin radius.

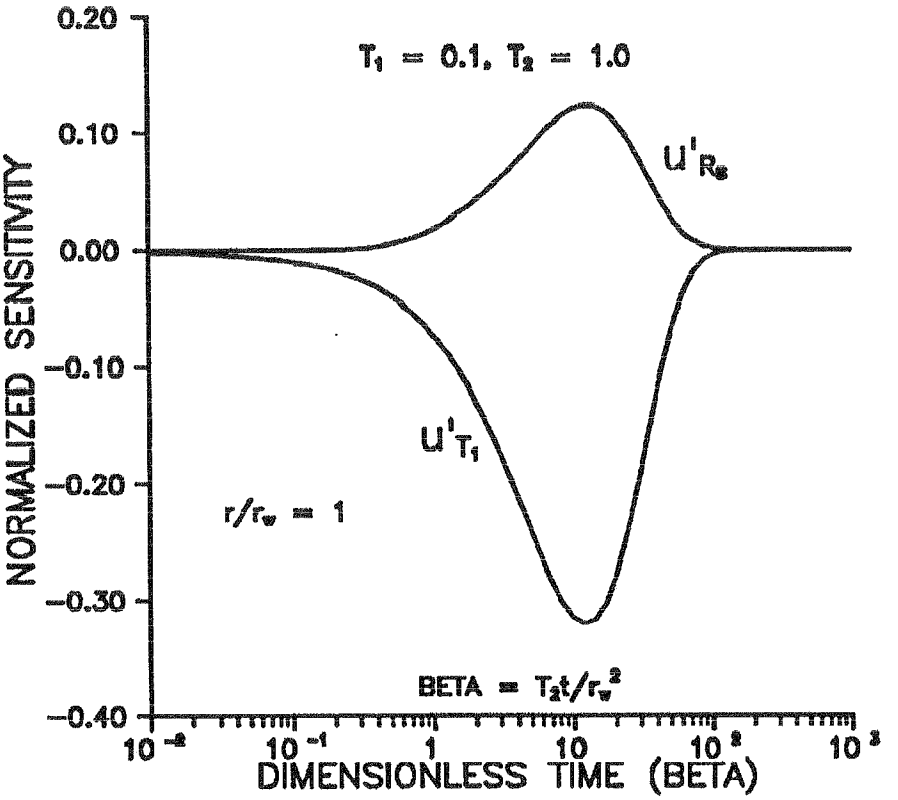

Figure II.D.6 Comparison of $u_{T_1}^{'}$ and $u_{R_s}^{'}$ at the slugged well.

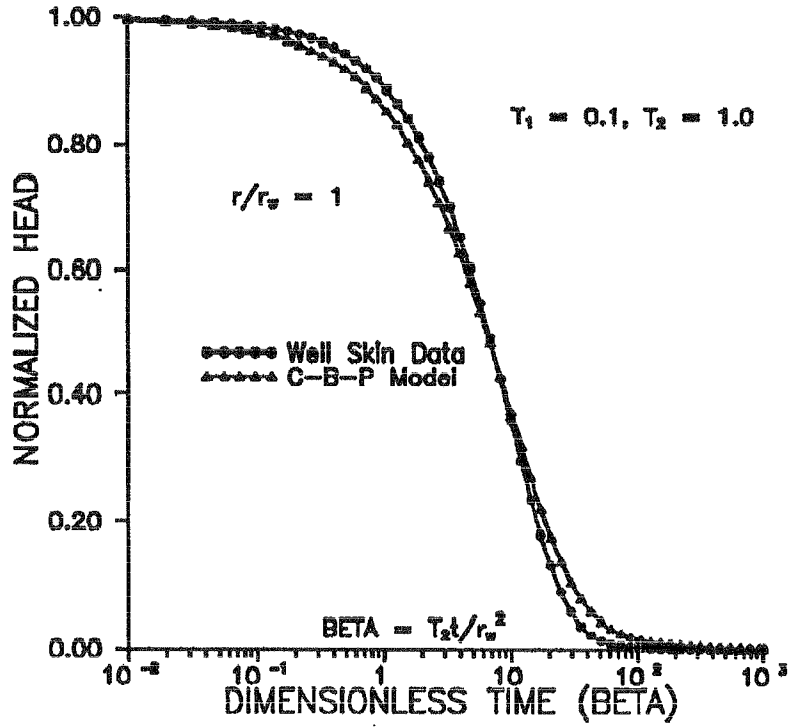

Figure II.D.7 Fit of well skin data to the C-B-P model.

D. AN ASSESSMENT OF THE NGUYEN AND PINDER METHOD FOR SLUG TEST ANALYSIS

A manuscript describing the work of this section was submitted to the journal Ground Water Monitoring and Remediation in January of 1994. A revised version of the manuscript was accepted in July of 1994, and the article was published in volume 14, number 4 of Ground Water Monitoring and Remediation in October of 1994. The remainder of this section consists of a reprint of that article.

An Assessment of the Nguyen and Pinder Method for Slug Test Analysis

by James J. Butler Jr. and Zafar Hyder

Abstract

The Nguyen and Pinder method is one of four techniques commonly used for analysis of response data from slug tests. Limited field research has raised questions about the reliability of the parameter estimates obtained with this method. A theoretical evaluation of this technique reveals that errors were made in the derivation of the analytical solution upon which the technique is based. Simulation and field examples show that the errors result in parameter estimates that can differ from actual values by orders of magnitude. These findings indicate that the Nguyen and Pinder method should no longer be a tool in the repertoire of the field hydrogeologist. If data from a slug test performed in a partially penetrating well in a confined aquifer need to be analyzed, recent work has shown that the Hvorslev method is the best alternative among the commonly used techniques.

Introduction

At sites of suspected ground water contamination, a slug test is often the preferred method for obtaining in situ estimates of hydraulic conductivity. In addition to its clear logistical and economic advantages over alternative approaches such as pumping tests, the slug test can provide useful information about spatial variations in flow properties. Such information about the degree of heterogeneity that exists at a site, which is difficult to obtain from conventional constant-rate pumping tests (Butler and Liu 1993), can be valuable for the prediction of contaminant movement and the design of remediation schemes.

Currently, most analyses of response data from slug tests are performed using one of four techniques. These techniques are (1) the Hvorslev (1951) method for slug tests in fully and partially penetrating wells in confined aquifers; (2) the Bouwer and Rice (1976; Bouwer 1989) method for slug tests in wells in unconfined aquifers screened below the water table; (3) the Cooper et al. (1967) method for slug tests in fully penetrating wells in confined aquifers; and (4) the Nguyen and Pinder (1984) method for slug tests in partially penetrating wells in confined aquifers. Note that the first two methods are based on approximate representations of the slug-induced flow system, while the latter two techniques use more complete descriptions of the relevant physics.

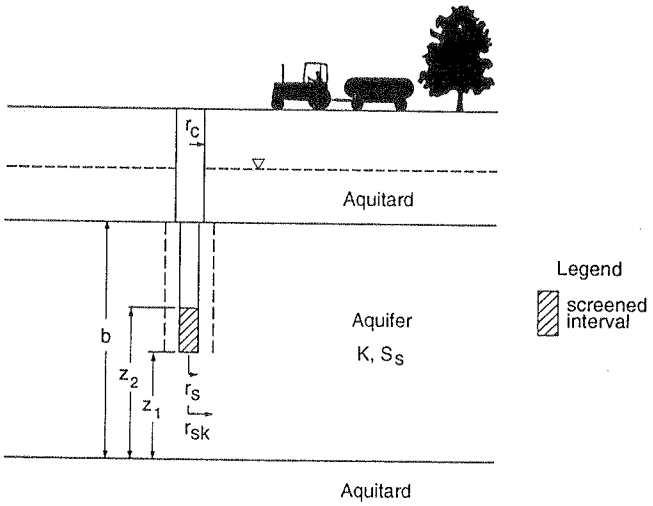

Figure 1. Cross-sectional view of a hypothetical confined aquifer (notation explained in text except for r_{sk}, radius of the gravel pack).

This paper focuses on the Nguyen and Pinder method for slug-test analysis. At the time of its publication, the Nguyen and Pinder method appeared to be the first rigorous approach for analyzing response data from slug tests in partially penetrating wells in confined aquifers. Analytical solutions for slug tests in partially penetrating wells that have been developed since the introduction of this method (e.g., Dougherty and Babu 1984; Hayashi et al. 1987) have not been widely adopted for parameter estimation, so many still consider the Nguyen and Pinder method the most appropriate approach for analysis of slug tests in partially penetrating wells in confined aquifers (e.g., Palmer and Johnson 1989). Although the method is used by field practitioners, currently taught in industry short courses on aquifer-test analysis (e.g., NGWA 1993), and recommended in technology transfer publications of the U.S. Environmental Protection Agency (e.g., Palmer and Johnson 1989), the Nguyen and Pinder method has not undergone the same degree of theoretical and field evaluation as the other three commonly used approaches have. Results from the limited field research on the technique have raised questions about the reliability of the resulting parameter estimates (e.g., Nichols 1985; Campbell et al. 1990; Brother and Christians 1993). These researchers reported that the Nguyen and Pinder estimates of hydraulic conductivity were not consistent with those obtained using other approaches. Given that this method is currently being used in the field and that there are questions concerning the reliability of its estimated parameters, a more thorough assessment is clearly needed. Such an assessment is the primary objective of this work.

This paper presents a complete theoretical evaluation of the Nguyen and Pinder method. This evaluation demonstrates that the parameter estimates obtained using this method are of very low quality due to errors in the derivation of the solution upon which the technique is based. A field evaluation will substantiate the results of the theoretical assessment. The paper will conclude with recommendations concerning the field applicability of the technique and possible alternative approaches.

Overview of Nguyen and Pinder Model

Model Definition

Although Nguyen and Pinder (1984) present a general mathematical model that can be employed for both pumping and slug tests, the focus of this work will be on the slug-test case. The problem of interest is the head response produced by the instantaneous introduction of a slug of water into the screened or open section of a well partially penetrating a confined aquifer, as shown in Figure 1. For the purposes of this development, the aquifer in Figure 1 is considered homogeneous and isotropic. The partial differential equation representing the flow of ground water in response to an instantaneous introduction of a slug at a central well can be written in cylindrical coordinates as:

$$\frac{\partial^2 s}{\partial r^2} + \frac{1}{r}\frac{\partial s}{\partial r} + \frac{\partial^2 s}{\partial z^2} = \left(\frac{S_s}{K}\right)\frac{\partial s}{\partial t} \qquad (1)$$

where:

s = Change in head relative to static, (L)
K = Hydraulic conductivity, (L/T)
S_s = Specific storage, (1/L)
t = Time, (T)
r = Radial direction, (L)
z = Vertical direction, z = 0 at the bottom of the aquifer and increases upward, (L).

Note that, except for the designation of spatial and temporal derivatives, the notation employed here will be that of Nguyen and Pinder.

The initial and boundary conditions are as follows:

$$s(r,z,0) = 0,\ r_s<r<\infty,\ 0\le z\le b \qquad (2)$$

$$\frac{\partial s(r,0,t)}{\partial z} = \frac{\partial s(r,b,t)}{\partial z} = 0,\ r_s<r<\infty,\ t>0 \qquad (3)$$

$$s(\infty,z,t) = 0,\ 0\le z\le b,\ t>0 \qquad (4)$$

$$\frac{1}{(z_2 - z_1)}\int_{z_1}^{z_2} s(r_s,z,t)\,dz = H(t),\ t>0 \qquad (5)$$

$$2\pi r_s K\int_{z_1}^{z_2}\frac{\partial s(r_s,z,t)}{\partial r}\,dz = \pi r_c^2\frac{dH(t)}{dt} \qquad (6)$$

where:

b = Aquifer thickness, (L)
r_s = Radius of well screen, (L)
r_c = Radius of well casing, (L)
z_1 = Distance from the bottom of the aquifer to the bottom of the screen, (L)
z_2 = Distance from the bottom of the aquifer to the top of the screen, (L)
$z_2 - z_1$ = Screen length, (L)
$H(t)$ = Head in well relative to static, (L).

Note that Equation 6, which is the flow boundary at the well screen, is presented in an integral form. Most contributions in the well hydraulics literature concerned with the transient response of partially penetrating wells have assumed a constant horizontal hydraulic gradient along the well screen as a mathematical convenience (e.g., Hantush 1964; Dougherty and Babu 1984). The error introduced by this assumption has been shown to be very small for wells commonly employed in field applications (Butler et al. 1993). In addition, this simplification allows a solution to be readily found, thus avoiding the problems that are discussed in the following section.

Although not explicitly stated, the following additional initial and boundary conditions are also employed in the later mathematical development:

$$H(0) = H_0 \tag{7}$$

$$\frac{\partial s(r_s,z,t)}{\partial r} = 0,\ 0<z<z_1,\ z_2<z<b,\ t>0 \tag{8}$$

where:

H_0 = Height of initial slug, (L).

Model Solution

Equations 1 through 8 describe the flow conditions modeled by Nguyen and Pinder. They attempted to derive an analytical solution to this mathematical model using conventional integral transform methodology. The key points of their derivation are given in the Appendix. In summary, a Laplace transform in time followed by a finite Fourier cosine transform in the z direction produces a modified Bessel equation in Fourier-Laplace space. Transform-space analogues of boundary conditions 4 and 6 are then employed to evaluate the equation constants. The basic problem with the Nguyen and Pinder method for slug-test analysis is that Equation 6 is undefined (i.e., cannot be written in terms of the dependent variable) in Fourier-Laplace space. As shown in the Appendix, Nguyen and Pinder attempted to circumvent this problem by performing an inverse Fourier transform prior to evaluating one of the constants. This step introduced an error that causes the remainder of the mathematical manipulations described by Nguyen and Pinder to be incorrect.

The problems produced by the undefined boundary condition prevented Nguyen and Pinder from presenting a solution in the conventional sense. All of their equations are given in terms of the deviation from static being a function of the temporal derivative of this same deviation. However, they were able to manipulate these equations to obtain expressions that can be used to estimate specific storage and hydraulic conductivity. Their expressions for parameter estimation are:

$$S_s = \frac{r_c^2\ C_3}{r_s^2\ (z_2 - z_1)} \tag{9}$$

$$K = \frac{r_c^2\ C_3}{4C_4\ (z_2 - z_1)} \tag{10}$$

where:

C_3 = The absolute value of the slope of a log-log $H(t)$ vs. t plot
C_4 = The absolute value of the slope of a semilog $-dH(t)/dt$ vs. $1/t$ plot.

The estimation procedure proposed by Nguyen and Pinder is straightforward. The slope of a log-log $H(t)$ vs. time plot is used to estimate specific storage from Equation 9. That slope along with the slope of a semilog $-dH(t)/dt$ vs. $1/t$ plot is then used to estimate hydraulic conductivity with Equation 10. In the field example presented by Nguyen and Pinder, a straight line is fit to the large-time data and the early-time data are ignored. Unfortunately, because of the error in the model derivation, the estimates produced by the procedure outlined above must be viewed with considerable skepticism. Furthermore, Nichols (1985) shows that there is a theoretical inconsistency (deviation from static is independent of hydraulic conductivity) that follows from Equation 9. This inconsistency, which is undoubtedly a product of the model error, casts further doubt on the reliability of estimates obtained using Equations 9 and 10.

Ramifications of the Model Error

In order to explore the ramifications of the model error for parameter estimation, a simple numerical experiment was performed in which a slug test in a partially penetrating well in a confined aquifer was simulated using a semianalytical solution. Parameter estimates were computed from the simulated response data using Equations 9 and 10 and then compared to the original parameter values employed in the semianalytical solution. This experiment used the semianalytical solution of Hyder et al. (in press), which has been extensively checked using both analytical (e.g., Dougherty and Babu 1984) and numerical (e.g., Butler et al. 1994) approaches, to simulate the slug test. The aquifer and well construction parameters given in Table 1 were used for this simulation. A well of a small aspect ratio (screen length/screen radius) was used to accentuate the partially penetrating nature of the well. Figure 2a displays a log-log $H(t)$ vs. time plot of the simulated responses.

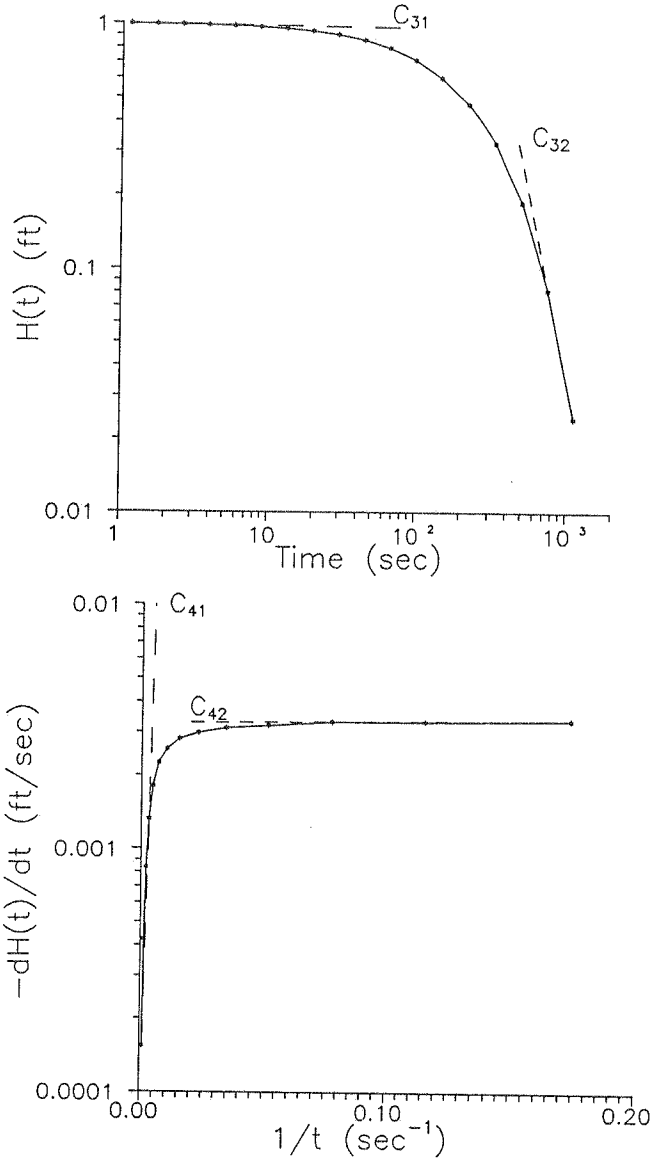

Figure 2. Nguyen and Pinder data plots for simulated slug test: (a) Log-log H(t) vs. time plot (C_{31} and C_{32} designate the absolute values of the slopes of straight lines fit to the early- and late-time portions of the plot, respectively); (b) Semilog negative head derivative (-dH(t)/dt) vs. inverse time plot (C_{41} and C_{42} designate the absolute values of the slopes of straight lines fit to the small and large inverse time portions of the plot, respectively).

Straight lines have been fit to the steepest (late time) and flattest (early time) portions of the plot in order to bound the specific storage estimates that might be obtained using Equation 9. Specific storage estimates of 0.00743 feet^{-1} and 3.64 feet^{-1} were obtained using the early and late time slopes, respectively. Note that the estimate obtained from the late time slope, which is the slope used by Nguyen and Pinder in their example, lies outside the range of physical plausibility.

A semilog $-dH(t)/dt$ vs. $1/t$ plot of the simulated responses is given in Figure 2b. Again, straight lines have been fit to the steepest (late time or early inverse time) and flattest (early time) portions of the plot to bound the hydraulic conductivity estimates that might be obtained using Equation 10. Note that four separate estimates of hydraulic conductivity can be obtained from

Table 1
Parameter Set for Slug Test Simulation

$K = 2.83$ ft/day
$S_s = 3.05e-6$ ft^{-1}
$r_s = r_c = 0.082$ ft
$z_2 - z_1 = 0.82$ ft
$b = 52.5$ ft
$H_0 = 1.0$ ft
$z_1 = 25.84$ ft

combinations of the two slope choices on Figure 2a and the two slope choices on Figure 2b. Table 2 lists the parameter estimates obtained using the various approaches. Based on the procedure outlined by Nguyen and Pinder, the most appropriate conductivity value would be 1.20 ft/d, which is 42 percent of the hydraulic conductivity employed in the semianalytical solution. However, given the lack of a clear-cut slope on Figures 2a and 2b, the use of a slope that produced a physically implausible specific storage estimate (3.64 feet^{-1}) for the conductivity estimate, and the considerable spread of estimates shown on Table 2, it is apparent that the relative close agreement between the conductivity estimate and the actual value is simply a function of chance.

A series of additional numerical experiments was performed to verify the results of the above analysis. In all cases, the estimates obtained using Equations 9 and 10 were found to be quite different from the actual parameter values. Thus, the ramifications of the model error appear to be of practical significance.

Table 2
Nguyen and Pinder Estimates from Simulated Slug Test

Parameter Estimates	Slopes Employed in Calculation
$S_s = 0.00743$ ft^{-1}	C_{31}
$S_s = 3.64$ ft^{-1} [a]	C_{32}
$K = 0.00245$ ft/day	C_{31}, C_{41}
$K = 12.8$ ft/day	C_{31}, C_{42}
$K = 1.20$ ft/day [a]	C_{32}, C_{41}
$K = 630$ ft/day	C_{32}, C_{42}

[a] Estimates obtained following the procedure employed in Nguyen and Pinder (1984).

Field Evaluation

The theoretical findings of the previous section can be substantiated with field data. Recently, the Kansas Geological Survey conducted a well testing program as part of a regional study of the Dakota Aquifer in Kansas (Butler and Liu 1994). At one site in Lincoln County, Kansas, two wells (0.167 feet and 0.083 feet in radius [r_c]), screened over similar depth intervals, are located

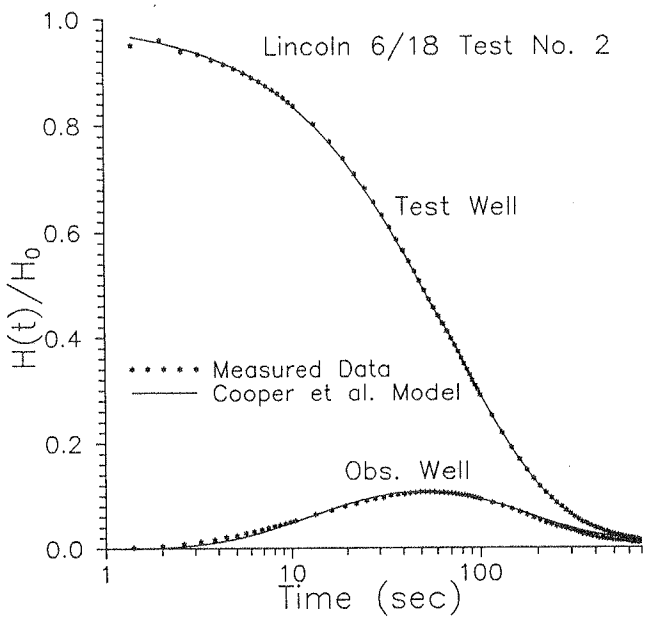

Figure 3. Semilog normalized head ($H(t)/H_0$) vs. time plot of Lincoln County slug-test data and best-fit Cooper et al. (1967) model.

21.2 feet apart. A series of slug tests was carried out to estimate the hydraulic conductivity and specific storage of the Dakota Aquifer at this site. These tests introduced a slug at the larger of the two wells and measured the responses at the test well and at the observation well. Measurements at the observation well were taken using a transducer placed below a packer located just above the top of the screen. The packer minimized effects associated with wellbore storage at the observation well. Note that an observation well was employed in these tests as a result of the theoretical work of McElwee et al. (1991), which shows that use of observation wells with slug tests can greatly improve the reliability of parameter estimates.

Table 3
Cooper et al. Estimates from Lincoln County Slug Test

	Estimated Value[a]	Lower Bound[b]	Upper Bound[b]
K	3.46 ft/day	3.45 ft/day	3.48 ft/day
S_s	$2.59e-6$ ft^{-1}	$2.53e-6$ ft^{-1}	$2.65e-6$ ft^{-1}

[a] Root-mean-squared deviation of 0.0035 feet. The following well construction parameters were employed for the test well: $(z_2-z_1) = 22$ feet, $r_c = 0.167$ feet, and $r_s = 0.333$ feet. Note that the screen length and radius were set equal to the length and radius of the gravel pack for the analysis because the gravel pack is much more permeable than the formation.

[b] Lower and upper bounds represent approximate 95 percent confidence intervals.

The response data were analyzed using an augmented version of the Cooper et al. (1967) method that allows inclusion of observations from points other than the test well. Plots of the measured data and the best-fit Cooper et al. model for both the test and observation wells are given in Figure 3. The small difference between the measured data and the best-fit model, in

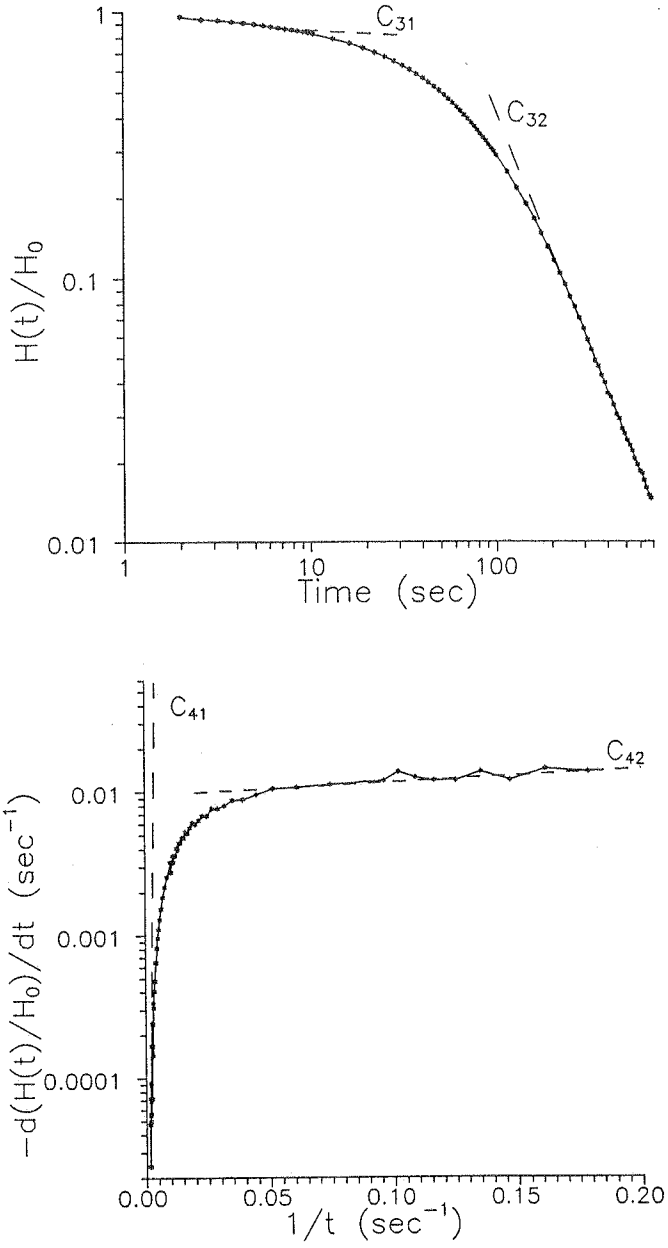

Figure 4: Nguyen and Pinder data plots for Lincoln County slug test: (a) Log-log normalized head ($H(t)/H_0$) vs. time plot (C_{31} and C_{32} designate the absolute values of the slopes of straight lines fit to the early- and late-time portions of the plot, respectively); (b) Semilog negative normalized head derivative ($-d(H(t)/H_0)/dt$) vs. inverse time plot (C_{41} and C_{42} designate the absolute values of the slopes of straight lines fit to the small and large inverse time portions of the plot, respectively).

conjunction with the results of the theoretical work of McElwee et al. (1991), indicates that the parameter estimates (given in Table 3) have good realiability. The model fitting, which was done using an automated well test analysis package developed at the Kansas Geological Survey (Bohling and McElwee 1992), also produces approximate confidence intervals for the estimated parameters. Those confidence intervals are given in Table 3.

Figure 4a presents the log-log normalized head vs. time plot of the data from the test well. As with Figure 2a, straight lines have been fit to the steepest (late time) and flattest (early time) portions of the plot to

bound the specific storage estimates that might be obtained using Equation 9. Table 4 lists the two specific storage estimates. The specific storage estimate obtained using the late-time straight line (0.0218 feet^{-1}) is close to four orders of magnitude larger than the specific storage estimated from the Cooper et al. analysis.

Figure 4b displays the semilog normalized $-dH(t)/dt$ vs. $1/t$ plot of the data. Again, straight lines have been fit to the steepest (late time) and flattest (early time) portions of the plot to bound the hydraulic conductivity estimates that might be obtained using Equation 10. Note that, as with the numerical example, four separate estimates of hydraulic conductivity can be obtained from combinations of the two slope choices on Figure 4a and the two slope choices on Figure 4b.

Table 4
Nguyen and Pinder Estimates from Lincoln County Slug Test

Parameter Estimates	Slopes Employed in Calculation
S_s = 0.000595 ft^{-1}	C_{31}
S_s = 0.0218 ft^{-1} [a]	C_{32}
K = 0.00107 ft/day	C_{31}, C_{41}
K = 1.58 ft/day	C_{31}, C_{42}
K = 0.0393 ft/day [a]	C_{32}, C_{41}
K = 58.0 ft/day	C_{32}, C_{42}

[a] Estimates obtained following the procedure employed in Nguyen and Pinder (1984).

Table 4 lists the parameter estimates obtained using the four slope combinations. Based on the procedure outlined by Nguyen and Pinder, the most appropriate conductivity value would be 0.039 ft/d, which is about two orders of magnitude smaller than the hydraulic conductivity estimated using the Cooper et al. solution.

Clearly, some difference should be expected between Cooper et al. model estimates and Nguyen and Pinder model estimates as a result of different assumptions of these two models concerning vertical flow in response to the slug-induced disturbance. The model of Cooper et al. assumes that the well is fully screened across the tested formation, so there is no possibility of vertical flow. The Nguyen and Pinder model, on the other hand, assumes a well that is partially screened across an isotropic formation. Thus, in this model, there will be a component of vertical flow. Extensive theoretical work (Hyder et al. in press), however, has shown that such dissimilar representations of the slug-induced vertical flow will produce a difference in hydraulic conductivity estimates of less than a factor of two for an aspect ratio of the well used in this test ($(z_2-z_1)/r_s \approx 66$). This is a far cry from the discrepancy of two orders of magnitude found here. Thus, the large difference in the computed parameters must be considered an illustration of the ramifications of the error in the Nguyen and Pinder model. As with the numerical experiments, the ramifications of the model error appear to be of practical significance.

Summary and Conclusions

The major results of this theoretical and field evaluation of the Nguyen and Pinder method for the analysis of response data from slug tests in partially penetrating wells in confined aquifers are as follows:

1. The Nguyen and Pinder method does not have a firm theoretical foundation as a result of its use of a boundary condition that is undefined in the transform space in which a solution was proposed. An attempt to circumvent this undefined boundary condition introduces further error that propagates into the expressions used for parameter estimation.
2. The errors in the theoretical development produce parameter estimates that may differ from the actual parameter values by orders of magnitude. The limited assessment done here indicates that the specific storage estimates tend to be too high while the hydraulic conductivity estimates are spread over a wide range.

This evaluation concludes that the Nguyen and Pinder method should not be used for slug-test analysis. If response data from a slug test performed in a partially penetrating well in a confined aquifer are to be analyzed, the best approach would be to use one of the existing analytical solutions that consider variants of this configuration (e.g., Dougherty and Babu 1984; Hayashi et al. 1987; Hyder et al. in press). Since these solutions are not widely available, the next best approach would be to employ the model of Hvorslev (1951). Recent work (Hyder et al. in press) shows that the Hvorslev method should produce reasonable approximations of hydraulic conductivity for the same conditions covered by the Nguyen and Pinder method. The Hvorslev method, however, is not a panacea and must be used with care in cases of high specific storage, low-permeability well skins, and anisotropy (Chirlin 1989; Demir and Narasimhan 1994; Hyder et al. in press).

Acknowledgment

This research was supported in part by the U.S. Geological Survey (USGS), Department of the Interior, under USGS award number 14-08-0001-G2093. The views and conclusions contained in this document are the authors' and do not necessarily represent the official policies, either expressed or implied, of the U.S. government.

Appendix

In this section, a brief overview of the mathematical derivation of the solution discussed in the main text is presented. The equation numbering will be the same as that given in Appendix A of Nguyen and Pinder (1984). The only difference between the equations given here and those of Nguyen and Pinder will be the notation used for derivatives and constants and the neglecting of their pumping-rate term (Q).

Equations 1 through 8 in the main text constitute the mathematical model of interest here. Nguyen and Pinder attempt to find a solution to this model by

employing classical integral transform techniques (Churchill 1972). Using initial conditions 2 and 7, Nguyen and Pinder apply the Laplace transform to Equations 1 and 3 through 6 to produce the following set of equations in Laplace space:

$$\frac{\partial^2 \bar{s}}{\partial r^2} + \frac{1}{r}\frac{\partial \bar{s}}{\partial r} + \frac{\partial^2 \bar{s}}{\partial z^2} = \left(\frac{S_s}{K}\right) p\bar{s} \qquad \text{(A1)}$$

$$\frac{\partial \bar{s}\ (r,0)}{\partial z} = \frac{\partial \bar{s}\ (r,b)}{\partial z} = 0 \qquad \text{(A2)}$$

$$\bar{s}\ (\infty,z) = 0 \qquad \text{(A3)}$$

$$\frac{1}{(z_2 - z_1)} \int_{z_1}^{z_2} \bar{s}\ (r_s,z)\,dz = \bar{H} \qquad \text{(A4)}$$

$$2\pi r_s K \int_{z_1}^{z_2} \frac{\partial \bar{s}\ (r_s,z)}{\partial r}\,dz = \pi r_c^2\ (p\bar{H} - H_0) \qquad \text{(A5)}$$

where:

$\bar{s}$, $\bar{H}$ = The Laplace transform of s and H(t), respectively
p = The Laplace transform variable.

Using the no-flow boundary condition given in A2, Nguyen and Pinder then apply a finite Fourier cosine transform in the z direction to Equations A1 and A3 to produce the following equations in Fourier-Laplace space:

$$\frac{\partial^2 \bar{s_c}}{\partial r^2} + \frac{1}{r}\frac{\partial \bar{s_c}}{\partial r} - \left(\frac{S_s}{K} p + (\frac{\pi n}{b})^2\right)\bar{s_c} = 0 \qquad \text{(A6)}$$

$$\bar{s_c}(\infty) = 0 \qquad \text{(A7)}$$

where:

$\bar{s_c}$ = The Fourier-Laplace transform of s
n = The Fourier transform variable.

Note that Nguyen and Pinder do not apply a Fourier transform to the wellbore flow condition given by Equation A5 because this condition is undefined in Fourier-Laplace space, i.e., the application of a finite Fourier cosine transform to A5 will not produce an expression in terms of $\bar{s_c}$.

The Fourier-Laplace solution to A6 is straightforward, because A6 is simply a form of the modified Bessel equation (Haberman 1987). The solution can be written as:

$$\bar{s_c}(r) = A_{1n} I_0(\alpha_n r) + A_{2n} K_0(\alpha_n r) \qquad \text{(A8)}$$

where:

$$\alpha_n^2 = \frac{S_s}{K} p + \left(\frac{\pi n}{b}\right)^2,\ n = 0, 1, 2, \ldots$$

A_{1n}, A_{2n} = Constants
I_0 = Modified Bessel function of the first kind of order 0
K_0 = Modified Bessel function of the second kind of order 0.

Note that the equation constants are a function of n and p.

The standard procedure for the evaluation of the constants in an equation such as A8 is to employ the boundary conditions. Application of A7, the boundary condition at an infinite radial distance from the well, to A8 results in constant A_{1n} being equal to 0 for all n. Thus, A8 is reduced to:

$$\bar{s_c}(r) = A_{2n} K_0(\alpha_n r). \qquad \text{(A9)}$$

At this point, Nguyen and Pinder face a problem because the boundary condition at $r = r_s$ is undefined in Fourier-Laplace space. Rather than redefining the wellbore boundary condition into a form that yields an expression in terms of $\bar{s_c}$, they incorrectly attempt to circumvent this problem by applying an inverse finite Fourier cosine transform to A9 before evaluating the constant. The expression that Nguyen and Pinder give for the inverse finite Fourier cosine transform is:

$$\bar{s}\ (r,z) = \frac{A_{2n}}{b}\left[K_0(\alpha_0 r) + 2\sum_{n=1}^{\infty} K_0(\alpha_n r)\cos\left(\frac{n\pi z}{b}\right)\right]. \qquad \text{(A10)}$$

Note that the constant A_{2n}, which is a function of n, has been taken out of the infinite series summation. Although moving A_{2n} out of the infinite series summation greatly simplifies the problem and allows the constant to be readily evaluated, this manipulation is mathematically incorrect and introduces further error into the proposed solution. Thus, even though the remaining manipulations outlined by Nguyen and Pinder in their Appendix A are performed without error, the errors previously described make all remaining expressions developed in the derivation, including the expressions for parameter estimation, incorrect and therefore of little practical value.

In summary, the derivation of Nguyen and Pinder has two interrelated problems. First, the boundary condition at the well screen is undefined in the transform

space in which Nguyen and Pinder propose a solution to their mathematical model. Second, an attempt to circumvent this problem through an application of an inverse Fourier transform is in error because a constant coefficient in Fourier-Laplace space is assumed to be independent of n. The theoretical and practical ramifications of these two problems are discussed in the main text.

References

Bohling, G.C., and C.D. McElwee. 1992. SUPRPUMP: An interactive program for well test analysis and design. *Ground Water* 30, no. 2: 262-68.

Bouwer, H. 1989. The Bouwer and Rice slug test — An update. *Ground Water* 27, no. 3: 304-9.

Bouwer, H., and R.C. Rice. 1976. A slug test for determining hydraulic conductivity of unconfined aquifers with completely or partially penetrating wells. *Water Resour. Res.* 12, no. 3: 423-28.

Brother, M.R., and G.L. Christians. 1993. In situ slug test analysis: A comparison of three popular methods for unconfined aquifers. In *Proc. of the 7th national outdoor action conf.,* 597-607. Dublin, Ohio: NGWA.

Butler, J.J., Jr., and W.Z. Liu. 1993. Pumping tests in nonuniform aquifers: The radially asymmetric case. *Water Resour. Res.* 29, no. 2: 259-69.

Butler, J.J., Jr., and W.Z. Liu. 1994. Analysis of 1991-1992 slug tests in the Dakota aquifer of central and western Kansas. Open-File Rept. 93-1c. Lawrence, Kansas: Kansas Geological Survey.

Butler, J.J., Jr., G.C. Bohling, Z. Hyder, and C.D. McElwee. 1994. The use of slug tests to describe vertical variations in hydraulic conductivity. *Jour. of Hydrology* 156: 137-62.

Butler, J.J., Jr., C.D. McElwee, and Z. Hyder. 1993. Slug tests in unconfined aquifers. Contribution No. 303. Manhattan, Kansas: Kansas Water Resources Research Inst.

Campbell, M.D., M.S. Starrett, J.D. Fowler, and J.J. Klein. 1990. Slug tests and hydraulic conductivity. In *Proc. of the petroleum hydrocarbons and organic chemicals in ground water: Prevention, detection, and restoration conf.,* 85-99. Dublin, Ohio: NWWA.

Chirlin, G.R. 1989. A critique of the Hvorslev method for slug test analysis: The fully penetrating well. *Ground Water Monitoring Review* 9, no. 2: 130-38.

Churchill, R.V. 1972. *Operational mathematics.* New York: McGraw Hill.

Cooper, H.H., J.D. Bredehoeft, and I.S. Papadopulos. 1967. Response of a finite-diameter well to an instantaneous charge of water. *Water Resour. Res.* 3, no. 1: 263-69.

Demir, Z., and T.N. Narasimhan. 1994. Towards an improved interpretation of Hvorslev tests. *ASCE J. of Hydraulics* 120, no. 4: 477-94.

Dougherty, D.E., and D.K. Babu. 1984. Flow to a partially penetrating well in a double-porosity reservoir. *Water Resour. Res.* 20, no. 8: 1116-22.

Haberman, R. 1987. *Elementary applied partial differential equations.* Englewood Cliffs, New Jersey: Prentice-Hall Inc.

Hantush, M.S. 1964. Hydraulics of wells. In: *Advances in hydrosciences,* Vol. 1, ed. V.T. Chow, 281-432. New York: Academic Press.

Hayashi, K., T. Ito, and H. Abe. 1987. A new method for the determination of in situ hydraulic properties by pressure pulse tests and application to the Higashi Hachimantai geothermal field. *J. Geophys. Res.* 92, no. B9: 9168-74.

Hvorslev, M.J. 1951. Time lag and soil permeability in groundwater observations. Bull. no. 36. Vicksburg, Mississippi: Waterways Exper. Sta., Corps of Engrs., U.S. Army.

Hyder, Z., J.J. Butler Jr., C.D. McElwee, and W.Z. Liu. In press. Slug tests in partially penetrating wells. *Water Resour. Res.*

McElwee, C.D., J.J. Butler Jr., G.C. Bohling, and W.Z. Liu. 1991. The use of observation wells with slug tests. Open-File Report 91-63. Lawrence, Kansas: Kansas Geological Survey. (See also McElwee, C.D., J.J. Butler Jr., G.C. Bohling, and W.Z. Liu. 1991. The use of observation wells with slug tests (abstract). *EOS* 72, no. 44: 220.)

National Ground Water Association. 1993. Analysis and design of aquifer tests, including slug tests and fracture flow. In *1994 catalog of ground water and environmental education,* 17-18. Dublin, Ohio: NGWA.

Nichols, E.M. 1985. Determination of the hydraulic parameters of salt marsh peat using in-situ well tests. Master's thesis, Civil Eng. Dept., Mass. Inst. Tech.

Nguyen, V., and G.F. Pinder. 1984. Direct calculation of aquifer parameters in slug test analysis. In *Groundwater hydraulics,* ed. J. Rosenshein and G.D. Bennett. AGU Water Resour. Monogr. No. 9: 222-39. Washington, D.C.: American Geophysical Union.

Palmer, C.D., and R.L. Johnson. 1989. Determination of physical transport parameters. In Transport and fate of contaminants in the subsurface, 29-40. EPA/625/4-89/019. Cincinnati, Ohio: Environmental Protection Agency.

Biographical Sketches

James J. Butler Jr. *is an associate scientist with the Geohydrology Section of the Kansas Geological Survey (1930 Constant Ave., The University of Kansas, Lawrence, KS 66047) He holds a B.S. in geology from the College of William and Mary, and an M.S. and Ph.D. in applied hydrogeology from Stanford University. His primary research interest is the development of field methodology for site characterization.*

Zafar Hyder *is a doctoral candidate in the Department of Civil Engineering at the University of Kansas and a research assistant at the Kansas Geological Survey. He holds master's and bachelor's degrees in civil engineering from the University of Connecticut and Bangladesh University of Engineering and Technology, respectively. His research interests include aquifer characterization and analytical and numerical modeling of subsurface flow and transport.*

F. HYDRAULIC TOMOGRAPHY IN TWO-DIMENSIONAL GROUNDWATER FLOW

Abstract

The head drop between any two points on a streamline is given by a line integral of the flux along the streamline multiplied by the hydraulic resistivity (inverse of hydraulic conductivity). This integral provides the basis for a tomographic method for estimating the distribution of hydraulic resistivities from measured heads in a steady-gradient flow field. Streamline trajectories and flux integrals are computed from a finite difference solution for stream function values based on an estimate of the resistivity distribution. Computing flux integrals along a number of streamlines with known heads at each end results in a system of linear equations which can be solved for an updated set of resistivities. Stream function values and flux integrals are recomputed and the process repeats until the resistivity estimates converge. This section includes numerical examples involving the estimation of the resistivity distribution in a vertical plane.

Introduction

As discussed in *Yeh's* [1986] review of the groundwater inverse problem, most research on aquifer parameter estimation has been cast either in terms of reducing an equation error criterion (direct method) or in terms of reducing an output error criterion (indirect method). In the direct method, the head is assumed to be known and specified exhaustively (typically, at all nodes in a finite difference or finite element grid) and the groundwater flow equation is recast as a first-order partial differential equation in the unknown transmissivity or hydraulic conductivity (assuming all source and sink terms and boundary conditions are known). Head gradient terms, estimated by differences of heads at computational nodes, appear in the left-hand side coefficients in this equation. Examples of application of the direct method include *Frind and Pinder* [1973], *Neuman* [1973], and the important early work by *Nelson* [1960, 1961, 1968].

In the indirect formulation of the inverse problem, the unknown aquifer parameters are iteratively adjusted until model-predicted heads and observed heads are sufficiently close, usually in the least squares sense. In most formulations, the indirect inverse problem depends on the calculation of the Jacobian or sensitivity matrix, where each element (i,j) is given by the partial derivative of a model output value, h_i, to model parameter j. In general, the sensitivity to each unknown parameter is itself a function of time and spatial location.

Sensitivity to the hydraulic conductivity in a certain region of the flow domain obeys an equation of essentially the same form as the equation for the head itself. The inverse problem can be approached by solving a set of 1+M partial differential equations at each iteration, the first describing the head field itself and each of the remaining M equations describing the distribution of the sensitivity to each of the M unknown parameters. As demonstrated in *Yeh* [1986] and *McElwee* [1982], in the sensitivity equation a term involving the head gradient appears in place of the source/sink term in the original equation for head. This head gradient is now evaluated from numerical differentiation of the computed head field, rather than from interpolation between observed head values, as in the direct inverse solution.

Neuman [1980] and *Carrera and Neuman* [1986] present a conjugate gradient minimization approach for solving the indirect inverse problem. The derivative of the objective function (sum squared output error) to each model parameter is derived from an adjoint state function. This method does not require computation of the Jacobian matrix and so does not require solution of the sensitivity equations at each iteration. Evaluation of the head gradient is still required, however, to compute the derivative of the objective function with respect to unknown conductivity values.

Any method for estimating aquifer conductivities (or transmissivities) depends in some way on the evaluation of head gradient terms because of the close relationship between the inverse problem and the Cauchy problem. In an appendix, *Neuman* [1980] discusses the causes for ill-conditioning of the inverse problem in terms of the one-dimensional Cauchy problem. The conductivity at each point in a one-dimensional flow problem is given uniquely by the specific flux at that point divided by the hydraulic gradient. The same condition applies along each flow line in a two- or three-dimensional flow field. If all source terms are known, conductivity can be determined uniquely along each flow line that crosses a surface where Cauchy data (either conductivity or flux) are specified. A specified flux boundary would constitute such a surface.

The relationship between the Cauchy problem and the inverse problem is also discussed in the papers by *Nelson* [1960, 1961, 1968]. *Nelson* [1961] describes a method for solving the direct inverse problem that involves flow net analysis. This is essentially a means of solving the one-dimensional Cauchy problem along each streamtube. A similar method has recently been presented by *Scott* [1992]. *Scott* [1992] derives his streamtube representation from a flow net based on a spline fit to the observed heads in a region, while *Nelson* [1961] uses an orthogonal regression fit. A large amount of head data are required to create an accurate representation of the piezometric surface in either case. Both authors also assume that the distribution of recharge and discharge along each streamtube is known.

Given the transmissivity at any point along the streamtube and the distribution of recharge and discharge, the transmissivity at any other point on the streamtube can be determined uniquely. If the recharge is unknown, only the ratio of transmissivity to recharge can be determined.

The method proposed here shares characteristics both of the indirect solution methods and the direct solution methods based on flow net analysis. A reformulation of the Cauchy problem shows that the head drop between any two points along a streamline is given by the line integral of the specific flux multiplied by the hydraulic resistivity along that streamline. This can also be seen as an integral version of Darcy's law, applied along a streamline. If the model domain is discretized into constant-resistivity zones, then the head drop along each streamline is given by a linear combination of the resistivities encountered along that streamline, with coefficients given by the integral of the specific flux within each constant resistivity zone.

In this study, streamline trajectories and values for specific flux along each streamline are derived from a finite difference solution for the stream function based on the current estimate of the resistivity distribution. Accumulating flux integral information along a number of streamlines connecting points with known heads leads to a system of linear equations yielding a vector of resistivity correction terms. These corrections are used to create an updated set of resistivity values. New stream function values, streamline trajectories, flux integrals, and resistivity corrections are then computed based on the new resistivities. The process continues until resistivity estimates converge. This approach is very similar to that used in seismic tomography [*Peterson et al.*, 1985].

The streamline trajectories and the specific fluxes are derived from the finite difference solution for the stream function using a modified version of a path-tracing algorithm presented by *Pollock* [1988]. *Pollock* [1988] presented a method for tracing advective flow paths based on the heads computed using a block-centered finite difference formulation. His method uses a linear interpolation of each velocity component within a model cell from the velocities computed at the cell faces. In *Pollock* [1988], the cell-face velocities (fluxes scaled by porosity) are derived from the differences of heads computed at the centers of adjacent model cells. In this work, the flux field within each cell is derived from bilinear interpolation of the fluxes at the cell faces, as in *Pollock* [1988]. However, the cell-face fluxes are derived from differences of stream function values at the corners of each cell, using a mesh-centered formulation, rather than from differences of heads in adjacent cells. This study presents the development of a formula for the integral of the flux along a

streamline in each model cell, providing the link between the path-tracing algorithm and the tomographic system of equations.

The original approach in this work was to base the streamline and flux integral calculations on head values computed using a block-centered finite difference formulation, as in *Pollock* [1988]. However, we discovered that there are two important reasons for basing the path-tracing and flux integral computations on a mesh-centered solution for stream functions instead. One reason is that flux values computed from differences of computed stream function values are inherently more accurate than those computed from differences of computed head values, as pointed out by *Frind and Matanga* [1985]. Secondly, the block-centered formulation uses harmonic averages of adjacent cell conductivities to represent cell face conductivities. As pointed out by *Desbarats* [1992a], the resulting distribution of cell-face conductivities tends to underestimate the distribution of cell-by-cell conductivities. As a result, the flux integral calculation, which uses cell-by-cell conductivities, sees a higher overall conductivity than the finite difference model for heads. This inconsistency leads to convergence problems for the inverse technique, since the resistivity corrections derived from the tomographic equations are not necessarily the optimal ones for computing a head field which will result in improved flux integral predictions.

Pollock's method is applicable to general time-varying, three-dimensional problems and can be used to compute particle position along a flow path as a function of time. His presentation is in terms of actual flow velocities, rather than Darcy velocity (specific flux). The two are equivalent, except for a scaling by the value of porosity. For a steady state flow field, a flow path coincides with a streamline. We are only interested in integrals of specific flux along a streamline, so we are interested in time only as a convenient variable of integration. Thus, we can use specific flux in place of flow velocity in Pollock's formulation, recognizing that we are working with a time variable that is scaled by the porosity. This has no effect on the resulting flux integral or on the trajectory of the streamline (assuming a constant porosity). The streamline tracing algorithm is not limited to use with finite difference models. *Cordes and Kinzelbach* [1992] present a modification of Pollock's algorithm applicable to velocity fields computed using finite element techniques. The computation of the flux integral could be added to their algorithm as well.

After the stream function solution is obtained and the streamlines are identified, the flux is integrated along each streamline. Flux integral components in each model cell are added to the appropriate entry in the coefficient matrix for the tomographic system of equations. An arbitrary zonation may be imposed on the model domain to reduce the number

of unknown resistivities. This estimation process is also iterative, since the stream function and streamline distributions depend on the current estimate of the resistivities.

This method (iteratively) identifies the 'characteristics' of the flow system, which coincide with the flow lines in an isotropic system [*Neuman*, 1973]. Since the head drop along any streamline depends only on the resistivities encountered by that streamline, this inverse procedure depends less on the spreading of Cauchy information across the flow field, described as the 'cross-characteristic influence of Cauchy data' by *Neuman* [1973]. This should improve the conditioning of the inverse problem. Another feature of this method is that the head drop along each streamline is a linear function of the sequence of resistivities along the streamline. Given the true model, exact parameter variances and covariances can be computed, since no second order information is being neglected in the forward computation.

The current work is concerned with determining the distribution of hydraulic conductivities (actually resistivities) in a vertical plane, rather than the distribution of transmissivity in a horizontal plane. However, this primarily involves a difference in terminology. The tomographic method could just as easily be applied to determining transmissivity in the horizontal plane.

The current work employs a very simple flow configuration, a vertical rectangular plane between two wells, one extracting water along a limited vertical interval and the other injecting the same amount of water, also along a limited vertical interval. For simplicity, a Cartesian coordinate system is used and local isotropy (within each model cell) is assumed. We are ignoring the fact that the flow to a well is actually radial and the complications caused by anisotropy in the conductivity. However, these simplifications are only for the purpose of demonstrating and testing the method. The theory is applicable to more complex and realistic flow configurations, as long as steady-gradient conditions have been achieved. The method does not require strict steady state conditions, since it depends only on head differences. Heads may be falling or rising at a uniform rate across the flow domain when measurements are taken.

The Finite Difference Model

The differential equation describing the stream function, ψ, in a two-dimensional vertical plane with heterogeneous, isotropic hydraulic resistivity, R, is

$$\frac{\partial}{\partial x}\left(R\frac{\partial \psi}{\partial x}\right)+\frac{\partial}{\partial y}\left(R\frac{\partial \psi}{\partial y}\right)=0 \qquad \text{(II.F.1)}$$

where x is the horizontal coordinate and y is the vertical coordinate (positive upward). As described in *Frind and Matanga* [1985], interior sources and sinks can be included in the stream function formulation by inserting a cut in the model domain connecting the interior source/sink point to the domain boundary, allowing the source/sink term to appear as an external boundary condition. We do not include interior source/sink terms in the current work. They could be incorporated without substantially affecting the hydraulic tomography formulation. However, heads would have to be known at all interior source/sink points, since each such point is the starting or ending point for a certain set of streamlines.

Using the convention adopted by *Frind and Matanga* [1985], the components of specific flux in the x and y directions, q_x and q_y, are related to the stream function by

$$q_x=\frac{\partial \psi}{\partial y} \qquad q_y=-\frac{\partial \psi}{\partial x} \qquad \text{(II.F.2)}$$

(Alternatively, the negative sign may be applied to the y derivative to obtain q_x. The choice is arbitrary.)

In this work, only specified flux boundary conditions are used. These result in first-type (Dirichlet) boundary conditions on the stream function. Following *Frind and Matanga* [1985], if ψ_0 represents the stream function at the point Γ_0 on the boundary, then the stream function along the boundary, Γ, is given by

$$\psi(\Gamma)=\psi_0(\Gamma_0)+\int_{\Gamma_0}^{\Gamma}\mathbf{q}_0\cdot\mathbf{n}\,d\Gamma \qquad \text{(II.F.3)}$$

where $\mathbf{q}_0$ represents the specified boundary flux and $\mathbf{n}$ is the unit normal to the boundary. Thus, stream function values at boundary nodes in a finite difference model are obtained by summing specified boundary fluxes, proceeding around the model boundary in either a clockwise or counterclockwise sense.

Figure II.F.1 is a sketch of a node in a mesh-centered finite difference grid, along with its neighboring nodes and cells. In our formulation, each cell in the model is labeled with the pair of indices identifying the node in its upper right-hand corner. The centered-difference approximation of the derivatives in Equation II.F.1 involves the resistivities at points half-way between nodes, at the midpoints of cell faces. These resistivities are computed as

arithmetic averages of the two adjacent cell resistivities. Thus, the resistivity between node (i,j) and node (i+1,j) is approximated as

$$R_{i+1/2,j} = \frac{R_{i+1,j} + R_{i+1,j+1}}{2} \qquad \text{(II.F.4)}$$

From the perspective of the head field for a linear flow system, hydraulic conductivities in series average harmonically and conductivities in parallel average arithmetically [*McDonald and Harbaugh*, 1984]. Thus, if we were solving for head using the mesh-centered formulation shown in Figure II.F.1, it would be appropriate to use the arithmetic average of the conductivities to represent the conductivity midway between the nodes. Since resistivity plays the same role in the stream function equation as does conductivity in the head equation, the same averaging laws apply to R in the stream function formulation as apply to K in the head formulation.

A mesh-centered finite difference formulation leads to the following equation for each node (i,j):

$$a_{xi,j}\Psi_{i-1,j} + a_{yi,j}\Psi_{i,j-1} + b_{i,j}\Psi_{i,j} + c_{xi,j}\Psi_{i+1,j} + c_{yi,j}\Psi_{i,j+1} = d_{i,j} \qquad \text{(II.F.5)}$$

where the coefficients for interior nodes are given by

$$a_{xi,j} = \frac{R_{i-1/2,j}}{\Delta x^2} \qquad \text{(II.F.6a)}$$

$$c_{xi,j} = \frac{R_{i+1/2,j}}{\Delta x^2} \qquad \text{(II.F.6b)}$$

$$a_{yi,j} = \frac{R_{i,j-1/2}}{\Delta y^2} \qquad \text{(II.F.6c)}$$

$$c_{yi,j} = \frac{R_{i,j+1/2}}{\Delta y^2} \qquad \text{(II.F.6d)}$$

$$b_{i,j} = -\left(a_{xi,j} + a_{yi,j} + c_{xi,j} + c_{yi,j}\right) \qquad \text{(II.F.6e)}$$

$$d_{i,j} = 0 \qquad \text{(II.F.6f)}$$

Since only Dirichlet boundary conditions are employed, equations for boundary nodes could be eliminated from the system of equations, with equations for adjacent nodes being modified

appropriately. However, for simplicity of coding, the boundary node equations are retained using

$$b_{i,j} = 1 \tag{II.F.7a}$$

$$a_{xi,j} = a_{yi,j} = c_{xi,j} = c_{yi,j} = 0 \tag{II.F.7b}$$

$$d_{i,j} = \psi_{i,j} \tag{II.F.7c}$$

$\psi_{i,j}$ at a boundary node is obtained from summation of the specified boundary flux at each node multiplied by the appropriate cell dimension (Δx for bottom and top nodes, Δy for left and right nodes). A value of zero is assigned for the stream function at the lower left-hand node, (i,j) = (0,0), and the summation proceeds in a counterclockwise fashion.

The program used for this study solves the system of equations using a simple alternating direction implicit technique [*Wang and Anderson,* 1982]. For each direction, the appropriate terms in Equation II.F.5 are moved to the right-hand side, modifying the d vector and resulting in a tridiagonal left-hand coefficient matrix. The method of treating boundary nodes shown in Equation II.F.7 facilitates the production of the tridiagonal coefficient matrix for the entire set of nodes, since boundary nodes need no special treatment aside from the initial computation of their coefficients.

The Streamline-Tracing Algorithm

The streamline-tracing algorithm is derived from that described by *Pollock* [1988], with some minor modifications. The first modification is that the algorithm is recast entirely in terms of specific flux values (Darcy velocities), rather than actual flow velocities. Pollock was interested in tracing the advective transport of particles with time, and so developed his algorithm in terms of flow velocity, v. Flow velocity, v, and specific flux, q, are related by

$$v = \frac{q}{n} \tag{II.F.8}$$

where n is the porosity of the medium. We are not interested in the time of travel along a path, but only in the path trajectory and the integral of flux along the path. Thus, the algorithm presented here works directly in terms of specific fluxes using a time given by $t = t_r/n$, where t_r is the real-world travel time. We use this time only as a convenient variable of

integration. However, actual travel time along a path could be derived from it simply by multiplying by the porosity.

The second modification is the use of a slightly different set of coordinates. Pollock works with global coordinates. The streamline-tracing algorithm presented here, however, uses a local coordinate system in each cell, with x ranging from -Dx/2 to Dx/2 and y ranging from -Dy/2 to Dy/2. Figure II.F.2 is a sketch of a single cell in the finite difference model showing the locations of the cell-face fluxes and one possible flow path through the cell. q_{x1} is the x component of flux at the left face, q_{x2} is the x component of flux at the right face, q_{y1} is the y component of flux at the bottom face, and q_{y2} is the y component of flux at the top face. The flux field is given by

$$q_x(x) = q_{x0} + A_x x \qquad \text{(II.F.9a)}$$

$$q_y(y) = q_{y0} + A_y y \qquad \text{(II.F.9b)}$$

where

$$q_{x0} = \left(q_{x2} + q_{x1}\right)/2 \qquad \text{(II.F.10a)}$$

$$q_{y0} = \left(q_{y2} + q_{y1}\right)/2 \qquad \text{(II.F.10b)}$$

and

$$A_x = \left(q_{x2} - q_{x1}\right)/\Delta x \qquad \text{(II.F.11a)}$$

$$A_y = \left(q_{y2} - q_{y1}\right)/\Delta y \qquad \text{(II.F.11b)}$$

The final, and most important, modification of Pollock's algorithm is that we derive the cell-face fluxes from differences of stream function values computed at nodes located at the corner of each cell, rather than from differences of head values computed at nodes located at the center of adjacent cells (scaled by the cell face conductivity). For example, in *Pollock* [1988] q_{x2} for cell (i,j) is given by

$$q_{x2} = -\frac{K_{i+1/2,j}}{\Delta x}\left(h_{i+1,j} - h_{i,j}\right) \qquad \text{(II.F.12)}$$

where $K_{i+1/2,j}$ is the cell-face conductivity on the right-hand face, $h_{i,j}$ is the head in cell (i,j), and $h_{i+1,j}$ is the head in the cell (i+1,j). In our formulation, however, the right-hand cell-face flux is given by

$$q_{x2} = \frac{(\psi_{i,j} - \psi_{i,j-1})}{\Delta y} \qquad \text{(II.F.13)}$$

where $\psi_{i,j}$ is the stream function value computed at node (i,j), at the upper right-hand corner of cell (i,j), and $\psi_{i,j-1}$ is the stream function value computed at the lower right-hand corner of cell (i,j).

Pollock's development of the equations describing a flow path will be briefly summarized here, being recast in terms of specific flux values and local coordinates. Given the above expressions for the flux components and the entry location of a streamline in local coordinates, the flux components, q_{xp} and q_{yp}, at the entry point, (x_p,y_p), can be obtained from Equation II.F.9. A particle moving through the cell from this entry point will then follow a trajectory determined by the following relationships

$$\frac{dq_x(t)}{dt} = A_x q_x(t) \qquad \text{(II.F.14a)}$$

$$\frac{dq_y(t)}{dt} = A_y q_y(t) \qquad \text{(II.F.14b)}$$

The right-hand sides of Equation II.F.14 are derived from application of the chain rule. A_x is dq_x/dx and $q_x(t)$ is the current value of dx/dt for the particle. Equation II.F.14 can be integrated, to give the following expressions for the flux components as a function of time

$$q_x(t) = q_{xp}\exp(A_x t) \qquad \text{(II.F.15a)}$$

$$q_y(t) = q_{yp}\exp(A_y t) \qquad \text{(II.F.15b)}$$

The trajectory of the streamline is given by integrating equation Equation II.F.15 and requiring that $(x(0),y(0)) = (x_p,y_p)$, yielding

$$x(t) = \frac{1}{A_x}\left(q_{xp}\exp\left(A_x t\right) - q_{x0}\right) \qquad \text{(II.F.16a)}$$

$$y(t) = \frac{1}{A_y}\left(q_{yp}\exp\left(A_y t\right) - q_{y0}\right) \qquad \text{(II.F.16b)}$$

The travel time in the cell is determined by testing the potential travel times to each face of the cell. The minimum positive (physically meaningful) value is the actual travel time, t_c. For example, the potential travel time to the right face is given by

$$t_{x2} = (1/A_x)\ln(q_{x2}/q_{xp}) \qquad \text{(II.F.17)}$$

if A_x is non-zero or

$$t_{x2} = \left(\frac{\Delta x}{2} - x_p\right)\Big/ q_{x0} \qquad \text{(II.F.18)}$$

if A_x is zero (q_x is constant). It is possible for all the candidate travel times to be non-positive if the cell represents a sink. This possibility is not allowed in the current work, since no sources or sinks are included in the model. A very long (theoretically infinite) travel time would indicate that the cell is located at a stagnation point in the flow field. Pollock points out that another special case can occur when a flow divide passes through the model cell, meaning, for example, that q_{x1} and q_{x2} are of opposite sign.

Once the travel time in the cell is determined, the coordinates of the exit point, (x_e,y_e), can be calculated by plugging the travel time into Equation II.F.16:

$$x_e = \frac{1}{A_x}\left(q_{xp}\exp(A_x t_c) - q_{x0}\right) \qquad \text{(II.F.19a)}$$

$$y_e = \frac{1}{A_y}\left(q_{yp}\exp(A_y t_c) - q_{y0}\right) \qquad \text{(II.F.19b)}$$

The particle moves into the appropriate neighboring cell (or in rare cases exits out the corner to a diagonally adjacent cell) and the process continues until the streamline reaches a boundary.

The Tomographic Equations

Assuming isotropy, Darcy's law reduces to a simple one-dimensional relationship along a streamline:

$$q_s(s) = -K(s)\frac{dh}{ds} \qquad \text{(II.F.20)}$$

where $q_s(s)$ is the specific flux (L/T) along the streamline, K(s) is the hydraulic conductivity (L/T) and dh/ds is the directional derivative of head along the streamline (dimensionless). The total head drop, H, along the streamline is given by rearranging Darcy's law and integrating:

$$H = \int_0^{L_s} R(s) q_s(s) ds \qquad \text{(II.F.21)}$$

where L_s is the total length of the streamline and R is hydraulic resistivity (T/L), the inverse of K.

In a finite difference model the resistivity is not a continuous spatial function, but is instead discretized into cell-by-cell values. Assuming that a streamline encounters N different cells, each with a discrete resistivity, R_i, the head drop along the streamline is given by

$$H = \sum_{i=1}^{N} \left(R_i \int_{si} q_s(s) ds \right) \qquad \text{(II.F.22)}$$

where the integral is evaluated separately along the streamline path within each cell, i.

The evaluation of the flux integral within a cell is simplified by recognizing that $q_s(s)ds$ is the same as $q_s^2(t)dt$, since $ds = q_s(t)dt$. Furthermore, $q_s^2(t) = q_x^2(t)+q_y^2(t)$, so that the flux integral within a cell conveniently reduces to the sum of two simple integrals

$$\int_{si} q_s(s) ds = \int_0^{t_c} q_s^2(t) dt = \int_0^{t_c} q_x^2(t) dt + \int_0^{t_c} q_y^2(t) dt \qquad \text{(II.F.23)}$$

Squaring and integrating the expression for $q_x(t)$ in Equation II.F.15 yields

$$\int_0^{t_c} q_x^2(t) dt = \frac{q_{xp}^2}{2A_x} \left(\exp(2A_x t_c) - 1 \right) \qquad \text{(II.F.24)}$$

if A_X is non-zero and

$$\int_0^{t_c} q_x^2(t) dt = q_{x0}^2 t_c \qquad \text{(II.F.25)}$$

if A_x is zero ($q_x(x)$ is constant). The corresponding expressions for the y-component integral are analogous. The addition of Equations II.F.23 -II.F.25 to Pollock's algorithm provides the means for reducing the complex dependence of the head field on the entire field of hydraulic conductivity to a simple set of one-dimensional equations expressing the linear dependence of the head drop between two points on the sequence of resistivities encountered by the streamline between those two points.

To reduce the number of unknown parameters, model cells may be grouped into larger zones of constant resistivity. If M is the number of zones, j is the zone index, and N_j is the number of cells in zone j, then the line integral is given by

$$H = \sum_{j=1}^{M}\left(R_j \sum_{i=1}^{N_j} \int_{si} q_s(s)ds \right) \qquad \text{(II.F.26)}$$

This is the formulation used in the program developed for the present study. The user is allowed to specify an arbitrary zonation of the resistivity field. Each zone may consist of one contiguous region of constant R, or several separate regions, all of the same R. For example, it would be possible to specify a two-zone model with alternating layers of zone-1 resistivity and zone-2 resistivity.

If measured heads are available at both ends of a streamline, these two values can be subtracted to yield an observed head drop. Subtracting the head drop predicted by Equation II.F.26 from the observed head drop yields a head drop residual, here denoted by DH. Since the relationship between head drop and resistivity along a streamline is linear, the head drop residual could be accounted for by a series of corrections, DR_j, to the zonal resistivities along the flow path. The corrections would need to satisfy

$$\Delta H = \sum_{j=1}^{M}\left(\Delta R_j \sum_{i=1}^{N_j} \int_{si} q_s(s)ds \right) \qquad \text{(II.F.27)}$$

Any set of resistivity corrections that satisfied Equation II.F.27 would allow the predicted head drop along the streamline to exactly match the observed head drop along the streamline, provided that the trajectory of the streamline and the flux integral computed on the basis of the new resistivities were the same as those computed on the basis of the old resistivities. The changes in the streamline trajectory and in the flux integral induced by the change in R values leads to the iterative nature of the parameter estimation process.

If heads have been measured at a number of data points within the model domain, these data points can be used as the beginning points of streamlines. The streamline that passes through a point can be thought of as two streamlines starting from that point, one moving forward, in the positive flux direction, and the other moving backward. In the absence of sources and sinks, each streamline beginning from a point within the model domain is constrained to end on a boundary interval with a non-zero flux, either a specified head boundary or a specified non-zero flux boundary. If heads are also known at all such boundaries, then observed head drops can be computed along each streamline. For each streamline, Equation II.F.26 gives the predicted head drop along that streamline. The head drop residual can then be computed for each streamline. Equation II.F.27 can then be applied, resulting in a set of linear equations

$$\sum_{j=1}^{M} \Delta R_j c_{k,j} = \Delta H_k \qquad k = 1, N_s \tag{II.F.28}$$

where N_S is the number of streamlines and

$$c_{k,j} = \sum_{i=1}^{N_j} \int_{si;k} q_s(s) ds \tag{II.F.29}$$

The integral shown in Equation II.F.29 is evaluated over the path of streamline k in cell i. This result is added into the $c_{k,j}$ entry for the zone, j, to which cell i belongs.

Least squares techniques can now be used to solve the set of Equations II.F.28 for the optimal correction values, DR_j. These values are then added to the current R estimates and the heads, streamline trajectories, flux integrals and predicted head drops are recomputed. The process continues until the parameter estimates converge or until a specified maximum number of iterations has occurred.

Examples

The initial example simply tests the accuracy of the streamline trajectory and flux integral calculations in a synthetic heterogeneous aquifer. The model domain is nine units on a side, with the upper and lower boundaries representing confining units and the left and right boundaries representing a pair of wells, one injecting water along a limited interval (on the left) and the other extracting the same amount of water along a limited interval (on the right). The spatial distribution of the natural log of the hydraulic resistivity is shown in Figure II.F.3.

This synthetic field was generated using sequential Gaussian simulation [*Deutsch and Journel*, 1992]. The specified variogram was spherical with a sill of 1.0, a range of 1.2 units in the vertical direction, and a range of 24 units in the horizontal direction. Thus, the horizontal range of the log-resistivity field is about 2.7 times the horizontal dimension of the model domain. In contrast, the vertical range is about 13% of the vertical dimension of the model domain. This results in a tendency for the synthetic field to exhibit an imperfectly layered structure similar to that exhibited by natural aquifers. The range of resistivity values corresponding to the log resistivities shown in Figure II.F.3 is 0.04 to 22 (dimensions L/T), or about 2.7 orders of magnitude variation.

Figure II.F.4 displays the head and stream function contours resulting from a single test performed in the synthetic aquifer. In this test water was injected at a rate of 0.5 units (in terms of specific flux, L/T) at each of the six nodes between y=4 and y=5 (inclusive) on the left side and extracted at the same rate along the same vertical interval on the right side. The remaining boundaries are zero-flux boundaries. The two sets of contours are generated from two separate program runs, one for the head solution and one for the stream function solution. The variable resistivity results in a fairly complex flow pattern. The channeling of flow through low-resistivity (high-conductivity) lenses is most evident in the stream function contours, especially near the lower portion of the injection interval on the left-hand side.

The plus signs posted on Figure II.F.4 represent the locations of 27 data points used in this and following program runs. Forward solutions for a set of head fields, using a known resistivity field, are computed for each simulated suite of tests. Head values computed at the posted locations are taken as input data for the subsequent inverse runs. For reasons discussed earlier, the inverse runs base the streamline trajectory and flux integral calculations on stream function solutions, rather than head solutions. At each iteration of an inverse run, streamlines are traced from each data point, at which the head is known, to each non-zero flux boundary. The flux integral along each streamline provides a prediction of the head drop between these two points. These predicted head drops are compared to the observed head drops provided by taking the difference between the observed head at the data point and the observed head at the boundary point where the streamline terminates. In this case the observed heads are provided by the forward solution for the head field. In a real-world application, these values would be provided by measurements in the field.

Figure II.F.5 is a comparison between the head drops computed from the flux integral, using a stream function solution based on the true resistivity field shown in Figure II.F.3, and those calculated from differences of heads computed at the 27 data points and the boundary points intersected by the streamlines. This plot shows that the flux integral results are

consistent with the computed head field, providing some confirmation of the validity of the flux integral formulation.

Before attempting any kind of parameter estimation for groundwater flow systems, a reduction in the dimensionality of the parameter space must be performed. For the purposes of estimating hydraulic conductivity, this reduction is often accomplished by an arbitrary segmentation of the flow domain into a finite number of zones, each characterized by a constant hydraulic conductivity. This discretization of the spatial variability of the conductivity field is one form of model error. Before exploring the effects of this kind of model error on the tomographic method, we will first present results of synthetic tests performed in two simpler aquifers, one consisting of nine constant-resistivity layers and the other consisting of 81 constant-resistivity blocks. The zonations used for parameter estimation will correspond exactly with the geometry of the true conductivity field. This allows us to evaluate the performance of the tomographic method in the absence of model error.

The solid line on Figure II.F.6 represents the true hydraulic resistivity for the simple nine-layer aquifer. This layered resistivity field was created by taking a geometric average of the resistivities of all the cells in sequential five-cell thick layers of the resistivity field shown in Figure II.F.3. Thus, each constant-resistivity layer in the simplified model contains 45 cells in the x direction (the full width of the model domain) and five cells in the vertical direction. The hydraulic tomography program was run in forward mode in order to simulate four different test scenarios in the nine-layer aquifer. The four scenarios examined were a nine-test sequence using nine observation points per test, a nine-test sequence using 27 observation points, a 17-test sequence using nine observation points, and a 17-test sequence using 27 observation points. The forward runs were used to produce head solutions, rather than stream function solutions, in order to provide synthetic head data for the inverse runs. For each test, the heads computed either at all 27 observation points shown in Figure II.F.4 or only those at the nine observation points at x=4.5 were taken as observed heads.

Each test in the suite of nine tests consisted of injecting water at six nodes (bounding a five-cell interval) at the left end of one of the constant-resistivity layers and extracting water at the same rate along the same vertical interval on the right side. The injection rate corresponded to a specific flux rate of 0.5 (L/T) at each node. The fifth test in this sequence, for example, used the same boundary conditions as were used to produce the results shown in Figure II.F.4. The 17-test scenario consisted of the same nine tests with pumping and injection at either end of each layer, plus eight more tests in which the pumping and injection intervals were adjacent to different layers. In the first of these 'crossed' tests, the injection

interval was adjacent to the bottom layer and the pumping interval was adjacent to the top layer. For the next test the injection interval moved up one layer while the pumping interval moved down one layer, and so forth. The middle test of this sequence (with both pumping and injection intervals adjacent to layer five) was included in the original nine tests, and so is skipped in the crossed tests.

The forward runs to produce head data for each test employed specified flux boundary conditions at the pumping and injection intervals. This resulted in the production of a variable head profile over the pumping and injection intervals. These vertically varying heads were averaged over all the nodes in the pumping or injection interval in order to create the boundary heads used as data for the inverse run. In reality, pumping in a well induces a variable flux profile and an essentially constant head along the well intake. Nevertheless, in the absence of data of the sort provided by a flowmeter log, only one flux value and one head value can be assigned to a pumping or injection interval anyway.

Table II.F.1 displays summary statistics for the various tests scenarios in the nine-layer aquifer. The first column displays the correlation between the actual and estimated layer resistivities and the second column displays the root mean squared deviation between these two values. The dashed lines on Figure II.F.6 represent the estimated resistivities for the 9- and 17-test scenarios using nine data points. Figure II.F.7 shows crossplots of true and estimated resistivities for all four test scenarios. Overall, the 17-test scenarios provide a marginally better match to the true resistivity values In the nine tests with the pumping and injection intervals at the same vertical location, flow in the middle of the tested domain is primarily horizontal, with vertical flow restricted to the left and right edges, as shown in Figure II.F.4. The eight additional crossed tests induce more vertical flow in the center of the domain, potentially allowing for better definition of horizontal variation of the resistivity in this region. However, since the properties are assumed to be constant in the horizontal direction, the increased number of more vertical streamlines in the center of the domain contribute little additional information.

Surprisingly, the tests with only nine data points produce somewhat better resistivity estimates (as measured by $\text{cor}(R,\hat{R})$ in Table II.F.1) than those with 27 data points. The streamlines emanating from the 18 data points closer to the left and right edges tend to be more curved than those emanating from the nine data points in the middle of the domain. In addition, those streamlines traveling from each set of 'side' data points to the far well are the longest ones. Increased length and curvature leads to increased potential for inaccuracies in the flux integral calculations. Thus, in this case, it is possible that the additional information

provided by the flux integrals along these streamlines does not offset the deleterious effects of inaccuracies in their calculation.

Figure II.F.8 displays the natural log resistivity field used for the next set of simulated test suites. Each 5X5 block of cells in the 45X45 model grid is represented by a single resistivity value, resulting in a 9X9 array of constant resistivity blocks. The resistivity value assigned to each block is the geometric mean of the cell resistivities for the 25 cells within that block in the fully heterogeneous aquifer shown in Figure II.F.3. The resulting log resistivities for this 81-block aquifer range from -1.90 to 1.97, meaning the actual resistivities range from 0.15 to 7.2. Again, the simulated tests will be analyzed using a zonation corresponding exactly with the true zonation shown in Figure II.F.8 (81 5X5 blocks).

Six different test scenarios were originally used to examine the 81-block aquifer, employing 17, 29 and 45 tests with either nine or 27 data points for each test, as in the nine-layer aquifer tests. The 17-test suite was the same as that described for the nine-layer aquifer. The 29-test suite consisted first of 15 tests, with injection along a four-node (three-cell) vertical interval on the left side and pumping along the same vertical interval on the right side, followed by 14 crossed tests, in a pattern similar to that described for the 17-test scenario. Finally, the 45-test suite employed two-node (one-cell) intervals, with pumping and injection intervals first at the same vertical levels, and then crossed. A greater number of smaller test intervals results in an increased amount of vertical flow. The increased importance of vertical flow should result in a better definition of the horizontal variation in the resistivity. The vertically varying heads along each pumping and injection interval are again averaged before being input as data for the inverse runs.

Analysis of these simulated tests revealed the need for the imposition of bounds on the resistivity estimates. Without bounds, the tomographic inverse algorithm was attempting to drive some resistivity values to zero. Therefore the program was modified so that no resistivity correction would move the corresponding resistivity estimate outside the user-defined upper and lower bounds. This results in a slight alteration of the resistivity correction vector computed using Equation II.F.28. However, the alteration does not appear to adversely affect the overall performance of the algorithm. The upper and lower limits used in the following analyses were 0.1 and 10, respectively. Some experimentation revealed that the value of the imposed lower bound did influence the quality of the estimates somewhat. Therefore, some prior knowledge of a test site would be important in order to define a reasonable lower bound for the resistivities. The upper limit is somewhat less important and can probably be widely overestimated without any harmful results. None of the resistivity

estimates ever started increasing without bound. In fact, the high resistivities were consistently underestimated (meaning low conductivities were overestimated).

Table II.F.2 displays summary statistics for all six simulated test scenarios. The correlation and rms deviation results for the resistivities are displayed in terms of natural log resistivity, since the true resistivities are approximately lognormally distributed in this case. The correlations between true and estimated resistivities increase both with increasing number of tests and increasing number of data points. However, all the correlations are fairly low. The rms deviations decrease with an increasing number of tests, but increase slightly with an increasing number of data points.

The spatial distributions of the estimated resistivities for the test scenarios using 27 observation points are shown in Figures II.F.9A-II.F.9C. Crossplots of the same results are shown in Figures II.F.10A-II.F.10C. The crossplots show clearly that a number of estimated resistivities have been driven to the lower bound of 0.1. Comparison of Figures II.F.8 and II.F.9C shows that the 45-test estimates are indeed beginning to pick up some of the features seen in the true resistivity field. A fairly coarse view of the true resistivity field would split it into five horizontal bands, alternating low-high-low-high-low. This pattern is also beginning to show up in the 45-test results. Note that the definition of the vertical variation is really quite good at the left and right ends of the model domain, immediately adjacent to the wells, while the results are much more ambiguous in the center of the domain.

Due to the fairly disappointing results of the above attempts to identify the spatial variation in the 81-block aquifer, another set of simulations were run to test the influence of the head averaging along the pumping and injection intervals. The data from the test scenarios with 27 observation points were analyzed again, this time using the exact heads computed at the boundary intervals as input data. The summary statistics for these analyses are presented in Table II.F.3. The spatial distribution of the estimates are shown in Figures II.F.9D-II.F.9F and the crossplots of true and estimated resistivity are shown in Figures II.F.10D-II.F.10F. Clearly, the use of the exact head profiles along the pumping and injection intervals leads to a dramatic improvement in the estimates. This is encouraging, since it is possible that the averaging of flux values over a pumping/injection interval that would occur when performing a real test would not have as harmful an effect on the estimates as does the averaging of head values over the interval that occurs when analyzing the synthetic tests.

More surprisingly, the quality of the estimates actually decreases with the increasing number of tests in this case. This implies that the detailed descriptions of a smaller number

of head profiles over longer intervals actually contains more information than detailed descriptions of a larger number of head profiles over shorter intervals. This advantage is lost when only average heads are known over these intervals. Note that the 45-test results do not vary greatly between the analyses using averaged and exact heads. This is not surprising, since heads are averaged over only a two-node interval, so that the averaged heads are not greatly different from the exact heads.

The above sets of experiments show that the experimental configuration described here allows much better definition of vertical variation than it does of horizontal variation. This is a fairly straightforward consequence of the predominantly horizontal nature of the applied stresses and is a well-known characteristic of crosshole seismic tomography [*Peterson et al.*, 1985]. If similar stressed intervals could be placed along the top and bottom boundaries of the aquifer an equally good description of the horizontal variation could be obtained. Fortunately, the most significant variations in hydraulic conductivity occur in the vertical direction at most sites.

The final sequence of simulated tests is carried out in the fully heterogeneous aquifer shown in Figure II.F.3. The same test suite is used for all analyses, the 17-test scenario with 27 data points, described above. Computed heads along the pumping and injection intervals are averaged before being used as input data. Six different zonation schemes are used to analyze the test results, three layered zonations and three zonations using rectangular or square blocks. Figure II.F.11 presents the spatial distributions of the estimated resistivities when the test data are analyzed using the six different zonation schemes. Figure II.F.12 presents the corresponding crossplots of true and estimated resistivities. Since each zone represents a large number of model cells, and therefore a large number of true resistivities, there is no unique value to which to compare each zonal estimate. The 'true' resistivities are represented on Figure II.F.12 by a range of spatial averages of all the resistivities in each zone, with the harmonic average at the left end of each line and the arithmetic average at the right end. The geometric average is represented by the small vertical line in between. These averages are special cases of a general spatial power average [*Desbarats*, 1992b]. Expressed as a discrete average over all N cells in a given zone, the spatially averaged resistivity for each zone is given by

$$R_\omega = \left(\frac{1}{N} \sum_{i=1}^{N} R_i^\omega \right)^{1/\omega}, \quad \omega \neq 0 \qquad \text{(II.F.30)}$$

and

$$R_\omega = \exp\left(\frac{1}{N}\sum_{i=1}^{N}\ln R_i\right), \quad \omega = 0 \qquad \text{(II.F.31)}$$

The harmonic, geometric, and arithmetic averages correspond to w=-1, w=0, and w=1, respectively. One would expect the harmonic and arithmetic averages to provide bounds on the effective resistivities for each zone. From the perspective of the head solution for one-dimensional linear flow, resistivities in series (varying along the direction of flow) would be averaged arithmetically and resistivities in parallel (varying perpendicularly to the direction of flow) would be averaged harmonically. This is the inverse of the averaging rules for conductivities in one-dimensional flow. In addition, *Desbarats* [1991] has demonstrated that the geometric average of point support-scale transmissivities provides a good estimate of effective block-scale transmissivities for various block geometries in two-dimensional linear flow and that the same relationship applies for resistivities. It is impossible to define strictly correct effective resistivities for the simulations performed here, due to the variety of flow configurations experienced by different portions of the model domain during different tests and due to the small dimensions of the zones in comparison to the horizontal and vertical correlation scales of the resistivity field. Nevertheless, it is expected that the range of averages shown approximates the range of 'correct' estimates for the zonal resistivities.

Both the gray-scale (Figure II.F.11) and crossplot (Figure II.F.12) representations show that the layered zonation runs do a good job of reproducing the major features of the true resistivity field. The 9-layer zonation consists of five-cell thick zones and the 15-layer zonation consists of three-cell thick zones. Both produce good estimates overall. The 23-layer zonation consist of 22 two-cell thick layers and one one-cell thick layer (at the top). The results here are still reasonably pleasing, although the correlation with the actual resistivities is beginning to break down.

The three 'block' zonation schemes are derived from the 9-layer zonation, with each layer being successively broken down into three 15X5 blocks (27-block zonation), five 9X5 blocks (45-block zonation), and nine 5X5 blocks (81-block zonation). As expected from the earlier experiments with the 81-block aquifer, the experimental configuration presented here does not allow for reasonable estimation of the horizontal variation of the resistivity and the estimates for all three block zonations are poor. Fortunately, many aquifers do exhibit pronounced stratification in their hydraulic properties and for many purposes can be adequately represented by a layered model.

Concluding Remarks

The synthetic examples described above demonstrate the validity of the proposed inverse method. This method could be applied essentially without modification to planar flow problems, such as horizontal flow in a confined aquifer, provided enough data were available to allow reliable estimates. To be applied to the experimental configuration described here, stressing different isolated intervals of two different wells in order to characterize the hydraulic conductivity distribution between them, the method has to be modified to account for the dual radial flow system involved. This is the subject of ongoing work.

The practicality of the method remains to be tested in the field. One reason for presenting numerical tests based on a two-well (pumping and injection) configuration is that this configuration is expected to produce steady state (actually, steady-gradient) more rapidly than a single-well configuration. Once steady state has been obtained in the field, a fairly large number of head data must be obtained, including measured heads in the pumping and injection wells. These heads must be accurate and all referenced to the same datum, since the parameter estimation process works with differences in measured head. To obtain a reasonable number of streamlines, the testing process needs to be repeated a number of times, using different pumping and injection intervals.

	cor(R,$\hat{R}$)	rmsd(R,$\hat{R}$)	cor(h,$\hat{h}$)	rmsd(h,$\hat{h}$)
9 tests, 9 obs.	0.91	0.83	0.94	0.12
9 tests, 27 obs.	0.89	0.90	0.95	0.13
17 tests, 9 obs.	0.95	0.81	0.96	0.11
17 tests, 27 obs.	0.93	0.80	0.96	0.12

TABLE II.F.1. Correlation (cor) and root mean squared deviation (rmsd) between true and estimated resistivities (R and $\hat{R}$) and between observed and predicted heads (h and $\hat{h}$) for different test scenarios in the simple nine-layer aquifer; 'obs.' is the number of observation points employed in each test.

	cor(lnR,ln$\hat{R}$)	rmsd(lnR,ln$\hat{R}$)	cor(h,$\hat{h}$)	rmsd(h,$\hat{h}$)
17 tests, 9 obs.	0.28	1.14	0.82	0.40
17 tests, 27 obs.	0.38	1.17	0.91	0.19
29 tests, 9 obs.	0.36	1.08	0.86	0.18
29 tests, 27 obs.	0.45	1.09	0.93	0.12
45 tests, 9 obs.	0.52	0.99	0.94	0.08
45 tests, 27 obs.	0.56	0.97	0.96	0.06

TABLE II.F.2. Correlation and root mean squared deviation between natural logs of true and estimated resistivities and between observed and predicted heads for different test scenarios in the 81-block aquifer using averaged heads along pumping and injection intervals.

	cor(lnR,ln$\hat{R}$)	rmsd(lnR,ln$\hat{R}$)	cor(h,$\hat{h}$)	rmsd(h,$\hat{h}$)
17 tests	0.79	0.67	0.96	0.14
29 tests	0.77	0.71	0.98	0.14
45 tests	0.67	0.82	0.97	0.05

TABLE II.F.3. Correlation and root mean squared deviation between natural logs of true and estimated resistivities and between observed and predicted heads for different test scenarios (all using 27 observation points) in the 81-block aquifer using exact heads along pumping and injection intervals.

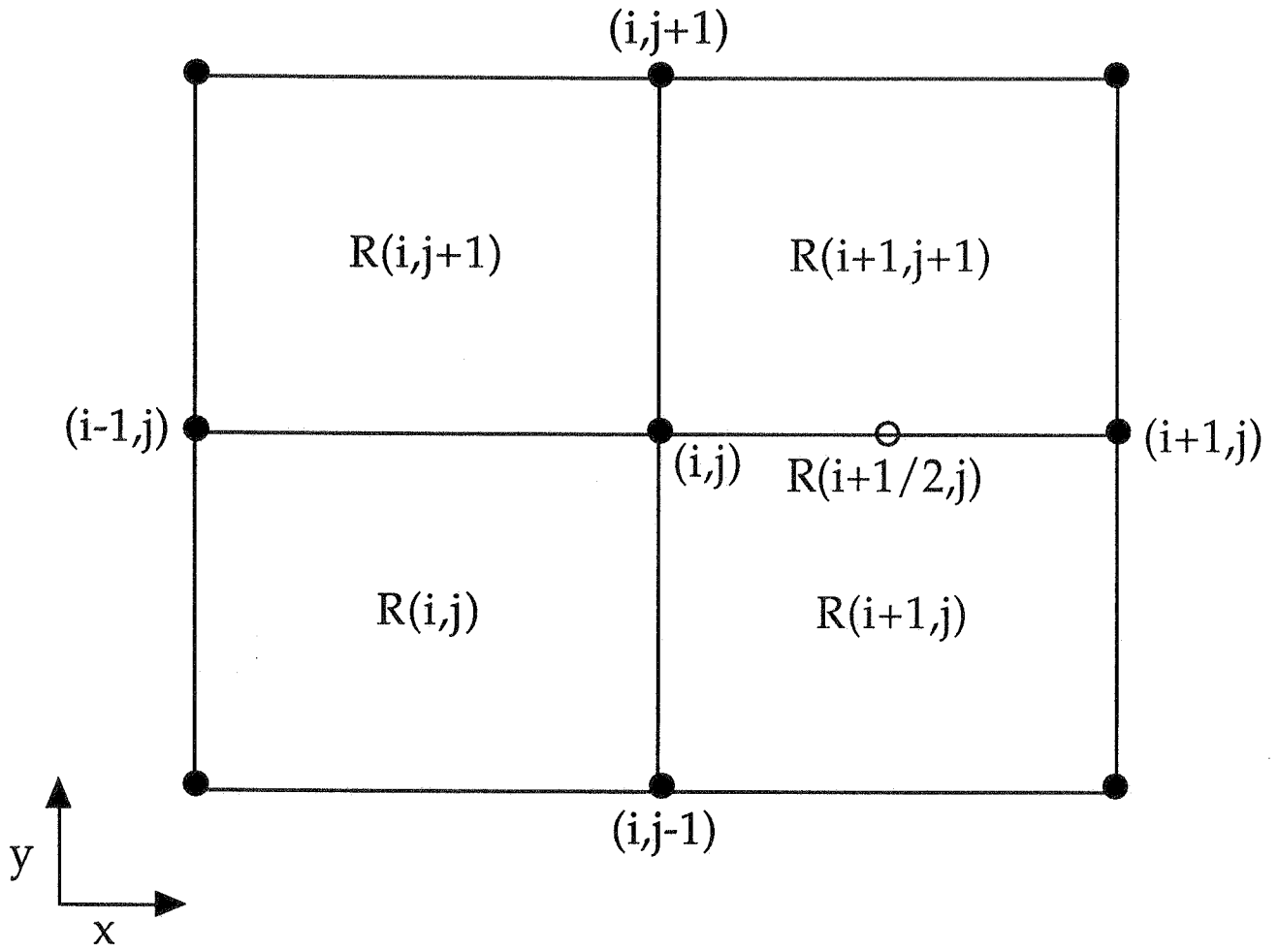

Fig. II.F.1. Computational node (i,j) and adjacent nodes and cells in a mesh-centered finite difference formulation.

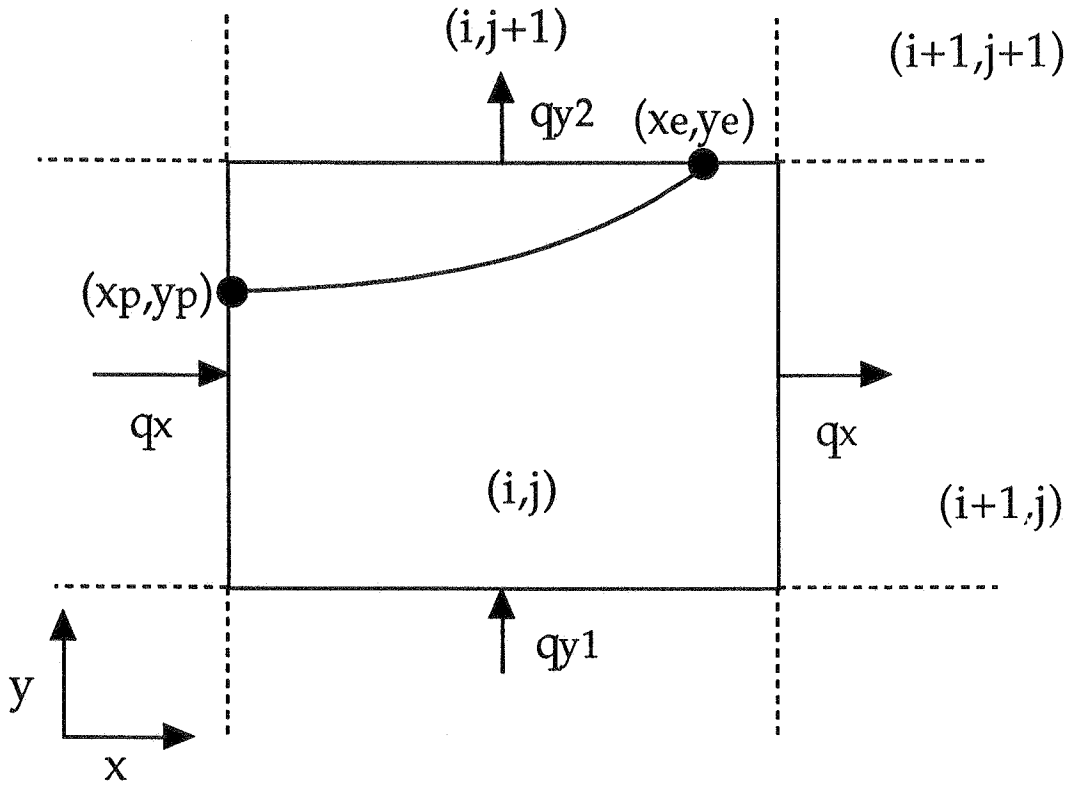

Fig. II.F.2. Typical finite difference cell, with one possible pathline shown. [After *Pollock*, 1988, Figure 2.]

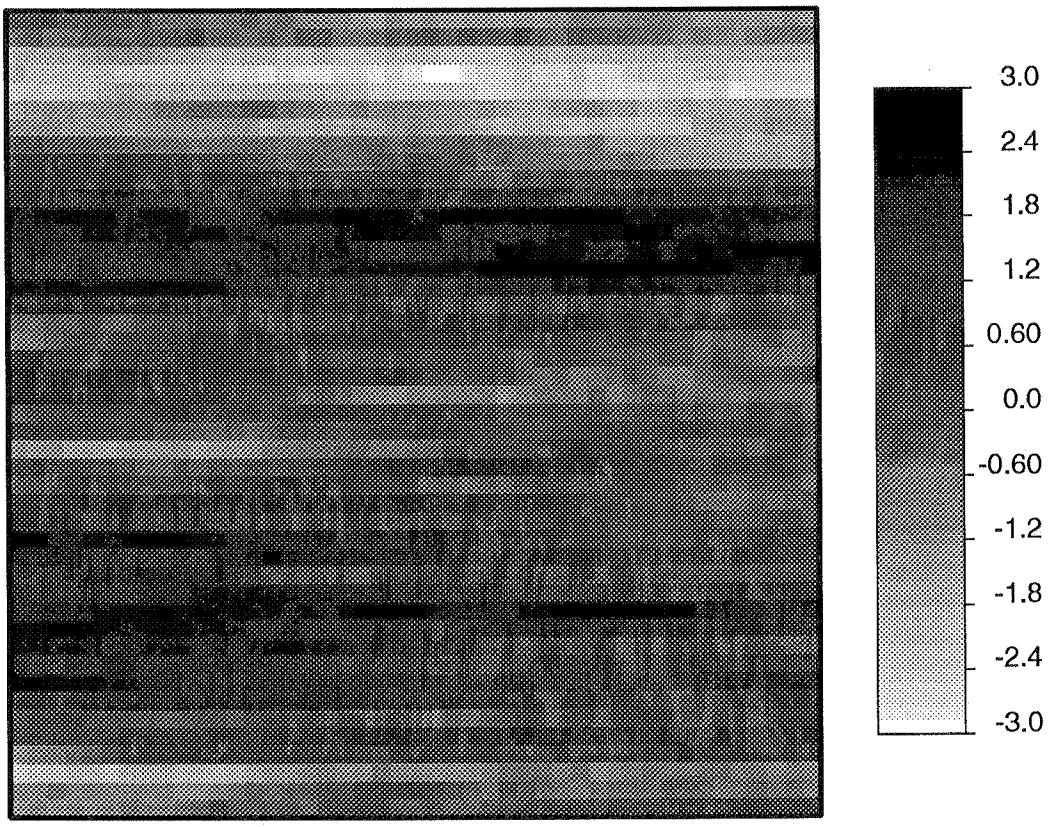

Fig. II.F.3. Natural log of true hydraulic resistivity in tested region, nine units on a side. Grid cells are 0.2 units on a side, resulting in a 45X45 array of grid cells.

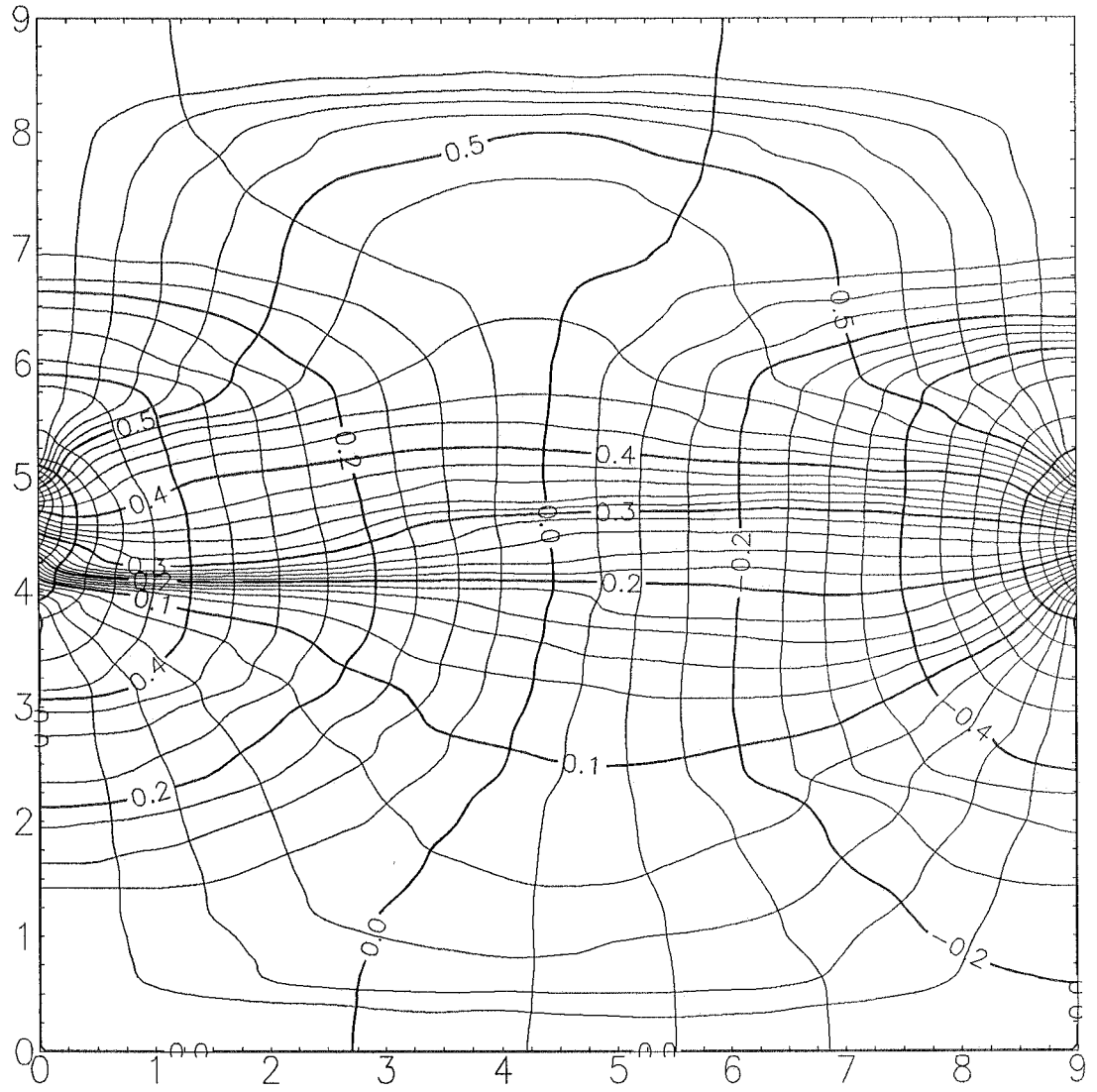

Fig. II.F.4. Contours of head solution (contours near vertical in center of domain) and stream function solution (contours near horizontal in center of domain) for a single test in the resistivity field shown in Figure II.F.3. Plus signs represent data points used in single-test forward run.

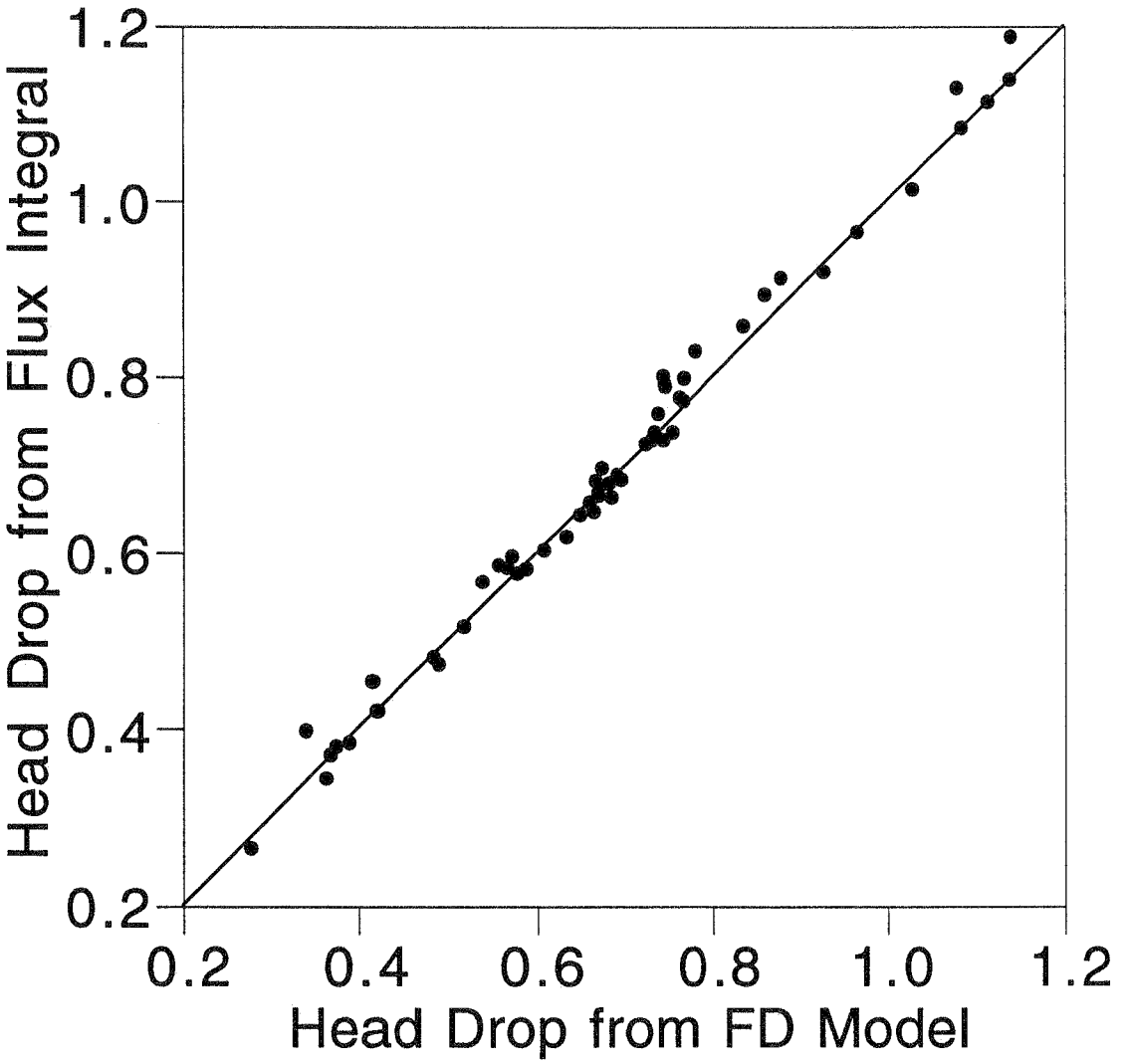

Fig. II.F.5. Head drops calculated from flux integrals along streamlines versus head drops computed from differences of heads computed at finite difference model nodes at each end of streamline.

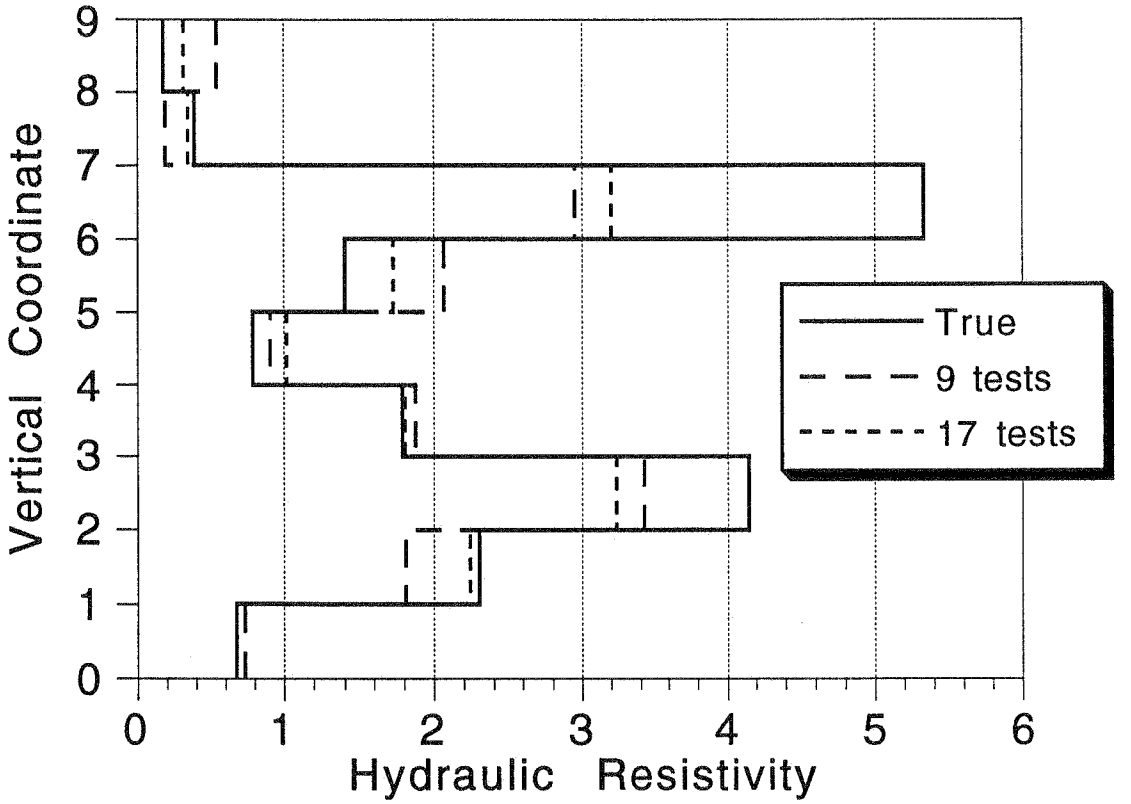

Fig. II.F.6. True and estimated hydraulic resistivities for tests in simple nine-layer aquifer versus height above aquifer base; estimates from nine- and 17-test inverse runs using nine observation points for each test.

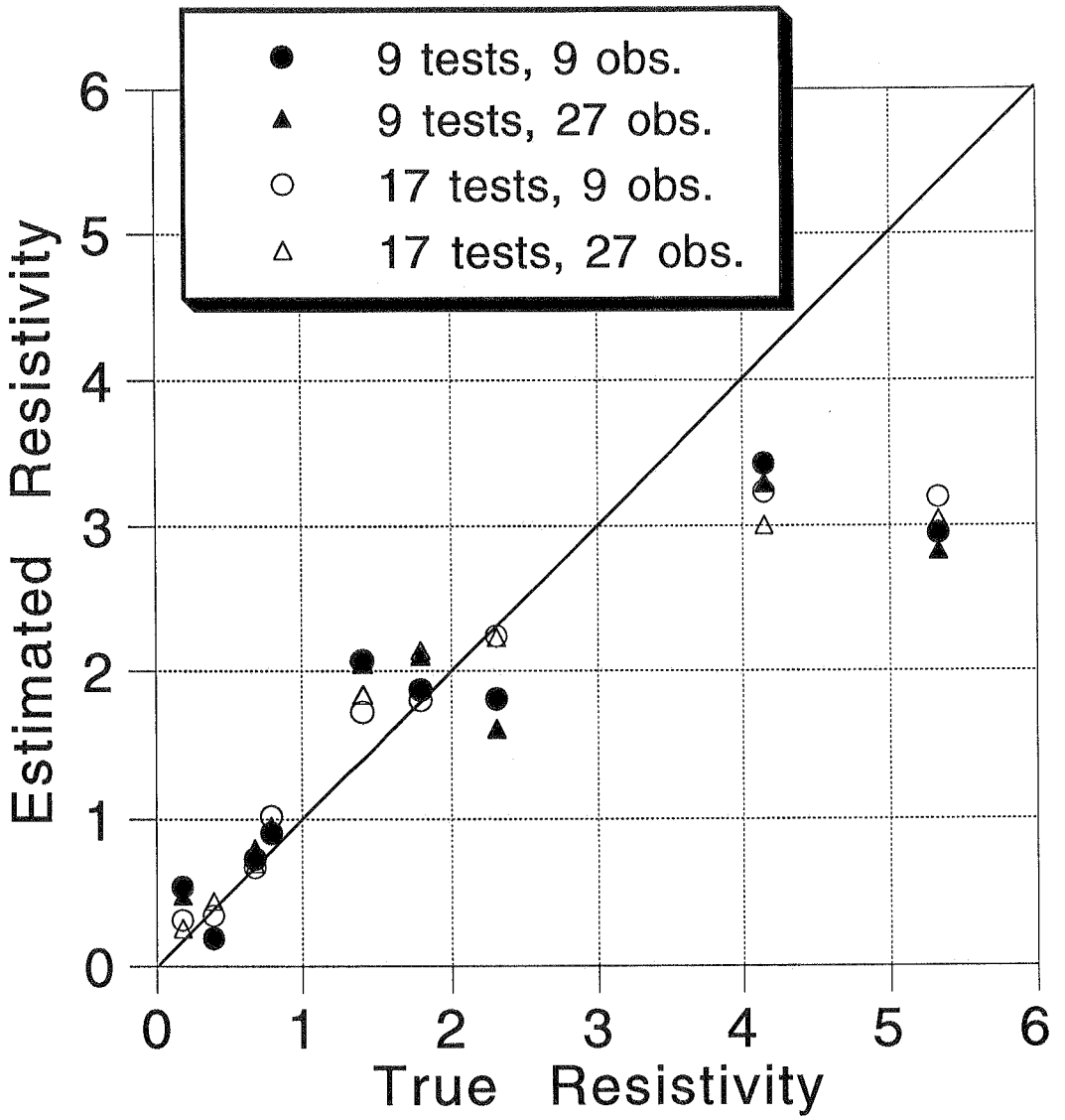

Fig. II.F.7. Crossplots of true and estimated resistivities for tests in nine-layer aquifer using different test scenarios.

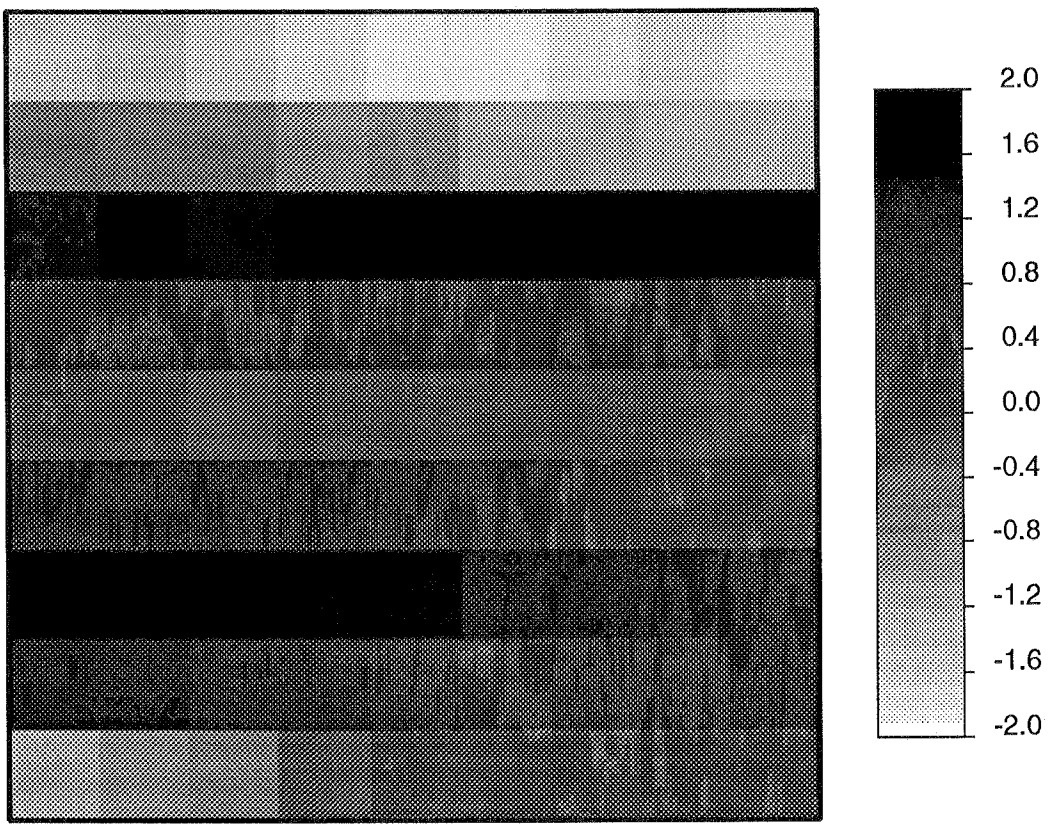

Fig. II.F.8. Natural log of true hydraulic resistivity in 81-block aquifer. Each block consists of a 5X5 array of cells.

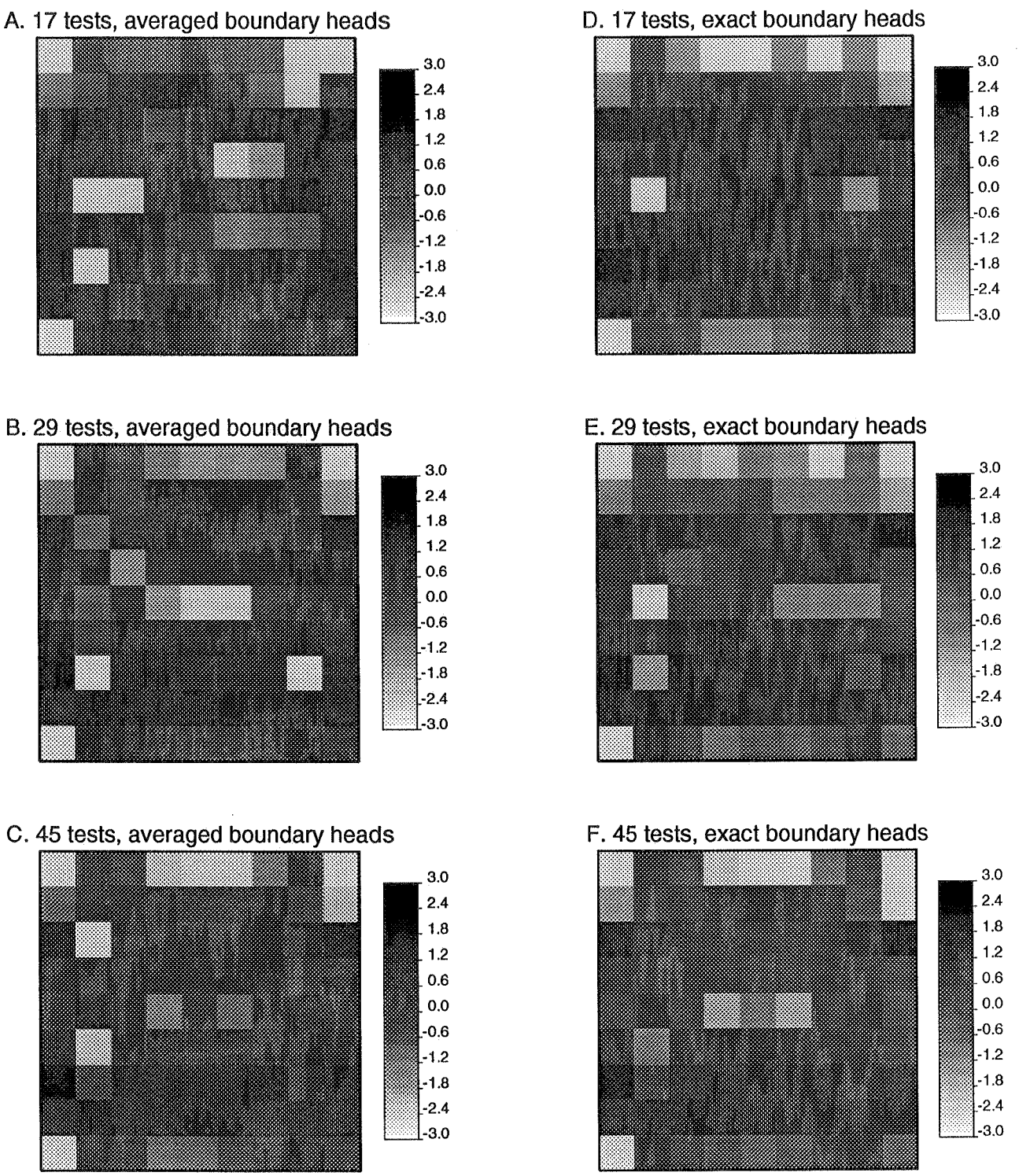

Fig. II.F.9. Spatial distributions of natural logs of estimated hydraulic resistivities for different test scenarios in 81-block aquifer, all using 27 observation points per test. Results of inverse runs using averaged heads along the pumping and injection intervals are shown on the left and those using exact heads are shown on the right.

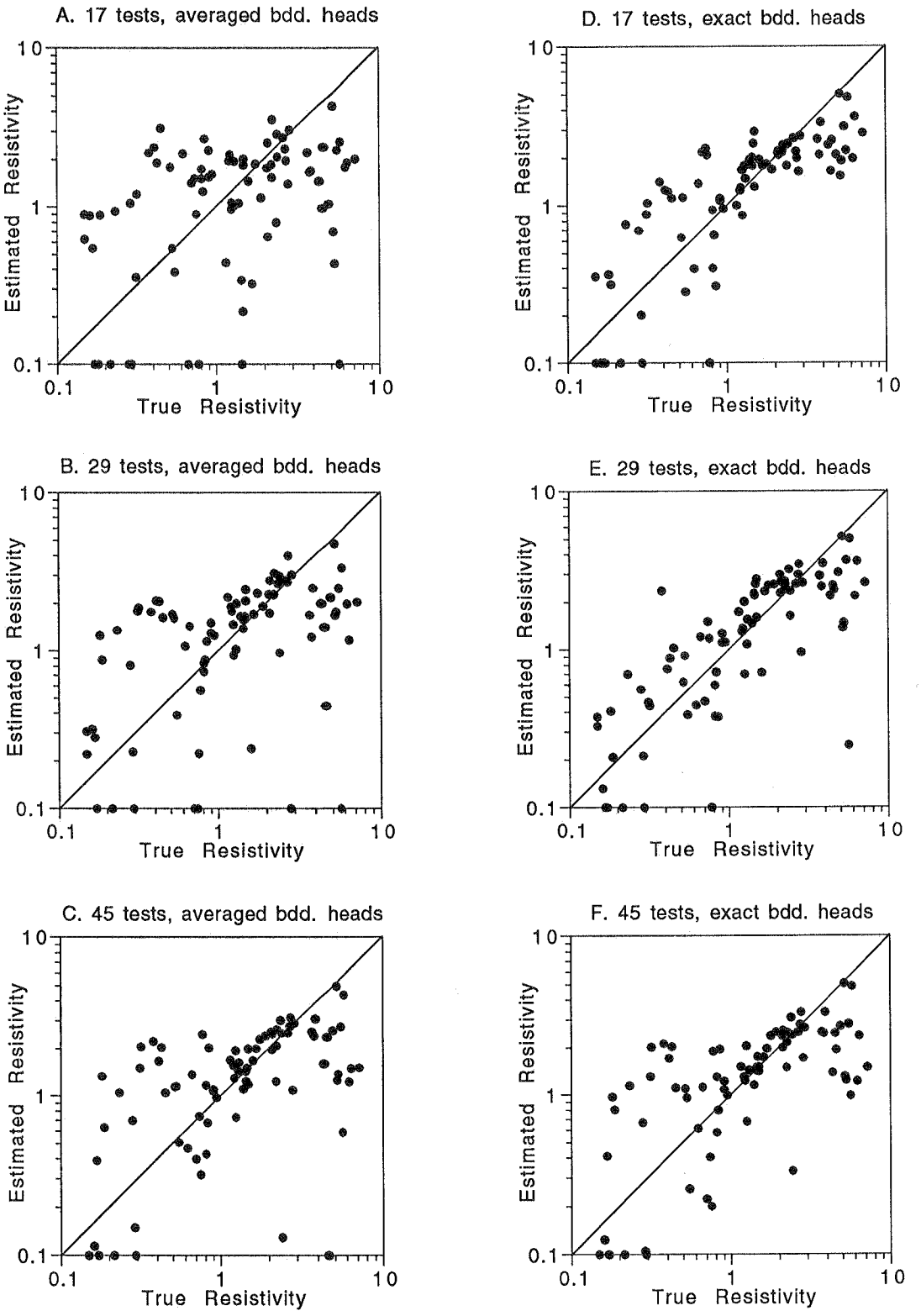

Fig. II.F.10. Crossplots of true and estimated hydraulic resistivities for different test scenarios in 81-block aquifer, all using 27 observation points per test.

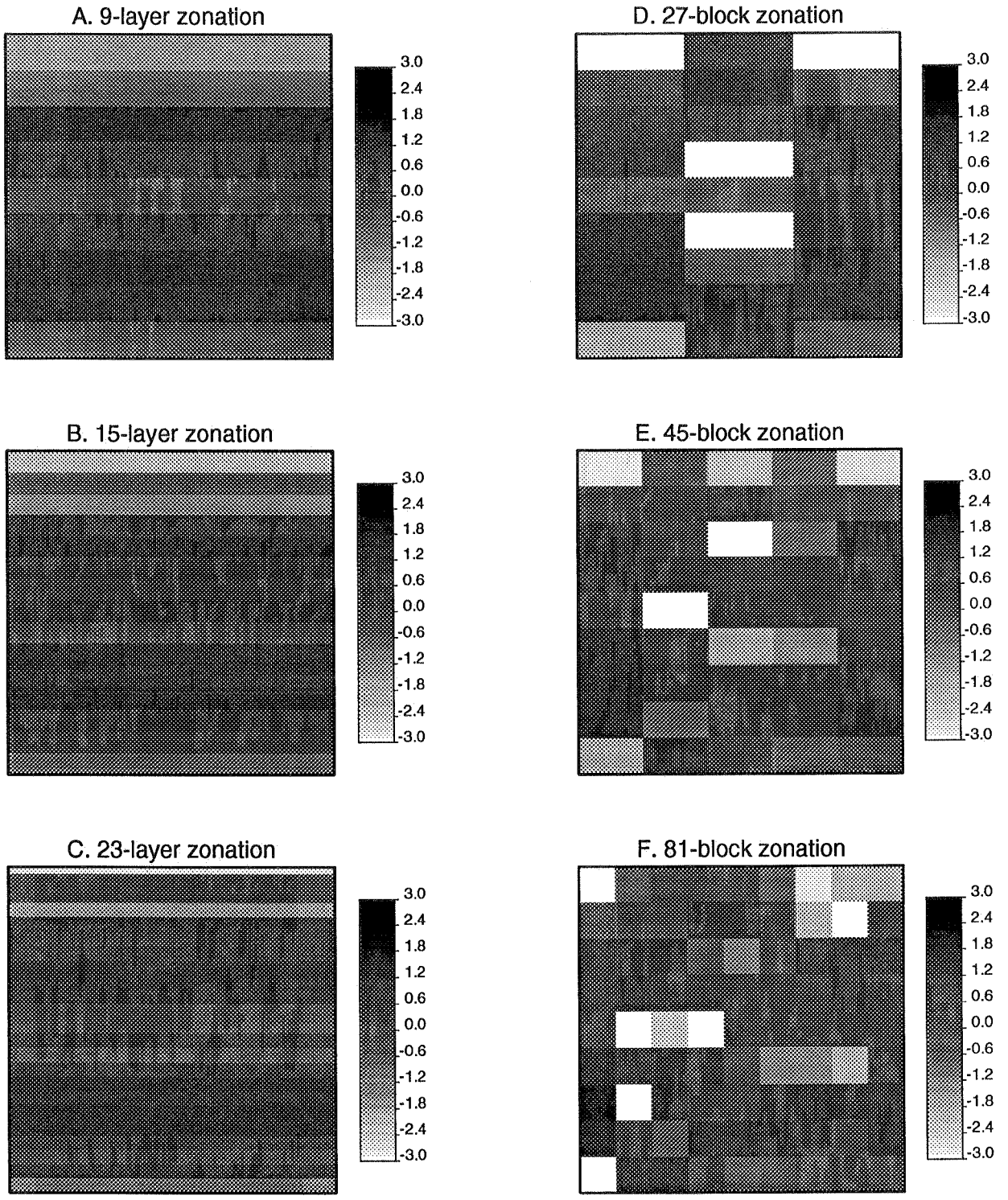

Fig. II.F.11. Natural logs of estimated resistivities using different zonations and a single test scenario (17 tests, 27 data points, averaged boundary heads) in the fully heterogeneous aquifer (shown in Figure II.F.3).

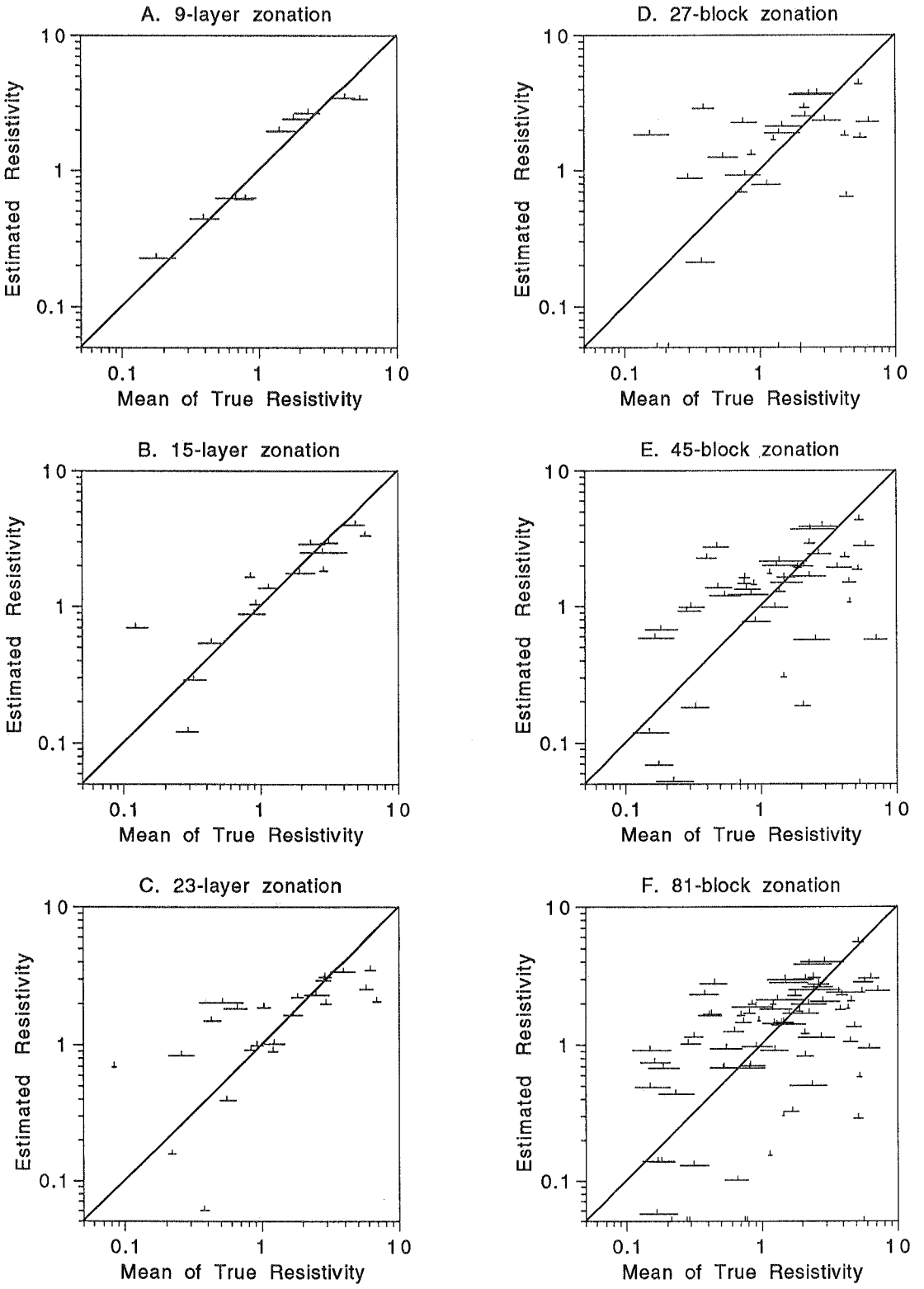

Fig. II.F.12: Estimated zonal resistivities versus range of mean resistivities for all cells in each zone. The lines representing the range of means extend from the harmonic mean (left end) to the arithmetic mean (right end), with the geometric mean represented by the small vertical line in between.

III. FIELD INVESTIGATIONS OF SLUG TESTS

A. KGS MULTILEVEL SLUG-TEST SYSTEM

In 1989, a slug-test system was developed at the KGS for the purpose of performing slug tests in wells of small diameters (0.05 m ID) located in highly permeable alluvial units (McElwee and Butler, 1989). This equipment served as the basis of a multilevel slug-test system that is being developed for the research described in this report. A prototype straddle-packer system for multilevel slug tests has been constructed at the KGS (see Figure 1 of Section II.B for a schematic drawing of this system). The prototype system consists of two packers (each approx. 0.67 m in length when fully inflated) that are used to seal off the test interval from adjacent portions of the well screen. A section of 0.025 m ID PVC (SCH 40) pipe is connected to the central flow-through pipe of the top packer of the pair. A series of sections of the 0.025 m ID PVC pipe runs to a third packer located above the top of the screened interval. This pipe allows the pressure pulse initiating a slug test to be confined to the straddle-packer interval. The central flow-through pipe of the middle packer is closed off prior to testing. A slug test is initiated by adding or removing water to the casing above the third packer and then opening the central flow-through pipe in the middle packer. As with the original KGS slug-test system (McElwee and Butler, 1989), the central flow-through pipe is opened by the mechanical lowering of a plug attached to pump rods. Note that other initiation mechanisms, such as via pneumatic means (e.g., Orient et al., 1987) or water displacement using a solid object of a known volume, could also be employed with this system. Although the test interval can be up to several meters in length, it cannot be less than 0.29 m in the present configuration.

After the completion of testing at one level, the packers are deflated and the string of packers and pipes is moved until the straddle-packer interval is opposite the next zone to be tested. The string can be moved without modification until the top of the third packer is raised above the static water level or lowered below the top of the screen. At that point, a section of PVC pipe must be either removed or added, respectively, to the pipe string connecting the straddle packer to the top packer, prior to further tests. In this manner, a series of multilevel slug tests can be readily performed across the entire screened interval of a well in a relatively short period of time. At shallow depths the string of packers and pipes can be lifted manually, while at deeper depths a special tripod and winch arrangement, which was

constructed during the first year of this project, is employed. Note that the packers used in this system were designed and constructed at the KGS. Commercially available packers for use in 0.05 m ID wells have central flow-through pipes that are 0.0125 m ID or smaller. Packers with larger flow-through pipes (0.025 m and 0.019 m) were designed in an effort to reduce the influence of the flow-through pipe diameter on test responses. The hope was that the parameters estimated from the response data would be reflective of properties in the aquifer, and not the diameter of the flow-through pipe.

As stated above, slug tests are initiated by adding or removing water from the cased section of the well above the third packer. In all cases, pressure transducers (PS7000 and PS9000 series, Instrumentation Northwest, Inc.) placed above the third packer are employed to monitor water-level responses in the test well. During the field season, the transducers are calibrated in the laboratory on a monthly to bimonthly basis using the equipment described in subsection IV.B. Between laboratory calibrations, transducer functioning is checked in the field by measuring the height of the column of water above the transducer using an electric tape (Model 101 flat tape water meter, Solinst Canada Ltd.). The transducers are connected to one of two types of data acquisition devices: a stand-alone datalogger (21X datalogger, Campbell Scientific, Inc.), or a data acquisition card (PC/IEEE 488 General Purpose Interface Board, IOtech, Inc.) placed in a personal computer.

In the following section, the use of this equipment in an initial series of multilevel slug tests at GEMS is described.

B. MULTILEVEL SLUG TESTS AT GEMS

Multilevel Tests at GEMS 2-5

The prototype KGS slug-test system described in the previous section was employed in a series of multilevel slug tests at GEMS. GEMS well 2-5 (depth = 20.67 m, screen length = 9.14 m), which is screened essentially through the entire sand and gravel section at the site, was used for these tests. An initial series of tests was run in which the slug consisted of the volume of water required to raise water levels 3.07 meters in the cased section of the well (H_0=3.07 m). As shown in Figure III.B.1, the slug-test responses measured at the different depths were very similar. Note that Table III.B.1 lists the depths corresponding to each test interval. Although the variation in hydraulic conductivity values calculated from permeameter tests performed on core samples taken from a nearby well (GEMS 2-6) at these same depths was not large (Butler et al., 1991), a greater variation in slug-test responses than that shown on Figure III.B.1 was expected. Therefore, the decision was made to repeat the series of slug tests using H_0's of different magnitudes to see if greater discrimination between test intervals would be possible using a different H_0. Figure III.B.2 shows a plot for slug tests over the same intervals as Figure III.B.1 using a H_0 of approximately 1.65 m. A comparison of the two figures shows that, although there is little difference between tests using the same H_0, there is a considerable difference between tests using different H_0's. Normalized plots of the slug-test responses from a series of tests in the third test interval using differing H_0's are presented in Figure III.B.3. Note the dramatic dependence of the slug-test responses on the magnitude of H_0. Dependence relationships of this form were seen in all the tested intervals. Table III.B.1 summarizes the parameters calculated from the slug-test responses for a subset of the tested intervals. In all cases, the higher the H_0, the lower the calculated conductivity. The inverse relationship between the magnitude of H_0 and the calculated conductivity existed over the entire range of H_0's employed in these tests. Experiments have shown that differences in H_0 as small as 0.03 meters (e.g., Figure III.B.3) will still produce conductivity differences in the direction predicted from this relationship. Thus, the small differences in H_0 that exists between the tests shown on Figure III.B.1 or Figure III.B.2 could largely explain the differences displayed on those plots. Note that when special care was taken to ensure that the same volume was used for the slug in repeat tests at a given interval, the plots of the responses for the repeat tests coincided.

It is important to note that the theory from which the conventional methodology used for slug-test analysis (e.g., the CBP or Hvorslev models) was developed holds that slug-test responses should be independent of H_0. In other words, plots of responses from slug tests performed using different H_0's normalized by the H_0 used in each test should coincide. Clearly, the multilevel slug tests at GEMS are being affected by processes not considered in the standard theory. It is doubtful, however, that these additional processes are solely responsible for the smaller-than-expected variation seen in the vertical. Based on the simulation results described in Section II.B, we suspect that the small variation with depth is also a result of a high-permeability skin that formed during well installation.

The dependence of slug-test responses on H_0 was not the only anomalous behavior observed during the multilevel slug tests at GEMS. Figures III.B.1 - III.B.3 are plots of slug-test responses presented in the format of the Hvorslev method (log head versus arithmetic time). Note the concave downward form of the curves. Conventional theory dictates that these plots should be concave upward or straight lines (Chirlin, 1989; McElwee et al., 1990). Nothing in the conventional theory would allow for concave downward plots. Additional indications that the multilevel slug tests at GEMS are being affected by processes not considered in the standard theory are seen in Figures III.B.4 and III.B.5, where the response data are fitted using conventional approaches (CBP and Hvorslev techniques). The systematic deviations displayed on these plots between the fitted model and the data are characteristic of the behavior observed in every multilevel slug test performed in GEMS well 2-5.

Clearly, the processes that are producing these anomalous responses need to be explained before much useful information can be obtained from multilevel slug tests at GEMS. The decision was therefore made to suspend multilevel slug testing and to concentrate on trying to explain the observed behavior. The objectives of this phase of the research project thus shifted to the definition of the underlying mechanisms causing the anomalous behavior, and the incorporation of these mechanisms into a general theory that could be the basis of new techniques for the analysis of slug-test response data. In the following pages, a series of field experiments, which were performed in an attempt to define the relevant processes, are described. These experiments led to the development of nonlinear flow models that are described in the next section.

Field Experiments to Explain Anomalous Behavior

A series of field experiments was designed to investigate possible explanations for the observed behavior. Factors that could be causing the observed behavior include the following: 1) Frictional flow losses - these could occur in the cased region of the well above the top packer, within the PVC pipe connecting the straddle packer to the top packer, within the packer flow-through pipes, and within the well screen; 2) Non-Darcian flow within the aquifer in the vicinity of the well screen; 3) Aquifer heterogeneities; and 4) Measured pressure not reflective of water level position - the transducers used in the field tests are measuring pressure, which may not always equate to the position of the water level.

An extensive series of field experiments was designed to test the possibility of frictional flow losses in each of the components of the system listed above. In order to simplify the testing procedure, the multilevel slug-test system was not used for these experiments. Instead, all experiments were carried out using a single packer inflated in the cased region of a well with a short screened interval. This configuration allows for a long length of well casing between the top of the packer and the static water level.

GEMS well 10-1 (depth = 17.25 m, screen length = 0.76 m, diameter = 0.051 m) was selected for the initial series of tests. The packer was placed just above the screened region and two transducers were placed in the well above the packer. One transducer was placed immediately above the packer (7.59 m below static water level) and one was placed slightly below the static water level (0.58 m below static water level). Thus, there was 7.01 m of casing separating the two transducers. If there are significant flow losses within the casing, normalized plots of the data from the two transducers should differ. Figure III.B.6 displays data from two tests of this series: Test 1, which employed an H_0 of 1.07 m, and Test 6, which employed an H_0 of 6.83 m. Note that for both tests the early-time data display pressure oscillations that are attributed to the water hammer effects accompanying the opening of the flow-through pipe in the packer. In both tests, the transducer closest to the packer displays the largest early-time pressure oscillation, consistent with a water hammer explanation (Parmakian, 1963). After the early-time pressure transients have passed, there is little to no difference between the normalized pressure measurements from the two transducers. Thus, frictional flow losses within the cased region of the well do not appear to be an important mechanism for these tests. Note that Figure III.B.6 clearly indicates that the dependence of slug-test responses on H_0 is seen with

the single packer setup. Note also that a Hvorslev plot of the tests of Figure III.B.6 will display a marked concave downward curvature. Thus, the same behavior was observed in the single packer tests as in the multilevel slug tests. This would imply that the PVC pipe employed in the multilevel system is not primarily responsible for the observed behavior.

The next series of field tests was designed to assess whether frictional losses within the flow-through pipe of the packer could be an explanation for the observed behavior. In order to test the importance of this mechanism, a transducer must be placed below the packer and isolated from the region above the packer. Unfortunately, there is not enough room in a 0.051 m ID well to place such a transducer-packer arrangement. Therefore, work was shifted to GEMS well 0-6 (depth = 24.69 m, screen length = 1.52 m, diameter = 0.127 m), which at the time of these tests was the only large-diameter monitoring well at the site. Unfortunately, GEMS well 0-6 is screened in the bedrock underlying the alluvial deposits, so the velocity of the slug-test induced flows is somewhat lower than in the wells sited in the sand and gravel section of the alluvium. Preliminary testing, however, did reveal that the slug-test responses at this well displayed a similar dependence on H_0. In addition, a slight downward curvature was seen on Hvorslev plots of tests when a very large H_0 (7.39 m) was employed. Thus, even a well sited in material of lower permeability displayed much of the same anomalous behavior.

A simple transducer-packer arrangement was constructed at the KGS for this set of experiments. The transducer cable was run through the central flow-through pipe of the packer until the bottom of the packer, a short distance above the location of the plug used to initiate the slug tests, at which point it was passed out of the flow-through pipe at a T connection. A compression fitting was placed on the cable at the T connection to ensure that no water leaked to/from the flow-through pipe along the transducer cable. This setup enabled the transducer to be placed below the packer, isolated from the region above the packer. A series of experiments was performed in the field and laboratory to ensure a watertight seal was obtained with the compression fitting and that the transducer was truly isolated from the cased region above the packer. Neither in these experiments nor in any of the following tests was there any indication of leakage in this system.

Figure III.B.7 displays the head data from a test (H_0 = 6.88 m) using the transducer-packer arrangement. The upper transducer is located above the packer, 0.46 m below the static water level. The lower transducer is located below the packer, 11.88 m below the static water level (total distance between the two

transducers is 11.42 m). The plotted data show that there are differences between the two transducers in the early portions of the test. These differences, however, become negligible later in the test. Some flow losses do seem to occur within the packer flow-through pipe, but, since the differences do not extend through the entire test, they are probably not the primary reason for the observed head dependence. A comparison of Figures III.B.6 and III.B.7 shows that recovery to the static water level in the bedrock well takes much longer than in the wells sited in the sand and gravel section. The velocities in the flow-through pipe in the wells in the sand and gravel section are clearly much greater than in the bedrock well and thus the effect of frictional losses in the flow-through pipe should be larger. However, given that a similar dependence on H_0 is observed in the bedrock and alluvial wells, frictional losses in the flow-through pipe are probably not the primary mechanism producing the anomalous responses. Note that for the four tests of this series performed with H_0's less than or equal to 2.33 m, the difference between the readings from the two transducers was at the same level as experimental noise.

In order to further assess the role of the packer flow-through pipe in the production of the observed behavior, an additional series of experiments was run in which the packer arrangement was not employed. Instead, PVC pipes (0.06 m OD) of differing lengths (1.60 and 3.10 m), which had been filled with sand and sealed at both ends, were used to perform the slug tests. A slug test was initiated by rapidly lowering a PVC pipe below the static water level, causing a rise in water levels. Pipes of different lengths cause the H_0's to be different (H_0 = 0.36 m for short pipe and = 0.69 m for large pipe). Figure III.B.8 displays the results from two tests of this series. As with tests using the packer, a dependence on H_0 is observed. Thus, flow losses in the central flow-through pipe in the packer do not appear to be the primary mechanism producing the observed dependence on H_0. Note that repeat tests were performed as part of this series, and the pattern displayed on Figure III.B.8 was reproduced in the repeat tests.

In the final year of this research, an additional series of tests was performed in order to further confirm the results of Figure III.B.8. In these tests, a pneumatic approach (see Section III.E) was used to introduce the pressure disturbance. Tests were performed at GEMS well 06 as well as at GEMS well 00-1 (depth = 17.04 m, screen length = 0.76 m, diameter = 0.051 m, screened in the sand and gravel interval). Figure III.B.9 shows the results of the tests at GEMS well 06, with one of the tests from Figure III.B.8 shown for comparison purposes. Although repeat tests were not performed at GEMS well 06, there does seem to be an apparent head

dependence in these data. Figure III.B.10 shows the results of the tests performed at GEMS well 00-1. Since the responses from the GEMS 00-1 test series were oscillatory in nature, the head dependence was different in form from that seen in the other tests. In this case, the head dependence was displayed in the amplitude and timing of the peaks of the normalized oscillations. As shown in Figure III.B.10, the amplitude of the normalized oscillations was considerably larger in the low H_0 test. In addition, the timing of the peaks was slightly lagged in the high H_0 test. Although only two tests are displayed on Figure III.B.10, repeat tests demonstrated that this head dependence was reproducible. Thus, this later set of experiments confirm the earlier results that flow losses in the central flow-through pipe in the packer are not the primary mechanism producing the dependence of test responses on H_0.

Frictional losses in the well screen appear to be a possible explanation for the observed behavior. Unfortunately, there is not an easy way of testing the importance of this mechanism in the field. An initial attempt at assessing the importance of frictional losses in the well screen was made using the transducer-packer arrangement discussed earlier. In this case, a piece of well screen (1.52 m in length) was screwed on to the bottom end of the flow-through pipe. The transducer situated below the packer was located outside this section of screen. The idea was to mount a piece of screen whose slot size was smaller than that used in the well screen at GEMS well 0-6. If frictional losses in this screen are important, measurements from the transducer located below the packer outside the mounted screen should differ from the measurements from transducers above the packer. A series of experiments with screens of two different slot sizes were performed. In all cases, the responses were similar to those of Figure III.B.7. There were no additional losses of any significance. We suspect, however, that this result may be more of a function of experimental design (i.e. slot sizes of mounted screen are too large, slots of screen in well are encrusted with mud, etc.), so further tests are planned both in the laboratory and field in an attempt to better assess the importance of this mechanism.

Aquifer heterogeneities could perhaps be invoked as an explanation of the observed phenomenon. However, simulations that were performed as part of the theoretical work described in Section II.B demonstrated that aquifer heterogeneities are not going to produce a dependence on H_0 in perfectly stratified systems. This result will apply to a system of discontinuous layers as well.

Most slug tests in moderate to highly permeable media are performed using submersible pressure transducers to record changes in water levels. These

transducers are assumed to be measuring the hydrostatic pressure exerted on the sensor by the overlying column of water. Actually, however, these sensors are measuring both static and dynamic components of pressure. If the dynamic component of pressure is significant, the measured pressures will not be reflective of actual water levels. Potentially, this effect could be contributing to the observed behavior at GEMS.

A series of experiments was performed in order to assess the difference between the pressure measured by the transducers and the actual water level in the well. GEMS well 0-6 was employed for this series of experiments because it was the only large-diameter well located at GEMS at the time of these experiments, and the experimental setup required a 0.01 m ID well or larger. These experiments used a single packer inflated a short distance above the well screen. A transducer was placed above the packer, several meters below the static water level. An ultrasonic distance transmitter (LV401 non-contact ultrasonic level/distance transmitter, Omega Engineering, Inc.), placed over the top of a 0.05 m ID drop pipe held in position by chain vice grips, was used to provide an independent measurement of the position of the actual water level. This transmitter measures the position of the water level using the travel time of an ultrasonic signal reflecting off the water surface. A comparison of the ultrasound data and the pressure transducer data should reveal any errors arising from use of pressure transducers to record changes in water levels. Note that the ultrasonic transmitter was placed in a drop pipe so that reflections off the pump rods used with the packer could be avoided. The ultrasonic transmitter had been preset at the factory for measurement in air at a temperature of 20°C. Thus, immediately prior to performing this series of slug tests, the ultrasonic transmitter was calibrated to reflect the air temperature at the onset of the test period. The manufacturer estimates that there is an approximate 1 percent shift in accuracy per 10°C deviation from 20°C.

Figure III.B.11 displays plots of the ultrasound and transducer data (both adjusted so that the static water level is the reference point) and their difference for one of the slug tests performed in this series of experiments. Note that nonnegligible differences are displayed at two intervals on the plot. The first interval encompasses the initial seconds of the slug test. Clearly, there are pressure oscillations during this period that are not due to actual movement of the water level in the well. We feel that these oscillations are due to the earlier-described water hammer effects and do not play a role in the anomalous behavior observed at larger times. The second interval occurs at the end of the plotted record and is due to the water level

beginning to fall outside of the range of the ultrasonic distance transmitter that we were employing for this series of experiments. Although we were only able to compare the ultrasound and transducer data over a limited range of distances, it is clear that the assumption that a pressure transducer is measuring the hydrostatic pressure exerted by the overlying column of water is appropriate for slug tests performed in wells screened in moderately permeable systems such as the bedrock in which GEMS well 0-6 is screened. Note that the results displayed in Figure III.B.11 are reflective of all the tests performed as part of this series of experiments at GEMS well 0-6, regardless of the H_0. Since the data for GEMS well 0-6 do display a pronounced dependence on H_0 (Figure III.B.9), transient dynamic pressure effects do not appear to be a primary explanation for the observed head dependence.

Non-Darcian flow within the aquifer in the vicinity of the well screen is also a possible explanation for the observed behavior. Since velocities in the well screen and the adjacent portions of the aquifer will be dependent on H_0 and the radius of the well screen (r_w), an additional series of tests was performed near the end of this research project to assess if there was an H_0 below which or a r_w above which test responses would not be dependent on H_0. Two large diameter wells were drilled in the sand and gravel aquifer underlying GEMS in the later phases of this project. One of these wells, GEMS well 0-9 (depth = 17.29 m, screen length = 0.76 m, diameter = 0.102 m), was the site of an extensive series of tests (total of 16 tests) in which H_0 was varied between 0.02 m and 6.07 m. These tests were done in a cyclic fashion, going from a low H_0 to a high H_0 and then back to a low H_0. A high-accuracy pressure transducer (In-Situ PTX-161 series 0-5 psig transducer) was used for tests with low H_0 in order to reduce the effect of sensor noise on response data. The response data from three tests of this series are shown in Figure III.B.12. A summary of test results is shown in Figure III.B.13, where the time lag (t_0) of Hvorslev (1951) is plotted versus initial head (H_0). The curve labelled "Cycle Up" denotes the series of tests in which H_0 was progressively increased, while the curve labelled "Cycle Down" denotes the tests in which H_0 was progressively decreased. The difference between these two plots is considered to be another example of dynamic skin effects (see Section III.E). Unfortunately, as shown on Figures III.B.12 and III.B.13, no threshold behavior was observed during these tests. Although the noise level at a H_0 of 0.02 m made interpretation difficult, there was a clear head dependence in all tests with H_0 larger than 0.06 m. Thus, it does not appear from these data that one can avoid the nonlinearities producing the head-dependent responses by using lower initial heads and/or larger diameter wells. Further

laboratory and field tests are continuing in an attempt to clarify the origin of these nonlinearities.

Summary

An initial series of multilevel slug tests was performed at a well sited in the sand and gravel section at GEMS. The data from this series of tests indicated that the slug-test responses at this well were being affected by mechanisms not accounted for in the conventional theory. An inverse relationship between the magnitude of the induced slug (H_0) and the estimated conductivity, a concave downward curvature to data plotted in the Hvorslev format, and systematic deviations between the test data and the best-fit conventional models were the most obvious indications of these mechanisms. Additional experiments indicated that some of these processes also affect slug-test responses in a well in the moderately permeable bedrock underlying the alluvial section at GEMS.

A large number of field experiments were performed in an attempt to identify the relevant mechanisms producing the observed behavior. The results of these experiments indicated that frictional flow losses in the well casing, in the PVC pipe string used in the multilevel slug-test system, and in the flow-through pipe in the packer were not the primary mechanisms producing the observed head dependence. Experiments to assess the importance of frictional flow losses within the well screen produced ambiguous results. A set of experiments to assess the magnitude of dynamic pressure effects on transducer measurements indicated that dynamic pressure effects are not a significant contributor to the observed behavior. Further experiments demonstrated that oscillatory tests also display a head dependence and that there is no apparent threshold H_0 below which nonlinear behavior is negligible in the sand and gravel deposits underlying GEMS. The general conclusion of the work to date is that non-Darcian flow losses in the screen and near-well portions of the aquifer are the most probable cause of the observed head dependence.

Although the work described here is ongoing, an important recommendation can be made about the performance and analysis of slug tests. A series of slug tests at a well should always be performed using at least two different H_0's (preferably differing by at least 0.5 m). If plots of the response data normalized by the corresponding H_0 all coincide, then one can feel confident that some variant of the conventional approach for analysis of slug-test data can be employed. As shown in the experiments described in this section, the use of only one H_0 in a series of slug tests could lead to considerable error in the estimated parameters. It is important

to note that the behavior described here has, to the best knowledge of the authors, never been reported on in the literature. This is not especially surprising due to the fact that H_0 is almost never varied during a program of slug testing and that most slug tests are performed and analyzed in a rather approximate fashion. However, if our ability to predict contaminant movement in the subsurface is to be improved, it is essential that the error being introduced into the modeling analyses by the use of incorrect parameter values be diminished.

Although field experiments directed at defining the relevant mechanisms producing the anomalous behavior have not yet been completed, considerable work has been done on the development of a theory to account for some of the observed behavior. In the next section of this report, a theory based on the incorporation of nonlinear flow losses and inertial effects into the model of Hvorslev (1951) is described and examples of application of the theory to data from wells at GEMS are presented.

Interval (m)	K_{HV} (10^{-3} m/s)	K_{CBP} (10^{-3} m/s)	H_0 (m)
20.07 - 20.36	0.2105	0.0682	6.88
20.07 - 20.36	0.2136	0.0693	6.86
20.07 - 20.36	0.3499	0.1124	1.66
20.07 - 20.36	0.2856	0.0921	3.06
20.07 - 20.36	0.2960	0.0956	3.12
19.77 - 20.05	0.3499	0.1135	1.65
19.77 - 20.05	0.2785	0.0904	3.04
19.77 - 20.05	0.2881	0.0938	3.01
19.77 - 20.05	0.2045	0.0664	6.85
19.46 - 19.74	0.3377	0.1098	1.74
19.46 - 19.74	0.2797	0.0911	3.05
19.46 - 19.74	0.2805	0.0913	3.03
19.46 - 19.74	0.2074	0.0676	6.86
19.15 - 19.43	0.3347	0.1085	1.62
19.15 - 19.43	0.2823	0.0917	3.04
19.15 - 19.43	0.2673	0.0864	3.28
19.15 - 19.43	0.2011	0.0652	6.85
18.83 - 19.12	0.3539	0.1177	1.58
18.83 - 19.12	0.2839	0.0922	3.03
18.83 - 19.12	0.2777	0.0900	3.19
18.83 - 19.12	0.2031	0.0660	6.87
18.52 - 18.81	0.3481	0.1124	1.60
18.52 - 18.81	0.2723	0.0882	3.23
18.52 - 18.81	0.2908	0.0943	2.94
18.52 - 18.81	0.2068	0.0672	6.90
18.22 - 18.50	0.3441	0.1111	1.69
18.22 - 18.50	0.2868	0.0929	3.01
18.22 - 18.50	0.2941	0.0955	2.99
18.22 - 18.50	0.2117	0.0688	6.92

Table III.B.1 - Results of Hvorslev (K_{HV}) and CBP (K_{CBP}) analyses for the multilevel slug tests using different initial heads (H_0). Interval nos. increase down table (top is no.2).

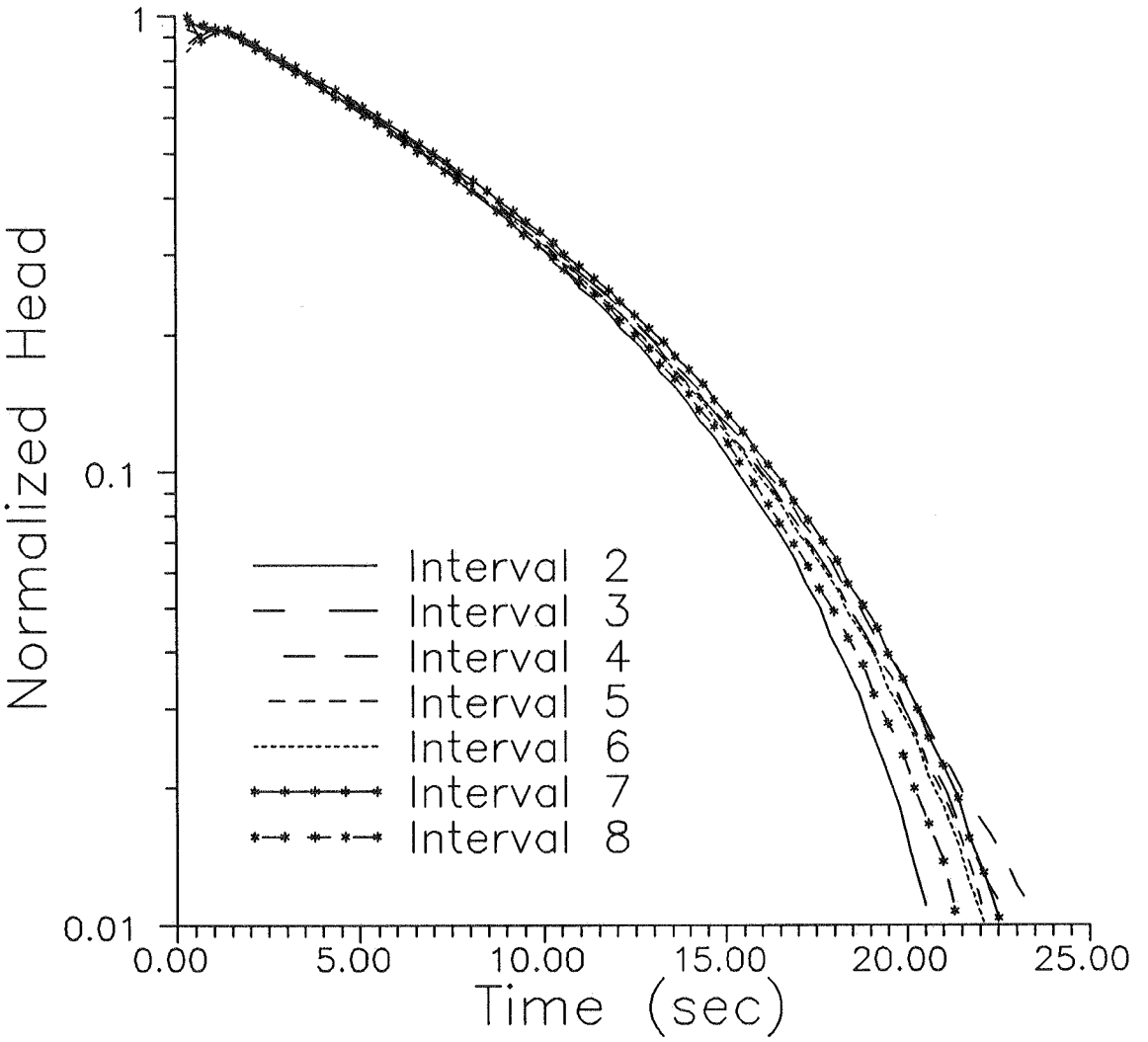

Figure III.B.1 - Normalized head (H/H_0) versus time plots for slug tests in seven intervals of GEMS well 2-5 (H_0 = 3.07 m). See Table III.B.1 for depths corresponding to each interval.

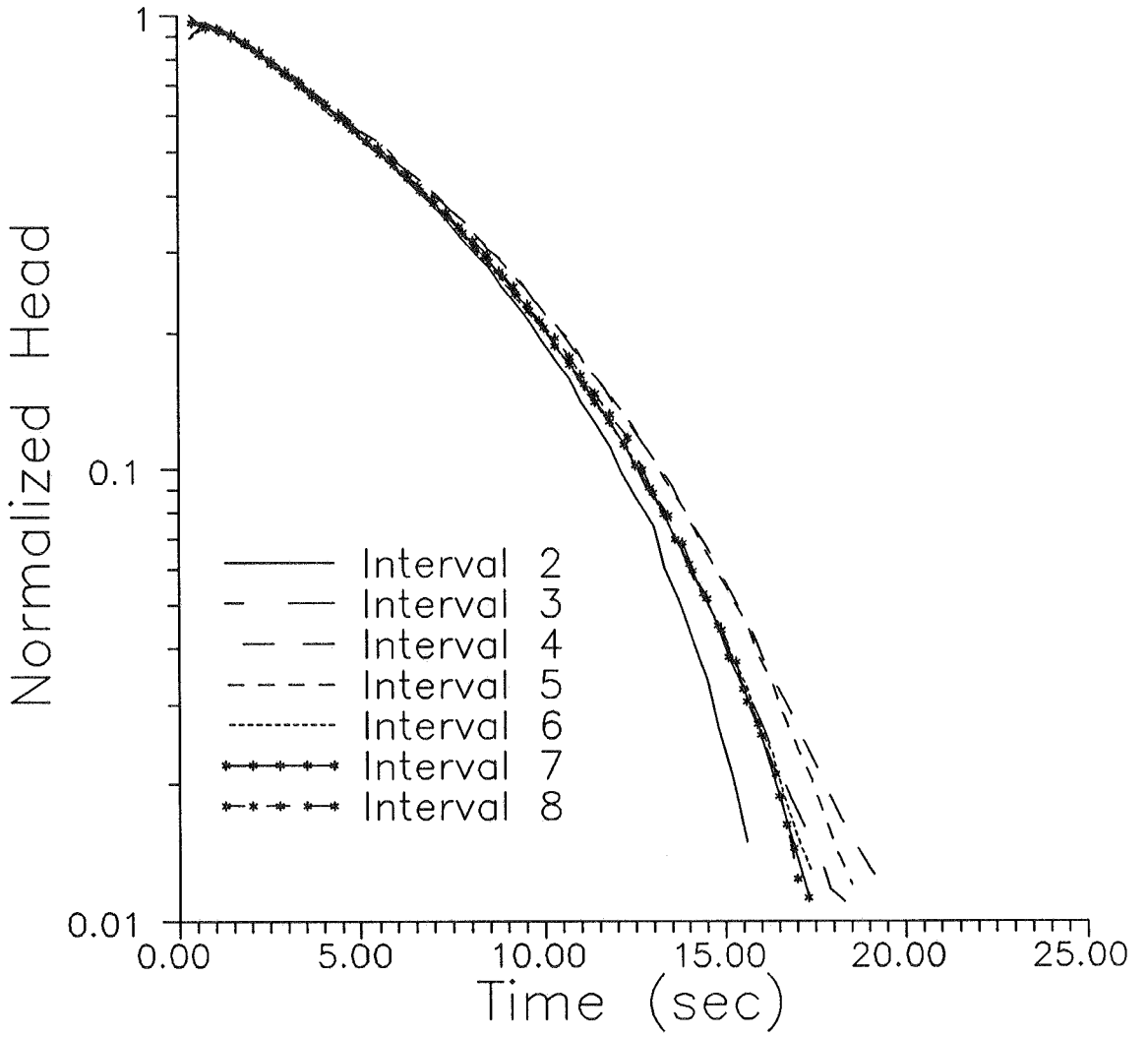

Figure III.B.2 - Normalized head (H/H_0) versus time plots for slug tests in seven intervals of GEMS well 2-5 (H_0 = 1.65 m). See Table III.B.1 for depths corresponding to each interval.

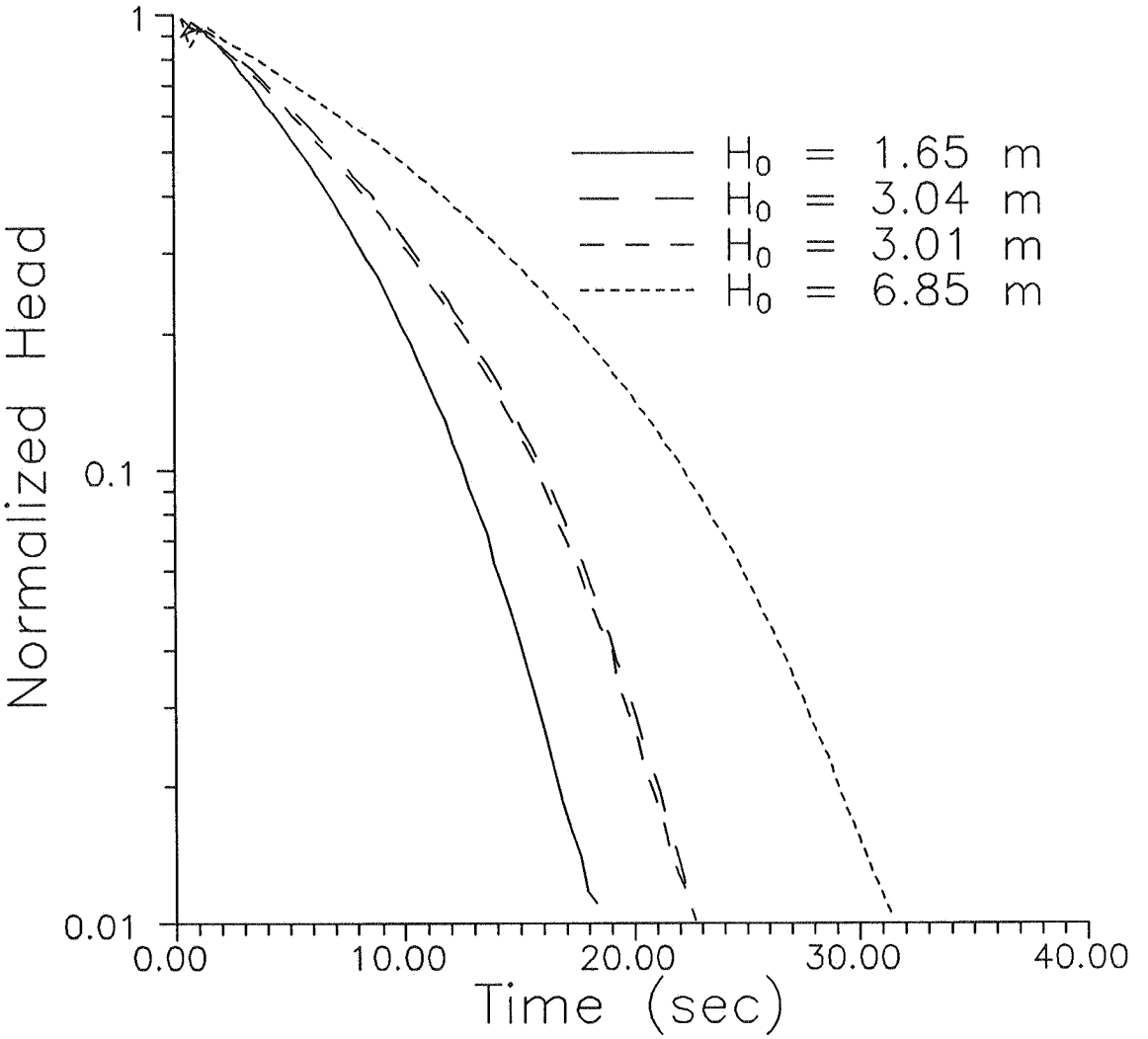

Figure III.B.3 - Normalized head (H/H_0) versus time plots for slug tests in the third interval (19.77-20.05 m) of GEMS well 2-5 using H_0's of different magnitudes.

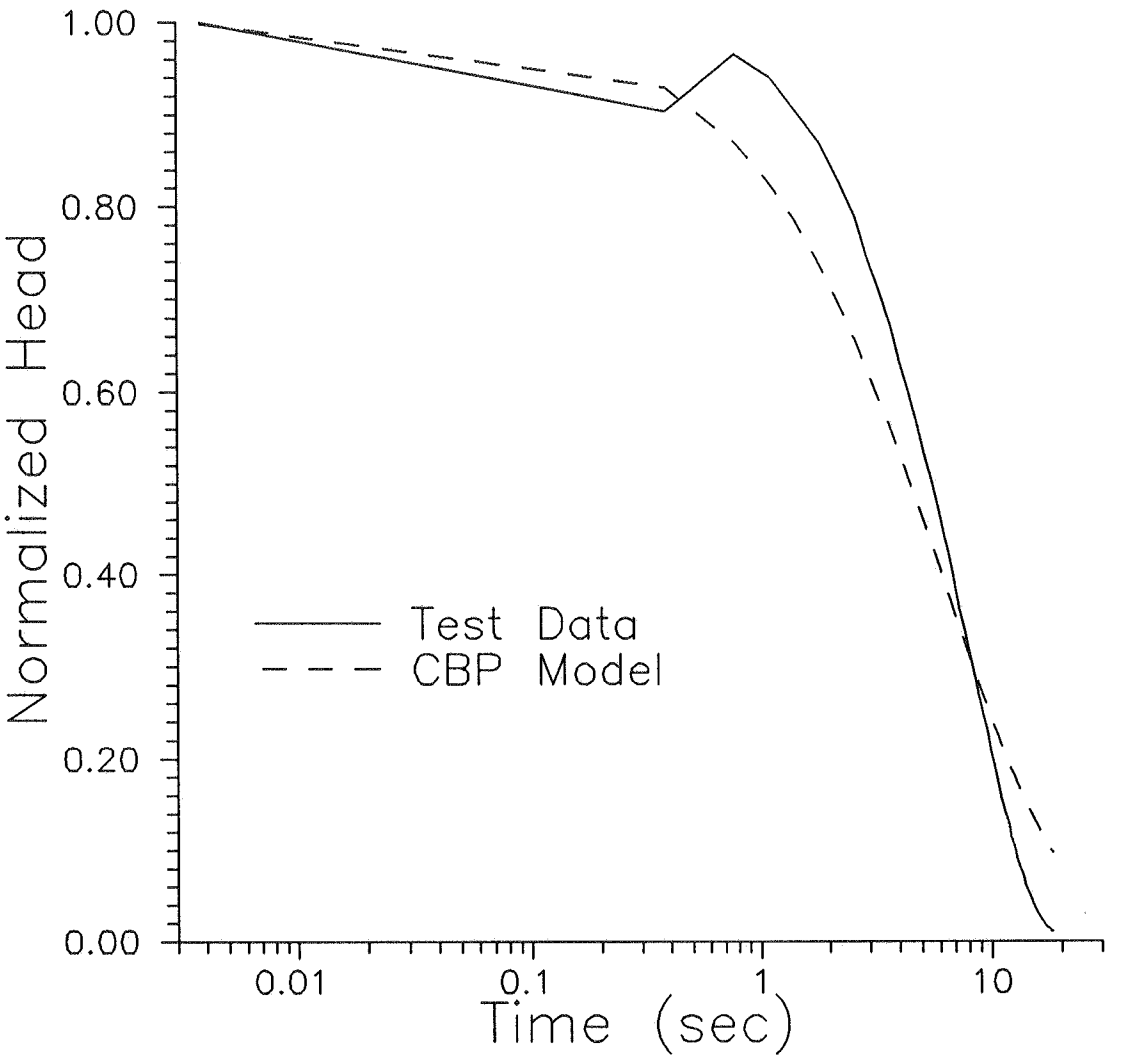

Figure III.B.4 - Normalized head (H/H_0) versus time plots of slug-test data from interval 3 (19.77-20.05 m) of GEMS well 2-5 and the best-fit CBP model.

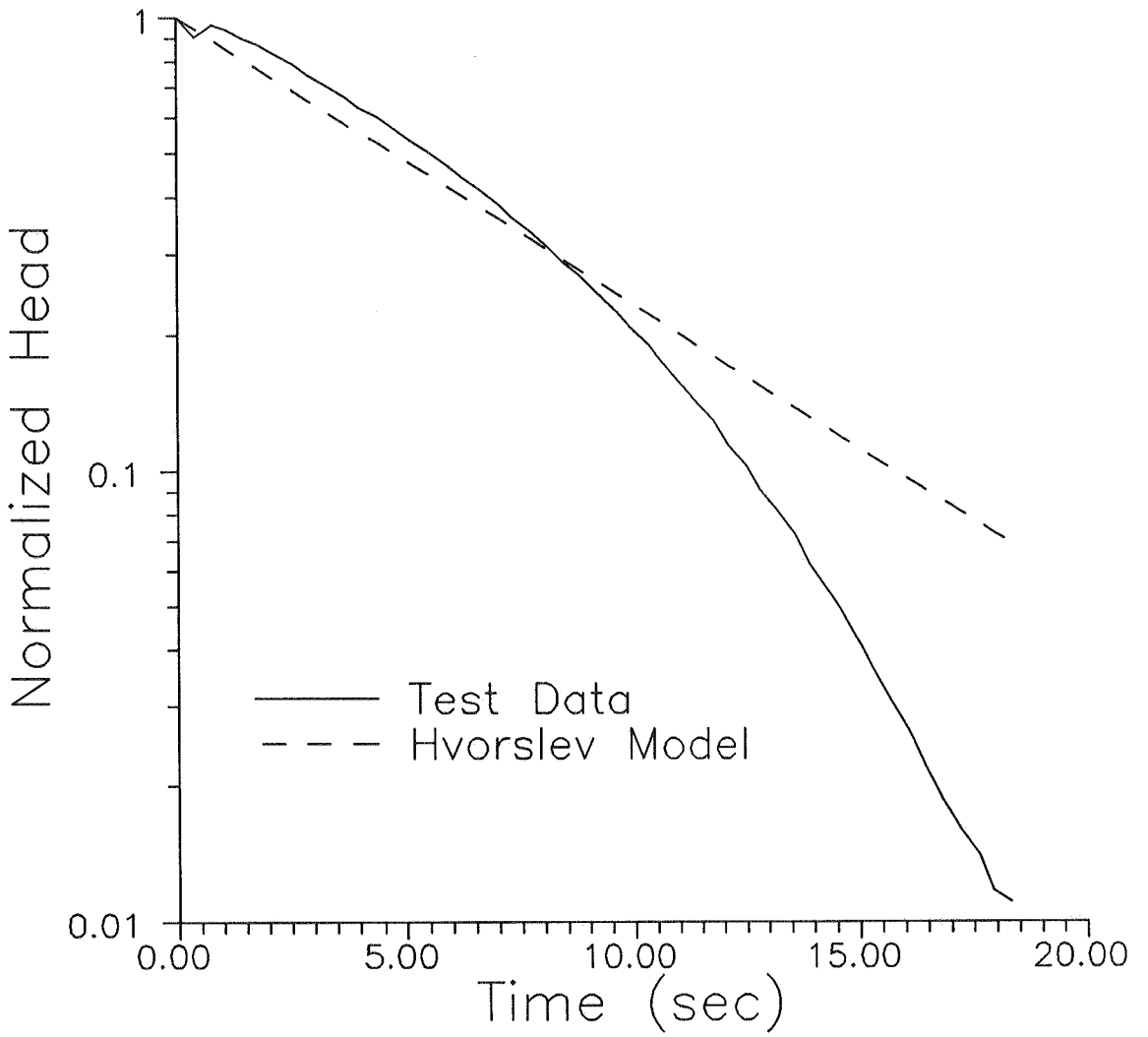

Figure III.B.5 - Normalized head (H/H_0) versus time plots of slug-test data from interval 3 (19.77-20.05 m) of GEMS well 2-5 and the best-fit Hvorslev model.

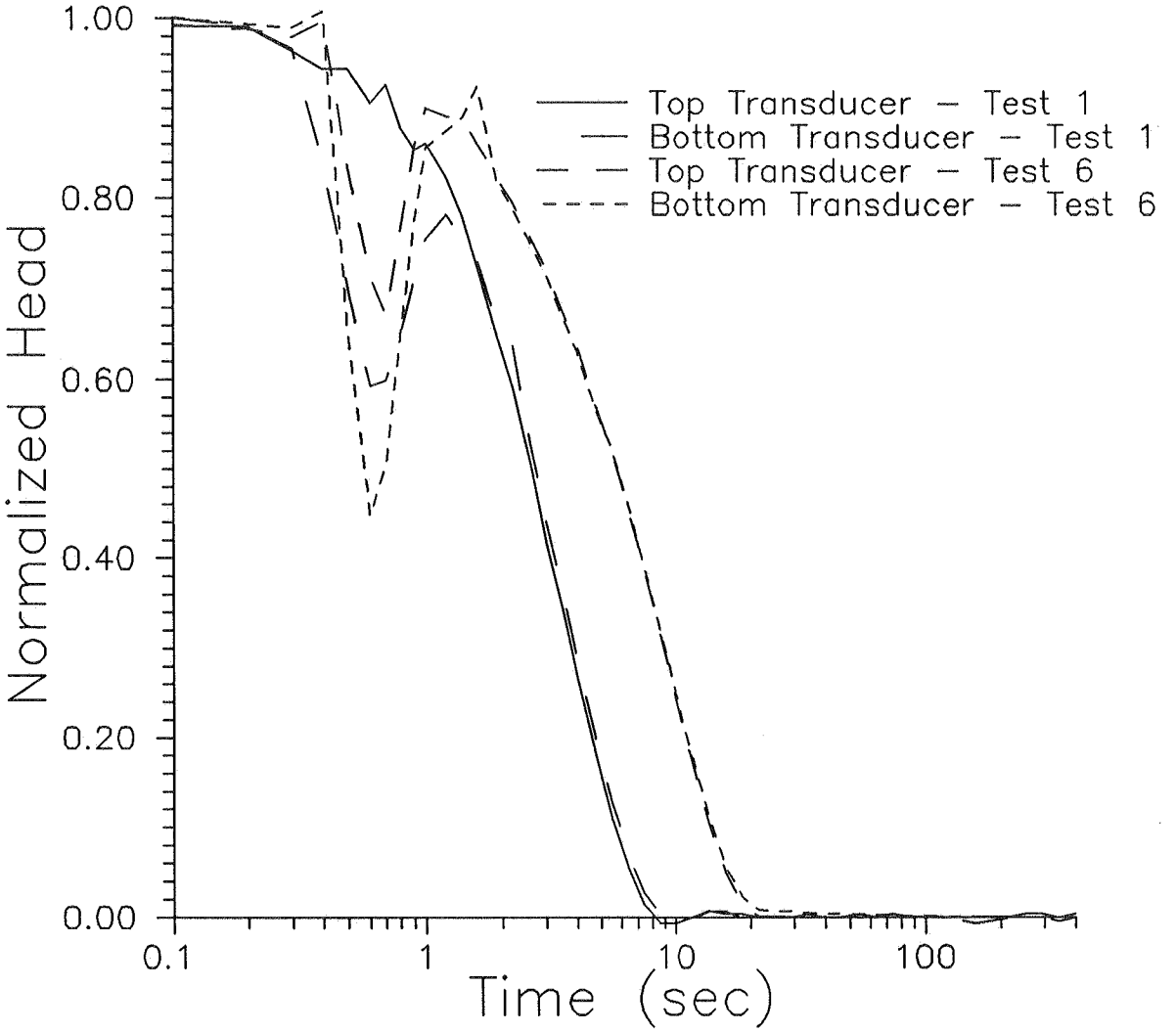

Figure III.B.6 - Normalized head (H/H_0) versus time plots for two slug tests at GEMS well 10-1 (H_{01} = 1.07 m; H_{06} = 6.83 m). Note that two transducers were used in each test.

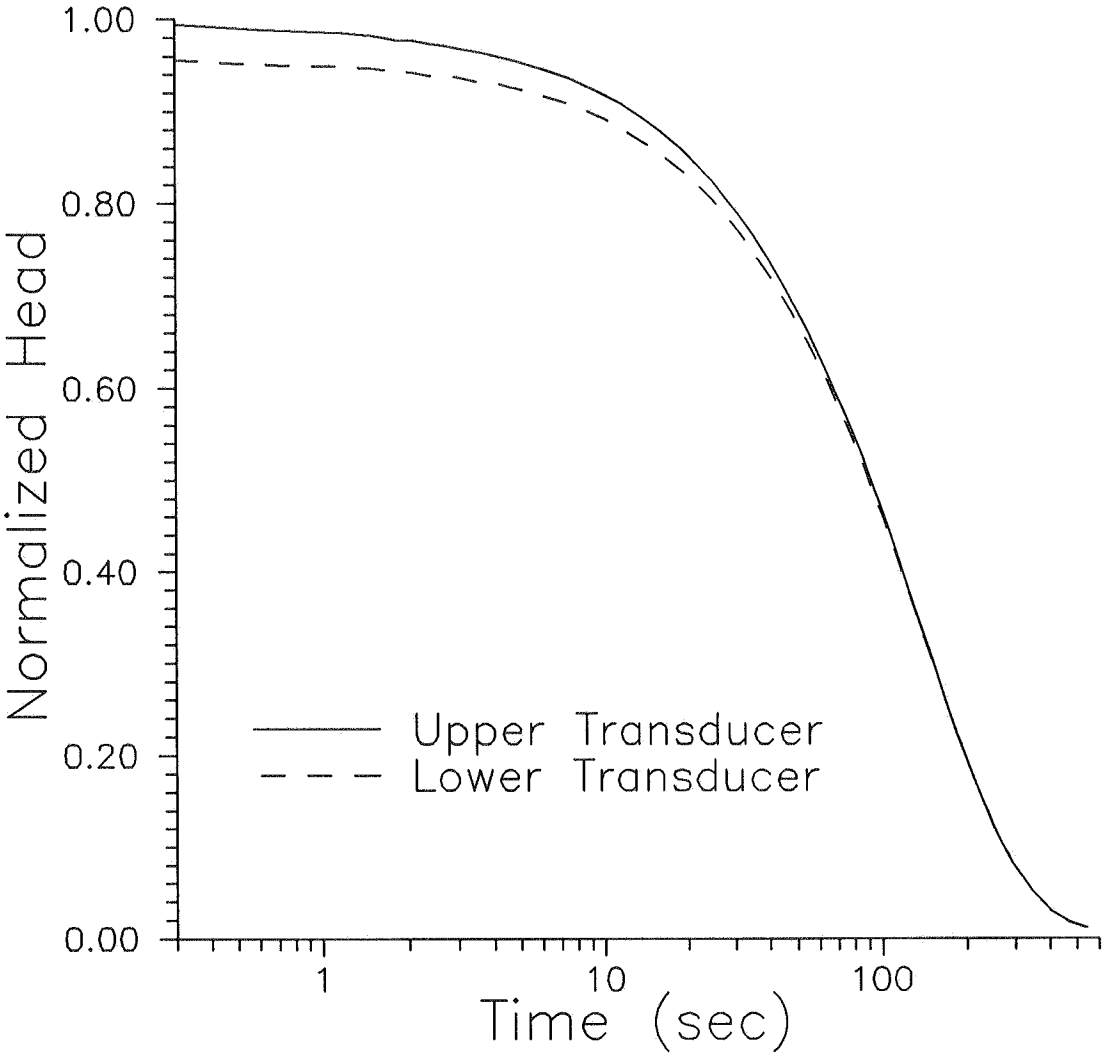

Figure III.B.7 - Normalized head (H/H_0) versus time plots for slug test at GEMS well 0-6 (H_0 = 6.88 m). Note that the transducer-packer arrangement described in the text was used in this test.

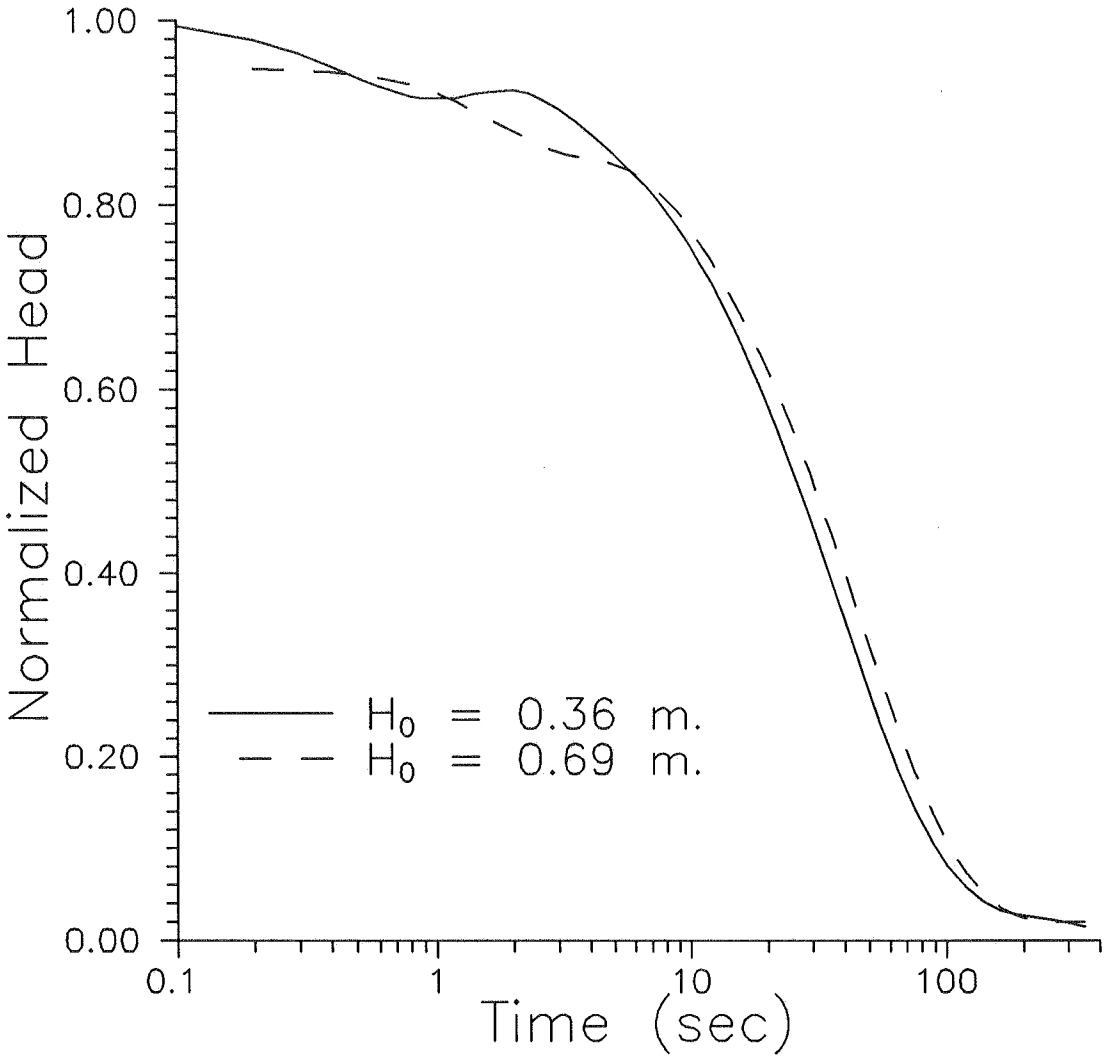

Figure III.B.8 - Normalized head (H/H_0) versus time plots for two slug tests at GEMS well 0-6 (H_{01} = 0.36 m; H_{02} = 0.69 m). Note that these slug tests were initiated using the PVC pipes described in the text.

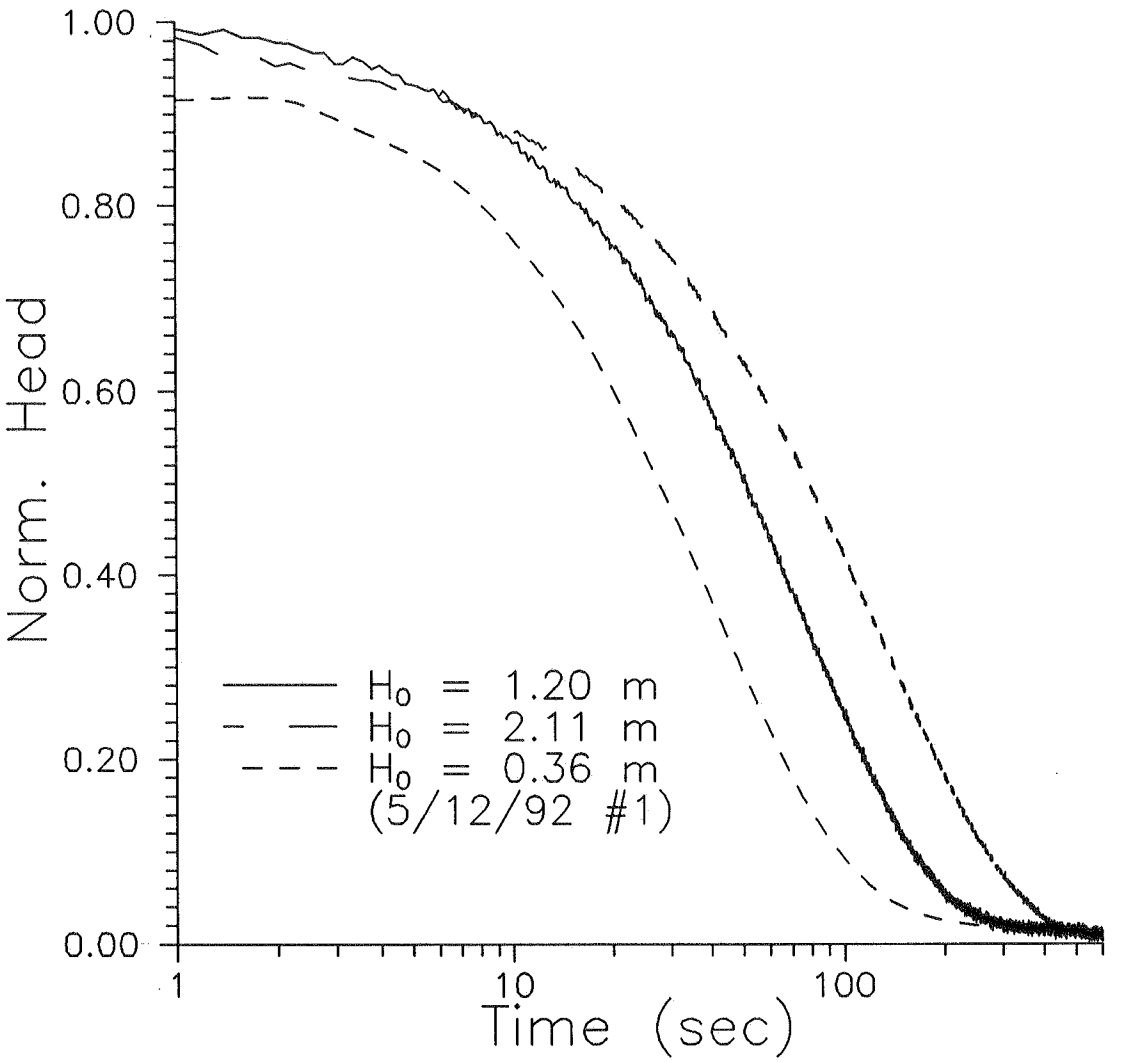

Figure III.B.9 - Normalized head (H/H_0) versus time plots for slug tests at GEMS well 0-6. Note that first two tests initiated using pneumatic means; 5/12/92 test #1 included for comparative purposes.

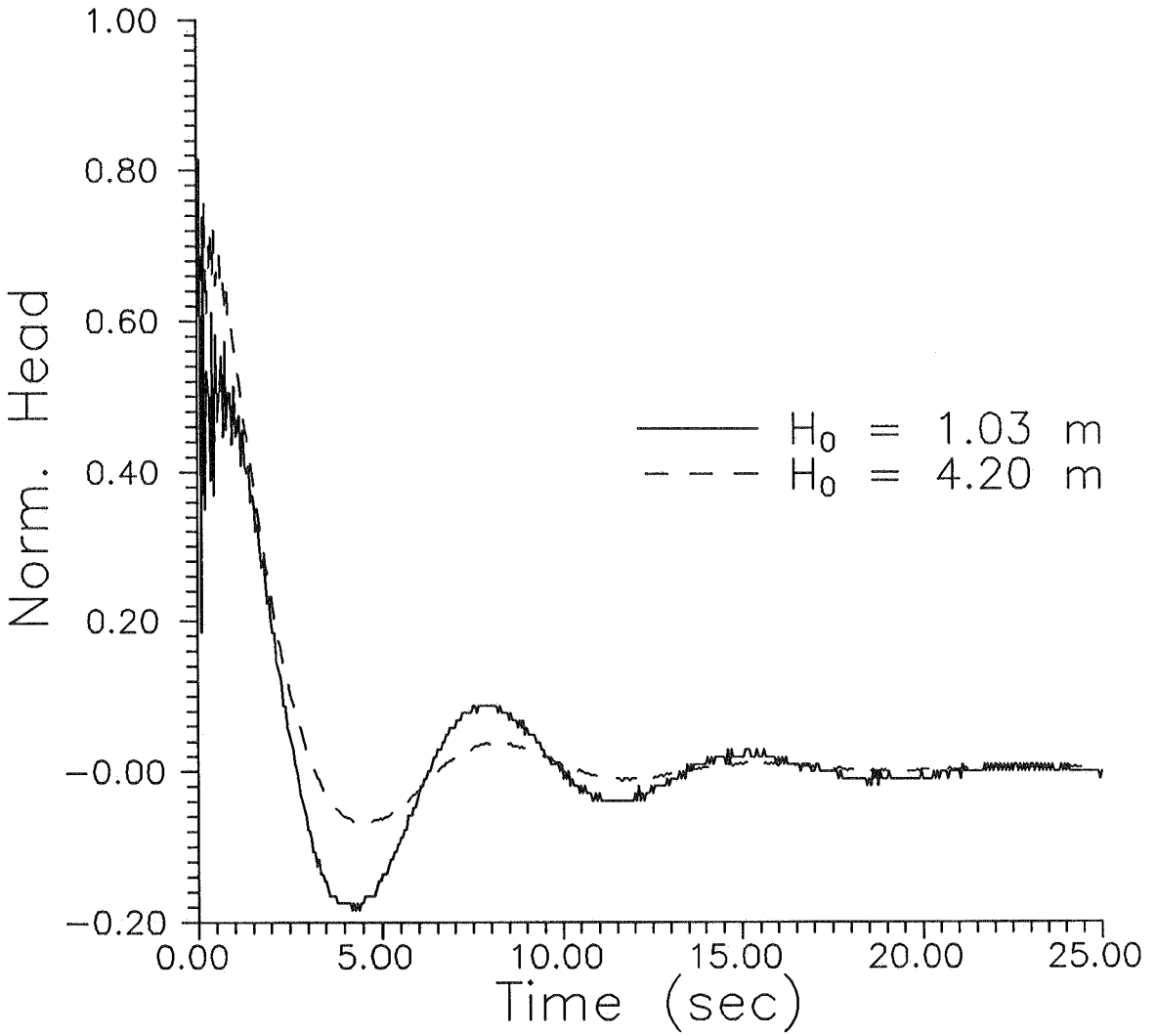

Figure III.B.10 - Normalized head (H/H_0) versus time plots for two slug tests at GEMS well 00-1. Note that if head data are not normalized, the head oscillations in the higher H_0 test are of larger amplitude than those in the lower H_0 test (see Figure 6 of Section III.E).

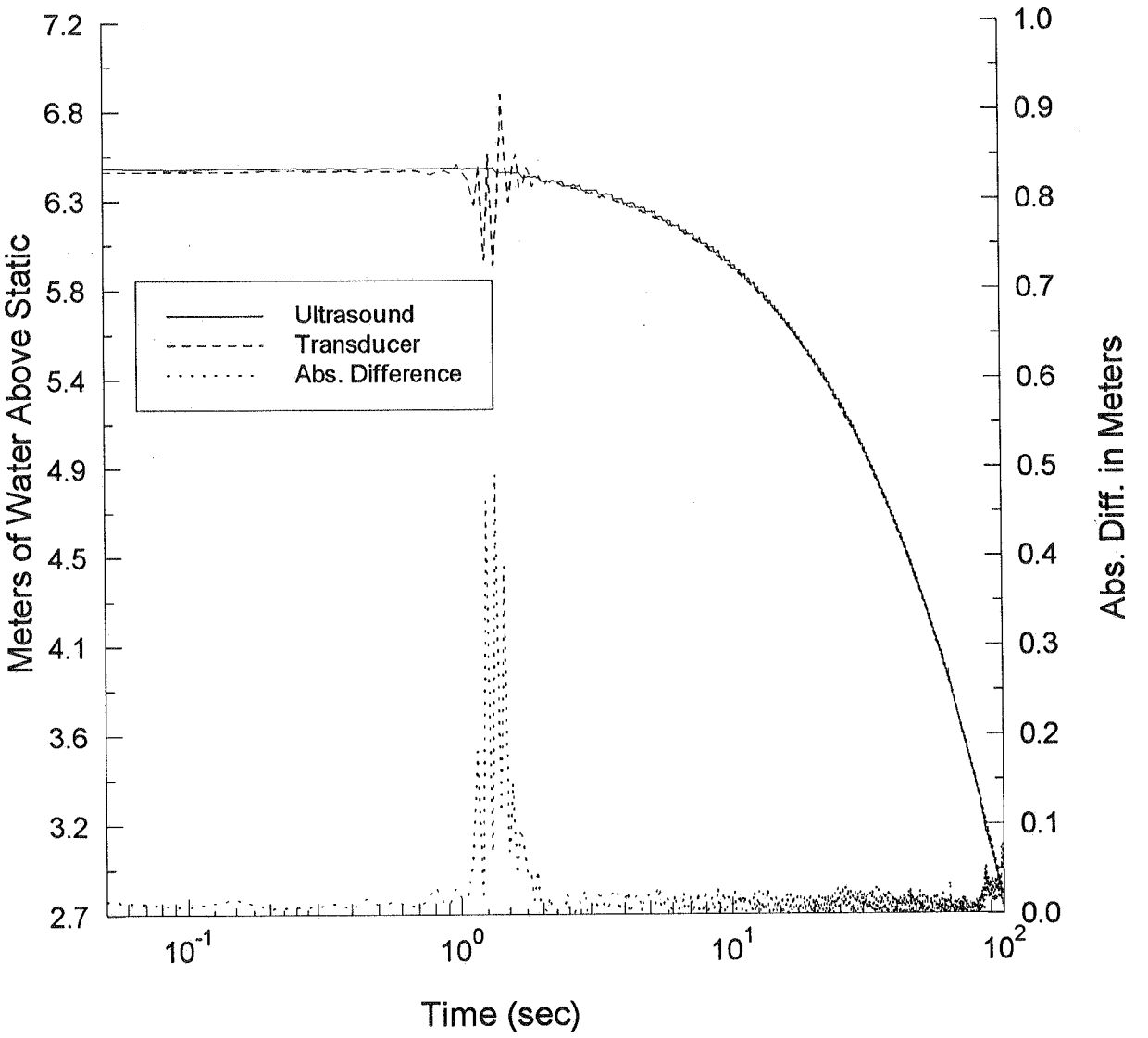

Figure III.B.11 - Meters of water above static versus time plot for a slug test at GEMS well 0-6 (H_0 = 6.46 m). Note that the height of the water column above static is being measured using both a pressure transducer and an ultrasonic distance transmitter. The absolute difference between these two measurements is also plotted.

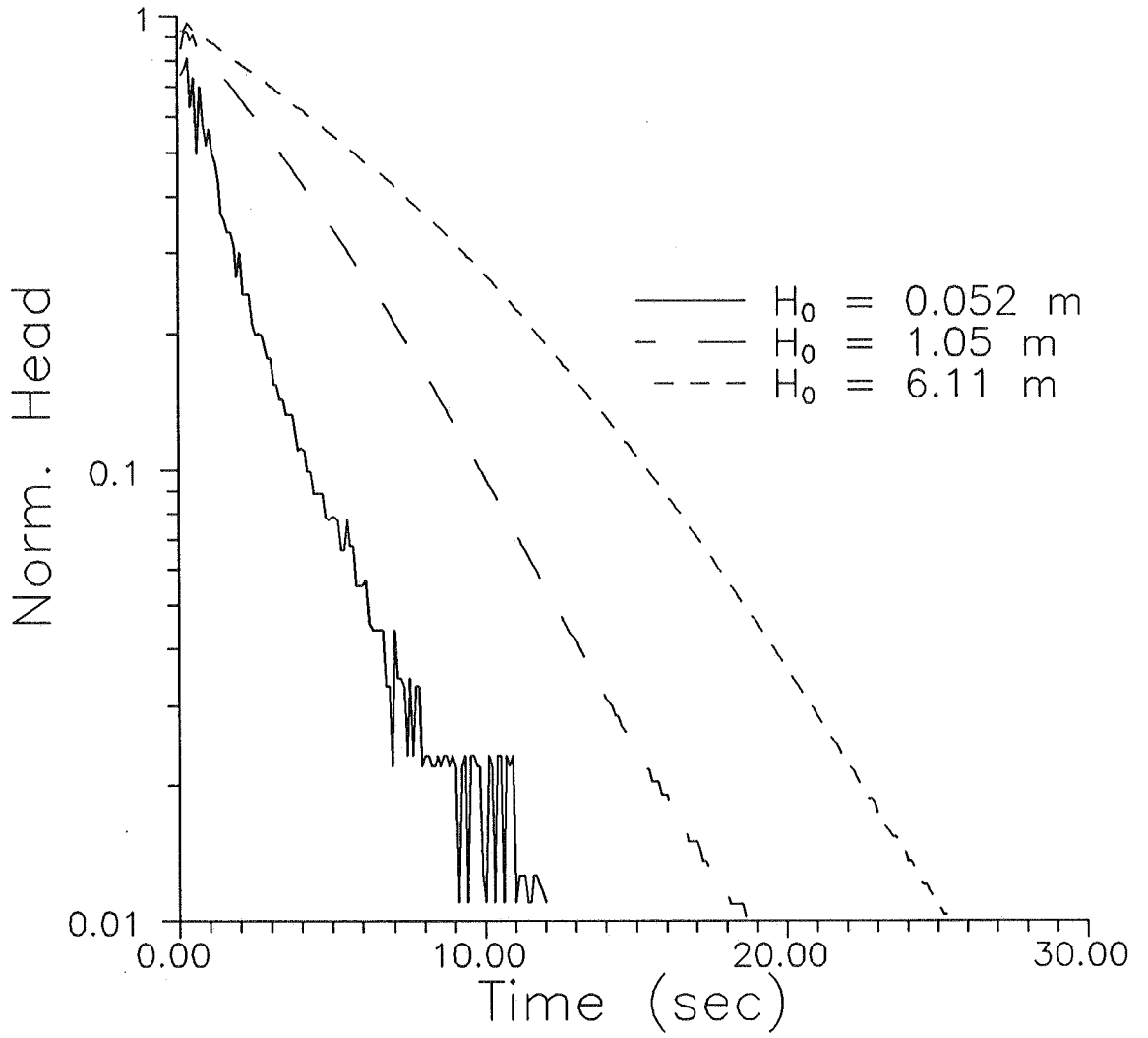

Figure III.B.12 - Normalized head (H/H_0) versus time plots for three slug tests at GEMS well 0-9.

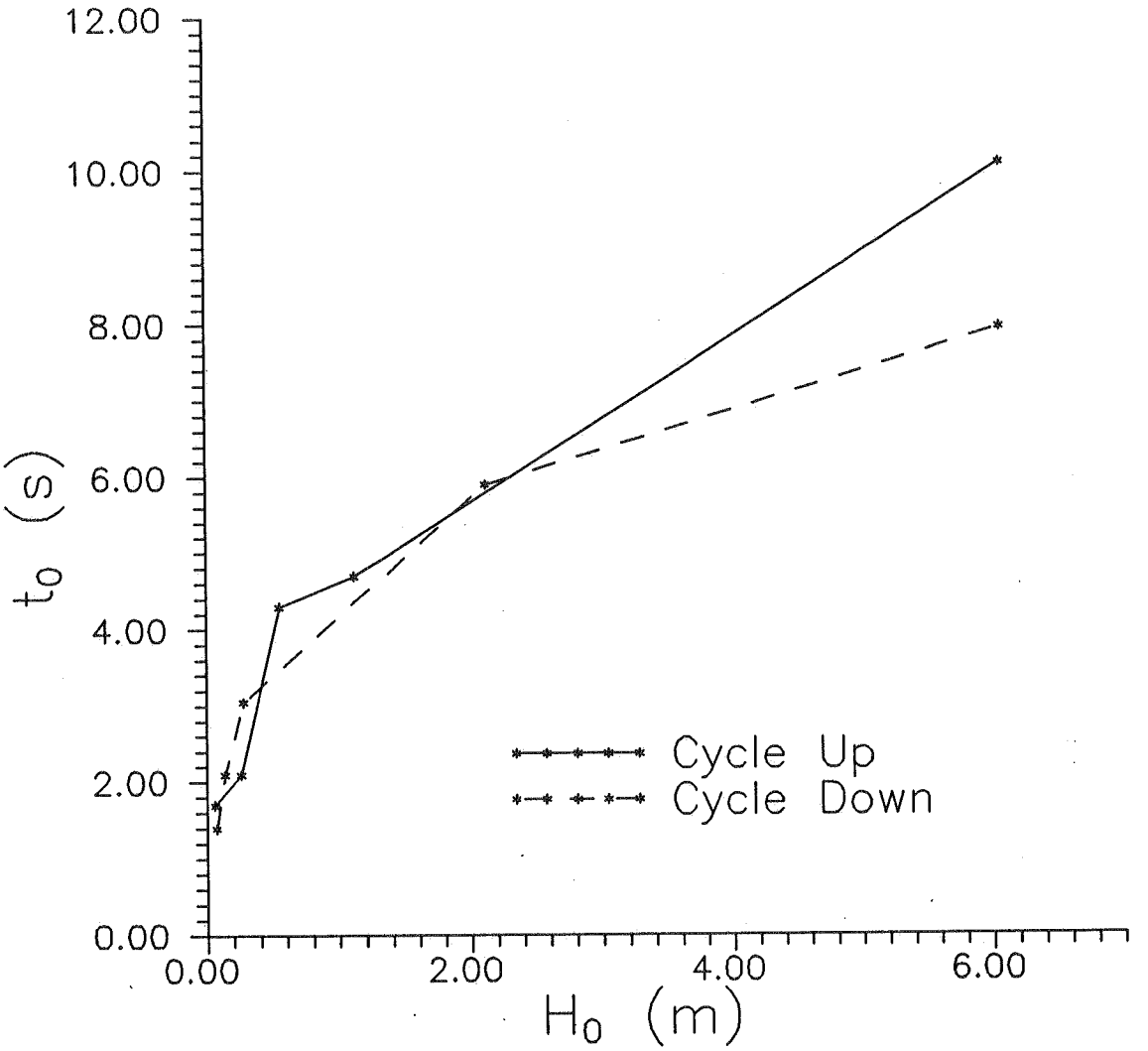

Figure III.B.13 - Plot of Hvorslev time lag (t_0 = time at which a normalized head of 0.37 is reached) versus initial head (H_0) for series of slug tests at GEMS well 0-9.

C. A GENERAL NONLINEAR MODEL FOR THE ANALYSIS OF SLUG-TEST DATA

Introduction

As discussed in the previous section, data from a large number of slug tests performed in the sand and gravel interval at GEMS indicate that slug-test responses at this site are being affected by mechanisms not accounted for in the conventional theory. An inverse relationship between the magnitude of the induced slug (H_0) and the estimated conductivity, a concave downward curvature to data plotted in the Hvorslev format, and systematic deviations between the test data and the best-fit conventional models are the most obvious indications of these mechanisms. Although most of the discussion of the previous section concerned tests that exhibited non-oscillatory responses, tests with oscillatory responses also displayed features that are not consistent with the conventional theory for oscillatory slug tests. Regardless of whether one speaks of oscillatory or non-oscillatory responses, the underlying conventional theory is linear in nature. For non-oscillatory responses, the conventional theory arises from either the work of Hvorslev (1951) or that of Cooper et al. (1967). The primary difference between these two theories lies in the manner in which they represent the influence of specific storage on slug-test responses. Analogues to these theories have also been developed for oscillatory responses. The model of Springer and Gelhar (1991) can be considered an extension of the model of Hvorslev to the oscillatory case, although technically it is an extension of the Bouwer and Rice (1976) method. Van der Kamp (1976) and Kipp (1985), among others, have developed oscillatory slug-test models that can be considered extensions of the Cooper et al. approach.

Kabala et al. (1985) are among the first to consider the use of a nonlinear model to represent slug-test responses in high-permeability media. After a numerical comparison of the linear and nonlinear forms of their slug-test model, they conclude that the linear model is appropriate in virtually all cases of practical significance. However, this conclusion and the form of their nonlinear model were not verified using field data. Concurrent with the work of this study, Stone and Clarke (1993) have developed a nonlinear slug-test model to study hydraulic properties in permeable subglacial media. Although their model does include a dependence on initial head, the authors do not explicitly recognize the importance of this dependence for field testing. The rather unconventional nature of their specific application of slug tests (testing of subglacial sediments) precludes them from making recommendations of practical significance for

more conventional hydrogeologic applications. Clearly, additional work is required to develop a general model that can be used for the analysis of slug-test data from wells sited in media of high permeability.

In this section, we develop a unified model for slug tests, in which we attempt to account for mechanisms not considered in the conventional theories. This model incorporates the effects of nonlinear terms, inertia, turbulence, radially nonuniform velocity distributions, viscosity within the wellbore, and differing casing and screen radii. We couple the wellbore and aquifer flow equations using the same set of assumptions as employed by Hvorslev (1951). Use of this model to fit data from multiple tests at a single well indicates that the relevant physics are apparently well represented by the model, although we cannot completely explain the large magnitude of one of the model parameters. Since this model requires that at least three parameters be estimated from test data, the field application of the approach may not be straightforward. We therefore have developed a simplified field approach based on the Hvorslev technique. Preliminary analyses of this simplified approach indicate that it has considerable promise.

Navier-Stokes Equation for the Borehole

The motion of water in a borehole can be described by the Navier-Stokes equations (Eskinazi, 1967). If we consider the borehole as a streamtube with average flow in the z direction (V), the z component equation is

$$\frac{\partial V}{\partial t} + V\frac{\partial V}{\partial z} = -g - \frac{\nabla P}{\rho} + \frac{\mu}{\rho}\nabla^2 V_* \qquad \text{(III.C.1)}$$

where V is the average (cross-sectional) velocity of the water in the borehole, g is the acceleration of gravity, P is the pressure, ρ is the density, μ is the viscosity, and V_* is the velocity at a point in the borehole. This expression is basically a force balance equation per unit fluid mass and can be integrated in the z direction over the length of the borehole shown in Figure III.C.1 to obtain an energy or work balance equation:

$$\int \frac{\partial V}{\partial t} dz + \int V dV = -g(h+z_0+b) - \int \frac{dP}{\rho} + \int \frac{\mu}{\rho} \nabla^2 V_* dz \qquad \text{(III.C.2)}$$

Note that in the remainder of this development we will assume that the length of the screen (b) is negligible in comparison with the water column length,

$$b << z_o + h(t) \qquad \text{(III.C.3)}$$

the water is incompressible (ρ is constant), and that the viscosity is constant. Integrating from the bottom of the screen to the top of the water in the borehole gives

$$\int \frac{\partial V}{\partial t} ds + \frac{V_T^2 - V_s^2}{2} = -g(h+z_0+b) + \frac{P_s - P_a}{\rho} + \int \frac{\mu}{\rho} \nabla^2 V_* dz \qquad \text{(III.C.4)}$$

where P_s and P_a are the pressures in the screen and at the top of the water column, respectively, and V_T and V_s are the water velocities at the top of the column and in the screen, respectively. The average velocity at the top of the water column is simply dh/dt. Thus, the velocities can be related by the conservation of mass flow:

$$\pi r_c^2 V_T = \pi r_c^2 \frac{dh}{dt} = 2\pi r_s b V_s \qquad \text{(III.C.5)}$$

where r_c and r_s are the casing and screen radii, respectively. Using equation (III.C.5) in equation (III.C.4) results in

$$\int \frac{\partial V}{\partial t} dz + \frac{1}{2}[1 - (\frac{r_c^2}{2r_s b})^2](\frac{dh}{dt})^2 = -g(h+z_0+b) + \frac{P_s - P_a}{\rho} + \int \frac{\mu}{\rho} \nabla^2 V_* dz \qquad \text{(III.C.6)}$$

The first and last terms of equation (III.C.6) require a little more explanation. The last term in equation (III.C.6) is the work done by viscous forces in the fluid column. Writing out the Laplacian operator gives

$$\int \frac{\mu}{\rho} \nabla^2 V_* dz = \frac{\mu}{\rho} \int [\frac{\partial^2 V_*}{\partial r^2} + \frac{1}{r}\frac{\partial V_*}{\partial r} + \frac{1}{r^2}\frac{\partial^2 V_*}{\partial \theta^2} + \frac{\partial^2 V_*}{\partial z^2}] dz \qquad \text{(III.C.7)}$$

If we assume that the flow is unchanging in the θ direction and that the cross section of the borehole is uniform and the fluid is incompressible then

$$\frac{\partial^2 V_*}{\partial \theta^2} = 0, \quad \frac{\partial^2 V_*}{\partial z^2} = 0 \qquad \text{(III.C.8)}$$

and equation (III.C.7) becomes

$$\int \frac{\mu}{\rho} \nabla^2 V_* dz = \frac{\mu}{\rho} \int [\frac{\partial^2 V_*}{\partial r^2} + \frac{1}{r}\frac{\partial V_*}{\partial r}] dz \qquad \text{(III.C.9)}$$

Note that if we have varying radii in the borehole due to changes in casing radius or the presence of an obstruction such as a packer or other equipment, then equation (III.C.8) is no longer correct and additional terms need to be added to equation (III.C.9) in order

to account for viscous work being performed at those locations. If we assume a parabolic distribution of velocities across the borehole as shown in Figure III.C.2, we can write

$$V_* = V_0[1 - r^2/r_c^2] \qquad \text{(III.C.10)}$$

This allows equation (III.C.9) to be written as

$$\int \frac{\mu}{\rho}\nabla^2 V_* dz = -\frac{4\mu}{r_c^2\rho}V_0\int dz = -\frac{4\mu}{r_c^2\rho}V_0(h+z_0+b) \qquad \text{(III.C.11)}$$

The average vertical water velocity is given by the rate of change of the height of the water column and is related to the maximum of the parabolic velocity distribution as follows

$$Q = \pi r_c^2\frac{dh}{dt} = \int V_* dA = 2\pi\int_0^{r_c} V_0[1-\frac{r^2}{r_c^2}]rdr = \frac{\pi r_c^2 V_0}{2} \qquad \text{(III.C.12)}$$

$$V_0 = 2\frac{dh}{dt}$$

where Q is the rate of water flow through the borehole. The final form for equation (III.C.11) can therefore be written as

$$\int \frac{\mu}{\rho} \nabla^2 V_* dz = -\frac{8\mu}{r_c^2 \rho}(h+z_0+b)\frac{dh}{dt} \qquad \text{(III.C.13)}$$

The first term in equation (III.C.6) can be manipulated as follows

$$\int \frac{\partial V}{\partial t} dz = \frac{\partial}{\partial t} \int V dz = \frac{\partial}{\partial t}\left[\frac{dh}{dt} \int \frac{\pi r_c^2}{A(z)} dz \right] \qquad \text{(III.C.14)}$$

by remembering that conservation of water flow requires that

$$\pi r_c^2 \frac{dh}{dt} = A(z)V(z) \qquad \text{(III.C.15)}$$

where dh/dt is the velocity in the casing with normal radius r_c and V(z) is the velocity where the cross-sectional area of the casing is A(z). If the cross-sectional area does not change with time and if the cross-sectional area is uniform in the z direction, then equation (III.C.14) becomes

$$\int \frac{\partial V}{\partial t} dz = (h + z_0 + b)\frac{d^2h}{dt^2} \qquad \text{(III.C.16)}$$

Additional acceleration work terms must be added to this equation if there are significant restrictions in the cross sectional area in the borehole. Thus, when a packer or multilevel slug-test system is employed, the effective length of the water column may be considerably larger than the nominal length $(h+z_0+b)$.

Substitution of equations (III.C.16) and (III.C.13) into (III.C.6) yields the following expression

$$(h + z_0 + b)\frac{d^2h}{dt^2} + \frac{1}{2}[1 - (\frac{r_c^2}{2r_sb})^2](\frac{dh}{dt})^2$$
$$= -g(h + z_0 + b) + \frac{P_s - P_a}{\rho} - \frac{8\mu}{r_c^2\rho}(h + z_0 + b)\frac{dh}{dt} \qquad \text{(III.C.17)}$$

which is an ordinary differential equation for the height of the water column above static in the borehole as a function of time. Notice that this equation is nonlinear in h.

Borehole and Aquifer Interaction

The pressure at the screen will depend on the head in the aquifer, which in turn depends on the aquifer parameters. If H(r) is the head in the aquifer relative to the static level shown in Figure III.C.1, we can write

$$P_s = P_a + g\rho[H(r_s,t) + z_o + b] \qquad \text{(III.C.18)}$$

(assuming that b is small so that the pressure across the screen is nearly constant in the vertical). Substitution of equation (III.C.18) into equation (III.C.17) yields the final form for the borehole equation, which couples to the aquifer-flow equation through H(r,t).

$$(h + z_0 + b)\frac{d^2h}{dt^2} + \frac{1}{2}[1 - (\frac{r_c^2}{2r_sb})^2](\frac{dh}{dt})^2 +$$
$$\frac{8\mu}{r_c^2\rho}(h + z_0 + b)\frac{dh}{dt} + g[h - H(r_s,t)] = 0 \qquad \text{(III.C.19)}$$

The general aquifer-flow equation can be written as

$$\nabla\cdot[bK\nabla H(r,t)] = S_s b\frac{\partial H}{\partial t} \qquad \text{(III.C.20)}$$

where K and S_s are the aquifer hydraulic conductivity and specific storage, respectively. This equation must be solved for H(r,t) concurrently with equation (III.C.19) in order to obtain the complete solution for h. The screen is the boundary between these two solutions and the following boundary condition applies.

$$Q(t) = -\pi r_c^2 \frac{dh(t)}{dt} = -2\pi bK[r\frac{\partial H(r,t)}{\partial r}]_{r_s} \qquad \text{(III.C.21)}$$

Hvorslev Style Approximation

The system of equations (III.C.19)-(III.C.21) is difficult to solve in general, so an approximation that simplifies the solution would be useful. Following Hvorslev (1951) and Bouwer and Rice (1976), we assume that the storage in the aquifer is negligible and consider the aquifer as going through a series of quasi steady states in response to the slug-induced disturbance. With this assumption, equation (III.C.21) can be taken to hold at any radius, not just at the screen. In that case, the following equation for H(r,t) can be obtained by integrating equation (III.C.21) over r:

$$H(r,t) = \left(\frac{r_c^2}{2bK}\right)\left(\frac{dh}{dt}\right)\ln\left(\frac{r}{r_e}\right) \qquad \text{(III.C.22)}$$

where r_e, which is the effective radius at which the effect of the slug-induced disturbance goes to zero, is treated as an empirical parameter. Evaluating equation (III.C.22) at r_s and substituting into equation (III.C.19) gives a single ordinary differential equation that must be solved for h(t).

$$(h + z_0 + b)\frac{\partial^2 h}{\partial t^2} + \frac{1}{2}[1 - (\frac{r_c^2}{2r_s b})^2](\frac{\partial h}{\partial t})^2 + [\frac{8\mu}{r_c^2 \rho}(h + z_0 + b) + g(\frac{r_c^2}{2bK})\ln(\frac{r_e}{r_s})]\frac{\partial h}{\partial t} + gh = 0 \quad \text{(III.C.23)}$$

Note that dropping the nonlinear, inertial, and viscous terms in equation (III.C.23) gives

$$\left[g\left(\frac{r_c^2}{2bK}\right)\ln\left(\frac{r_e}{r_s}\right)\right]\left(\frac{dh}{dt}\right) + gh = 0 \quad \text{(III.C.24)}$$

which is equivalent to the Hvorslev equation

$$Q = -\pi r_c^2 \frac{dh}{dt} = FKh \quad \text{(III.C.25)}$$

if we identify the Hvorslev shape factor (F) as

$$F = \frac{2\pi b}{\ln\left(\frac{r_e}{r_s}\right)} \quad \text{(III.C.26)}$$

Both F and r_e are empirical factors, so it does not matter which we use. In order to stay consistent with the widely used Hvorslev theory, we will write equation (III.C.23) as

$$(h + z_0 + b)\frac{\partial^2 h}{\partial t^2} + \frac{1}{2}[1 - (\frac{r_c^2}{2r_s b})^2](\frac{\partial h}{\partial t})^2 + [\frac{8\mu}{r_c^2 \rho}(h + z_0 + b) + g(\frac{\pi r_c^2}{FK})]\frac{\partial h}{\partial t} + gh = 0 \qquad \text{(III.C.27)}$$

If we use the usual Hvorslev expressions for F, this equation only has one unknown parameter, K. The rest of the physical parameters in equation (III.C.27) can be measured directly in the field or laboratory. Therefore, a least squares fit of the numerical solution of equation (III.C.27) to field data for h(t) should yield a value for K, the hydraulic conductivity of the aquifer.

To conserve writing effort we use the usual definition of the Hvorslev time lag

$$t_0 = \frac{\pi r_c^2}{FK} \qquad \text{(III.C.28)}$$

and define two more quantities

$$A = \frac{\left[1 - \left(\frac{r_c^2}{2r_s b}\right)^2\right]}{2g\pi r_c^2} \qquad \text{(III.C.29)}$$

and

$$M = \frac{8\mu}{g t_o r_c^2 \rho} \qquad \text{(III.C.30)}$$

With these definitions and dividing by gt_o, equation (III.C.27) can be written as

$$\frac{(h + z_o + b)}{gt_o}\frac{d^2h}{dt^2} + FKA\left(\frac{dh}{dt}\right)^2 + [M(h + z_o + b) + 1]\left(\frac{dh}{dt}\right) + \frac{h}{t_o} = 0 \qquad \text{(III.C.31)}$$

When the acceleration term is negligible and M =0, this is the same model as presented by McElwee et al. (1992) for the nonoscillatory case.

Limiting Case Solutions

Analytical solutions to equation (III.C.31) can be obtained in a couple of limiting cases. At t=0, the water column is at rest and dh/dt = 0. The velocity of the water column will be small at early times, so the velocity dependent terms of equation (III.C.31) can be dropped to give

$$(h_o + z_o + b)\frac{d^2h}{dt^2} + gh_o = 0 \qquad \text{(III.C.32)}$$

where h_0 is the initial height. Equation (III.C.32) can only be used for very early times, before the water column has moved much, because we are assuming the column height is approximately constant at h_0. With these assumptions, the solution to equation (III.C.32) is

$$h = h_o - \frac{g}{2}\left(\frac{h_o}{h_o + z_o + b}\right)t^2 \qquad \text{(III.C.33)}$$

This is simply the normal equation for a falling body under the action of gravity. However, the acceleration is not g but some fraction based on the quantities h_0, z_0, and b. In the case where $h_0 >> z_0 + b$, the column acceleration approaches g at early times.

Dropping only the velocity squared term (assuming small velocities) in equation (III.C.31) gives

$$(h + z_o + b)\frac{d^2h}{dt^2} + gt_o\left[M(h + z_o + b) + 1\right]\left|\frac{dh}{dt}\right| + gh = 0 \qquad \text{(III.C.34)}$$

which would be the usual damped harmonic oscillator equation except for the expression $(h + z_0 + b)$ which occurs in the coefficients and makes the equation nonlinear. In the case where $h_0 << z_0 + b$ (initial displacements are small), equation (III.C.34) can be approximated by

$$(z_o + b)\frac{d^2h}{dt^2} + gt_o\left[M(z_o + b) + 1\right]\left|\frac{dh}{dt}\right| + gh = 0 \qquad \text{(III.C.35)}$$

which is exactly the damped harmonic oscillator equation (Kreyszig, 1983). Three cases can be identified. The overdamped case is the classical one usually treated in older geohydrology literature (e.g., Hvorslev, 1951; Cooper et al., 1967):

$$g^2t_o^2\left[M(z_o + b) + 1\right]^2 > 4g(z_o + b) \qquad \text{(III.C.36)}$$

In this case, the water column does not oscillate at all. In these overdamped cases, the viscosity effects represented by M are usually much smaller than the damping due to the aquifer hydraulic conductivity, and thus can usually be ignored. If the quantities on both sides of equation (III.C.36) are equal, then critical damping is said to occur and there is no oscillation.

The third case, the underdamped case, occurs when

$$g^2t_o^2\left[M(z_o + b) + 1\right]^2 < 4g(z_o + b) \qquad \text{(III.C.37)}$$

In this case we have an exponentially decaying oscillation given by

$$h(t) = CExp\left[-\alpha t\right]\cos(\omega^* t - \delta) \qquad \text{(III.C.38)}$$

where

$$\alpha = \frac{gt_o\,[M(z_o + b) + 1]}{2(z_o + b)} \qquad \text{(III.C.39)}$$

and

$$\omega^* = \sqrt{\frac{g}{z_o + b} - \alpha^2} \qquad \text{(III.C.40)}$$

C and δ are given by the initial conditions on the displacement and the velocity of the water column. If $\alpha = 0$ in equation (III.C.40), which corresponds to no damping either by viscous forces or the aquifer, then ω^* is just the natural frequency of an undamped water column. Although a number of papers over the last two decades have dealt with the underdamped case (e.g., Van der Kamp, 1976), little has been done to treat the general case of responses that might lie anywhere in the domain from overdamped to underdamped and for which the small-velocity assumption may not be appropriate. Clearly, a general solution to equation (III.C.31) is needed.

Numerical Solution

Since the fully nonlinear equation (III.C.31) can not be solved analytically, we must resort to numerical techniques. Evaluating equation (III.C.31) at time n and using central difference formulae for the time derivatives results in

$$\frac{(h^n + z_o + b)}{gt_o}\left[\frac{h^{n+1} - 2h^n + h^{n-1}}{\Delta t^2}\right] + FKA\left(\frac{h^{n+1} - h^{n-1}}{2\Delta t}\right)^2 + [M(h^n + z_o + b) + 1]\left(\frac{h^{n+1} - h^{n-1}}{2\Delta t}\right) + \frac{h^n}{t_o} = 0 \qquad \text{(III.C.41)}$$

We have had good results applying a point iterative method (von Rosenberg, 1969) to equation (III.C.41). In order to apply this iterative method, an iteration index (m+1) will be introduced as a superscript in all single appearances of h at time level

n+1. In all terms where h squared at time level n+1 appears, we must evaluate one h at the new iteration level (m+1) and one h at the old iteration level (m).

$$\frac{(h^n + z_o + b)}{gt_o}\left[\frac{h^{n+1(m+1)} - 2h^n + h^{n-1}}{\Delta t^2}\right] + FKA\left(\frac{h^{n+1(m)} - h^{n-1}}{2\Delta t}\right)\left(\frac{h^{n+1(m+1)} - h^{n-1}}{2\Delta t}\right) + [M(h^n + z_o + b) + 1]\left(\frac{h^{n+1(m+1)} - h^{n-1}}{2\Delta t}\right) + \frac{h^n}{t_o} = 0$$

(III.C.42)

Rearranging equation (III.C.42) gives

$$h^{n+1(m+1)} = \frac{coef(n-1,m)h^{n-1} + coef(n)h^n}{coef(n+1,m)}$$

(III.C.43)

where

$$coef(n+1,m) = \left[1 + \left(M + \frac{2}{gt_o\Delta t}\right)(h^n + z_o + b) + FKA\left(\frac{h^{n+1(m)} - h^{n-1}}{2\Delta t}\right)\right],$$

(III.C.44)

$$coef(n-1,m) = \left[1 + \left(M - \frac{2}{gt_o\Delta t}\right)(h^n + z_o + b) + FKA\left(\frac{h^{n+1(m)} - h^{n-1}}{2\Delta t}\right)\right],$$

(III.C.45)

and

$$coef(n) = \left[\frac{4(h^n + z_o + b)}{g t_o \Delta t} - \frac{2\Delta t}{t_o} \right] . \qquad \text{(III.C.46)}$$

Equation (III.C.43) can now be solved iteratively for h at the new time level n+1.

This numerical solution has been incorporated into an automated well test analysis package called SUPRPUMP (Bohling and McElwee, 1992). As mentioned earlier, K, the hydraulic conductivity of the aquifer, is really the only parameter available for fitting in equation (III.C.31). However, initial attempts to fit the field data with equation (III.C.31) were not successful. We found that it was impossible to fit the overall shape of the oscillatory field data with only one parameter. The values of A and M in equations (III.C.29) and (III.C.30) were quite small and did not seem to fit the field data. The value of A calculated from equation (III.C.29) for our field data was about 0.02 sec^2/m^3, while the kinematic viscosity (μ/ρ) was about 10^{-6} m^2/sec. Therefore, neither of these parameters played an important role in the analysis of our data. We then decided to treat A as an adjustable parameter to be determined by fitting the data. McElwee et al. (1992) had reasonable success using this kind of model when no oscillating water column was observed. Unfortunately, when applied to oscillatory data, the model with two parameters (A and K) still did not give a good overall fit to the shape of the curve and, most troubling of all, a constant set of values for A and K did not seem to properly predict the head dependence of the slug-test responses. In the process of trying to fit the data, it was observed that if the length of the water column in the borehole was increased the general shape of the field data could be fit much better. Therefore, it appeared that something was missing in the original physical model on which equation (III.C.31) was based.

Revision of the Model

An alternate method of deriving the equation of motion for the water column during a slug test can be obtained by considering an energy balance equation (Hansen, 1967). Consider the water column inside the borehole (Figure III.C.1) to be a control volume. The change of energy within the control volume over time is determined by the work done at the free surface and the amount of energy that flows out the screen. In equation form this is

$$\frac{d}{dt}\int_{V_{cv}}\left(\frac{V^2}{2}+gz\right)\rho dV_{cv} - \int_{A_s}\left(\frac{P_s}{\rho}+\frac{V_s^2}{2}\right)V_{rn}\rho dA_s + \int_{A_T}P_a V_a dA_T = 0 \quad \text{(III.C.47)}$$

The first term is the rate of change of kinetic and potential energy in the borehole (control volume,V_{cv}). The second term is the rate at which energy flows out the screen area (A_s) due to a radial velocity (V_{rn}), where P_s and V_s are the screen pressure and velocity (V_{rn} will be assumed equal to V_s for the remainder of this derivation), respectively. The third term is the rate at which work is done by atmospheric pressure (P_a) on the moving upper surface. Note that this equation neglects viscous forces.

Assume that the pressure is constant over the screen area ($2\pi r_s b$) and on the upper surface of the water column (πr_c^2). In addition, assume that the velocity is uniform over the screen area (V_s) and the upper free surface (V_a). If we consider the water incompressible, the average screen velocity is related to the average borehole velocity (dh/dt).

$$V_s = \frac{r_c^2}{2r_s b}V_a = \frac{r_c^2}{2r_s b}\frac{dh}{dt} \quad \text{(III.C.48)}$$

Using the mean value theorem to average equation (III.C.47) over the control volume gives the result

$$\frac{d}{dt}\left\{\left[\frac{\overline{V^2}}{2}+\frac{g}{2}(h+z_o+b)\right]\pi r_c^2\rho(h+z_o+b)\right\}$$
$$-\left\{\left[\frac{P_s}{\rho}+\left(\frac{r_c^2}{2r_s b}\right)^2\frac{1}{2}\left(\frac{dh}{dt}\right)^2\right]\left(\frac{r_c^2}{2r_s b}\frac{dh}{dt}\right)2\pi r_s b\rho + P_a\pi r_c^2\frac{dh}{dt}\right\} = 0$$

(III.C.49)

The term involving $\overline{V^2}$ is the average kinetic energy per unit volume of the

borehole and needs further consideration. In actual fact, there will be velocity components inside the borehole other than the average vertical velocity describing the drop of the water column. These velocity components may be random in nature (turbulence) or axially circular (curl of velocity not zero), but when averaged over the borehole they do not contribute to the net flow of water out the screen. However, these velocity components may carry significant energy and must be considered when averaging the kinetic energy over the control volume, which is the entire borehole. Assume that the velocity field can be represented by a vertical component and a random component.

$$V = V_z + V_r \tag{III.C.50}$$

Using this form for the velocity in equation (III.C.49) gives

$$\begin{aligned}\overline{V^2}\rho\pi r_c^2(h + z_o + b) &= \int_{V_{cv}} V^2 \rho dV_{cv} = \int_{V_{cv}} (V_z + V_r)^2 \rho dV_{cv} \\ &= \int_{V_{cv}} (V_z^2 + 2V_z V_r + V_r^2)\rho dV_{cv}\end{aligned} \tag{III.C.51}$$

Since V_r is a random velocity component, we assume that the following integral will average to zero over the control volume.

$$\int_{V_{cv}} V_z V_r \rho dV_{cv} = 0 \tag{III.C.52}$$

Assume that V_z is given by a radial velocity distribution defined by equations (III.C.10) and (III.C.12).

$$V_z = 2\frac{dh}{dt}\left[1 - \frac{r^2}{r_c^2}\right] \tag{III.C.53}$$

The first term in equation (III.C.51) can now be evaluated. The last term in equation (III.C.51) requires some additional assumptions about the random component. Since the

random component is zero in a static situation and could logically be expected to increase proportionally to the average vertical velocity, it is reasonable to assume that

$$V_r = C\frac{dh}{dt} \tag{III.C.54}$$

where C is a constant of proportionality. With these assumptions, equation (III.C.51) can now be written as

$$\begin{aligned}\bar{V}^2\rho\pi r_c^2(h+z_0+b) &= (\frac{dh}{dt})^2\int_{V_{cv}}(4[1-\frac{r^2}{r_c^2}]^2+C^2)\rho dV_{cv} \\ &= (\frac{dh}{dt})^2[\frac{4}{3}+C^2]\rho\pi r_c^2(h+z_0+b)\end{aligned} \tag{III.C.55}$$

which shows that the average square velocity is larger than the square of the average velocity by a factor greater than one.

$$\bar{V}^2 = (\frac{dh}{dt})^2[\frac{4}{3}+C^2] = (\frac{dh}{dt})^2(1+\alpha^2) \tag{III.C.56}$$

where the α^2 term incorporates the effects of both a radially nonuniform velocity distribution and random components of velocity. Equation (III.C.56) implies that the kinetic energy of the water column can be significantly larger than one might suspect based on the average vertical velocity (dh/dt).

Substitution of equation (III.C.56) into equation (III.C.49) yields

$$\frac{d}{dt}[(\frac{1}{2}(\frac{dh}{dt})^2(1+\alpha^2) + \frac{g}{2}(h+z_0+b))\pi r_c^2\rho(h+z_0+b)]$$
$$-[\frac{P_s}{\rho}+(\frac{r_c^2}{2r_sb})^2\frac{1}{2}(\frac{dh}{dt})^2](\frac{r_c^2}{2r_sb}\frac{dh}{dt})2\pi r_sb\rho+P_a\pi r_c^2\frac{dh}{dt} = 0 \qquad \text{(III.C.57)}$$

Performing the differentiation and rearranging terms produces a form that is identical to equation (III.C.17), except for the neglect of the viscous term and the inclusion of the kinetic-energy multiplication factor:

$$(\frac{dh}{dt})[(h + z_0 + b)(1 + \alpha^2)\frac{d^2h}{dt^2} + \frac{1}{2}[(1 + \alpha^2) -$$
$$(\frac{r_c^2}{2r_sb})^2](\frac{dh}{dt})^2 + g(h + z_0 + b) - \frac{P_s - P_a}{\rho}] = 0 \qquad \text{(III.C.58)}$$

Thus, by considering an energy-based approach, we have derived the same basic equation as was obtained by starting from the Navier-Stokes equation. The essential difference between these two derivations is the contribution of kinetic energy. Since the kinetic energy contribution of velocity components other than those in the vertical direction may be considerable, a new parameter (α) has been added to the energy model to help account for the additional kinetic energy.

Equation (III.C.58) can be generalized to include a viscous term and acceleration work terms arising from changes in the casing radii (see discussion with respect to equation (III.C.16)). The final form for the mathematical model representing the motion of water in the borehole can therefore be written as

$$(h+z_0+b+\beta)(1+\alpha^2)\frac{d^2h}{dt^2} + \frac{1}{2}[(1+\alpha^2) - (\frac{r_c^2}{2r_s b})^2](\frac{dh}{dt})^2 + g(h+z_0+b) - \frac{P_s - P_a}{\rho} + \frac{8\mu}{r_c^2\rho}(h + z_0 + b)\frac{dh}{dt} = 0 \qquad \text{(III.C.59)}$$

where

β = acceleration work terms arising from changes in casing radii.

Coupling of this equation to the aquifer-flow equation can now be done in exactly the same manner as with equation (III.C.17) to produce:

$$\frac{(h+z_0+b+\beta)}{gt_0}(1+\alpha^2)\frac{d^2h}{dt^2} + FKA(\frac{dh}{dt})^2 + [M(h + z_0 + b) + 1]\frac{dh}{dt} + \frac{h}{t_0} = 0 \qquad \text{(III.C.60)}$$

Note that the A parameter in this equation is slightly different from the definition given in (III.C.29):

$$A = \frac{[(1+\alpha^2) - (\frac{r_c^2}{2r_s b})^2]}{2g\pi r_c^2} \qquad \text{(III.C.61)}$$

Data Analysis

The numerical method presented earlier can easily be adapted to the model presented by equation (III.C.60). The point iterative formula for the head at the latest time level is still given by equation (III.C.43).

$$h^{n+1(m+1)} = \frac{coef(n-1,m)h^{n-1} + coef(n)h^{n}}{coef(n+1,m)} \qquad \text{(III.C.43)}$$

Only the coefficients are changed slightly:

$$coef(n+1,m) = 1 + (M + \frac{2(1+\alpha^2)}{gt_0\Delta t})(h^n + z_0 + b) + \frac{2\beta(1+\alpha^2)}{gt_0\Delta t} + FKA(\frac{h^{n+1(m)} - h^{n-1}}{2\Delta t}) \qquad \text{(III.C.62)}$$

$$coef(n-1,m) = 1 + (M - \frac{2(1+\alpha^2)}{gt_0\Delta t})(h^n + z_0 + b) + \frac{2\beta(1+\alpha^2)}{gt_0\Delta t} + FKA(\frac{h^{n+1(m)} - h^{n-1}}{2\Delta t}) \qquad \text{(III.C.63)}$$

$$coef(n) = \frac{4(1+\alpha^2)}{gt_0\Delta t}(h^n + z_0 + b + \beta) - \frac{2\Delta t}{t_0} \qquad \text{(III.C.64)}$$

The model represented by equation (III.C.43) and equations (III.C.62)-(III.C.64) has four parameters (α, A, β, K) that may be adjusted to fit the field data. Since α and β are highly correlated, we have had good success fitting this model to the GEMS slug-test data by setting β to zero and solving for three parameters. The error introduced by this reduction appears considerably less than that introduced by use of the Hvorslev model to represent flow in the aquifer (see Section III.E). Figures III.C.3 and III.C.4 show the comparison between the fitted theoretical model and the field data for two

series of slug tests performed at GEMS. The theory describes the head dependence and the general shape of the field data very well. Both the nonoscillatory (Figure III.C.3) and oscillatory (Figure III.C.4) data are predicted very well by the theoretical model. Field data for a variety of initial slug heights are reproduced well for a single set of parameters (α, A, K). Figures III.C.5 and III.C.6 are plots of the field data and theoretical model for one particular value of the initial slug height. These plots allow one to better assess the quality of the fit of the theoretical model to the experimental data. In general, the fit is very good. Note that earlier models (McElwee et al., 1992) fit the non-oscillatory data reasonably well, but the parameters did have some dependence on the magnitude of the slug.

The results of these field analyses reveal several features of this model. First, the effect of the viscosity term appears to be insignificant. Second, since a α^2 of 0.58 is the best-fit value, this implies that velocity components other than in the z direction, a radially nonuniform velocity distribution, and acceleration work terms arising from changes in casing radii combine to produce an effective column length that is 58% larger than the nominal column length. Finally, the A parameter was estimated to lie in the range of 1.5-2.0 s^2/m^3 for these two sets of field data. This is much larger than would be calculated from equation (III.C.61). Clearly, some physical mechanisms have been left out of the model. These mechanisms apparently have the same mathematical form as the term involving A in equation (III.C.60), but with a much larger magnitude. Two possible mechanisms are non-Darcian flow and frictional losses within the well screen. Each of these mechanisms is explored further in the following pages.

Incorporation of Non-Darcian Flow into the Nonlinear Slug-Test Model

Non-Darcian flow arises when velocities within the porous media are large enough that the hydraulic gradient is no longer a linear function of the specific discharge. For this derivation, we will assume that the relationship between the hydraulic gradient and specific discharge under non-Darcian flow conditions can be expressed as

$$\frac{dH}{dr} = wv + Bv^2 \qquad \text{(III.C.65)}$$

where

v = specific discharge;

w, B = constants of proportionality (w=-1/K, B=0 for purely laminar flow).

Note that although the second power of the velocity is employed in equation (III.C.65), any arbitrary power could be incorporated into the derivation. The second power was employed here to be consistent with most past work on non-Darcian flow in porous media (e.g., Bear, 1972; Guppy et al., 1982).

Equation (III.C.65) can be rearranged and expressed in terms of the specific discharge using the quadratic formula:

$$v = -\frac{w}{2B} \pm \sqrt{\frac{w^2}{4B^2} + \frac{1}{B}\frac{dH}{dr}} = -\frac{w}{2B} \pm y \qquad \text{(III.C.66)}$$

Since the Hvorslev model of slug-induced flow in the aquifer is based on the assumption of incompressible matrix and pore fluids (i.e. specific storage is assumed negligible), the continuity equation for flow in the aquifer can be written in its steady-state form

$$\frac{1}{r}\frac{d}{dr}(rv) = \frac{dv}{dr} + \frac{v}{r} = 0 \qquad \text{(III.C.67)}$$

Substitution of equation (III.C.66) into equation (III.C.67) yields

$$\frac{\pm dy}{w \mp 2By} = \frac{dr}{2Br} \qquad \text{(III.C.68)}$$

A straight-forward integration of equation (III.C.68) results in

$$-\ln(w \mp 2By) = \ln(r) + \ln(C') \qquad \text{(III.C.69)}$$

where

C' = integration constant.

Use of the additive properties of logarithms enables equation (III.C.69) to be rewritten as

$$\ln[rC'(w \mp 2By)] = 0 \qquad \text{(III.C.70)}$$

Equation (III.C.70) can be readily solved for y producing the following expression:

$$y = \pm\frac{w}{2B} \mp \frac{1}{2BC'r} \qquad \text{(III.C.71)}$$

Substitution of equation (III.C.71) back into equation (III.C.66) yields an expression for the specific discharge:

$$v = -\frac{1}{2BC'r} \qquad \text{(III.C.72)}$$

Employing the boundary condition at the test well, an expression for the flow into/out of the well in response to the slug-induced disturbance can be written as

$$Q(t) = -\pi r_c^2\frac{dh(t)}{dt} = v_{r_s}A_s = -\frac{1}{2BC'r_s}2\pi r_s b \qquad \text{(III.C.73)}$$

where

A_s = surface area of the well screen;

r_s = radius of the well screen;

b = screen length.

Rearrangement of equation (III.C.73) leads to an expression for specific discharge in terms of the head in the test well:

$$v = -\frac{r_c^2}{2b}\frac{dh(t)}{dt}\frac{1}{r} \qquad \text{(III.C.74)}$$

Substitution of equation (III.C.74) back into equation (III.C.65) and integration in the radial direction yields

$$H = -w\frac{r_c^2}{2b}\frac{dh(t)}{dt}\ln(r) - B[\frac{r_c^2}{2b}\frac{dh(t)}{dt}]^2\frac{1}{r} + C'' \qquad \text{(III.C.75)}$$

where

C'' = integration constant.

If we assume that the head is unchanged from static conditions (= 0) at some distance r_e (effective radius) from the test well, then the integration constant can be written as

$$C'' = B[\frac{r_c^2}{2b}\frac{dh(t)}{dt}]^2\frac{1}{r_e} + w\frac{r_c^2}{2b}\frac{dh(t)}{dt}\ln(r_e) \qquad \text{(III.C.76)}$$

Substitution of equation (III.C.76) back into equation (III.C.75) yields an expression for the head within the aquifer

$$H = -w\frac{r_c^2}{2b}\frac{dh(t)}{dt}\ln(\frac{r}{r_e}) + B[\frac{r_c^2}{2b}\frac{dh(t)}{dt}]^2[\frac{1}{r_e} - \frac{1}{r}] \qquad \text{(III.C.77)}$$

An expression for head in the well screen can be obtained by setting $r=r_s$ in equation (III.C.77)

$$H(r_s,t) = (-w\frac{r_c^2}{2b}\ln(\frac{r_s}{r_e}) + B[\frac{r_c^2}{2b}]^2[\frac{r_s - r_e}{r_e r_s}][\frac{dh(t)}{dt}])\frac{dh(t)}{dt} \qquad \text{(III.C.78)}$$

By substituting -1/K for w, equation (III.C.78) can be rewritten into a non-Darcian flow analogue to equation (III.C.22)

$$H(r_s,t) = (\frac{r_c^2}{2bK}\ln(\frac{r_s}{r_e}) + B[\frac{r_c^2}{2b}]^2[\frac{r_s - r_e}{r_e r_s}][\frac{dh(t)}{dt}])\frac{dh(t)}{dt} \qquad \text{(III.C.79)}$$

Substitution of the definition of the Hvorslev time lag (equation (III.C.28)) into equation (III.C.79) and assuming $r_s << r_e$ yields

$$H(r_s,t) = -t_0[1 + B\frac{r_c^2 K}{2br_s \ln(\frac{r_e}{r_s})}\frac{dh(t)}{dt}]\frac{dh(t)}{dt} \qquad \text{(III.C.80)}$$

Substituting equations (III.C.18) and (III.C.80) into equation (III.C.58), generalizing as with equation (III.C.59), and dividing by gt_0 yields

$$\frac{(h+z_0+b+\beta)}{gt_0}(1+\alpha^2)\frac{d^2h}{dt^2} + FK(A + B\frac{r_c^2}{4\pi b^2 r_s})(\frac{dh}{dt})^2 + [M(h+z_0+b) + 1]\frac{dh}{dt} + \frac{h}{t_0} = 0 \qquad \text{(III.C.81)}$$

The A term of equation (III.C.61) can be redefined as

$$A = \frac{[(1 + \alpha^2) - (\frac{r_c^2}{2r_s b})^2 + 2gr_s B(\frac{r_c^2}{2r_s b})^2]}{2g\pi r_c^2} \qquad \text{(III.C.82)}$$

This allows equation (III.C.81) to be rewritten in the same form as equation (III.C.60). Thus, non-Darcian flow produces an increase in the magnitude of the A parameter.

Incorporation of Frictional Losses in the Well Screen into the Nonlinear Slug-Test Model

During a slug test in high-permeability media, there are very likely some head

losses due to friction in the well screen. If there is a head loss across the well screen due to friction in the screen slots, the head in the well will not be the same as the head in the portion of the aquifer immediately adjacent to the screen. A reasonable assumption is that the frictional losses are dependent on the flow rate (Q(t)). Based on this assumption, an equation can be written to relate the head in the well (h(t)) and the head in the immediately adjacent portions of the aquifer ($H(r_s,t)$):

$$H(r_s,t) = h(t) - Q(t)R \qquad \text{(III.C.83)}$$

where

R = resistance factor.

The resistance factor is undoubtedly proportional to some power of the velocity in the well casing. For this derivation, we will assume that R is proportional to the first power of the velocity:

$$R = (A^*)|V| = (A^*)\left|\frac{dh}{dt}\right| \qquad \text{(III.C.84)}$$

where

A^* = constant of proportionality.

In the case of frictional losses within the well screen, equation (III.C.18) must be rewritten (assuming $P_a=0$) as

$$P_s = g\rho[H(r_s,t) + z_0 + b + Q(t)R] \qquad \text{(III.C.85)}$$

Substituting equations (III.C.22), (III.C.84), and (III.C.85) into equation (III.C.58), employing the definition for Q(t) given in equation (III.C.21), and generalizing as with

equation (III.C.59) produces

$$\frac{(h+z_0+b+\beta)}{gt_0}(1+\alpha^2)\frac{d^2h}{dt^2} + FK(A + A^*)(\frac{dh}{dt})^2 + [M(h+z_0+b) + 1]\frac{dh}{dt} + \frac{h}{t_0} = 0 \qquad \text{(III.C.86)}$$

If non-Darcian flow is also added into the model, the $(A + A^*)$ term of equation (III.C.86) can be redefined as

$$A = \frac{[(1 + \alpha^2) - (\frac{r_c^2}{2r_sb})^2 + 2r_sB(\frac{r_c^2}{2b^2r_s})^2 + 2g\pi r_c^2A^*]}{2g\pi r_c^2} \qquad \text{(III.C.87)}$$

This redefinition allows equation (III.C.86) to be rewritten as

$$\frac{(h+z_0+b+\beta)}{gt_0}(1+\alpha^2)\frac{d^2h}{dt^2} + FKA(\frac{dh}{dt})^2 + [M(h+z_0+b) + 1]\frac{dh}{dt} + \frac{h}{t_0} = 0 \qquad \text{(III.C.88)}$$

Thus, both non-Darcian flow in the aquifer and frictional losses within the well screen

produce an increase in the magnitude of the A parameter. Note that additional work has shown that the similarity of the representations of non-Darcian flow and frictional losses within the well screen is only found when the power of the velocity to which resistance in the well screen is proportional is one less than the power of the velocity in the second term of equation (III.C.65). This relationship appears to arise from the quasi steady-state assumption that is the basis of the Hvorslev model.

The preceding derivations indicate that the large value estimated for A from the analysis of GEMS slug-test data may be partially explained by non-Darcian flow in the aquifer and/or frictional losses within the well screen. This explanation is consistent with the results of the field tests described in Section III.B. The conclusion of those field tests was that non-Darcian flow in the aquifer and/of frictional losses within the well screen were the most likely explanation for the anomalous slug-test responses observed at GEMS.

Although we may be able to explain the magnitude of the α and A parameters obtained from the analysis of slug-test data, we still have questions about when the actual four-parameter model can be reduced to the three-parameter model used here. Clearly, this issue must be resolved prior to use of this nonlinear model for routine field applications. Even in its three-parameter form, however, experience has shown that there is a considerable degree of correlation between model parameters, making it difficult to obtain unique estimates. In an effort to develop a more straightforward approach for estimation of hydraulic conductivity from slug tests performed in high-permeability media, we have developed an approximate approach for the analysis of test data. The description of this approach is described in the following subsection.

The Projection Method: An Approximate Approach for Analysis of Slug Tests in High-Permeability Formations

Equation (III.C.88) is the most general form of the nonlinear slug-test model. All previous work on slug tests in high-permeability formations in the hydrogeologic literature has employed a variety of assumptions to reduce equation (III.C.88) to the form given in equation (III.C.35). The critical assumption in this reduction is that the nonlinear terms become negligible when the magnitude of the initial head is small (both relative to (z_0+b) and in an absolute sense). Unfortunately, little if any field work has been done to verify the soundness of this assumption. Thus, the question of whether we can actually simplify equation (III.C.88) to (III.C.35) by keeping the size of the slug-

induced disturbance very small has not yet been answered. Clearly, this is an issue of some practical importance.

In order to assess the soundness of the small-H_0 assumption, a series of carefully controlled slug tests were performed at GEMS near the end of this project. Figure III.B.13 displays results from the most extensive of these series of tests (t_0 = Hvorslev time lag = time at which a normalized head of 0.37 is obtained). The critical feature to note from this series of tests is that there does not appear to be a minimum head value below which one can neglect the head dependence. Figure III.C.7 shows results from a series of tests at another GEMS well that are combined with theoretical results obtained using equation (III.C.88). The field results are from the tests displayed on Figure III.C.3, while the theoretical results are based on additional simulations using the same parameters as determined from the field testing. The open circle labelled "Hvorslev Model" was determined using the isotropic form of the model of Hvorslev (1951). There are several noteworthy features of this figure. First, as with Figure III.B.13, the plot approaches the y axis quite steeply. Thus, it appears that it is difficult to define what a "small" slug-induced disturbance should be in tests in high-permeability media. Second, a method for the analysis of slug tests is suggested by this plot. If one could do repeat tests at the same well using H_0 values from about 0.3-1.0 meters (H_0 values should be large enough so that the effects of background noise are small), one could fit a straight line to a plot of field-determined t_0 values. The y-intercept of that line (i.e. the projection of the line to H_0=0) would be a reasonable estimate of the t_0 that one would get from a simulation using the conventional Hvorslev model. In this particular case, the t_0 calculated from the projection is about 7% larger than the t_0 from the conventional Hvorslev model. The difference is apparently due to inertial and nonlinear effects that remain significant at very small H_0. Although the difference is not large at this well, the difference is much greater in the more permeable units. Figure III.C.8 displays theoretical results for parameters characteristic of a highly permeable aquifer. In this case, the t_0 estimate obtained from the projection would lead to a poor K estimate (about 50% of actual K) if it is used with the conventional Hvorslev model. Thus, a modification of the approach is required if it is going to be generally applicable in highly permeable media.

The "Hvorslev" t_0 estimates shown on Figures III.C.7-III.C.8 were obtained using the conventional form of the Hvorslev model. One reasonable modification to the proposed approach would be to develop a form of the Hvorslev model that incorporates inertial effects. As shown in the derivation earlier in this section, this would involve obtaining a solution to equation (III.C.35). Kipp (1985) obtained a solution to an

equation similar to (III.C.35) using the Theis model to represent slug-induced flow in the aquifer. Springer and Gelhar (1991) obtained a solution based on the Bouwer and Rice model of flow in the aquifer. As shown earlier, a solution using the Hvorslev model can be obtained in a similar manner.

A dimensionless form of equation (III.C.35) can be written in the following manner:

$$\frac{d^2h_D}{dt_D^2} + C^*\frac{dh_D}{dt_D} + h_D = 0 \qquad \text{(III.C.89)}$$

where

$h_D = h/H_0$;

$t_D = t(g/(z_0+b))^{0.5}$;

$$C^* = \frac{r_c^2 \ln(b/r_s)}{2bK}(g/(z_0+b))^{0.5}(M(z_0+b)+1) \quad .$$

Note that the C^* term incorporates the Hvorslev shape factor for a partially penetrating well (assuming $b/r_s > 8$). Note also that the $M(z_0+b)$ term is almost always very small, and therefore can be ignored for most practical applications.

Solutions to equation (III.C.89) can be readily obtained (see equations (III.C.36)-(III.C.40)), and can be expressed in graphical form as a series of type curves in which each curve is characterized by a particular value of C^*. Figure III.C.9 displays a series of type curves developed from the solution of equation (III.C.89). Kipp (1985) and Springer and Gelhar (1991) describe two approaches for estimation of hydraulic conductivity that are based on type curves such as those shown in Figure III.C.9. The basic idea is to determine a value for C^* by comparing field data to the type curves and then estimate K from that C^* value. Kruseman and de Ridder (1989) describe a related approach for the underdamped case only ($C^* < 2$) that employs the period of the oscillation, the ratio between two adjacent peaks or troughs, and a nomograph to estimate K.

Although a type-curve approach based on equation (III.C.35) may, at first glance, appear as a viable field method, it does neglect the mechanisms that introduce

nonlinearities into the slug-test responses. The validity of the approach therefore depends on how the type curves change with H_0 in the presence of these nonlinear mechanisms. Figure III.C.10 displays the solution to equation (III.C.88) as a function of H_0 for the same parameters as used in Figure III.C.8. The solution to equation (III.C.89) is also included for comparative purposes. There are four points to note from this figure. The first is that the shape of the type curves changes tremendously as a function of H_0. Second, given the strong dependence on H_0 and the range of H_0s feasible in field applications, it may be difficult to obtain a K estimate that is within a factor of two of the actual value using the type curves of Figure III.C.9. Third, even at extremely small H_0, there will still be a small difference between the solutions to equations (III.C.88) and (III.C.89). This difference is primarily a function of the α^2 term that is ignored in equation (III.C.89). Fourth, it appears that as H_0 decreases the plots converge quite smoothly on t_0. Thus, a modified version of the projection method described earlier could be viable in highly-permeable systems.

The approach proposed here is to recognize that there is a unique dimensionless t_0 value ($t_{0D} = t_0/(\sqrt{(z_0+b)/g})$) for each C^* curve. Figure III.C.11 is a plot of the relationship between t_{0D} and C^*. Since Figure III.C.10 indicates that there is a convergence on t_0 with decreasing H_0 and since one should know the value of (z_0+b), a t_{0D} value can be calculated from test data using the projection method. One can readily estimate C^* from Figure III.C.11 and then calculate K from the C^* value. There are two points concerning this approach that need to be emphasized. First, given the form of Figure III.C.11, estimation of t_0 from field data must be done quite carefully. Electronic data acquisition equipment is clearly required. Also, repeat tests must be performed at each H_0 value in order to assess the magnitude of dynamic-skin effects (see Section III.E). Second, additional inertial effects (i.e. the effects encapsulated in the α term) may not be negligible at small values of H_0. Thus, the K estimate obtained using the proposed approach will be lower than the actual estimate when such effects are significant. It is important to emphasize that these additional effects appear in the model as an uncertainty about the effective length of the water column. An example of the error in the K estimate is shown in Figure III.C.12, which is similar to Figure III.C.8 except that the value predicted from equation (III.C.89) is included on the plot. Figure III.C.13 is an expanded view of the 0.0-1.0 m range in H_0. Note that the projection line was calculated only using the two points denoted A (H_0=0.667 m) and B (H_0=0.305 m). This plot clearly shows the linear relationship at small heads that is the basis of the projection method. Although the projection method produces a higher t_0 due to the

neglected additional inertial effects, the difference in K values is now only 9%. Given the possible errors introduced by other approaches, this error appears acceptable.

Since this projection method was developed in the final phase of this research project, it has not yet been thoroughly tested using field data. The limited results that have been obtained, however, indicate that it holds considerable promise as a practical field method.

Summary

In this section, a new general nonlinear slug-test model was introduced. This model allows the effects of nonlinearities, inertia, turbulence, radially nonuniform velocity distributions, viscous work within the well casing, and changing casing radii to be assessed. Although the effect of viscous work within the well casing appears to be small, the other mechanisms may be important in tests in highly permeable media. Efforts to use an approximate three-parameter (α, A, K) form of this model to analyze GEMS slug-test data appear successful. The model reproduces the key features of the GEMS data. These include the dependence on the magnitude of the initial head and the concave downward curvature when data are plotted in the Hvorslev format. The final form of the model also helps explain the magnitude of the α and A parameters determined from analysis of GEMS slug-test data. Further work is clearly required in order to better understand the relationship between the α and β parameters, and when the actual four-parameter model can be reduced to the three-parameter model used in the applications of this section. Preliminary results, however, indicate that the error introduced by this reduction is considerably less than that introduced by use of the Hvorslev model to represent flow in the aquifer.

Although this model appears to incorporate the majority of the relevant mechanisms controlling slug-test responses, it may be difficult to use on a routine basis. In an effort to obtain a tool for routine field analyses, we have developed an approximate approach called the Projection Method. This approach is based on the idea that the nonlinear effects should become insignificant as the initial head goes to zero. Preliminary theoretical and field analyses of this approach appear quite promising. The major error in the estimated K is introduced through uncertainty concerning the effective length of the water column. It does not appear, however, that the error in K should exceed 10-15%. Further field and theoretical verification of this approximate approach is continuing.

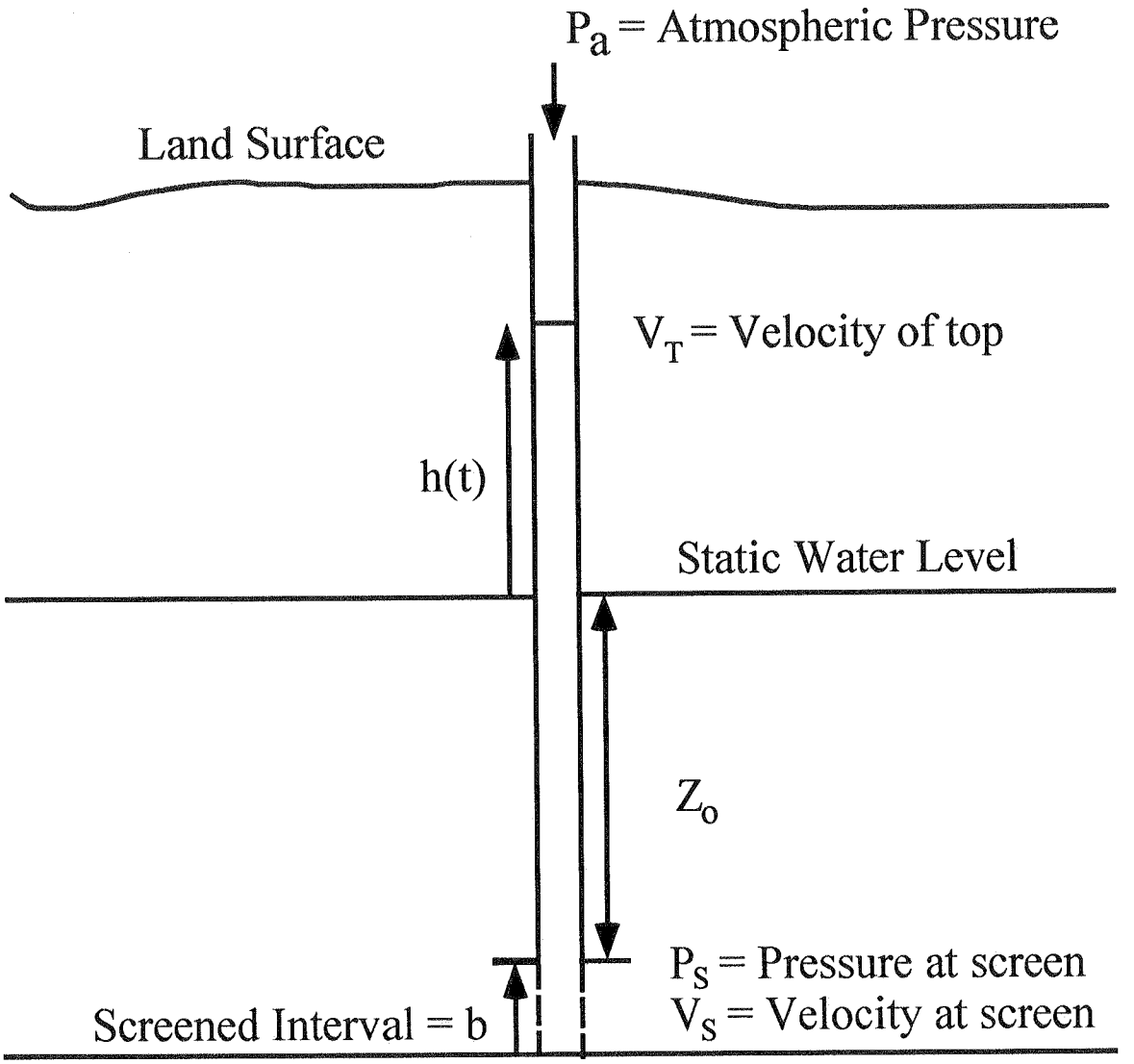

Figure III.C.1 - Cross-sectional view of slug-test configuration.

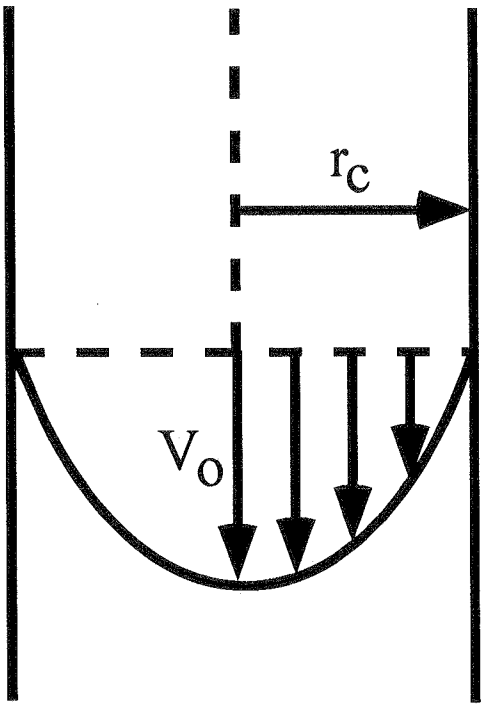

Figure III.C.2 - Assumed radial velocity distribution employed in nonlinear slug-test model derivation.

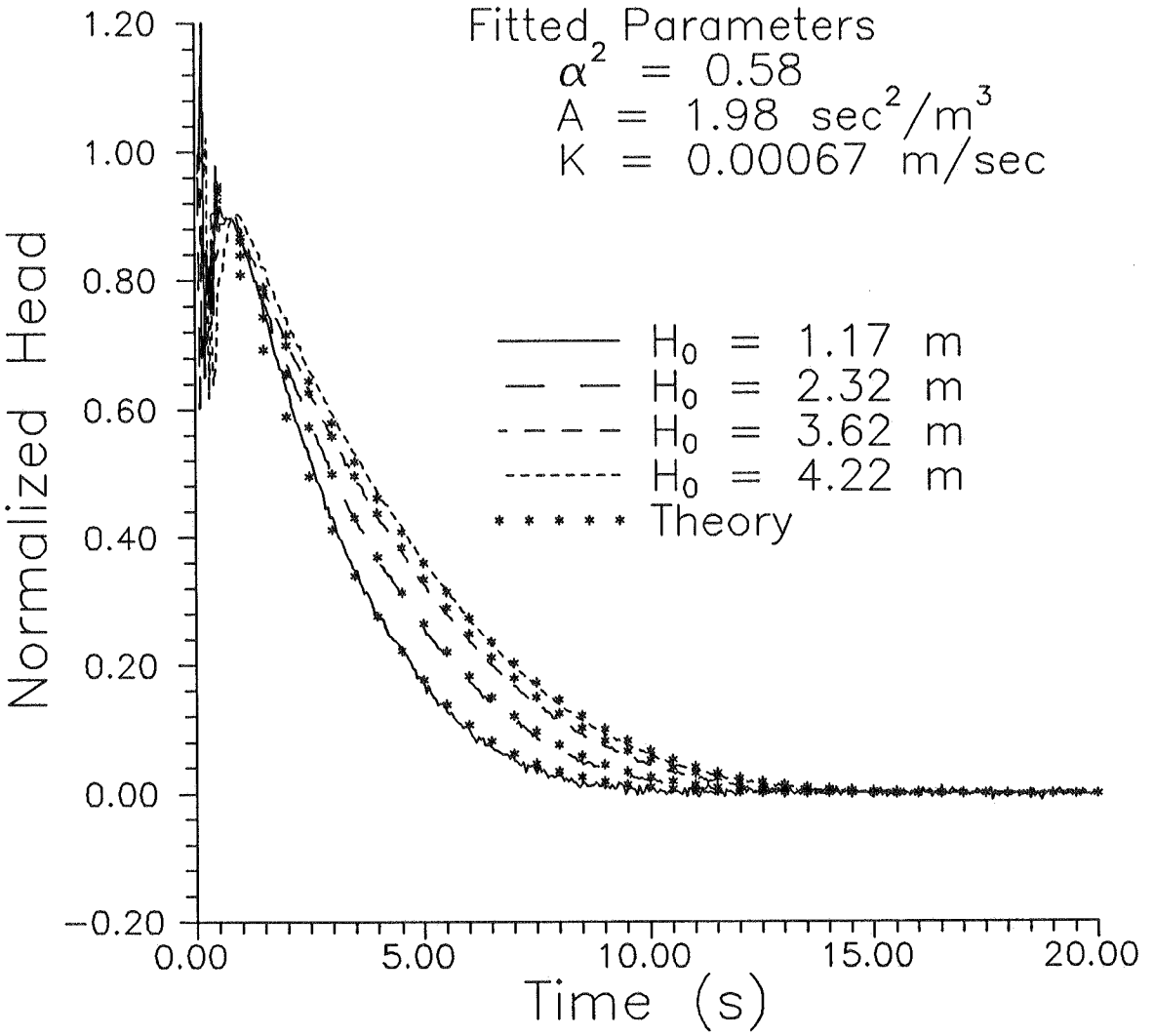

Figure III.C.3 - Normalized head versus time plot and the best-fit nonlinear model for a series of slug tests at GEMS well 02.

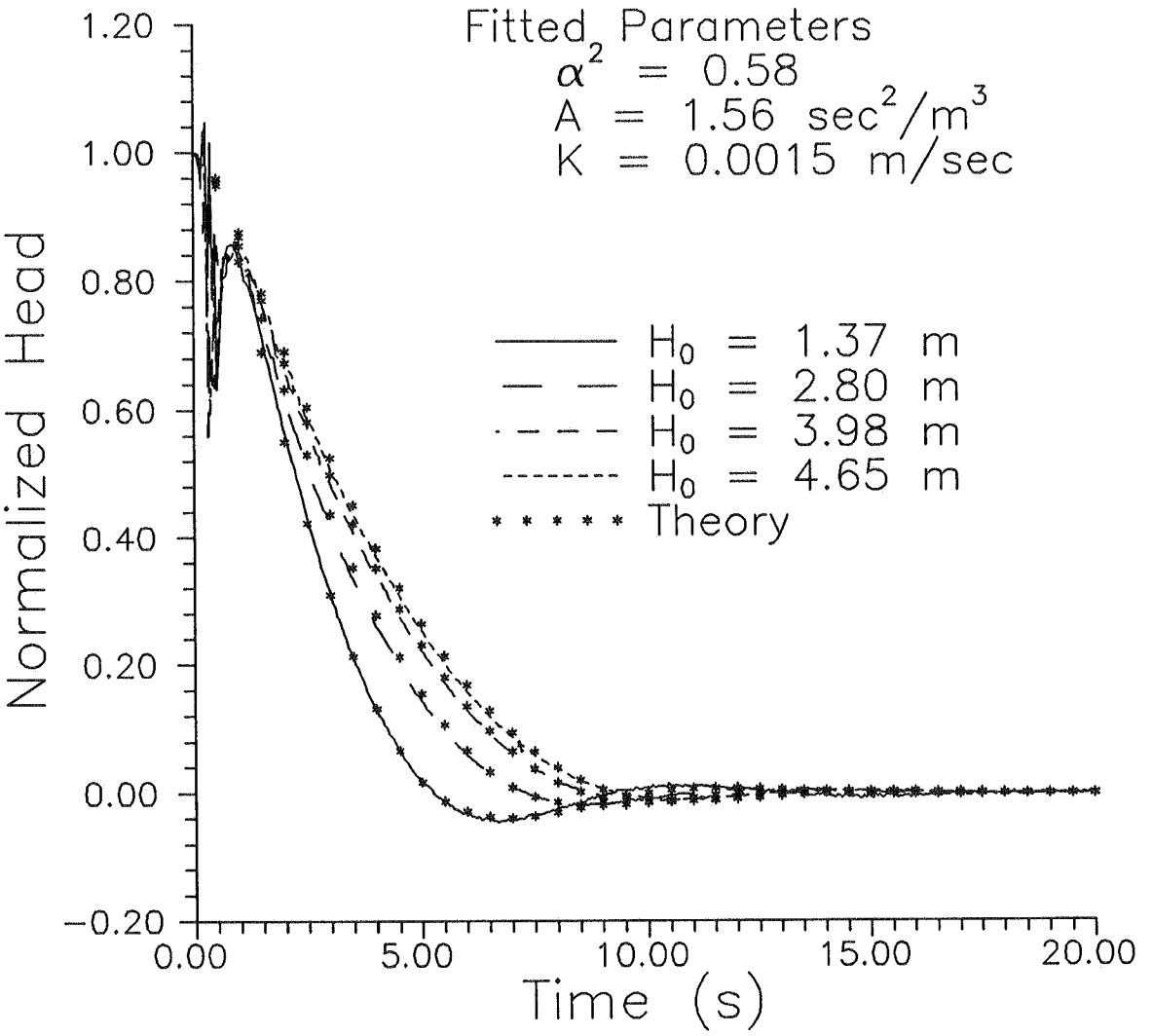

Figure III.C.4 - Normalized head versus time plot and the best-fit nonlinear model for a series of slug tests at GEMS well 07.

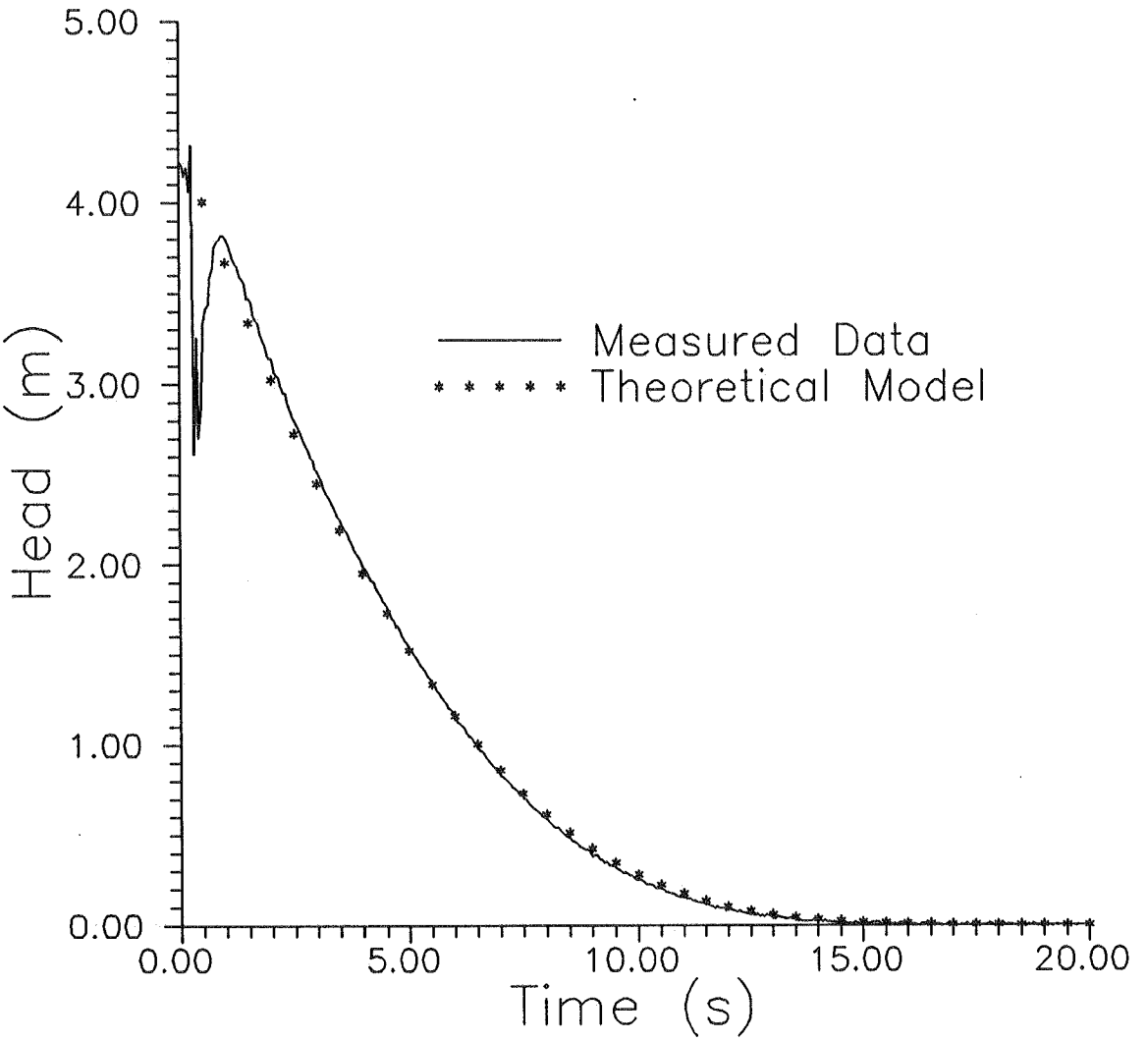

Figure III.C.5 - Head versus time plot and the best-fit nonlinear model for a single slug test at GEMS well 02 (fitted parameters as in Figure III.C.3).

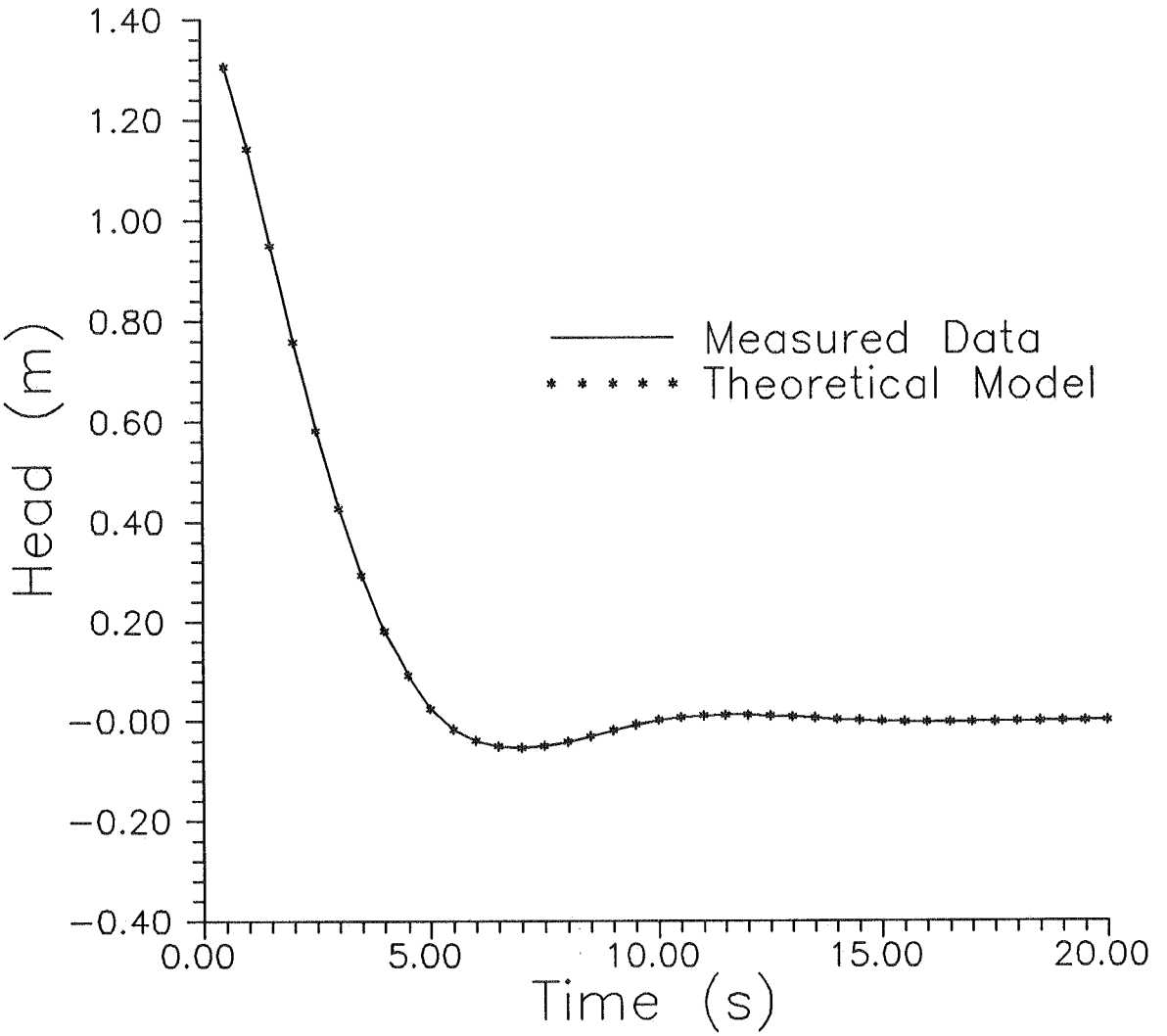

Figure III.C.6 - Head versus time plot and the best-fit nonlinear model for a single slug test at GEMS well 07 (fitted parameters as in Figure III.C.4).

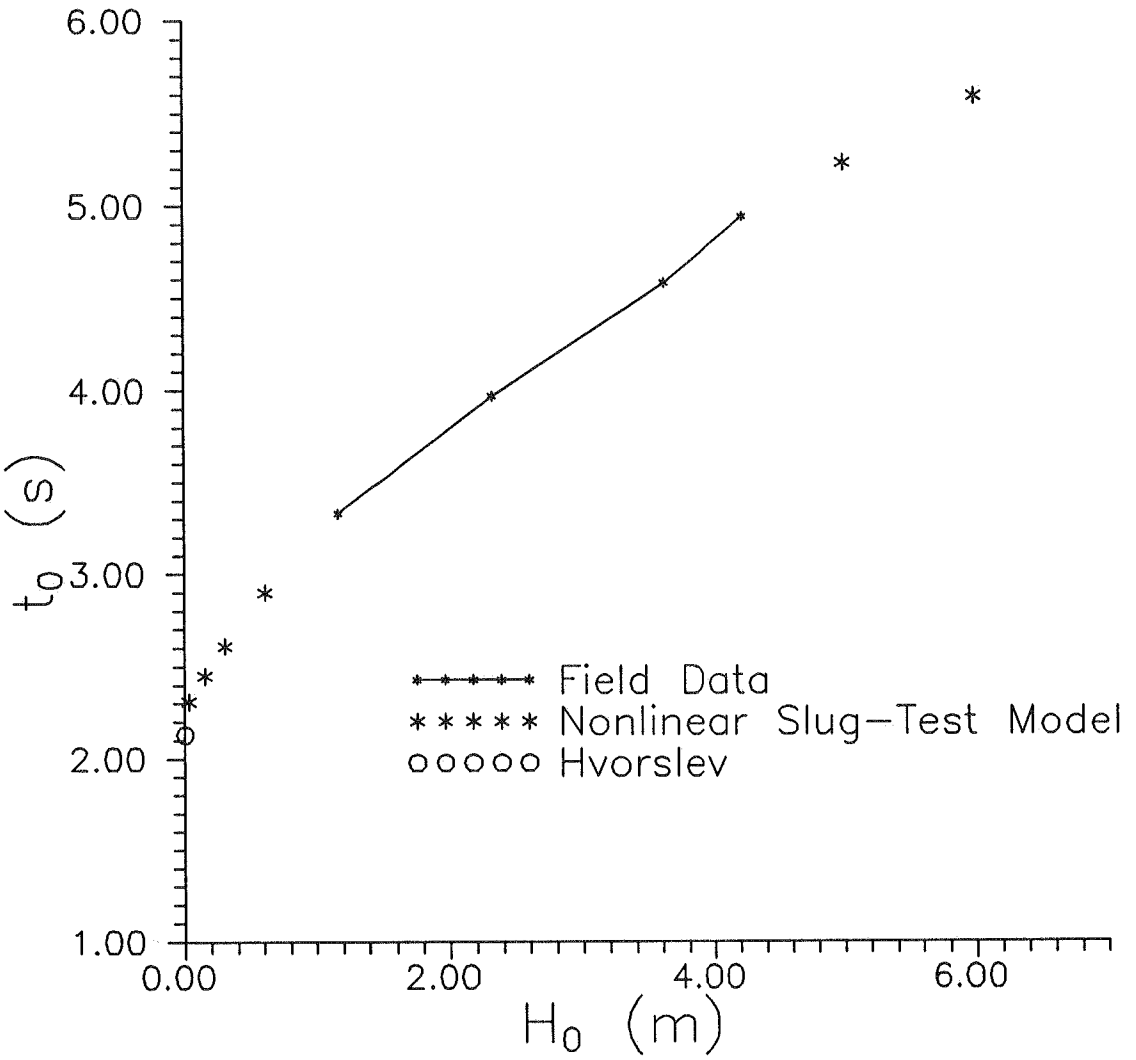

Figure III.C.7 - Plot of Hvorslev time lag (t_0) versus initial head (H_0) for slug tests at GEMS well #02. Nonlinear slug-test model simulations use same parameters as determined from analysis of field data with nonlinear model. Hvorslev model uses same K as in the nonlinear model simulations.

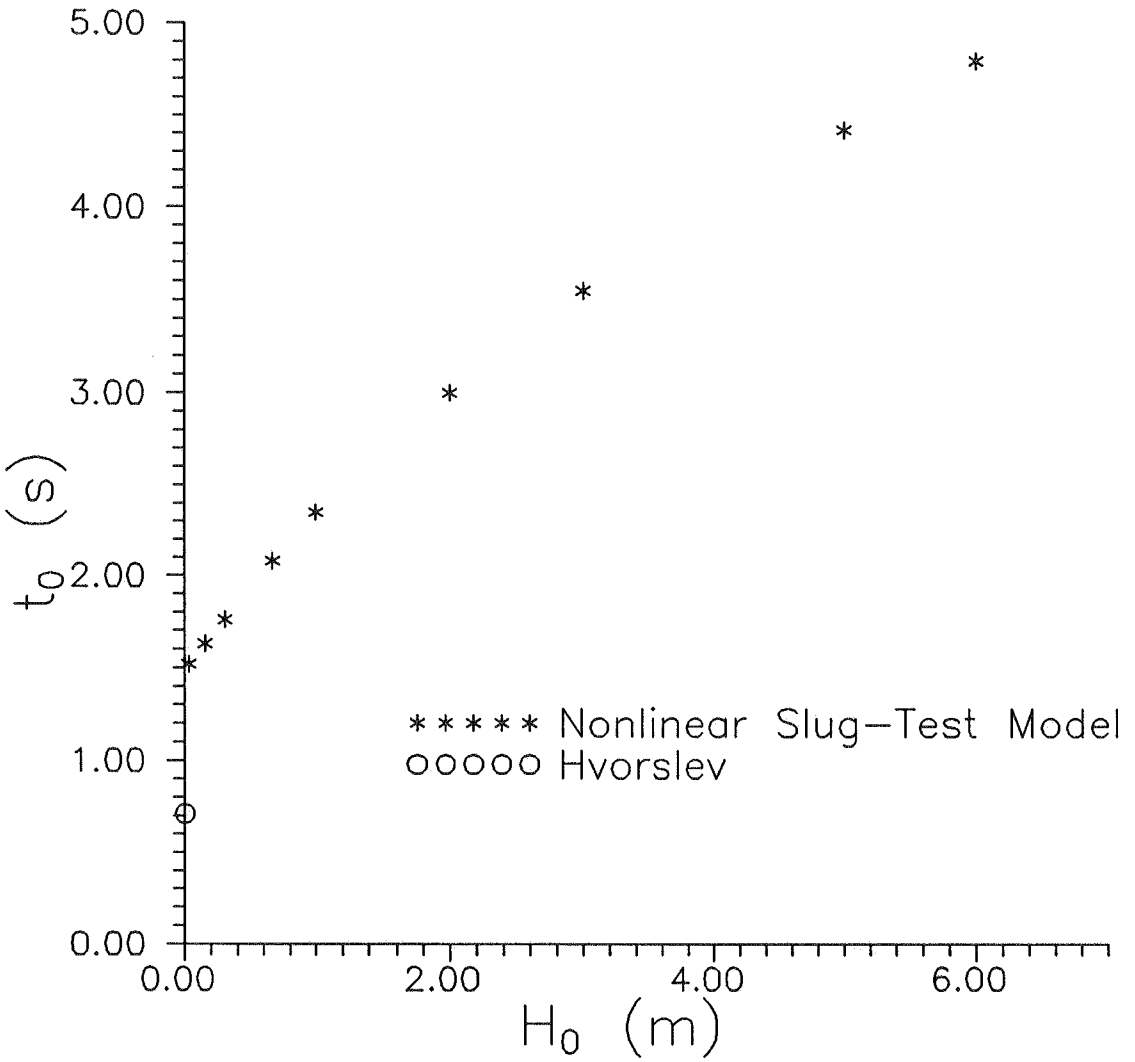

Figure III.C.8 - Plot of Hvorslev time lag (t_0) versus initial head (H_0) for simulated slug tests in a highly permeable aquifer (K=0.0020 m/s, A=1.98 s^2/m^3, α^2=0.58). Hvorslev model uses same K as in the nonlinear slug-test model simulations.

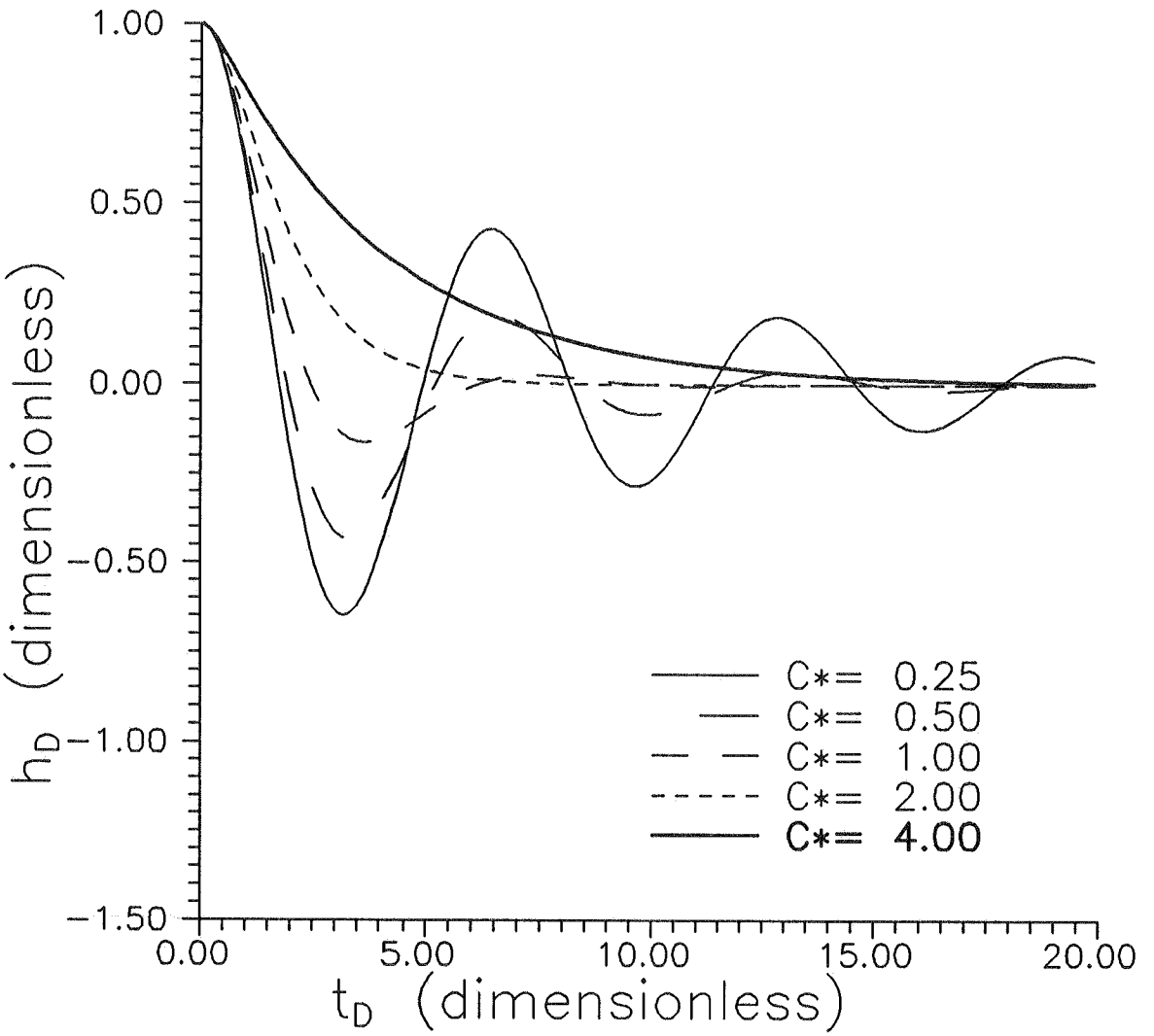

Figure III.C.9 - h_D versus t_D type curves for Hvorslev model with inertial effects. Each curve characterized by a unique C^* value (C^*, h_D, and t_D defined in equation (III.C.89)).

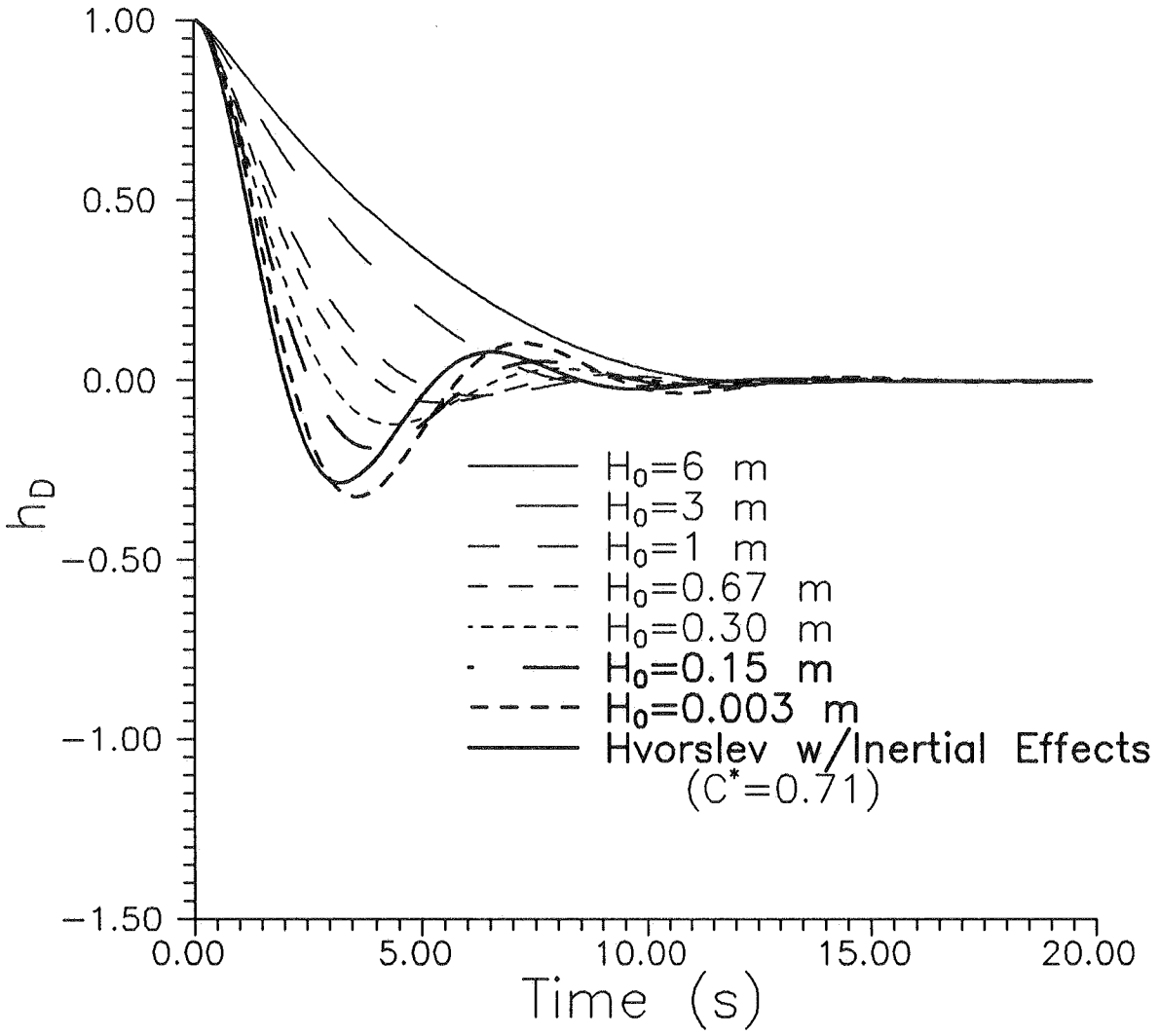

Figure III.C.10 - Plot of normalized head (h_D) versus time as a function of H_0 for simulated slug tests in a highly permeable aquifer (same parameters as in Figure III.C.8). Results of Hvorslev model with inertial effects are also plotted for comparison purposes.

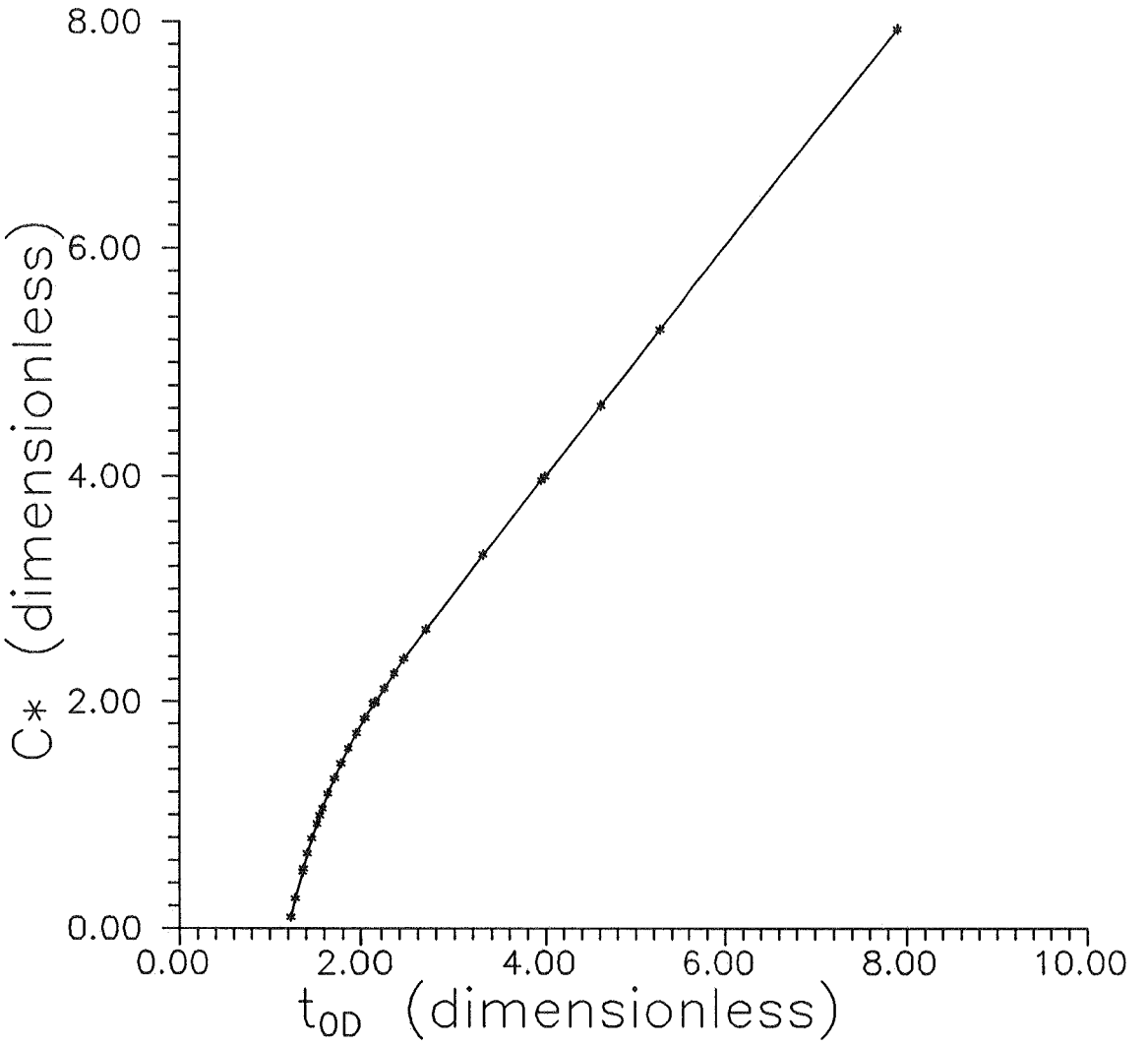

Figure III.C.11 - C^* versus t_{0D} plot for Hvorslev model with inertial effects (C^* defined in equation (III.C.89), $t_{0D} = t_0/(\sqrt{(z_0+b)/g})$).

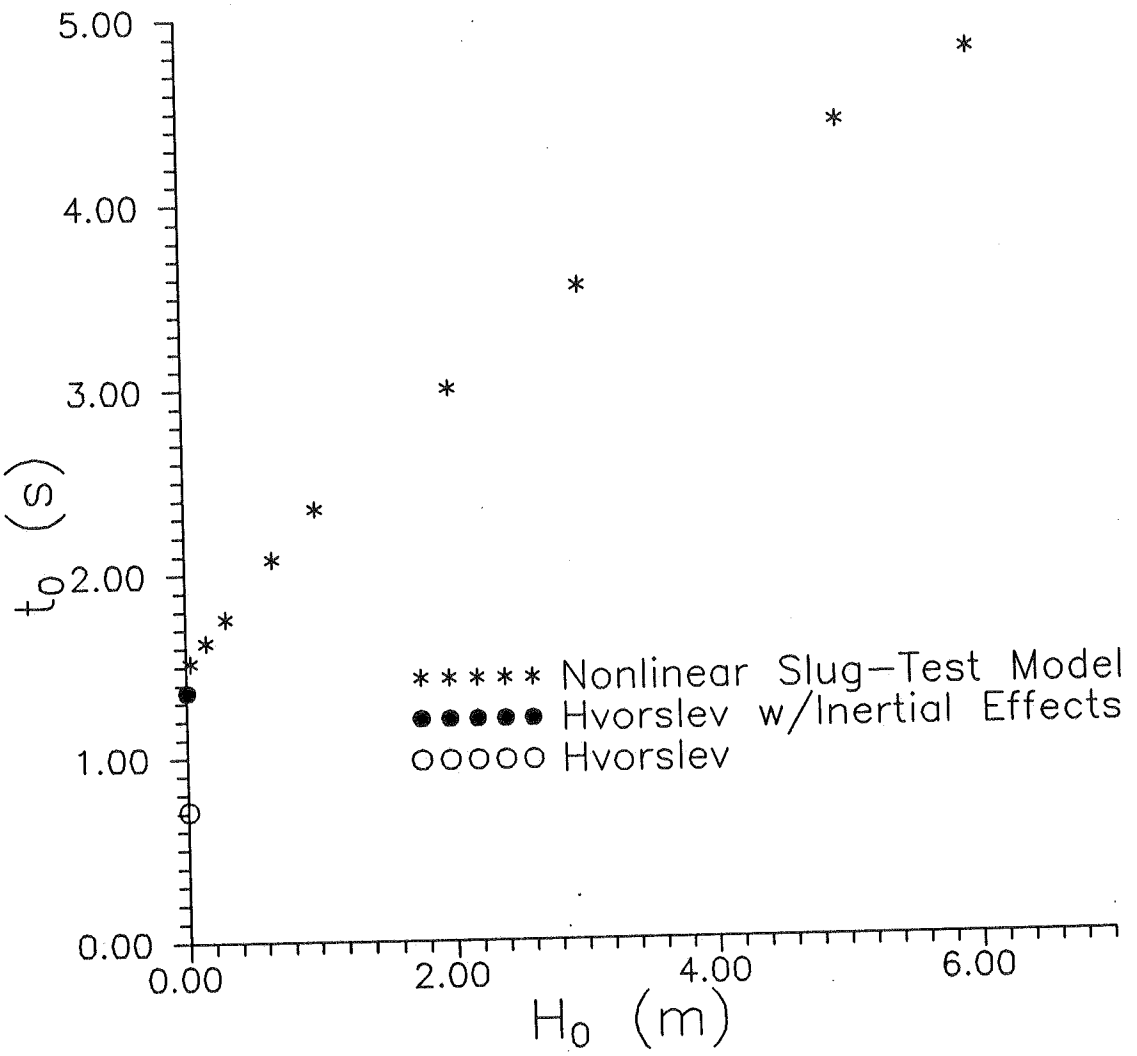

Figure III.C.12 - Plot of Hvorslev time lag (t_0) versus initial head (H_0) for simulated slug tests in a highly permeable aquifer (same parameters as in Figure III.C.8). The two variants of the Hvorslev model use same K as in the nonlinear slug-test model simulations.

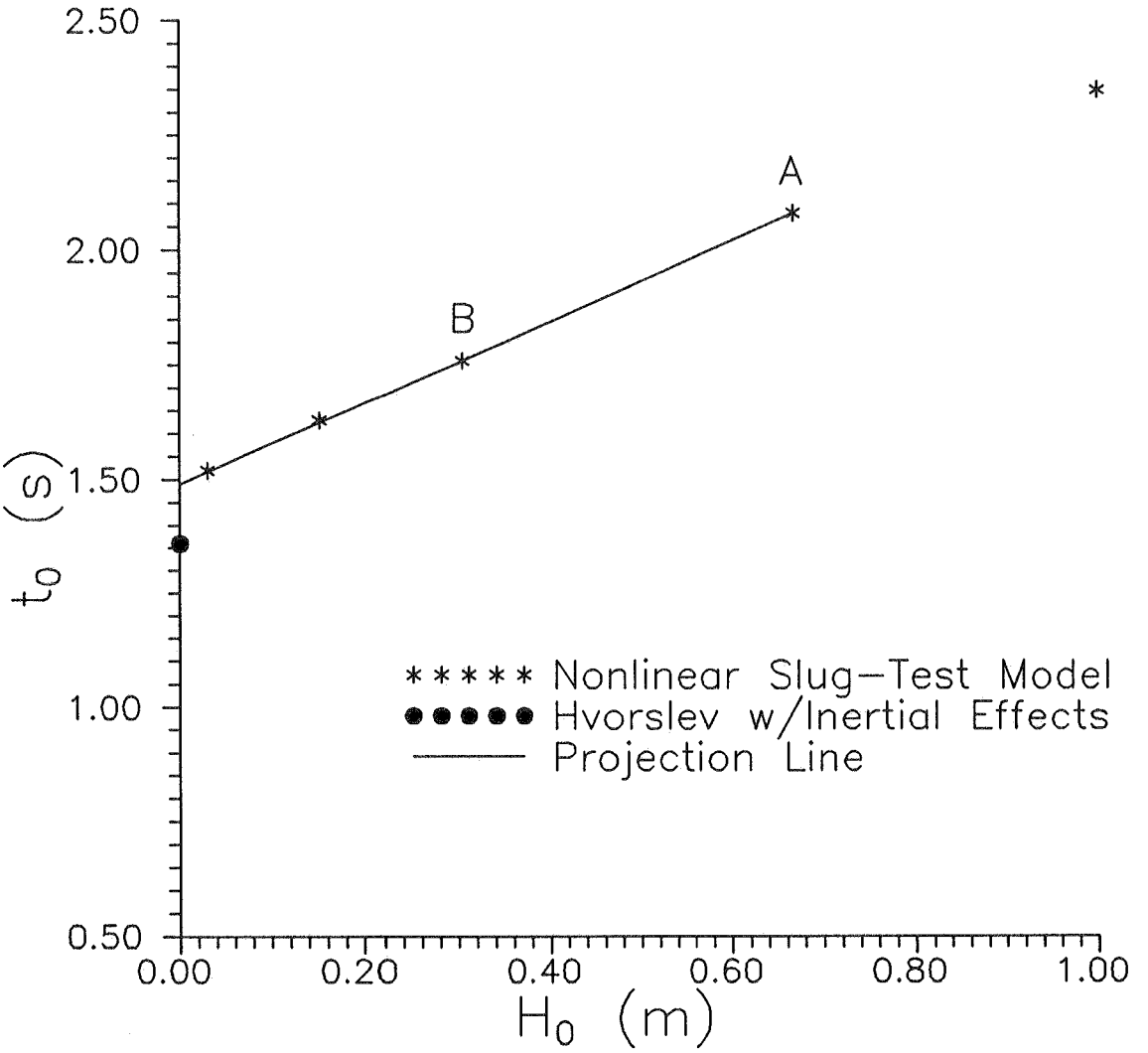

Figure III.C.13 - Plot of Hvorslev time lag (t_0) versus initial head (H_0) for simulated slug tests in a highly permeable aquifer (same parameters as in Figure III.C.8). The Hvorslev model with inertial effects uses same K as in the nonlinear slug-test model simulations. Points labelled A and B were used to calculate the slope of the projection line.

D. SLUG TESTS WITH OBSERVATION WELLS

Introduction

Traditionally, slug tests have been performed using a single well as both the site of the stress and the site at which measurements are taken. In Section II.C, theoretical and field results were reported that demonstrated the benefits of using observation wells other than the stressed well in slug tests. The most noteworthy of these results was the finding that the reliability of the parameter estimates can be improved through the use of observation wells. In the case of the storage parameter, the improvement is quite dramatic. The field experiment described in Section II.C involved wells approximately 6.5 meters apart. The transmission of the slug-induced pressure disturbance over that distance indicates that the estimated parameters from slug tests are reflective of conditions over a much larger volume of the formation than is normally considered to be influencing the results of a slug test. In cases where large volumetric averages of formation parameters are desired, slug tests may provide an alternative to pumping tests. Clearly, slug tests present several advantages to conventional pumping tests. These include the small amount of equipment and manpower required to perform a test, the relatively short duration of the test, and the need for only a small amount of water (if any) to be added/removed from the well during the course of the test. As discussed in Section II.B, the advantage of being able to initiate a slug test without adding or removing water from the well is very important for testing at sites of known or suspected contamination. However, if information about the hydraulic boundaries of a flow system is desired, slug tests do not provide a viable alternative to pumping tests.

To date, there has been very little field work reported on the use of observation wells with slug tests (henceforth designated as multiwell slug tests). One of the few contributions in this area outside of the research of this project has been the work of Novakowski (1989a) in which he presents an application of a semianalytical solution for the response in an observation well to a pressure disturbance introduced instantaneously at a central well. Both the observation well and the stressed well are assumed to be fully screened across the aquifer. Well-bore storage is accounted for at the stressed well and, in an approximate fashion, at the observation well. Recently, van Dyke et al. (1993) describe the use of multiwell slug tests at a monitoring site in New Jersey. Unfortunately, the method that they employ for the analysis of the response data, which follows the approach of Walter and Thompson (1982), ignores well-bore storage effects at the stressed and observation wells, thereby introducing a large amount of error into the parameter estimates.

In this section, additional field and theoretical work concerning multiwell slug tests is reported. A program of multiwell slug tests at the Geohydrologic Experimental and Monitoring Site (GEMS) is described. The estimated parameters obtained from these tests were considerably larger than expected. A theoretical examination of multiwell slug tests using a recently developed semianalytical solution is then presented. The results of this theoretical investigation provide one explanation for the larger than expected parameter estimates.

Field Testing at GEMS

Well 10-1 (depth 17.32 m, screen length 0.76 m) was selected as the test well for a program of multiwell slug tests because of its proximity to several groups of wells that could be used as observation wells (see Figure IV.B.1). The tests reported here involved using well 6-2 (depth = 21.55 m, screen length = 11.55 m, distance from 10-1 = 5.62 m) and well 00-1 (depth = 17.04 m, screen length = 0.76 m, distance from 10-1 = 6.61 m) as observation wells. In all cases, the slug test was initiated at 10-1 using the slug-test packer system described in Section III.A. Measurements at the observation wells were taken using a transducer attached to the bottom of a packer located beneath the static water level in the well. The packer enabled effects associated with wellbore storage at the observation well to be kept very small. The response data could thus be analyzed without considering the effects of wellbore storage at the observation well.

Figures III.D.1 and III.D.2 display the responses observed at wells 6-2 and 00-1, respectively, for a slug test performed at well 10-1. In all cases, the responses at the stressed well exhibited the anomalous behavior discussed in Sections III.B and III.C. Note the very low normalized heads measured at the two observation wells. The head changes at the observation wells were so small that the effective resolution of the transducers produced a stepped pattern in the measured responses. The responses at well 6-2 were approximately 33% smaller than those at 00-1, even though 6-2 is one meter closer to 10-1 than 00-1. Several explanations can be advanced for the difference between the responses at 6-2 and 00-1: 1) the well at 6-2 is screened for a considerable length, so head increases at the same vertical interval as the stressed well are dampened by vertical movement of water in the well; 2) the resolution of the transducers causes the measured difference in the responses to be greater than the actual difference; and 3) spatial variations (heterogeneities) in flow properties produce a lower diffusivity (K/S_s) between wells 10-1 and 6-2 than that between wells 10-1 and 00-1. Additional testing with a higher resolution pressure transducer and use of additional wells is currently being carried out to evaluate which of these explanations is the most

reasonable.

Figures III.D.3 and III.D.4 display the results of an analysis of the response data using the fully penetrating slug-test model of Cooper et al. (1967). Although the fits appear relatively good (especially considering the stepped nature of the measured responses), the parameter estimates are much larger than the results obtained from the single-well slug tests discussed in the previous section. In addition, the parameter values exceed the maximum values (for both K and S_s) that would be plausible for the sand and gravel aquifer at GEMS (e.g., Anderson and Woessner, 1992). In an attempt to explain the anomalously high parameter values that were obtained in the field tests, a further theoretical investigation of multiwell slug tests was undertaken. The results of the initial portion of this work are reported below.

Extension of Hyder et al. (1994) Solution to Case of Multiwell Slug Tests

The Cooper et al. model that was used in the analysis of the responses at wells 6-2 and 00-1 is based on the assumption that both the stressed well and the observation well are fully screened across the aquifer. Since well 10-1 is screened for only 0.76 meters of a 10.7 meter sequence of sand and gravel, the fully screened assumption of the Cooper et al. model is clearly being violated. In order to assess the error that is introduced into parameter estimates through use of a fully penetrating well model to analyze results from multiwell slug tests performed in partially penetrating wells, a recently developed semianalytical solution for slug tests in partially penetrating wells (Hyder et al., 1994; Liu and Butler, 1995, henceforth designated as the KGS model) was extended to the case of observation points at other than the stressed well.

Equations (1)-(9) of Hyder et al. (1994) describe the flow conditions of interest here. To work with the most general form of the solution, this derivation is performed using dimensionless equations. The dimensionless analogues of (1)-(9) of Hyder et al. (1994) are as follows:

$$\frac{\partial^2 \phi_i}{\partial \xi^2} + \frac{1}{\xi}\frac{\partial \phi_i}{\partial \xi} + \psi_i^2 \frac{\partial^2 \phi_i}{\partial \eta^2} = R_i \frac{\partial \phi_i}{\partial \tau} \qquad \text{(III.D.1)}$$

$$\phi_i(\xi,\eta,0) = 0,\ \xi \geq 1,\ 0 \leq \eta \leq \beta \qquad \text{(III.D.2)}$$

$$\Phi(0) = 1 \qquad \text{(III.D.3)}$$

$$\phi_2(\infty,\eta,\tau) = 0,\ \tau > 0,\ 0 < \eta < \beta \qquad \text{(III.D.4)}$$

$$\frac{\partial \phi_i(\xi,0,\tau)}{\partial \eta} = \frac{\partial \phi_i(\xi,\beta,\tau)}{\partial \eta} = 0,\ \xi > 1,\ \tau > 0 \qquad \text{(III.D.5)}$$

$$\int_{\varsigma}^{\varsigma+1} \phi_1(1,\eta,\tau)d\eta = \Phi(\tau),\ \tau > 0 \qquad \text{(III.D.6)}$$

$$\frac{\partial \phi_1(1,\eta,\tau)}{\partial \xi} = \frac{\gamma}{2}\frac{d\Phi(\tau)}{d\tau}\square(\eta),\ \tau > 0 \qquad \text{(III.D.7)}$$

$$\phi_1(\xi_{sk},\eta,\tau) = \phi_2(\xi_{sk},\eta,\tau),\ 0 \leq \eta \leq \beta,\ \tau > 0 \qquad \text{(III.D.8)}$$

$$\frac{\partial \phi_1(\xi_{sk},\eta,\tau)}{\partial \xi} = \gamma\frac{\partial \phi_2(\xi_{sk},\eta,\tau)}{\partial \xi},\ 0 \leq \eta \leq \beta,\ \tau > 0 \qquad \text{(III.D.9)}$$

where

$\phi_i = h_i/H_0$;

$\xi = r/r_w$;

$\eta = z/b$;

$\tau = (tbK_{r2})/(r_c^2)$;

$\psi_i = (A_i/a^2)^{.5}$;

$A_i = K_{zi}/K_{ri}$;

$a = b/r_w$;

$R_i = \gamma\alpha/2\lambda$, i = 1,

$= \alpha/2$, i = 2;

$\lambda = S_{s2}/S_{s1}$;

$\beta = B/b$;

Φ = head in the stressed well = H/H_0;

$\gamma = K_{r2}/K_{r1}$;

$\alpha = (2r_w^2 bS_{s2})/r_c^2$;

$\square(\eta)$ = boxcar function = 0, $\eta < \varsigma$, $\eta > \varsigma + 1$,

= 1, elsewhere;

$\varsigma = d/b$;

$\xi_{sk} = r_{sk}/r_w$.

A solution can be obtained for (III.D.1)-(III.D.9) through the use of integral transforms (Churchill, 1972). A Laplace transform in time followed by a finite Fourier cosine transform in the η direction produce a Fourier-Laplace space analogue to (III.D.1) of the following form:

$$\frac{\partial^2\overline{\phi_i}}{\partial\xi^2} + \frac{1}{\xi}\frac{\partial\overline{\phi_i}}{\partial\xi} - (\psi_i^2\omega^2 + R_i p)\overline{\phi_i} = 0 \qquad \text{(III.D.10)}$$

where

$\overline{\phi_i}$ = the Fourier-Laplace transform of ϕ_i, $f(\xi,\omega,p)$;

ω = the Fourier-transform variable = $(n\pi)/\beta$, n=0,1,2,..;

p = the Laplace-transform variable.

The Fourier-Laplace space solution to (III.D.10) is quite straightforward, as (III.D.10) is simply a form of the modified Bessel equation (Haberman, 1987). A solution can therefore be proposed in the form:

$$\overline{\phi_i} = C_i K_0(\nu_i \xi) + D_i I_0(\nu_i \xi) \qquad \text{(III.D.11)}$$

where

$\nu_i = (\psi_i^2 \omega^2 + R_i p)^{.5}$;

C_i, D_i = constants;

K_i = modified Bessel function of the second kind of order i;

I_i = modified Bessel function of the first kind of order i.

Using the transform-space analogues of auxiliary conditions (III.D.4) and (III.D.6)-(III.D.9), the constants in (III.D.11) can be evaluated. The transform-space expression for head at an arbitrary radial distance can be written as:

$$\overline{\phi_i}(\xi,\omega,p) = \frac{\gamma}{2}[1-p\Phi(p)]F_c(\omega)f_{i+1} \qquad \text{(III.D.12)}$$

where

$\Phi(p)$ = Laplace transform of $\Phi(t)$, the nondimensional form of H(t),

$$= \frac{\frac{\gamma}{2}\Omega}{[1 + \frac{\gamma}{2}p\Omega]}$$

$$\Omega = \int_{\varsigma}^{\varsigma+1} (F_c^{-1}(F_c(\omega)f_1))d\eta;$$

F_c^{-1} = inverse finite Fourier cosine transform;

$F_c(\omega)$ = finite Fourier cosine transform of $\square(z)$

$$= \frac{2}{\omega}\sin(\frac{\omega}{2})\cos(\frac{\omega(1+2\varsigma)}{2}),\ \omega = n\pi/\beta,\ n=1,2,3...,$$

$$= 1,\ \omega = 0;$$

$$f_1 = \frac{[\Delta_2 K_0(\nu_1)-\Delta_1 I_0(\nu_1)]}{\nu_1[\Delta_2 K_1(\nu_1)+\Delta_1 I_1(\nu_1)]};$$

$$f_2 = \frac{[\Delta_2 K_0(\nu_1\xi)-\Delta_1 I_0(\nu_1\xi)]}{\nu_1[\Delta_2 K_1(\nu_1)+\Delta_1 I_1(\nu_1)]};$$

$$f_3 = \frac{[\Delta_2 K_0(\nu_1\xi_{sk})-\Delta_1 I_0(\nu_1\xi_{sk})]K_0(\nu_2\xi)}{K_0(\nu_2\xi_{sk})\nu_1[\Delta_2 K_1(\nu_1)+\Delta_1 I_1(\nu_1)]};$$

$$\Delta_1 = K_0(\nu_1\xi_{sk})K_1(\nu_2\xi_{sk})-[\frac{N}{\gamma}]K_0(\nu_2\xi_{sk})K_1(\nu_1\xi_{sk});$$

$$\Delta_2 = I_0(\nu_1\xi_{sk})K_1(\nu_2\xi_{sk})+[\frac{N}{\gamma}]K_0(\nu_2\xi_{sk})I_1(\nu_1\xi_{sk});$$

$$N = \nu_1/\nu_2.$$

The application of an inverse finite Fourier cosine transform to (III.D.12) produces the following Laplace-space expression:

$$\phi_i(\xi,\eta,p) = \frac{\gamma/2}{(1+(\gamma/2)p\Omega)}\Omega_i \qquad \text{(III.D.13)}$$

where

$$\Omega_i = F_c^{-1}[F_c(\omega)f_i]$$

$$= \frac{f_i(n=0)}{\beta} + \frac{4}{\pi}\sum_{n=1}^{\infty}\frac{f_i(n)}{n}\sin(\frac{n\pi}{2\beta})\cos(\frac{n\pi(1+2\varsigma)}{2\beta})\cos(\frac{n\pi\eta}{\beta})$$

Equation (III.D.13) was developed for the case of an observation well that can be represented as a point (ξ,η). Although this approach might be reasonable for a well with an extremely short screen, it is clearly not appropriate in the general case. A more general approach would be to define the observation-well head as a vertical average:

$$\phi_{ow_i} = \frac{1}{\Delta\zeta}\int_{\zeta_1}^{\zeta_2}\phi_i(\xi,\eta,\tau)d\eta \qquad \text{(III.D.14)}$$

where

$$\Delta\zeta = \zeta_2 - \zeta_1;$$

$\zeta_i = z_i/b;$

z_i = distance from top of formation to top (i=1) or bottom (i=2) of observation-well screen.

Employing the transform-space analogue to (III.D.14), the application of an inverse finite Fourier cosine transform to (III.D.12) produces a Laplace-space expression equivalent to (III.D.13), except that the Ω_i expression is defined as

$$\Omega_i = \frac{1}{\Delta\zeta}\int_{\zeta_1}^{\zeta_2}\left(\frac{f_i(n=0)}{\beta} + \frac{4}{\pi}\sum_{n=1}^{\infty}\frac{f_i(n)}{n}\sin\left(\frac{n\pi}{2\beta}\right)\cos\left(\frac{n\pi(1+2\varsigma)}{2\beta}\right)\cos\left(\frac{n\pi\eta}{\beta}\right)\right)d\eta$$

$$= \frac{f_i(n=0)}{\beta} + \frac{4}{\pi\Delta\zeta}\sum_{n=1}^{\infty}\frac{f_i(n)}{n}\sin\left(\frac{n\pi}{2\beta}\right)\cos\left(\frac{n\pi(1+2\varsigma)}{2\beta}\right)\int_{\zeta_1}^{\zeta_2}\cos\left(\frac{n\pi\eta}{\beta}\right)d\eta \qquad \text{(III.D.15)}$$

The integral in (III.D.15) can be rewritten as

$$\int_{\zeta_1}^{\zeta_2}\cos\left(\frac{n\pi\eta}{\beta}\right)d\eta = \frac{\beta}{n\pi}\left[\sin\left(\frac{n\pi\zeta_2}{\beta}\right) - \sin\left(\frac{n\pi\zeta_1}{\beta}\right)\right]$$
$$= \frac{2\beta}{n\pi}\left(\cos\left(\frac{n\pi(\zeta_1+\zeta_2)}{2\beta}\right)\sin\left(\frac{n\pi\Delta\zeta}{2\beta}\right)\right) \qquad \text{(III.D.16)}$$

Substituting (III.D.16) into (III.D.15) produces the following expression for Ω_i:

$$= \frac{f_i(n=0)}{\beta} +$$
$$\frac{8\beta}{\Delta\zeta\pi^2}\sum_{n=1}^{\infty}\frac{f_i(n)}{n^2}\sin\left(\frac{n\pi}{2\beta}\right)\sin\left(\frac{n\pi\Delta\zeta}{2\beta}\right) \qquad \text{(III.D.17)}$$
$$*\cos\left(\frac{n\pi(1+2\varsigma)}{2\beta}\right)\cos\left(\frac{n\pi(\zeta_1+\zeta_2)}{2\beta}\right)$$

Equation (III.D.13) with the Ω_i definition given in (III.D.17) is employed to calculate observation-well heads in Liu and Butler (1995). Note that equation (III.D.13) is based on the assumption that the observation well has been packed off (i.e. well-bore storage effects can be neglected). Well-bore storage at the observation well could be included by utilizing an approach similar to that of Tongpenyai and Raghavan (1981) and Novakowski (1989a).

In the homogeneous (no skin) case,

$$\Omega_2 = \Omega_3 = \frac{f_i^*(n=0)}{\beta} +$$
$$\frac{8\beta}{\Delta\zeta\pi^2}\sum_{n=1}^{\infty}\frac{f_i^*(n)}{n^2}\sin\left(\frac{n\pi}{2\beta}\right)\sin\left(\frac{n\pi\Delta\zeta}{2\beta}\right) \qquad \text{(III.D.18)}$$
$$*\cos\left(\frac{n\pi(1+2\varsigma)}{2\beta}\right)\cos\left(\frac{n\pi(\zeta_1+\zeta_2)}{2\beta}\right)$$

where

$f_i^* = K_0(\nu\xi)/(\nu K_1(\nu))$

Note also that f_1 in the Ω term of (III.D.12) becomes $K_0(\nu)/(\nu K_1(\nu))$.

Theoretical and Field Analyses Using Extended Form of KGS Model

Equation (III.D.13) was employed to simulate a series of slug tests in a hypothetical aquifer with a hydraulic conductivity of 1.0e-3 m/s and a specific storage of 1.0e-5 m^{-1}. For the initial analysis discussed here, the well skin was assumed to have the same properties as the formation, which was considered isotropic with respect to hydraulic conductivity. This series of simulations was designed to examine the effect of the fully screened well assumption of the Cooper et al. model. A slug test was simulated for the case of a test well that is fully screened across a one-meter thick aquifer. A second simulation was performed for the case of a slug test in a well, also with a screen one meter in length, that is at the center of a very thick aquifer. Figure III.D.5 displays the simulated responses for an observation point located ten meters in the radial direction from the stressed well. In both cases, the observation point is at the same vertical position as the center of the screen. Note that the responses in the partially penetrating case are close to an order of magnitude smaller than those in the fully penetrating case. An analysis of the partially penetrating responses using the Cooper et al. model produced the results displayed in Figure III.D.6. Note that the estimated hydraulic conductivity and specific storage are 7.8 and 33 times, respectively, larger than the actual parameters employed in the simulations. Clearly, the misapplication of the Cooper et al. model to data from a partially penetrating well can produce parameter estimates that are much larger than the actual formation parameters.

Given this result, it is clear that the data from the multiwell slug tests at GEMS must be reanalyzed using the KGS model. Figure III.D7 displays the results of the reanalysis of the test at well 00-1. Note that the estimated hydraulic conductivity and specific storage values are 22 and 38 times, respectively, smaller than the parameters obtained in the fully penetrating case. Note also that the estimated conductivity of 3.4e-4 m/s (29.4 m/d) is in keeping with the results of the core analyses reported in Section IV.C.

Summary

In this section, the semianalytical solution of Hyder et al. (1994) was extended to the case of multiwell slug tests. An important assumption of the extension is that the observation well is packed off, so that wellbore storage effects at the observation well can be ignored. This solution can be used to provide one explanation for the

anomalously high hydraulic conductivity and specific storage estimates obtained from multiwell slug tests at GEMS when the Cooper et al. (1967) model was used in the analysis. These results clearly demonstrate that the Cooper et al. model should not be used to analyze multiwell slug tests in partially penetrating wells. Cooper et al. model estimates can easily be an order of magnitude or more too large. The parameter estimates obtained from the extended solution are in reasonable agreement with results of laboratory analysis of core data from GEMS.

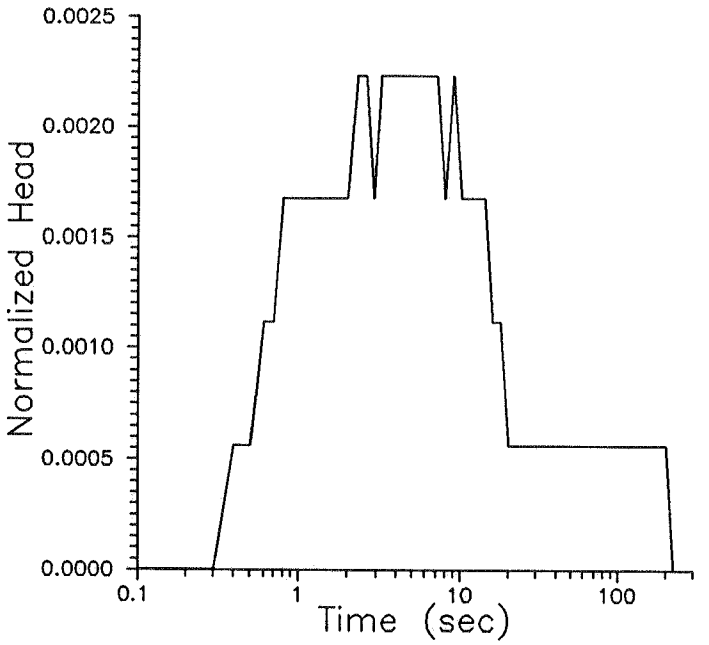

FIGURE III.D.1 - Normalized head ($h(t)/H_0$) versus time plot for well 6-2.

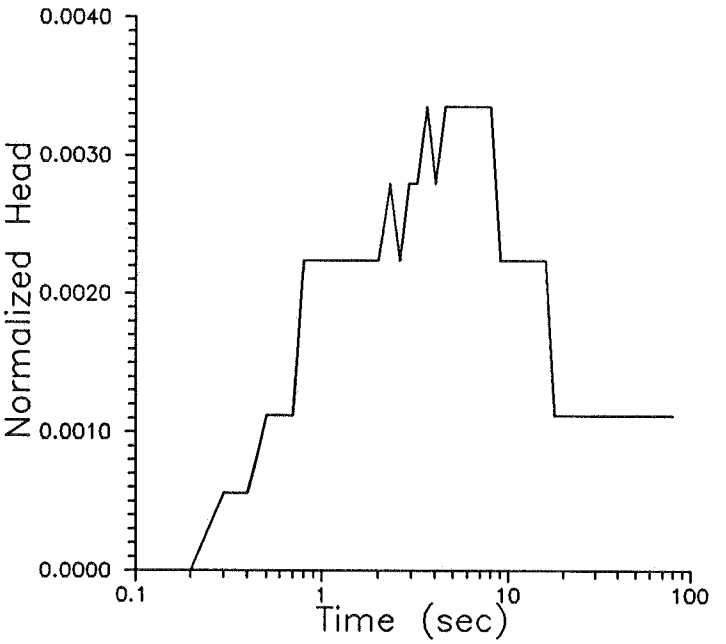

FIGURE III.D.2 - Normalized head ($h(t)/H_0$) versus time plot for well 00-1.

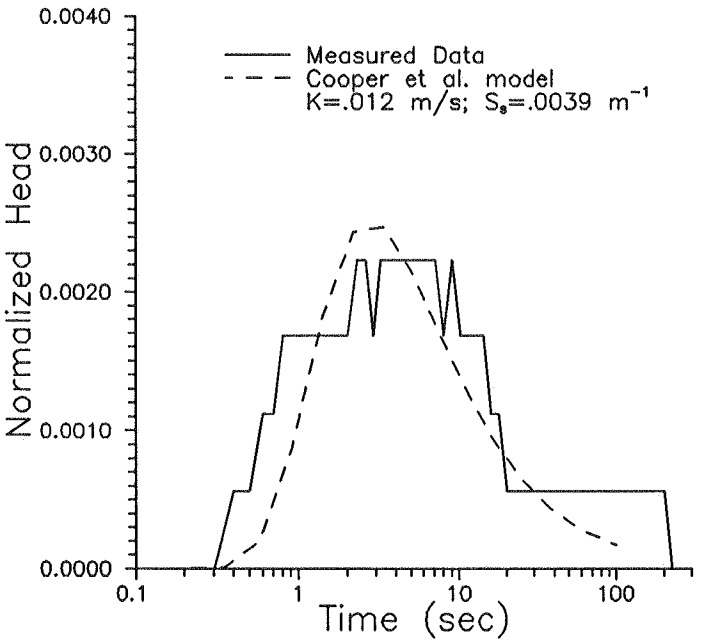

FIGURE III.D.3 - Normalized head versus time plot and the best-fit Cooper et al. model for well 6-2.

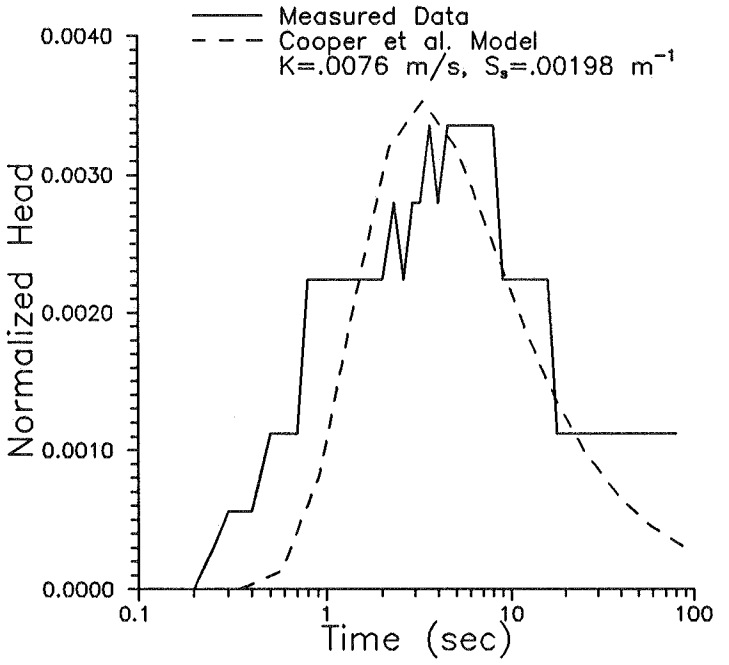

FIGURE III.D.4 - Normalized head versus time plot and the best-fit Cooper et al. model for well 00-1.

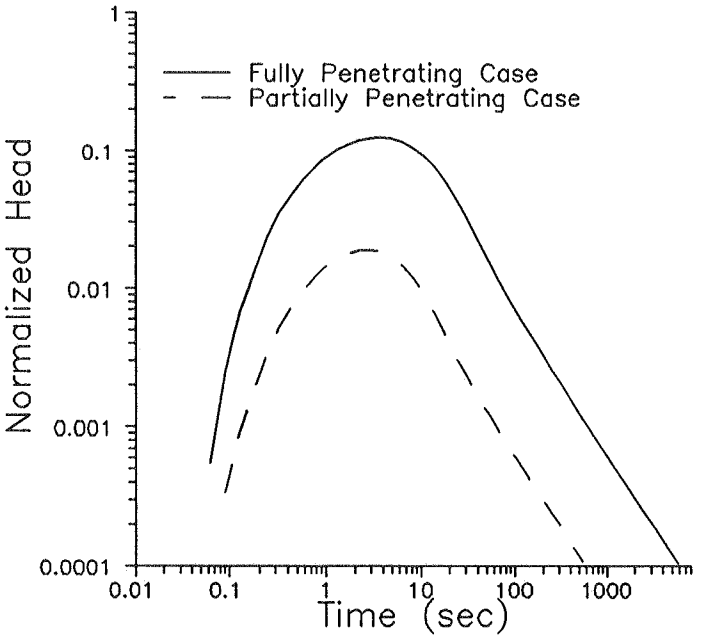

FIGURE III.D.5 - Normalized head versus time plot of simulated slug-test data (simulations employ the KGS model).

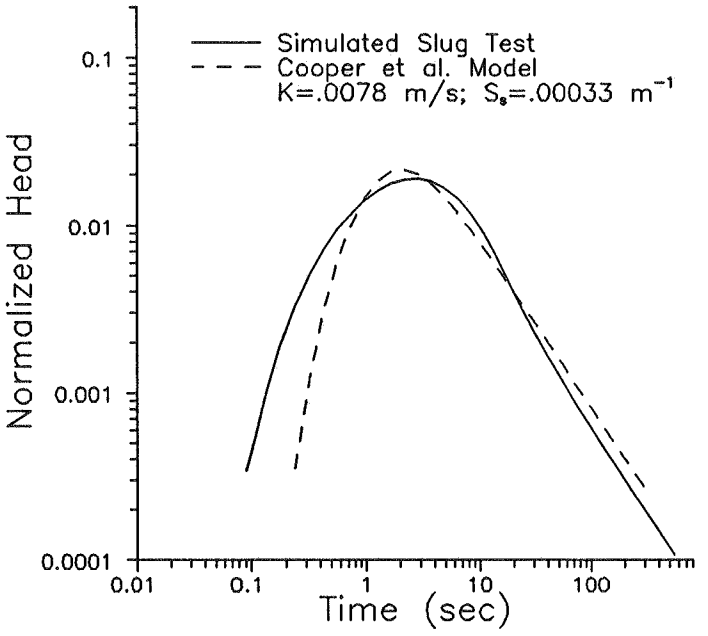

FIGURE III.D.6 - Normalized head versus time plot and the best-fit Cooper et al. model for the simulated partially penetrating well data of Figure III.D.5.

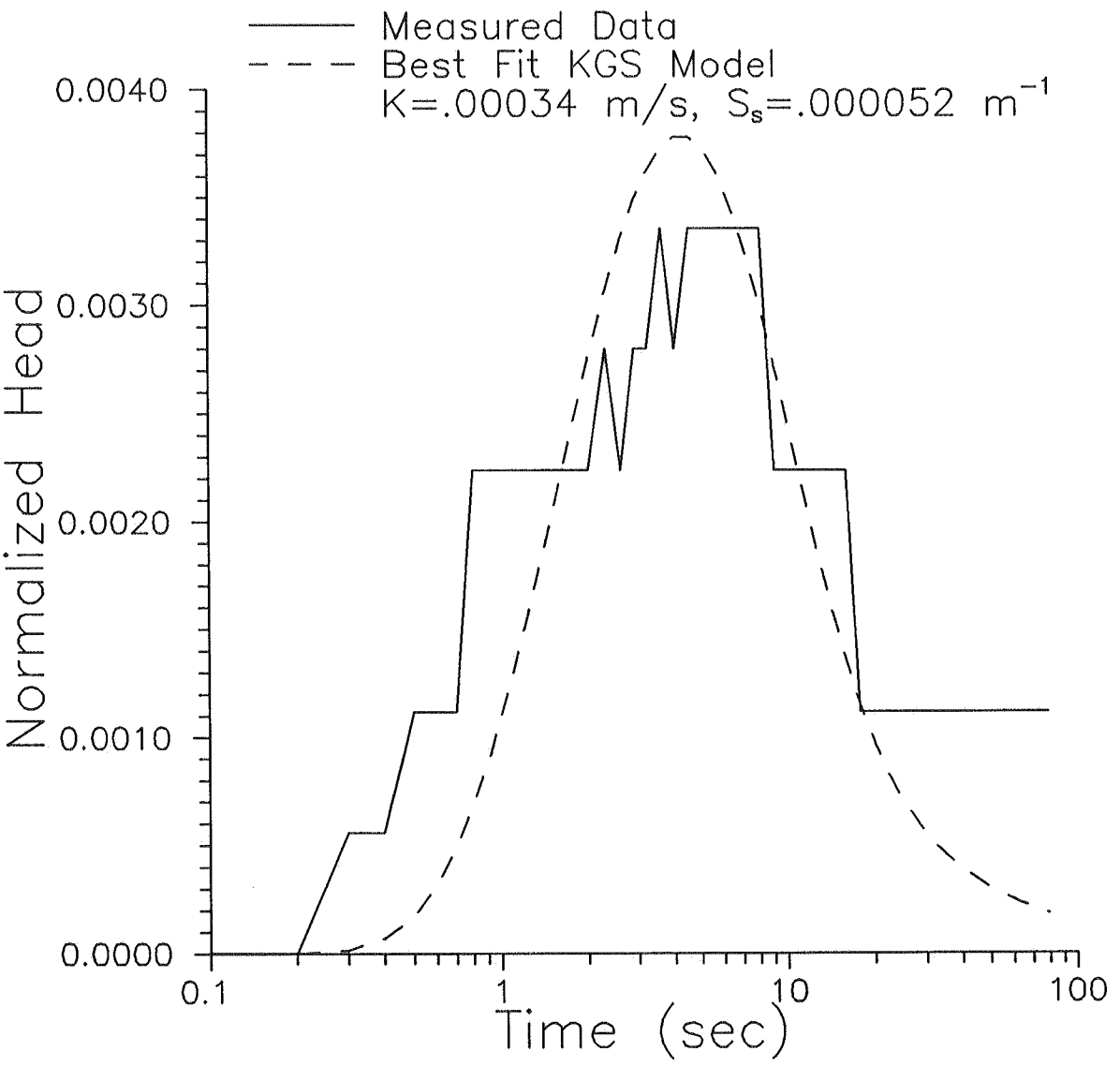

FIGURE III.D.7 - Normalized head versus time plot and the best-fit KGS model for well 00-1.

E. IMPROVING THE QUALITY OF PARAMETER ESTIMATES OBTAINED FROM SLUG TESTS

A manuscript describing the work of this section was submitted to the journal Ground Water in August of 1994. A revised version of the manuscript was accepted in May of 1995, and the article will be published in volume 34, number 3 of Ground Water in May of 1996. The remainder of this section consists of a preprint of that article.

IMPROVING THE QUALITY OF PARAMETER ESTIMATES OBTAINED FROM SLUG TESTS

James J. Butler, Jr., Carl D. McElwee, and Wenzhi Liu
Kansas Geological Survey
1930 Constant Ave.
Lawrence, KS 66047

Original Submission: August, 1994
Accepted Pending Final Revisions: January, 1995
Submission of Revised Manuscript: April, 1995
Revised Manuscript Accepted: May, 1995

Prepared for submission to
Ground Water

ABSTRACT

The slug test is one of the most commonly used field methods for obtaining in-situ estimates of hydraulic conductivity. Despite its prevalence, this method has received criticism from many quarters in the groundwater community. This criticism emphasizes the poor quality of the estimated parameters, a condition that is primarily a product of the somewhat casual approach that is often employed in slug tests. Recently, the Kansas Geological Survey (KGS) has pursued research directed at improving methods for the performance and analysis of slug tests. Based on extensive theoretical and field research, a series of guidelines have been proposed that should enable the quality of parameter estimates to be improved. The most significant of these guidelines are: 1) three or more slug tests should be performed at each well during a given test period; 2) two or more different initial displacements (H_0) should be used at each well during a test period; 3) the method used to initiate a test should enable the slug to be introduced in a near-instantaneous manner and should allow a good estimate of H_0 to be obtained; 4) data-acquisition equipment that enables a large quantity of high quality data to be collected should be employed; 5) if an estimate of the storage parameter is needed, an observation well other than the test well should be employed; 6) the method chosen for analysis of the slug-test data should be appropriate for site conditions; 7) use of pre- and post-analysis plots should be an integral component of the analysis procedure, and 8) appropriate well-construction parameters should be employed. Data from slug tests performed at a number of KGS field sites demonstrate the importance of these guidelines.

INTRODUCTION

The slug test is a widely used technique for the in-situ estimation of hydraulic conductivity at sites of suspected groundwater contamination (Kruseman and de Ridder, 1989; Chirlin, 1990). Parameter estimates obtained from slug tests can be used for a variety of purposes including prediction of contaminant transport, design of large-scale pumping tests, and design of remediation schemes. Recently, however, this technique has received a considerable amount of criticism in the groundwater literature (e.g., Osborne, 1993). A primary cause of this criticism is the discrepancy that is often observed between estimates obtained from slug tests and those obtained from other information collected as part of the site investigation (e.g., geologic and geophysical logs, core samples, pumping tests, etc.). Although spatial variability and the different scales at which the various information was obtained can explain a portion of the observed discrepancy (e.g., Butler, 1990), a significant component of this difference undoubtedly arises as a result of the somewhat casual attitude that is often directed at the performance and analysis of slug tests. Since slug tests have considerable logistical and economic advantages over alternative approaches, it is imperative that these tests be done in such a manner so as to yield parameter estimates of as high a quality as possible. The purpose of this paper is to propose practices for the performance and analysis of slug tests that should increase the quality of the resulting parameter estimates.

Since 1989, the Kansas Geological Survey (KGS) has pursued extensive theoretical and experimental research on slug tests in porous formations. A major component of this effort has been a thorough examination of currently accepted practices. This work has resulted in the definition of a series of guidelines for the design, performance, and analysis of slug tests. We have found that adherence to these guidelines can greatly improve the quality of parameter estimates obtained from a program of slug tests. The major purpose of this paper is to describe the most significant of these guidelines. In the following sections, each of the proposed guidelines is explained in detail. Tests from a variety of KGS field sites are used as examples to demonstrate the importance of the proposed guidelines.

PROPOSED SLUG-TEST GUIDELINES

1. THREE OR MORE SLUG TESTS SHOULD BE PERFORMED AT A GIVEN WELL

According to conventional theory (e.g., Cooper et al., 1967), data from repeat slug tests at the same well should coincide when graphed in a normalized format (measured deviations from static normalized by the magnitude of the initial displacement, i.e. the size of the slug (H_0)). Thus, the duration of a slug test should be independent of the size of the slug (H_0). Figure 1 is a plot of a series of slug tests from a well in Lincoln County, Kansas, in which the response data conform to conventional theory, despite a variation of almost a factor of four in the magnitude of the initial displacement (H_0).

Unfortunately, however, data from repeat slug tests at a well will not always plot in this ideal manner. Figure 2 displays data from a series of slug tests from another well at the same site in Lincoln County in which there was considerable variation in test responses. Since the pattern of responses shown on Figure 2 does not indicate a reproducible dependence on H_0 (test 3 on 5/21 and test 11 on 6/26 have similar H_0 but yield Cooper et al. hydraulic conductivity estimates that differ by close to a factor of two), this behavior is most likely an indication that the gravel pack or a portion of the formation in the vicinity of the well is being altered during the course of testing to form a low-permeability well skin. One possible explanation is that some fine material is being mobilized by the introduction of the slug and is moving in a manner that produces progressive decreases in formation permeability during the course of testing. Without doing a series of tests at a given well, this behavior would not be identified and thus properties reflective of the low-permeability skin could inadvertently be assigned to the formation. A minimum of three tests, preferably closely spaced in time, is recommended in order that the effects of an evolving (dynamic) skin can be separated from a dependence on H_0 (discussed in the next section). Clearly, considerable attention must be given to well construction and development in order to minimize the possibility of skin development during the course of testing. Note that Dax (1987) describes results from a series of slug tests at wells that are gradually being clogged through time as a result of accumulation of material in the well and incrustation of the well screen. The test responses displayed on Figure 2 are not thought to be a result of such a process of gradual clogging. The large differences in response time that are seen

between tests performed on the same day are strong evidence in support of the hypothesis of mobilization of fine material leading to a decrease in near-well permeability. Based on the authors' experience, the failure to recognize the existence of a low-permeability well skin is the largest source of error in parameter estimates obtained from slug tests. Butler (1996) proposes additional approaches to help assess the presence of a low-permeability well skin using slug tests.

2. TWO OR MORE DIFFERENT INITIAL DISPLACEMENTS SHOULD BE USED DURING TESTING AT A GIVEN WELL

As stated in the preceding section, conventional theory maintains that slug-test responses should be independent of the magnitude of the initial displacement (H_0). In confined formations of moderate to low permeability (K < 10-15 m/d, where K is hydraulic conductivity), this assumption appears quite sound (e.g., Figure 1 of this paper and Herzog (1994)). In very permeable systems, however, a dependence on H_0 is often seen as a result of non-Darcian flow losses. Figure 3 is a plot from a series of tests in the semiconfined alluvial aquifer underlying the Geohydrologic Experimental and Monitoring Site (GEMS) in Douglas County, Kansas. A very strong dependence on H_0 is seen in these data, producing an inverse relationship between H_0 and hydraulic conductivity estimates obtained using conventional methods (i.e. Hvorslev (1951) and Cooper et al. (1967)). The tests displayed on Figure 3 were performed on the same day in a series of cycles from low to high H_0. As shown in the figure, repeat tests with the same approximate H_0 from different cycles coincided, verifying that the observed behavior is a reproducible function of H_0 and not a result of an evolving skin. In order to identify a dependence on H_0, a series of tests in which H_0 varies between tests should be performed. A variation in H_0 of a factor of two or greater is recommended. In addition, the first and last tests should use the same H_0 so that the effects of an evolving skin can be separated from the H_0 dependence. Figures 4A and 4B display response data from such a test series in the unconsolidated aquifer underlying the Great Bend Prairie region of south-central Kansas. The coincidence of the normalized plots on Figure 4B indicates that the test responses are independent of H_0, the formation is not being altered during testing, and that the responses are independent of whether the slug was induced by raising or lowering the water level in the well. It is strongly recommended that such a series of tests always be performed. Failure to do so can potentially introduce considerable error into the hydraulic conductivity estimates obtained from a program of slug tests.

The first and last tests in the series shown in Figure 4 employed initial displacements of similar magnitude but differing signs. According to conventional theory, responses should be independent of whether the test was initiated by an injection (slug in) or withdrawal (slug out) mechanism. The results of the tests shown in Figure 4 (and all other slug tests performed by the authors in properly developed wells) indicate that, as long as the water level in the well is not driven below the top of the screen during the test, the responses will be essentially independent of the mechanism used for test initiation (i.e. injection versus withdrawal). However, in wells that have not undergone sufficient development, it is likely that there will be a dependence on the mechanism for test initiation due to an evolving skin. In addition, recent theoretical work (McElwee and Butler, 1994) indicates that in wells screened in very permeable formations it is possible that test responses are dependent on the mechanism used for test initiation. However, the very limited field data that have been collected to assess this theory have not displayed such a dependence.

The above discussion of the dependence of test responses on the magnitude of H_0 is appropriate for wells in confined formations and those in unconfined formations screened at least a certain minimum distance below the water table. In wells screened close to or across the water table, one may observe a dependence on H_0 as a result of changes in the effective length of the screen through which water flows into/out of the well during a test. In such wells, one may also observe a dependence of responses on the mechanism of test initiation (i.e. injection versus withdrawal). Dahl and Jones (1993) report a series of tests in which there is a clear dependence on H_0 and the mechanism of test initiation. Figure 5 reproduces one set of tests reported by Dahl and Jones (1993). These tests were performed at the same well using different initial displacements and different mechanisms of test initiation. Butler et al. (1994) have recently proposed an approximate analytical solution for withdrawal slug tests performed in wells screened across the water table that can model the dependence on H_0 arising from changes in the effective screen length during the course of a test. Butler et al. (1994) also provide estimates of the minimum distance that the top of the well screen must be below the water table in order for test responses to be independent of H_0.

3. THE SLUG SHOULD BE INTRODUCED IN A NEAR-INSTANTANEOUS FASHION AND A GOOD ESTIMATE OF THE INITIAL DISPLACEMENT SHOULD BE OBTAINED

Conventional methodology for the analysis of slug-test data requires that the slug-induced disturbance be introduced in an instantaneous fashion and that the magnitude of the initial displacement (H_0) be known. Thus, the method used to initiate a slug test must satisfy both of these requirements. In systems of moderate to low permeability, most common methods of test initiation will enable the slug to be introduced in a manner that can be considered instantaneous relative to the timing of the resulting head responses. In addition, measurements taken immediately after test initiation should yield a good estimate of H_0. In very rapidly responding systems, however, satisfying these requirements may prove difficult.

Figure 6 displays data from a series of tests performed in the same permeable alluvial aquifer as in Figure 3. In this case, the slug was introduced by pneumatic means (i.e. pressurizing the air column in the well casing (producing a depression of the water level) followed by a very rapid depressurization (e.g., McLane et al., 1990; Levy and Pannell, 1991)). The "actual H_0" values shown in Figure 6 (1.03 m and 4.20 m for tests 1 and 4, respectively) are based on measurement of the air pressure in the well casing using a pressure transducer placed at the top of the casing, while the head readings were taken using a submersible pressure transducer. The difference between the H_0 readings taken with the air pressure transducer and those taken with the submersible pressure transducer (0.20 m and 1.03 m for tests 1 and 4, respectively) is a result of the time for depressurization (on the order of several tenths of a second) being too slow for such a rapidly responding system. The use of the H_0 from the submersible pressure transducer, in conjunction with the lower-than-expected radial hydraulic gradient arising from the non-instantaneous slug introduction, will lead to an estimate of hydraulic conductivity that is lower than the actual conductivity of the formation. A comparison between the apparent H_0 (in this case the reading from the submersible pressure transducer) and the expected H_0 (in this case the reading from the air pressure transducer) is a simple way to assess if the instantaneous-introduction assumption is being upheld. A theoretical analysis indicates that a normalized difference between apparent and expected H_0 (difference normalized by the expected H_0) greater than 10% should be of concern in practical applications (Butler, 1996). Note that further testing at the same site showed that there was no difference between the H_0 readings in wells screened in material of

moderate to low permeability.

Although the example displayed in Figure 6 was from a pneumatic slug test, more severe problems would actually be expected in tests initiated by the addition or removal of a solid slug because of the longer time needed for introduction of the slug. Packer-based systems, in which the slug is introduced by opening the central pipe (mandrel) upon which the packer is mounted (e.g., Figure 4a of this paper and McElwee and Butler (1989)), provide one means of introducing the slug-induced disturbance in a near-instantaneous fashion in very permeable systems. This approach also enables a very good estimate of H_0 to be obtained. However, the inner diameter of the mandrel must be large enough so as to not significantly restrict flow. Note that Orient et al. (1987) and McLane et al. (1990), among others, suggest use of electric water-level indicators (electric tapes) to estimate H_0 for pneumatic slug tests. Although this approach can provide an approximate value of H_0, a high-accuracy pressure transducer mounted on top of the well casing will provide a better estimate in very permeable systems. Since high-accuracy air pressure transducers are inexpensive, can be readily added to the standard pneumatic-slug-test well head assembly, and can be readily connected to standard data-acquisition equipment, their use is strongly recommended for pneumatic slug tests.

4. APPROPRIATE DATA-ACQUISITION EQUIPMENT SHOULD BE EMPLOYED

Responses to a slug-induced disturbance can be measured either manually (electric tape, plopper, etc.) or electronically (pressure transducers connected to a data logger). For tests in wells screened in formations of moderate to low permeability, such as shown in Figure 1, manual methods can provide measurements of sufficient quality as long as a good estimate of H_0 is available. However, for tests in more permeable systems ($K > 10\text{-}15$ m/d), such as shown in Figures 3-6, electronic methods must be employed, as manual methods will not provide measurements of sufficient density or accuracy. Theoretical work (McElwee et al., 1995a) has shown that the quality of parameter estimates is closely tied to the density and accuracy of measurements. In very rapidly responding wells (e.g., Figures 3 and 6), data-acquisition rates of at least several hertz are needed in order to clearly define the nature of the responses. The need for rapid acquisition rates is of special concern in the case of oscillating responses where slow collection rates will produce aliasing and other effects that may make data interpretation and analysis difficult. Given the capabilities of currently available data-acquisition equipment, data collection rates of several hertz are easily obtainable and, therefore, should always be used when rapid

responses are expected.

5. AN OBSERVATION WELL SHOULD BE EMPLOYED FOR ESTIMATION OF THE STORAGE PARAMETER

It has frequently been observed that slug-induced responses at the test well are relatively insensitive to the value of the storage parameter (e.g., Cooper et al., 1967). McElwee et al. (1995a) have used a sensitivity-analysis approach to demonstrate that reliable estimates of the storage parameter will be difficult to obtain using the density and quality of data that are normally collected during a single-well slug test. A primary reason for this condition is that the measured responses at the test well are much more sensitive to transmissivity (Kb, where b is screen length) than to the storage parameter ($S_s b$, where S_s is the specific storage). The limited sensitivity to the storage parameter that does exist is highly correlated with the sensitivity to transmissivity. In addition, any uncertainties about the effective screen radius (nominal screen radius or radius of gravel pack or radius of developed zone) will have a much larger effect on estimates of the storage parameter than on estimates of transmissivity. Use of an observation well during a slug test can greatly improve this situation because the insensitivity and correlation effects are dramatically lessened (McElwee et al., 1995b). Uncertainties about the effective screen radius can also be considerably reduced when data from an observation well are used (Butler, 1996).

Figure 7 displays data from a multi-well slug test at the same site as in Figure 1. The two wells, which are screened over similar intervals, are 6.45 m apart. Owing primarily to uncertainty about the effective screen radius, the estimate of specific storage obtained using data from well Ln-2 alone is too large by a factor of between 3 and 4 (estimated $S_s=2.98\text{x}10^{-5}$ m^{-1}). When the analysis is performed using data from both wells (results shown in Figure 7), a specific storage estimate compatible with other information is obtained (estimated K=1.06 m/d; estimated $S_s=8.49\text{x}10^{-6}$ m^{-1}). Note that measurements from the observation well were taken using a transducer placed below a packer located just above the screen. The observation well was packed off in order to remove the lagging and damping of responses that occurs due to wellbore storage at the observation well (Novakowski, 1989a).

Although it may not be practical to install observation wells solely for use in slug tests, the density of pre-existing monitoring wells is often such that this technique can be readily employed. Generally, the observation well must be fairly close (within $\approx$ 10 m) to the test well and screened over a similar vertical interval in order that the responses to the slug-induced disturbance can be discerned from background noise.

The storage parameter must be quite small in order to employ wells at greater distances from the test well (Sageev, 1986; Karasaki et al., 1988; Novakowski, 1989a; Guyonnet et al., 1993).

6. METHOD CHOSEN FOR DATA ANALYSIS SHOULD BE APPROPRIATE FOR SITE CONDITIONS

Most analyses of slug-test data are performed using one of four techniques: 1) the method of Hvorslev (1951) for fully and partially penetrating wells in confined aquifers; 2) the method of Bouwer and Rice (1976) for wells in unconfined aquifers screened below the water table; 3) the method of Cooper et al. (1967) for fully penetrating wells in confined aquifers; and 4) the method of Nguyen and Pinder (1984) for partially penetrating wells in confined aquifers. Recent theoretical work at the KGS has focused on the quality of the estimates provided by these techniques.

Figure 8 displays the results of a theoretical analysis of the error introduced into hydraulic conductivity estimates when applying the Cooper et al. model to data from a partially penetrating well (see Hyder et al. (1994) for further details). The ψ quantity plotted on the x axis is the square root of the anisotropy ratio ($\sqrt{K_z/K_r}$) divided by the aspect ratio (b/r_w, where b is the screen length and r_w is the screen radius). The quantity plotted on the y axis is the hydraulic conductivity estimate provided by the Cooper et al. model (K_{est}, obtained using b as the formation thickness in the Cooper et al. model) divided by the actual conductivity value (K_r). A series of curves are shown for different values of the dimensionless storage parameter ($\alpha = (2r_w^2 S_s b)/r_c^2$, where r_c is the casing radius). Note that the α parameter used here is twice that defined by Cooper et al. (1967). Although the Cooper et al. estimates improve as ψ decreases (i.e. the proportion of vertical flow in response to the slug-induced disturbance decreases), Figure 8 shows that the Cooper et al. model will always provide an upper bound for the conductivity estimate. The quality of this bounding estimate will depend on the ψ and α values. For tests in wells of moderate to low aspect ratios sited in isotropic formations (i.e. the upper end of the plotted ψ range), Figure 8 indicates that the Cooper et al. model will provide estimates that are significantly greater than the actual formation conductivity for moderate to low α values.

Figure 9 displays results of a similar analysis for the partially-penetrating-well form of the Hvorslev method. In this variant of the Hvorslev method, an anisotropy ratio must be assumed, producing a ψ^* value (square root of assumed anisotropy ratio

divided by the aspect ratio) that is used in the analysis. This assumed ψ^* value may be quite different from the actual unknown ψ value of the well-formation configuration. Most standard references (e.g., Freeze and Cherry, 1979) recommend that the Hvorslev analysis be performed assuming an isotropic formation (i.e. $\psi^*=r_w/b$). The results displayed in Figure 9 indicate that this approach will produce a significant underestimation of hydraulic conductivity in moderately to highly anisotropic ($K_r>K_z$) formations, where the assumed ψ^* will be much greater than the actual ψ. Note that the results displayed in Figure 9 are for a single value of the dimensionless storage parameter (α). Hyder et al. (1994) discuss the dependence of these results on α.

Figure 10 displays results for a similar analysis of the Bouwer and Rice method. In this case, two plots are given so that the effect of aspect ratio and anisotropy can be evaluated separately. Again, anisotropy ($K_r>K_z$) will produce a considerable underestimation of hydraulic conductivity in wells of moderate to small aspect ratio. Note that Zlotnik (1994) has recently proposed an approach for incorporating anisotropy into the Bouwer and Rice analysis. However, this approach does require that the anisotropy be known prior to the analysis. Uncertainty regarding anisotropy will still produce errors of the magnitude shown on Figure 10b.

Hyder et al. (1994) and Hyder and Butler (1995) provide further details of the theoretical analyses of the Cooper et al., Hvorslev, and Bouwer and Rice techniques discussed above. Referral to plots such as Figures 8-10 prior to data analysis is strongly recommended. Given a parameter error that is deemed acceptable for a particular application, one can use these plots to select the most appropriate method to employ for analysis of the test data.

The fourth method for data analysis listed above, the Nguyen and Pinder method, is not recommended for the analysis of slug-test data. Butler and Hyder (1994) have recently shown that parameter estimates obtained using the Nguyen and Pinder method must be viewed with skepticism owing to an error in the analytical solution upon which that method is based. For slug tests performed in partially penetrating wells under conditions where Figures 8-10 indicate that the standard methods do not appear capable of providing acceptable parameter estimates, the recently introduced KGS model for slug tests in partially penetrating wells (Hyder et al., 1994; Hyder and Butler, 1995; Liu and Butler, 1995) can be employed for the analysis of the response data.

The above discussion pertains to conditions where conventional slug-test theory is applicable. However, in cases where test responses are dependent on H_0

and/or the mechanism of test initiation (e.g., Figures 3 and 5), conventional theory is no longer viable. McElwee and Butler (1994) propose an approach for the analysis of slug tests in highly permeable confined systems where a dependence on H_0 is observed. The model proposed by Butler et al. (1994) can be used for the analysis of data from withdrawal slug tests performed in wells screened across the water table when a dependence on H_0 is observed. As emphasized earlier, it is critical that the series of slug tests performed at a well be designed so as to assess whether conventional theory is applicable.

7. USE OF PRE- AND POST-ANALYSIS PLOTS SHOULD BE AN INTEGRAL COMPONENT OF THE ANALYSIS

Currently, the vast majority of analyses of slug-test data are performed using automated fitting programs or procedures involving manual fitting of straight lines to test data. Unfortunately, all too often, the analysis is performed by rote, with little attention paid to the form of the plots and the nature of the fit of the theoretical model to the test data. If the quality of parameter estimates from slug tests is to be improved, more attention must be paid to all aspects of the analysis. Three examples are briefly given here to demonstrate the importance of these issues. Further details about the tests used for these examples can be found in Butler et al. (1993) and Butler and Liu (1994).

Figure 11 displays data and the best-fit Cooper et al. model from a test at the Lincoln County site (screen radius (r_w) = 0.071 m, casing radius (r_c) = 0.025 m, screen length (b) = 3.96 m; estimated $K=5.79\times10^{-4}$ m/d assuming $S_s=3.28\times10^{-6}$ m^{-1} ($\alpha=2.10\times10^{-4}$)). Note that specific storage was assumed known for the analysis based on what was considered a reasonable estimate for the material in the screened interval. Although the relative closeness of the theoretical model to the field data might lead one to consider the model fit as reasonably good, the model fit must actually be considered rather poor. In our opinion, the existence of a systematic deviation between the theoretical model and the field data should be the primary criterion for determining the quality of a model fit. Since there is a clear systematic deviation shown in Figure 11, the fit must be considered rather poor. In this case, the systematic deviation can be readily explained by an assumed dimensionless storage parameter (α) that is too low. Justification for a higher α can be found in Figure 12, which is a plot of the data in a semilog Hvorslev format. The distinct concave upward curvature seen on this plot is strong evidence (for a well of this aspect ratio) that the storage parameter for the test interval is quite large (e.g.,

Chirlin, 1989). Therefore, the analysis was repeated without constraining the value of α. Figure 13 displays the very good fit that was then obtained (estimated $K=2.68\times10^{-4}$ m/d; estimated $\alpha=0.025$). The higher α value is most probably a result of a larger-than-anticipated S_s and/or effective well radius. Note that the hydraulic conductivity estimate decreased by over a factor of two between the analyses of Figures 11 and 13, a further indication of the attention that must be paid to deviations between the fitted theoretical model and the test data. Also note that the good agreement shown in Figure 13 between the Cooper et al. model and the test data would be predicted from Figure 8 for a well of this aspect ratio ($b/r_w=55$), given the large α value. Because this well is of a moderate aspect ratio, the test data were also analyzed using the confined isotropic form of the earlier described KGS model for slug tests in partially penetrating wells (note that the confined isotropic form of the KGS model is equivalent to the model of Dougherty and Babu (1984)). As would be predicted from Figure 8, the conductivity estimate was essentially the same as that obtained from the Cooper et al. model. This result is also in keeping with earlier theoretical work of Hayashi et al. (1987), who found that vertical flow due to a slug-induced disturbance decreases with increases in the storage parameter (i.e. at large values of the storage parameter, responses from fully penetrating well models and partially penetrating well models will coincide).

Figure 14 displays data and the best-fit Cooper et al. model from a test at a site in Pratt County, Kansas ($r_w=0.125$ m, $r_c=0.064$ m, $b=1.52$ m; estimated $K=42.0$ m/d assuming $S_s=3.28\times10^{-6}$ m^{-1} ($\alpha=3.80\times10^{-5}$)). Again, a systematic deviation between the measured data and the Cooper et al. model is shown. This type of deviation is often seen when applying a fully penetrating well model to data from a test in a partially penetrating well. The near-linear Hvorslev plot of the data shown in Figure 15 can be considered further support for the hypothesis of a deviation produced by a significant component of vertical flow. Hyder et al. (1994) note that a near-linear Hvorslev plot can be an indication of a significant component of vertical flow in response to a slug test in a partially penetrating well or a low-permeability well skin. Given the small aspect ratio ($b/r_w\approx12$) and the coincidence of plots of normalized responses from five repeat tests at this well, the partially penetrating well explanation was considered the most likely. The data were therefore reanalyzed using the KGS model for slug tests in partially penetrating wells. Figure 16 displays the fit resulting from an analysis with the confined isotropic form of the KGS model (estimated $K=17.6$ m/d assuming $\alpha=3.80\times10^{-5}$). It is important to emphasize that the dramatic improvement in model fit between Figures 14 and 16 was not accompanied

by an increase in the number of estimated parameters. The hydraulic conductivity estimate provided by the Cooper et al. model is 2.4 times larger than the KGS model conductivity estimate, an overprediction by the Cooper et al. model very close to what would be theoretically predicted from Figure 8 for a well of this aspect ratio in an isotropic formation, given the assumed α of 3.80×10^{-5}. Note that this assumed value of the dimensionless storage parameter (α) is much smaller than the estimate obtained in the previous example. Also note that in Figure 16, and a number of the other figures in this article, the normalized head data show a good deal of fluctuation at very early times. These fluctuations are related to test initiation and should be ignored when considering the quality of the match between the best-fit model and the test data.

A final example illustrates the effect of an evolving low-permeability well skin. Figure 17 is a plot of the test data and the best-fit Cooper et al. models from two tests in the series shown on Figure 2 (r_w=0.071 m, r_c=0.025 m, b=3.66 m; estimated $K_{5/21\ \#3}$=1.34 m/d and $K_{6/11\ \#11}$=0.62 m/d assuming $S_s=6.56 \times 10^{-6}$ m^{-1} ($\alpha=3.87 \times 10^{-4}$)). As shown in the figure, the nature of the deviation between the test data and the best-fit model changes between the two tests. Figure 18 displays data from these two tests in a semilog Hvorslev format. The degree of curvature of the plotted data is significantly smaller in test 11 than in test 3. The greater duration of the later test, the change in the nature of the deviation seen on Figure 17, and the decrease in the degree of curvature shown on Figure 18 are very strong evidence of a developing low-permeability skin. In the case of an evolving skin, the best option is to analyze data from tests before the skin becomes too pronounced. Test 3 of 5/21 was the first slug test performed at this well, so it should be the best test for analysis. The most likely explanation for the deviation between the theoretical model and test 3 data is that the assumed dimensionless storage parameter is too low. The curvature of test 3 data displayed in Figure 18 is strong support for this explanation. The results of a reanalysis of test 3 allowing the storage parameter to vary are shown in Figure 19 (estimated K=1.01 m/day; estimated $S_s=5.35 \times 10^{-5}$ m^{-1} ($\alpha=3.16 \times 10^{-3}$)). The agreement between the fitted model and the test data is significantly better in this case. Note that the conductivity estimate obtained from this analysis is within 5% of the value obtained from the analysis of a multiwell slug test performed at this site over the same vertical interval (see Figure 7). The estimated specific storage ($S_s=5.35 \times 10^{-5}$ m^{-1}), however, appears too large by a factor of six when compared to the value obtained from the multiwell test. This larger specific storage estimate is thought to be a result of the earlier-discussed insensitivity of test responses to the

dimensionless storage parameter and uncertainty concerning the effective screen radius.

Although the analysis of test 3 appears to have been somewhat successful, analysis of tests in wells that display an evolving skin will, in general, be very difficult, as all available test data may be affected by the skin. Clearly, proper well construction and development are essential in order to minimize the potential for the development of a well skin during a program of slug tests.

8. APPROPRIATE WELL-CONSTRUCTION PARAMETERS SHOULD BE EMPLOYED

The well-construction parameters are one of the more significant sources of uncertainty in the analysis of slug-test data. Specifically, the selection of values to use for the effective screen length and radius can introduce considerable error into the analysis. The effective screen length clearly has a very large impact on hydraulic conductivity estimates through its inclusion in the dimensionless time parameter ($\tau = (Kbt)/r_c^2$). Both quantities, however, will influence estimates from slug tests through the dimensionless storage parameter (α) and, in partially penetrating wells, the aspect ratio (effective screen length/effective screen radius). In formations of moderate to low permeability (K < 10-15 m/d), the gravel pack will usually be considerably more permeable than the formation itself. Therefore, as recommended by Palmer and Paul (1987) among others, the effective screen length should be the length of the gravel pack and the effective screen radius should be the radius of the gravel pack. In very permeable systems, it may be more difficult to decide if the gravel-pack dimensions or the nominal screen dimensions are the more appropriate quantities to employ. Careful sizing of the gravel pack, however, can largely remove this uncertainty from the analysis. In the examples of the preceding section, the radius of the gravel pack and the length of the gravel pack were used for r_w and b, respectively, in the analyses because the gravel pack was considerably more permeable than the formation in all cases. Butler (1996) provides further details concerning the effect of well-construction parameters on slug tests. Note that the recommendations of this section are based on the assumption of a properly developed well. Incomplete well development will clearly introduce a great deal of uncertainty into estimates of effective screen length.

CONCLUSIONS

The slug test has the potential to provide very useful information about the transmissive and storage properties of a formation. In order for the potential of this technique to be fully realized, however, considerable care must be given to all phases of test design, performance, and analysis. A series of guidelines has been outlined here that should allow the quality of parameter estimates obtained from a program of slug tests to be improved. Three very important points arising from these guidelines cannot be overemphasized: 1) it is critical that a series of slug tests at a given well be designed so as to assess whether conventional theory is applicable (i.e. is there a dependence on initial head or mechanism of test initiation, is there a well skin that is developing during the course of testing, etc.); 2) the analysis of the response data must be done using the most appropriate model for the test configuration and with considerable care; and 3) inattention to details of well construction and development can produce a situation in which it is virtually impossible to use slug tests to obtain parameter estimates that are representative of formation properties. Unfortunately, the authors have found through repeated experience that failure to consider the issues discussed in this article can produce parameter estimates that may differ considerably from reality. Finally, two additional points need to be emphasized. First, these guidelines developed out of research performed in flow systems for which a porous media representation is valid. The complexities of tests in fractured systems may give rise to additional guidelines of equal or greater importance than those outlined here. Second, although these guidelines developed from work done in formations of a wide range of hydraulic conductivity, this work did not involve tests in formations of extremely low hydraulic conductivity. Clearly, a number of additional issues need to be considered for slug tests in very low conductivity media (e.g., Neuzil, 1982; Palmer and Paul, 1987; Beauheim, 1994).

ACKNOWLEDGMENT

This research was sponsored in part by the Air Force Office of Scientific Research, Air Force Systems Command, USAF, under grant or cooperative agreement number, AFOSR 91-0298. This research was also supported in part by the U.S. Geological Survey (USGS), Department of the Interior, under USGS award number 14-08-0001-G2093. The views and conclusions contained in this document

are those of the authors and should not be interpreted as necessarily representing the official policies, either expressed or implied, of the U.S. Government.

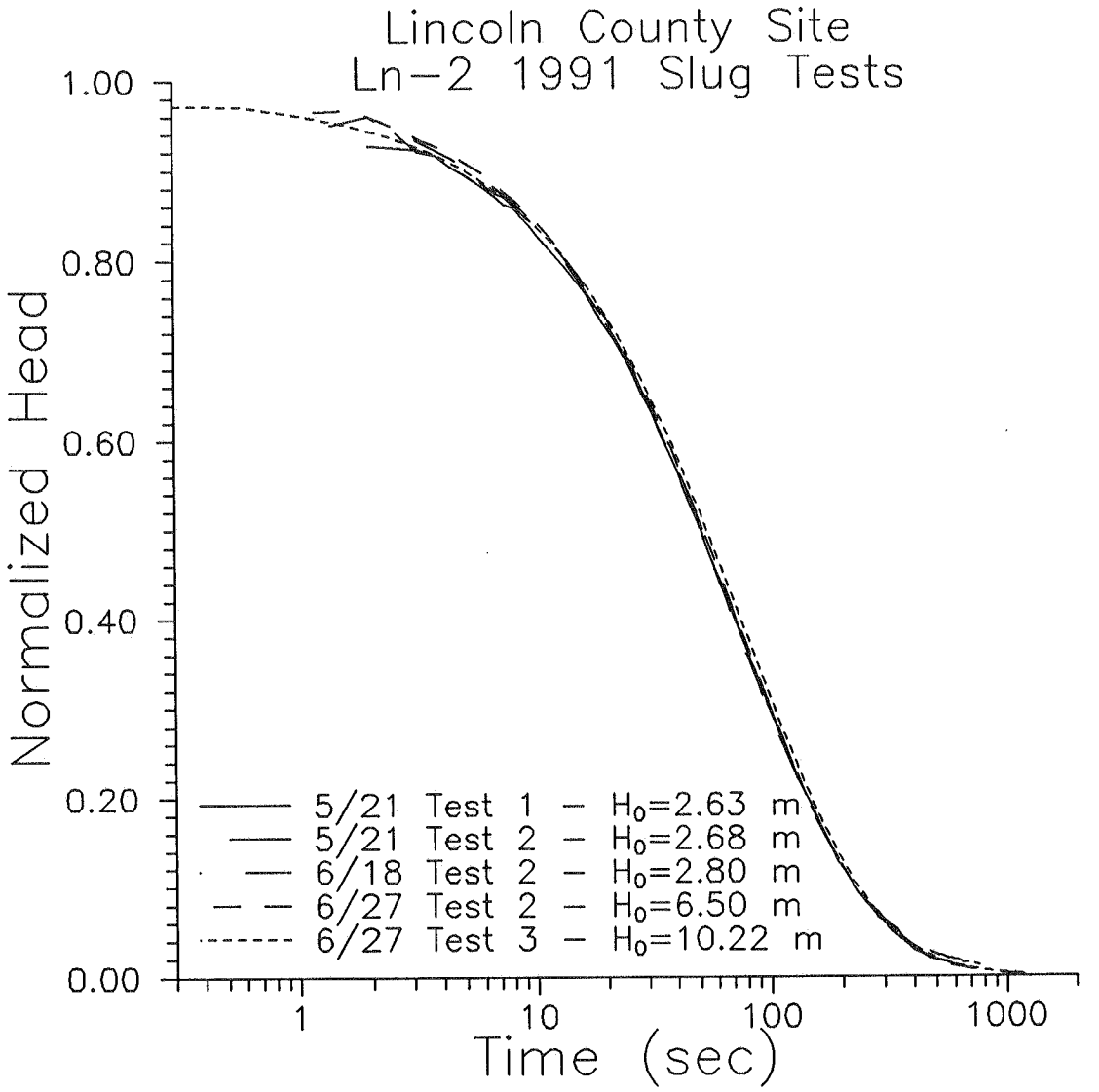

Figure 1 - Normalized head ($H(t)/H_0$) versus log time plot of a series of slug tests performed during May and June of 1991 in well Ln-2 at a site in Lincoln County, Kansas.

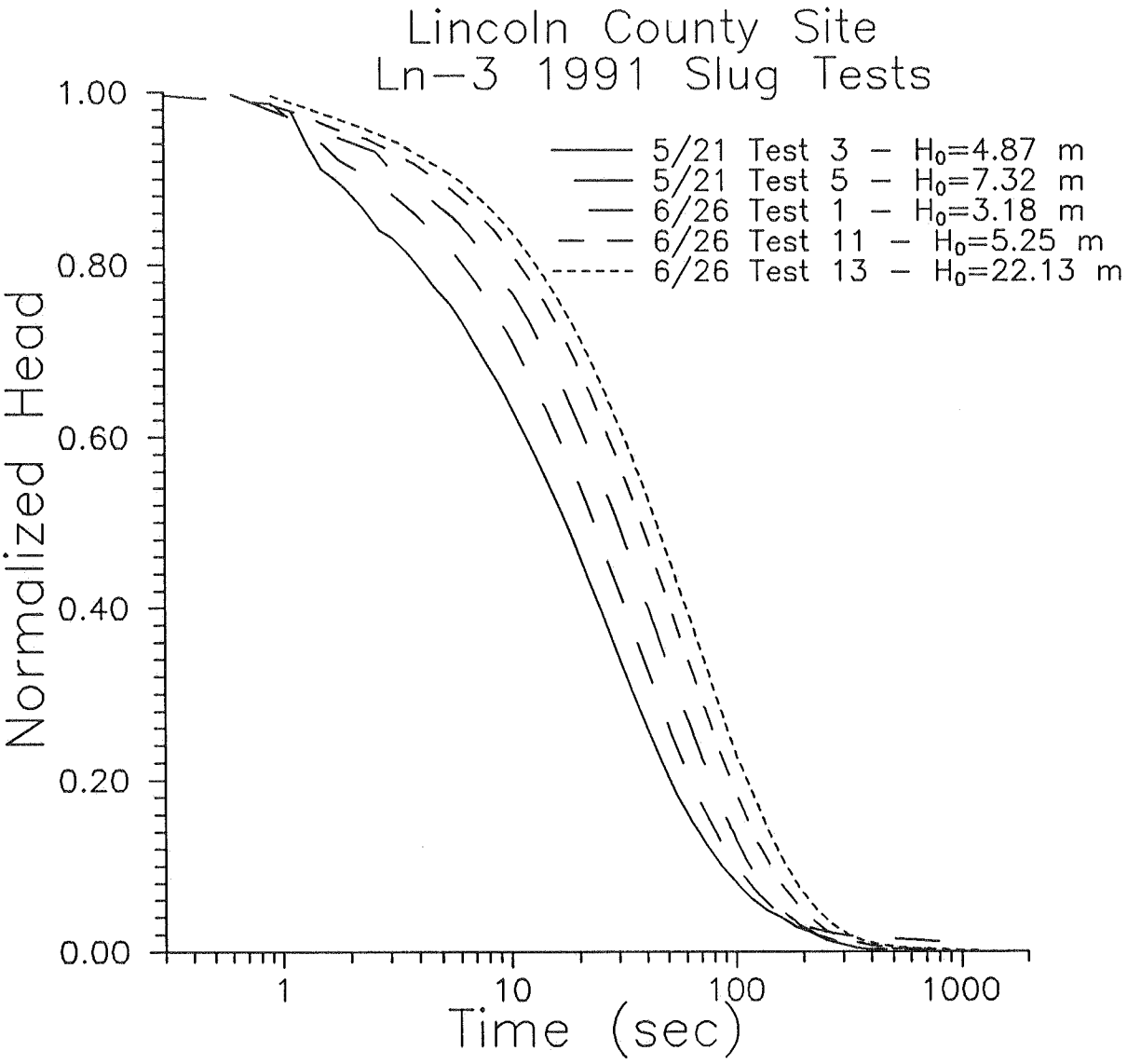

Figure 2 - Normalized head ($H(t)/H_0$) versus log time plot of a series of slug tests performed during May and June of 1991 in well Ln-3 at a site in Lincoln County, Kansas.

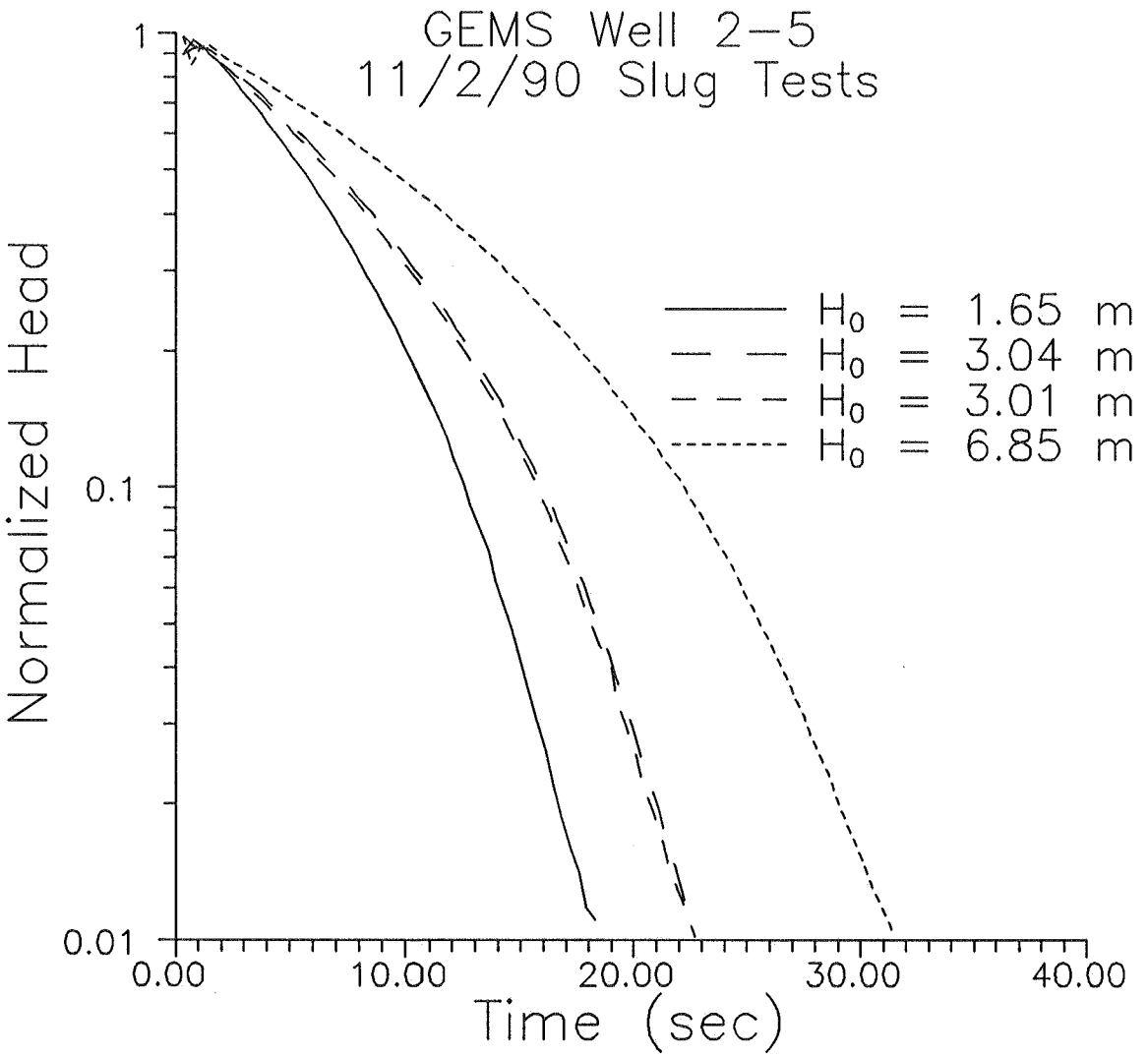

Figure 3 - Log normalized head ($H(t)/H_0$) versus time plot of a series of slug tests performed during November of 1990 in well 2-5 at the Geohydrologic Experimental and Monitoring Site (GEMS) in Douglas County, Kansas.

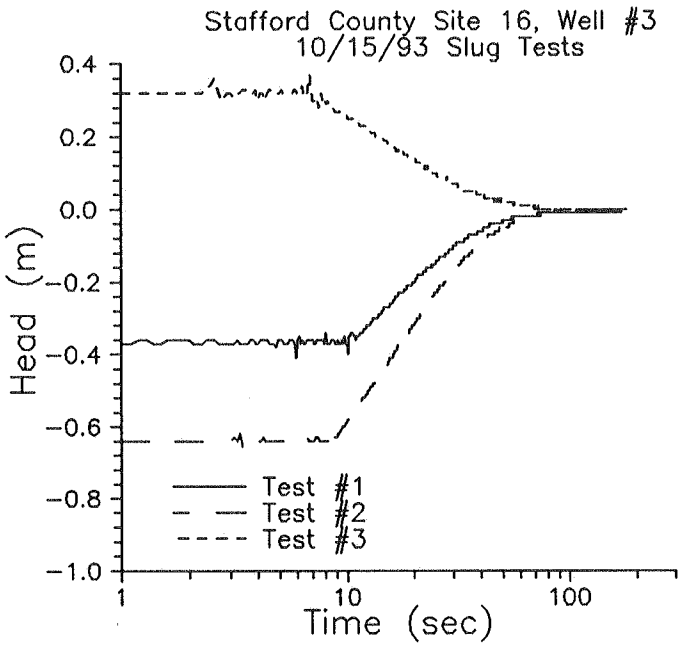

Figure 4 - Plots from a series of slug tests performed during October of 1993 in well 3 at site 16 in Stafford County, Kansas: a) Head versus log time (since initiation of data collection) plot of slug-test data;

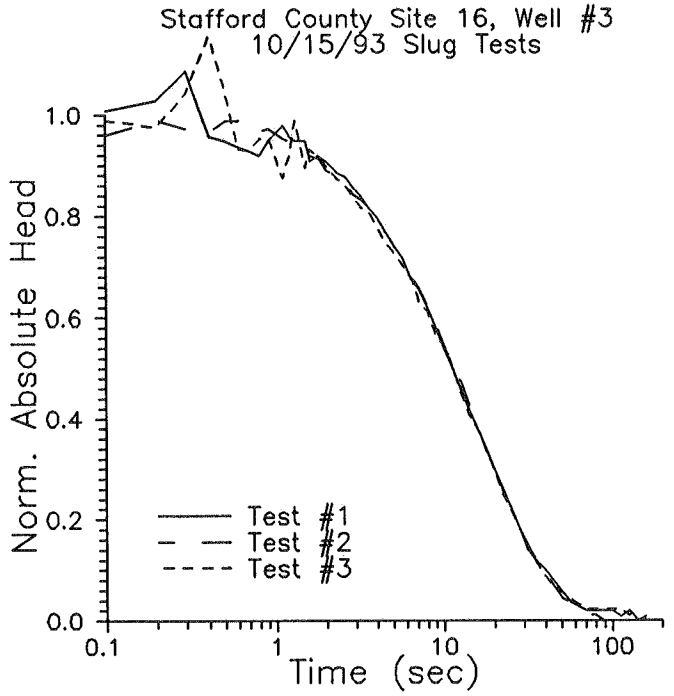

b) Normalized absolute head versus log time (since test initiation) plot of slug-test data.

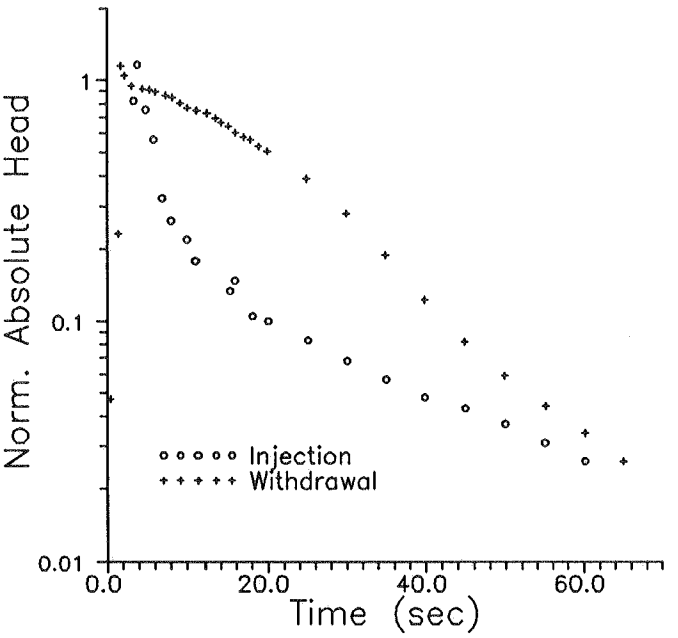

Figure 5 - Log normalized absolute head versus time plot of a series of slug tests reported by Dahl and Jones (1993): a) Injection and withdrawal slug tests using H_0=1.07 m;

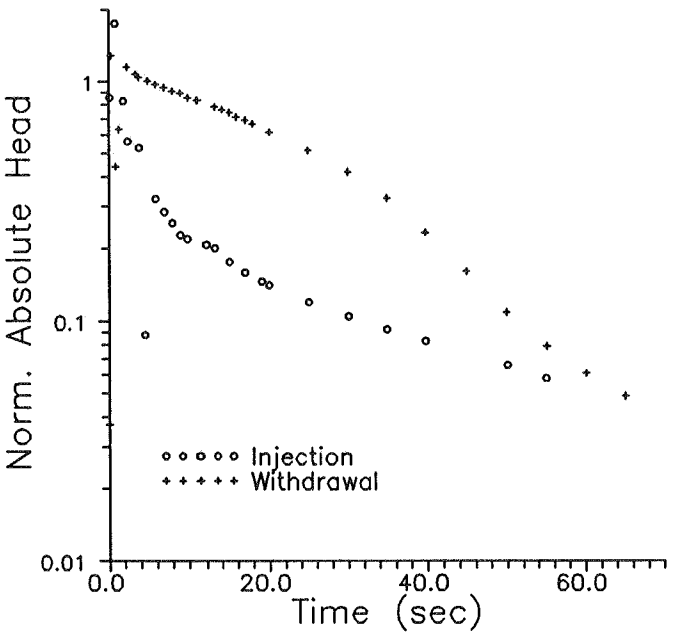

b) Injection and withdrawal slug tests using H_0=1.59 m.

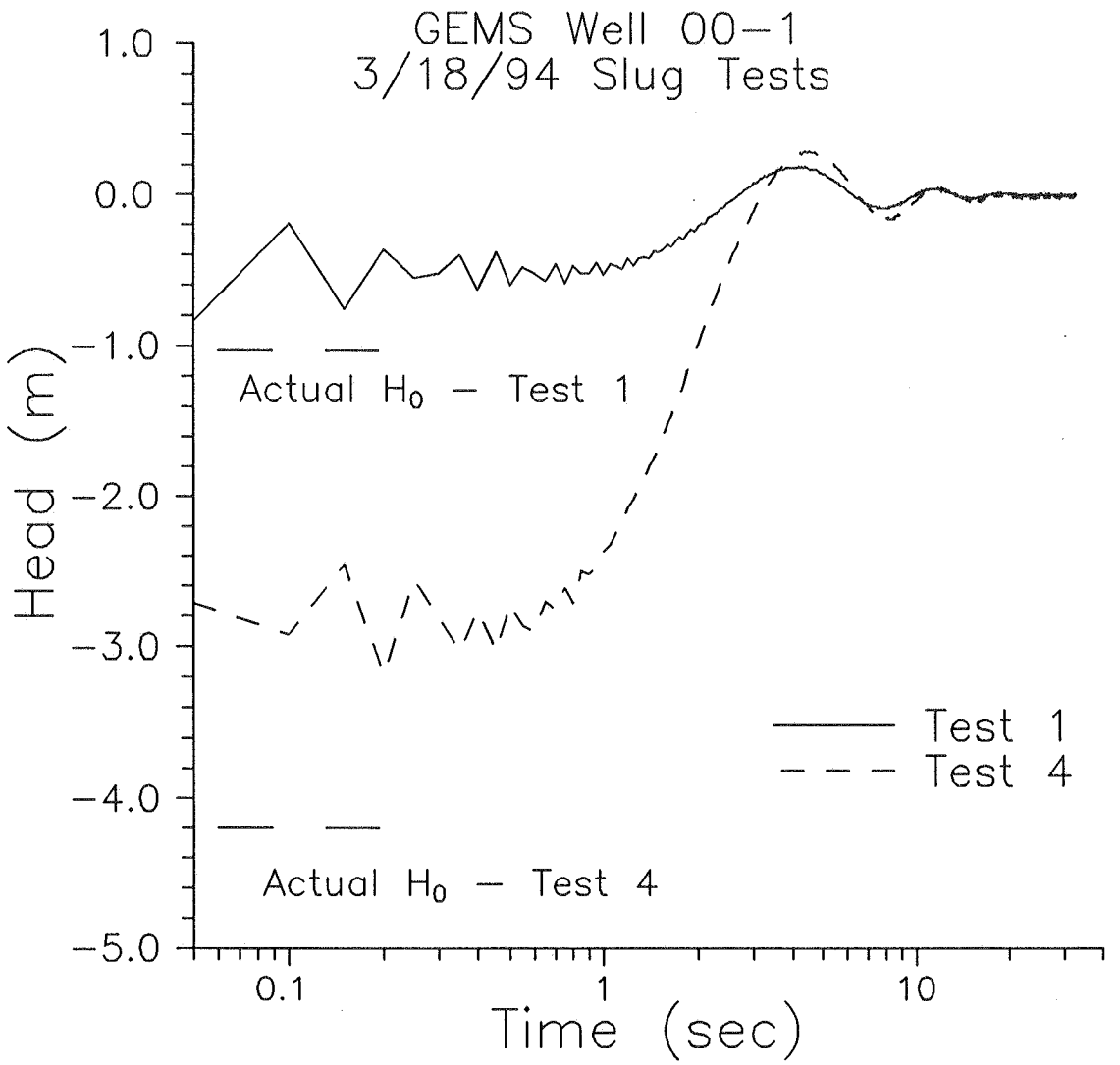

Figure 6 - Head versus log time plot of a pair of slug tests performed during March of 1994 in well 00-1 at GEMS in Douglas County, Kansas ("actual H_0" estimated from gas pressure transducer and denoted by large dashed lines).

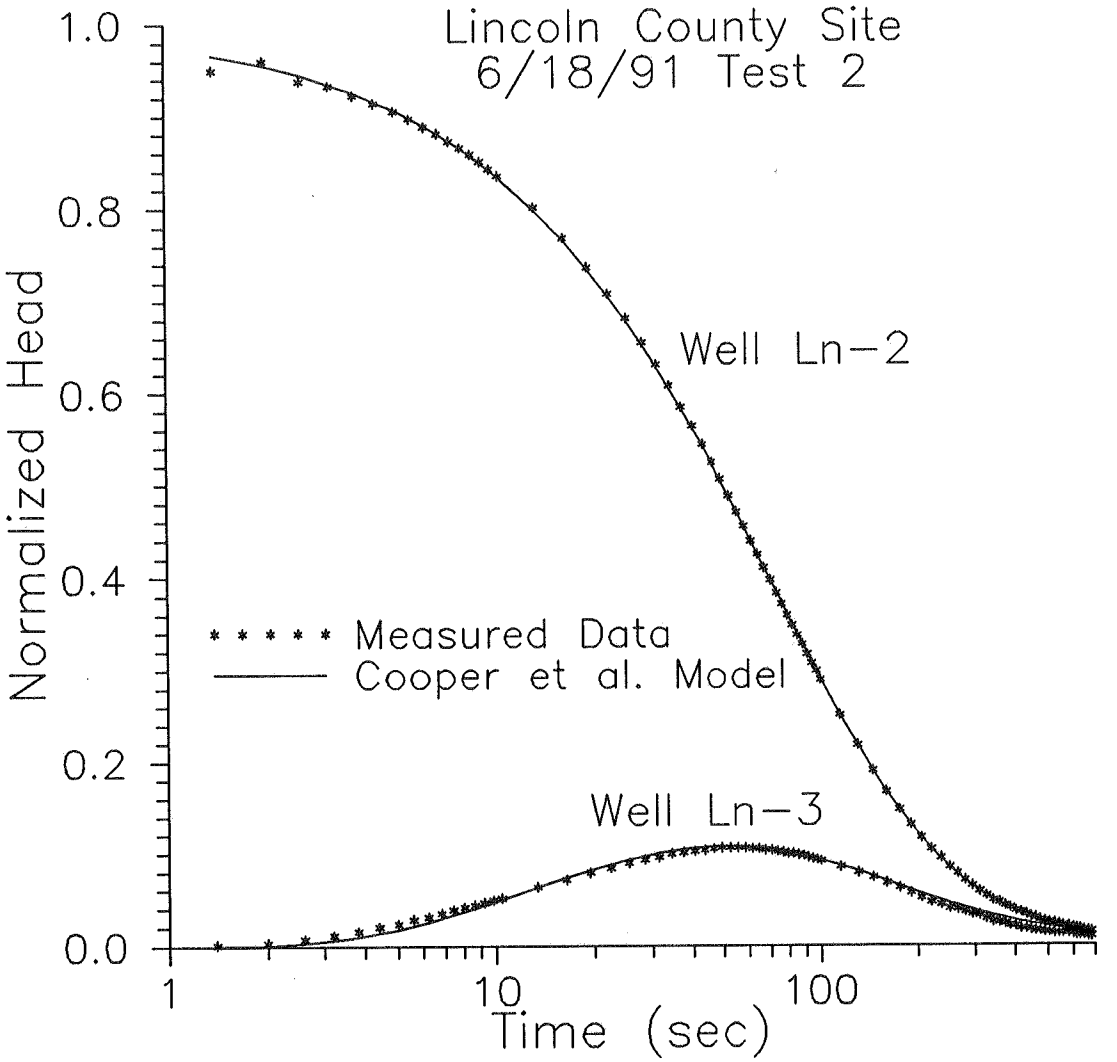

Figure 7 - Normalized head ($H(t)/H_0$) versus log time plot of Lincoln County slug-test data and best-fit Cooper et al. model (H_0=2.80 m).

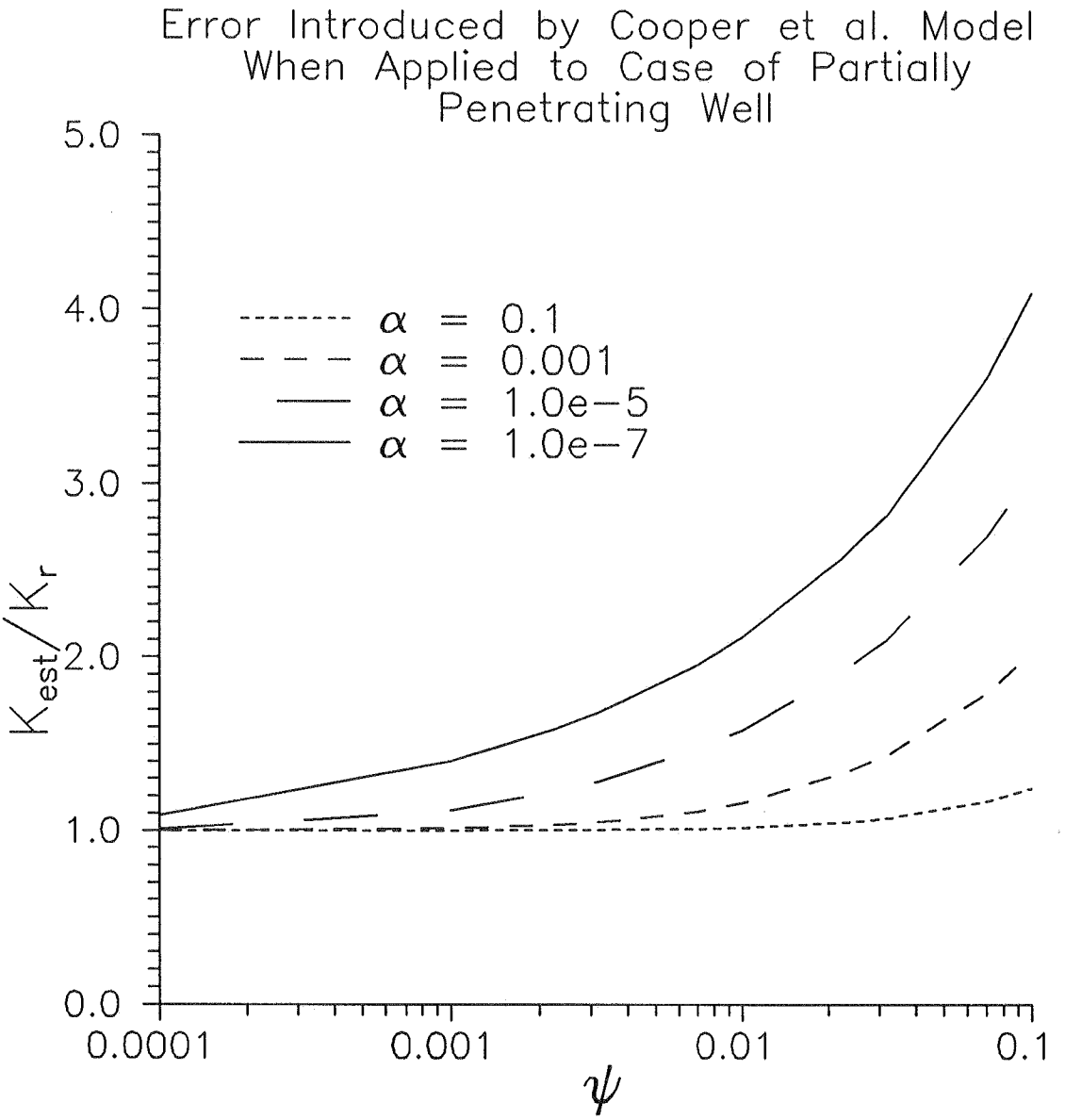

Figure 8 - Plot of conductivity ratio (Cooper et al. estimate (K_{est}) over actual conductivity (K_r)) versus ψ ($\sqrt{K_z/K_r}\,/\,(b/r_w)$) as a function of α ($(2r_w^2 S_s b)/r_c^2$) for the case of a partially penetrating well screened near the center of a very thick aquifer (after Hyder et al. (1994)).

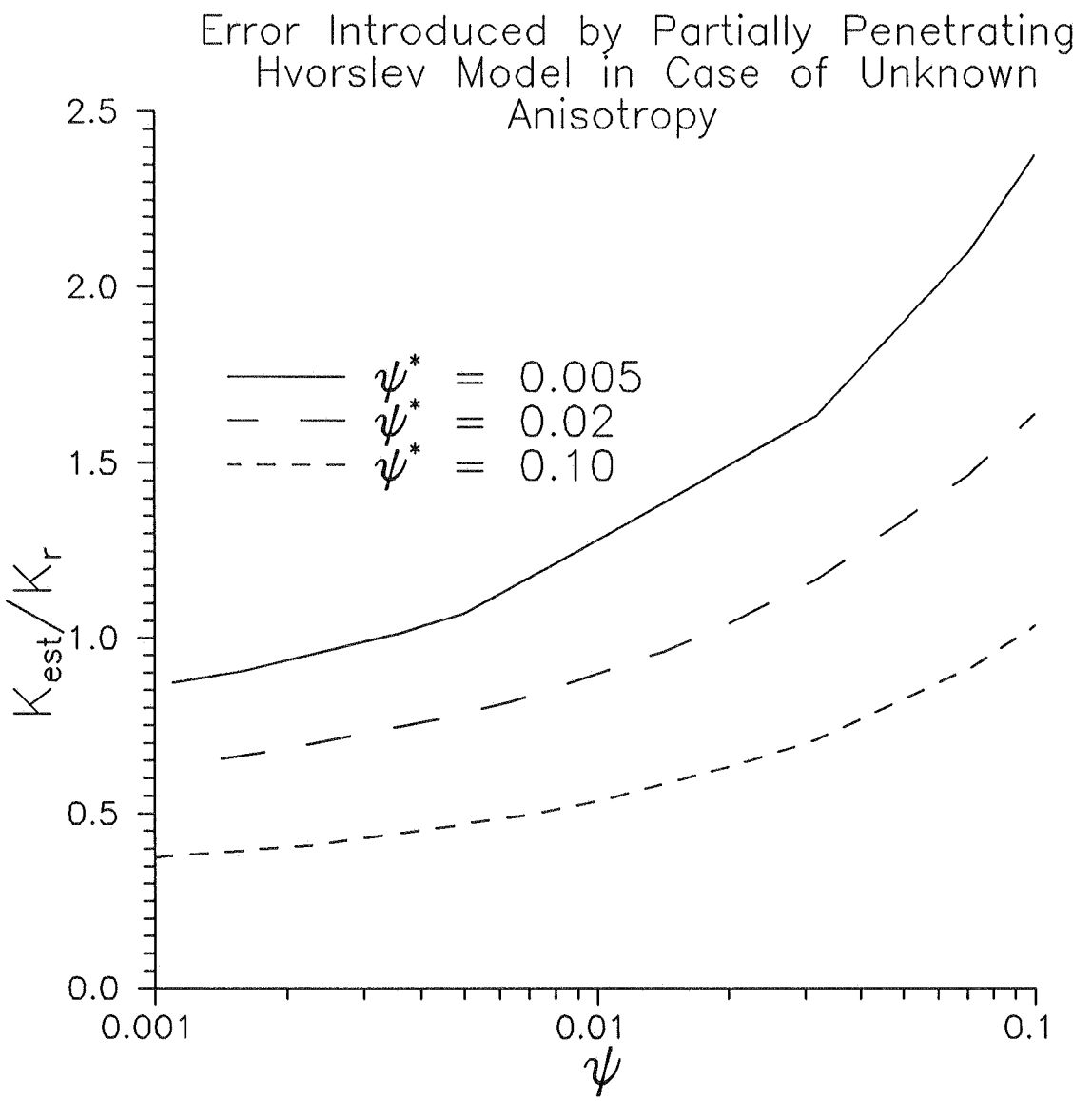

Figure 9 - Plot of conductivity ratio (Hvorslev estimate (K_{est}) over actual conductivity (K_r)) versus ψ ($\sqrt{K_z/K_r}\,/\,(b/r_w)$) as a function of ψ^* (ψ term with an assumed anisotropy ratio) for the case of a well screened near the center of a very thick aquifer and $\alpha=1.0\text{x}10^{-5}$ (after Hyder et al. (1994)).

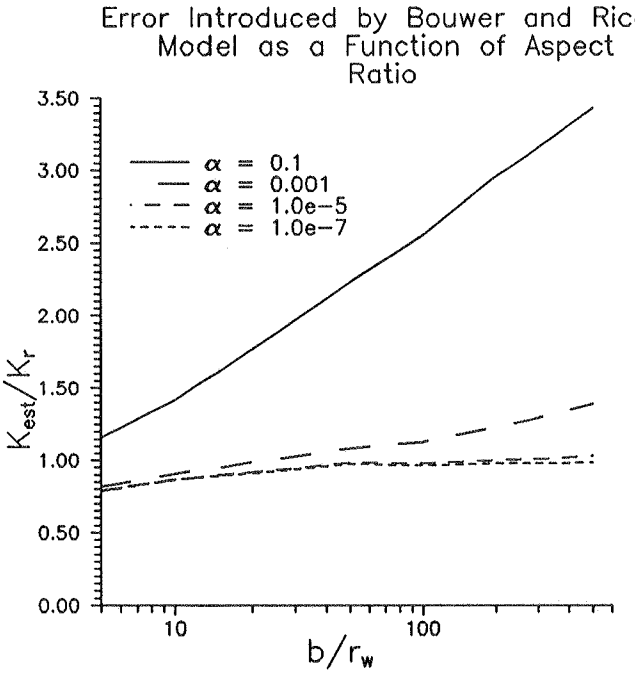

Figure 10 - Plots illustrating the error introduced by the Bouwer and Rice model for the case of a well screened near the center of a very thick aquifer (after Hyder and Butler (1995)): a) Plot of conductivity ratio (Bouwer and Rice estimate (K_{est}) over actual conductivity (K_r)) versus aspect ratio (b/r_w) as a function of α ($(2r_w^2 S_s b)/r_c^2$);

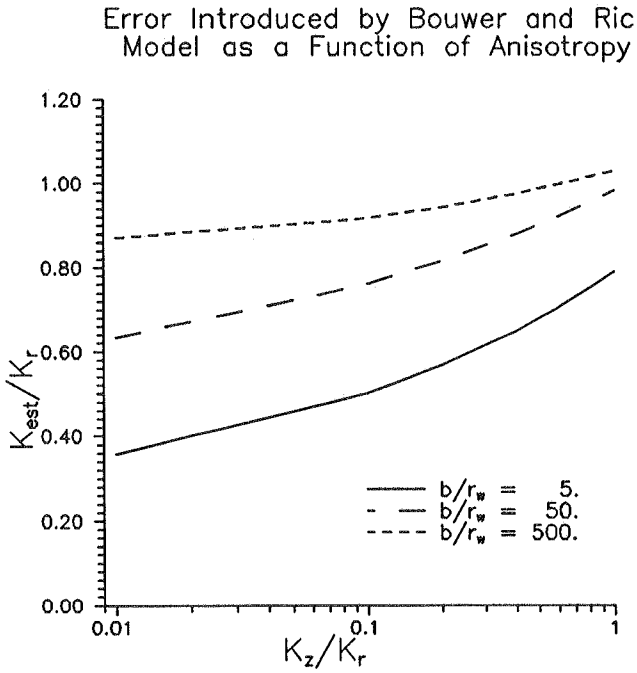

b) Plot of conductivity ratio versus anisotropy ratio (K_z/K_r) as a function of aspect ratio for $\alpha=1.0\text{x}10^{-5}$.

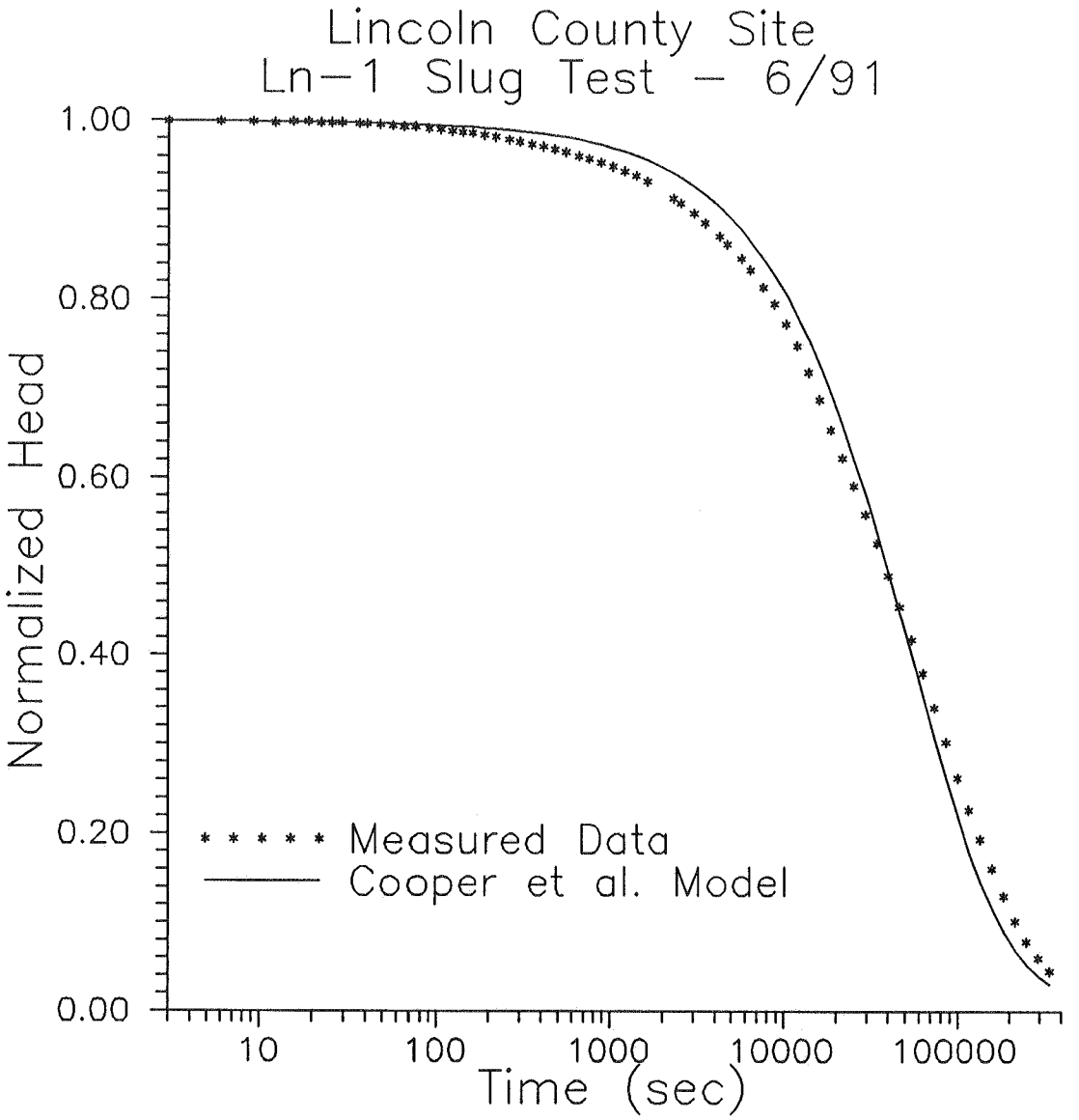

Figure 11 - Normalized head ($H(t)/H_0$) versus log time plot of 6/91 slug test performed in well Ln-1 at the Lincoln County site and the best-fit Cooper et al. model assuming $\alpha=2.10\text{x}10^{-4}$ ($H_0=10.35$ m; $K_{est}=5.79\text{x}10^{-4}$ m/d).

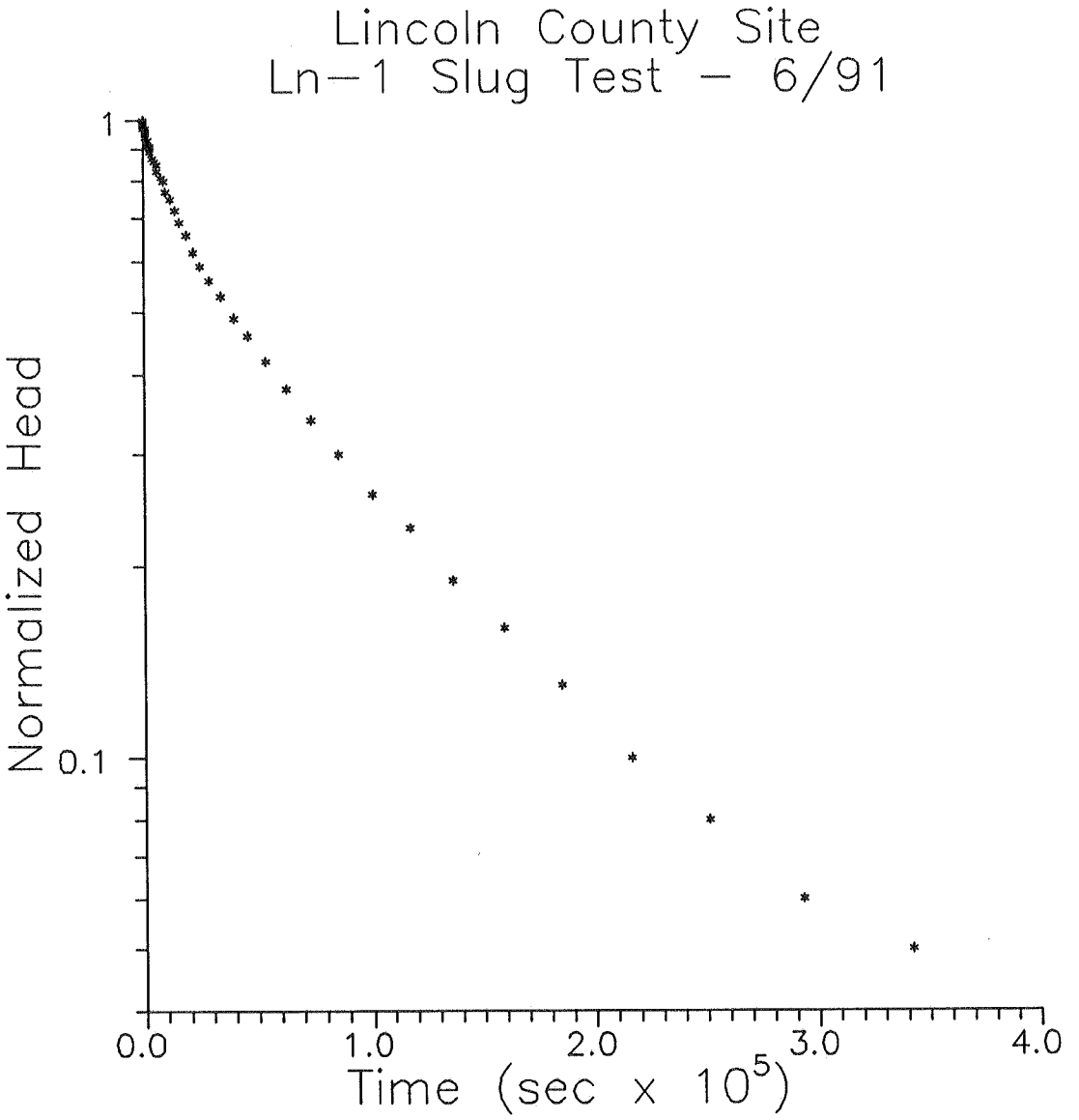

Figure 12 - Log normalized head ($H(t)/H_0$) versus time plot of 6/91 slug test from well Ln-1 at the Lincoln County site.

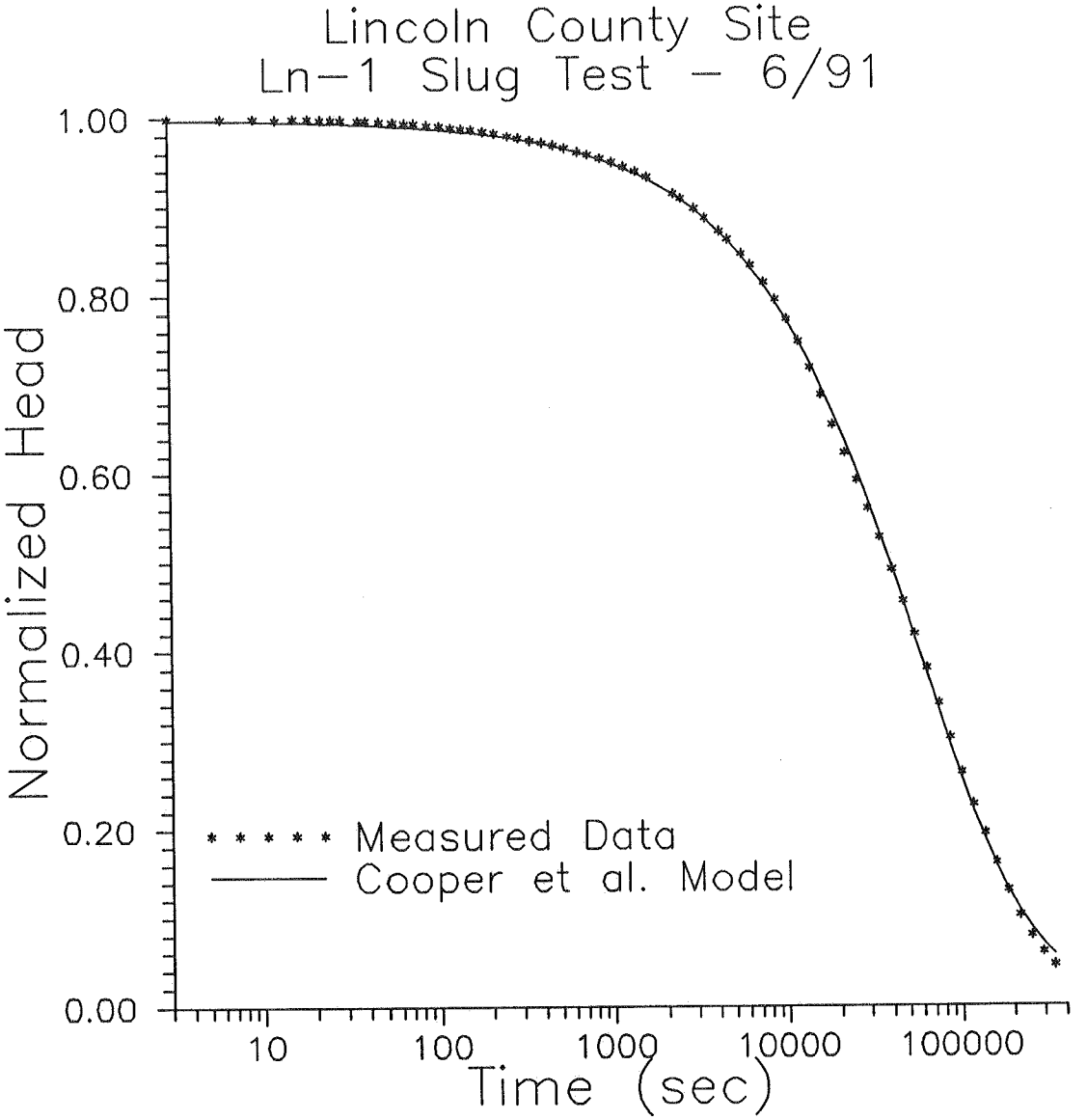

Figure 13 - Normalized head ($H(t)/H_0$) versus log time plot of 6/91 slug test from well Ln-1 at the Lincoln County site and the best-fit Cooper et al. model (K_{est}=2.68x10^{-4} m/d; no prior assumption concerning α).

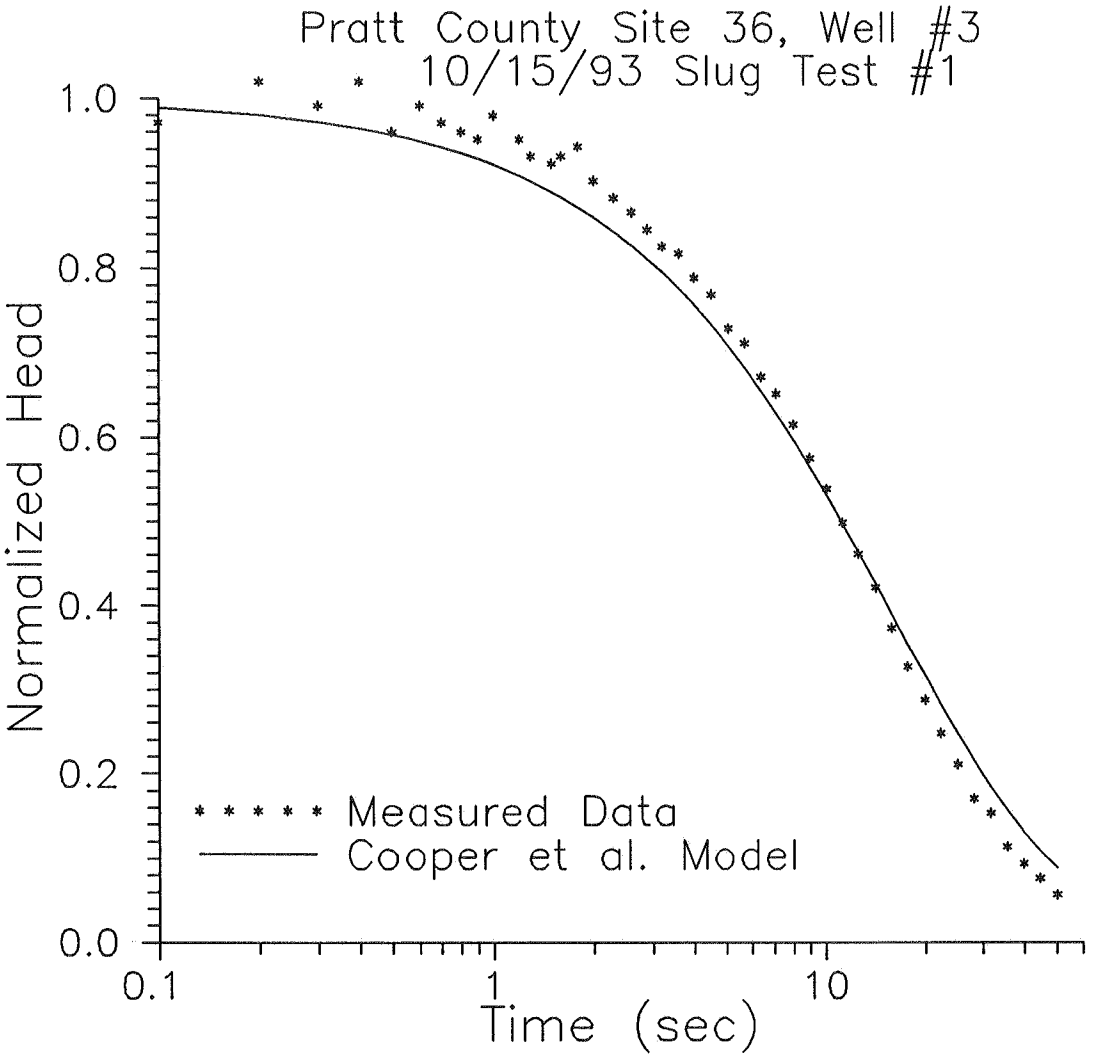

Figure 14 - Normalized head ($H(t)/H_0$) versus log time plot of 10/15/93 #1 slug test performed in well 3 at site 36 in Pratt County, Kansas, and the best-fit Cooper et al. model assuming $\alpha=3.80\text{x}10^{-5}$ ($H_0=0.38$ m; $K_{est}=42.0$ m/d).

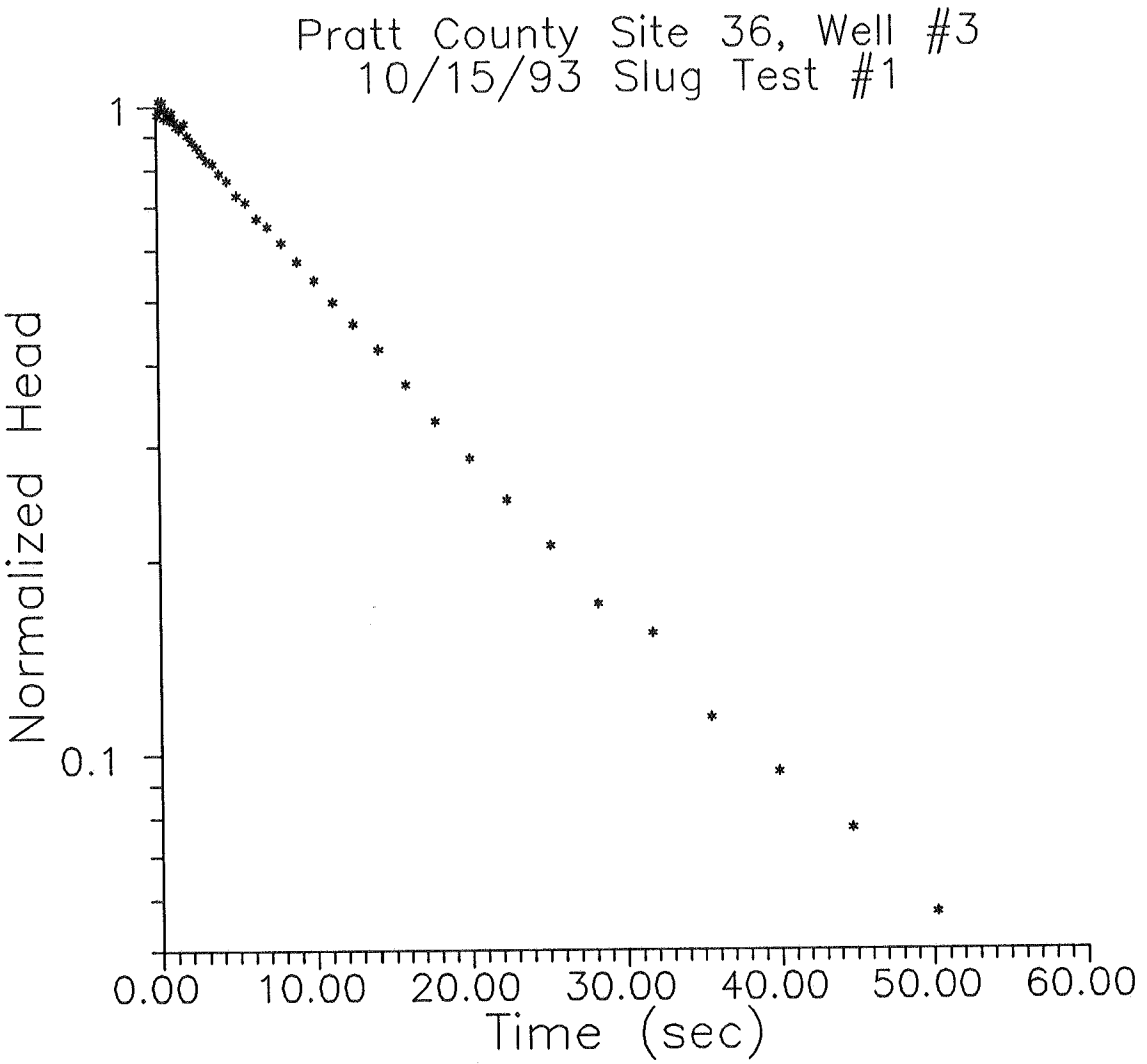

Figure 15 - Log normalized head ($H(t)/H_0$) versus time plot of 10/15/93 #1 slug test from well 3 at site 36 in Pratt County, Kansas.

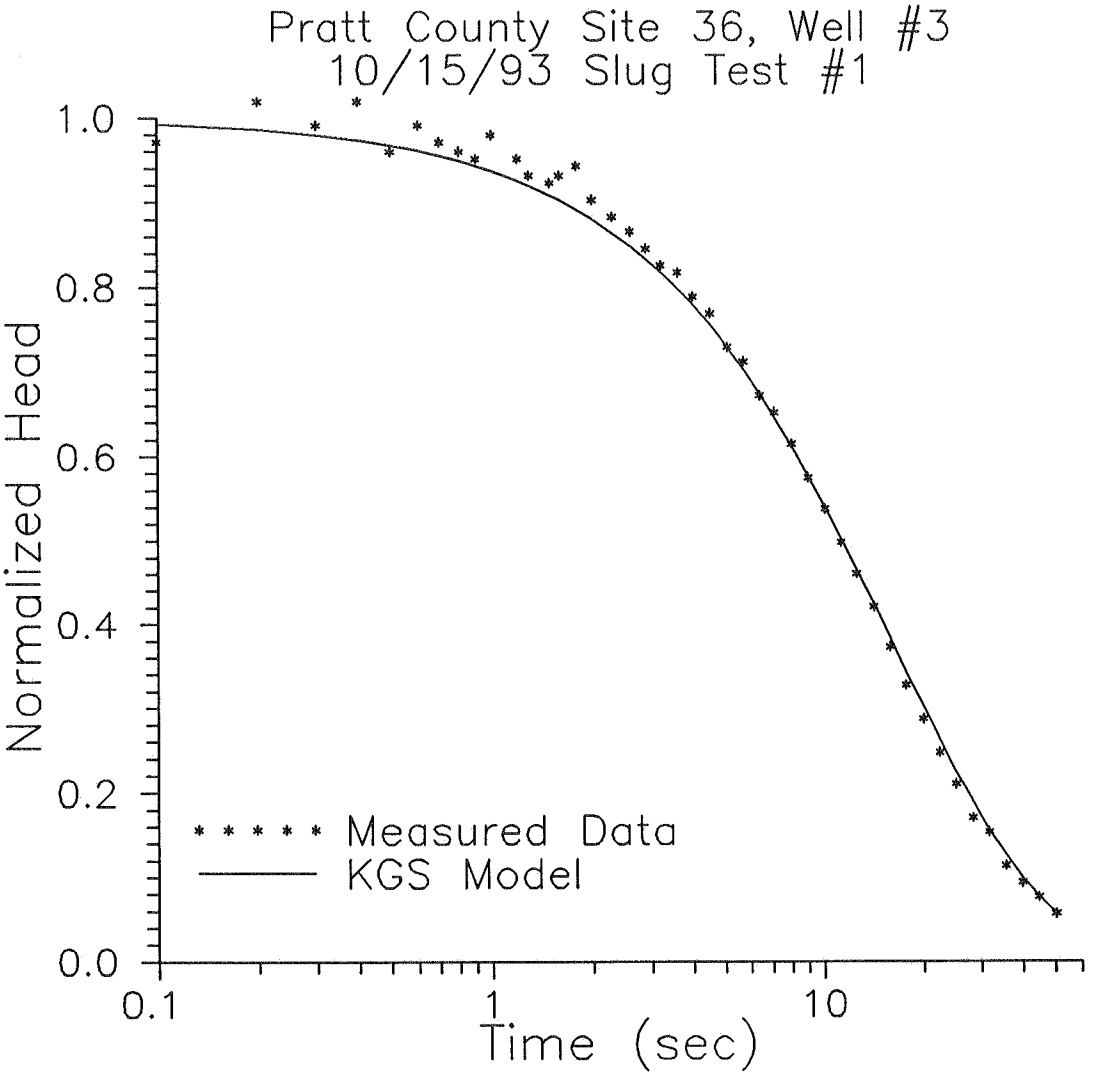

Figure 16 - Normalized head ($H(t)/H_0$) versus log time plot of 10/15/93 #1 slug test from well 3 at site 36 in Pratt County, Kansas, and the best-fit KGS model assuming $\alpha=3.80\text{x}10^{-5}$ ($K_{est}=17.6$ m/d).

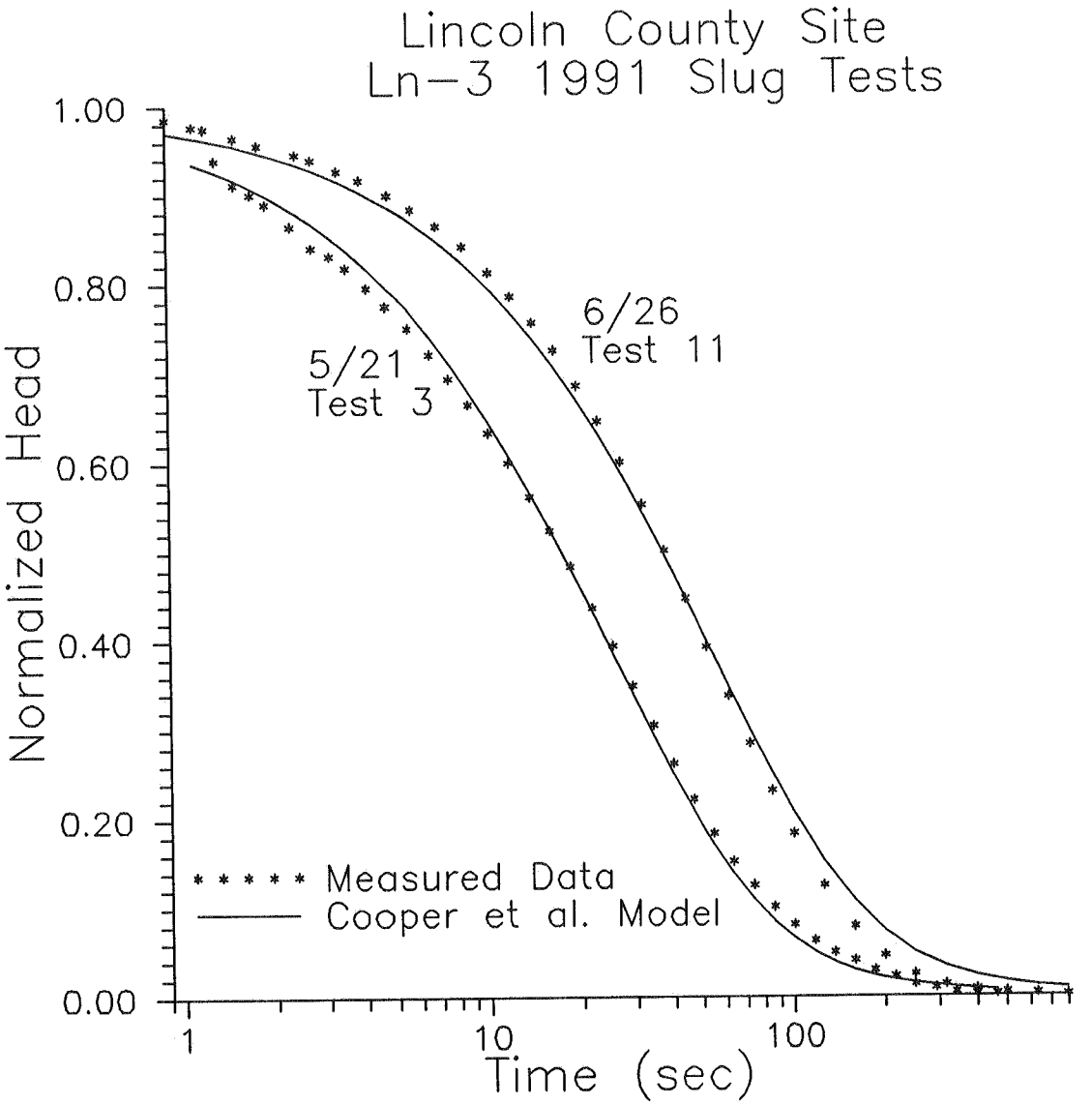

Figure 17 - Normalized head ($H(t)/H_0$) versus log time plot of 5/21/91 #3 (H_0=4.87 m) and 6/26/91 #11 (H_0=5.25 m) slug tests from well Ln-3 at Lincoln County site and the best-fit Cooper et al. models assuming $\alpha=3.87\text{x}10^{-4}$ (estimated $K_{5/21\ \#3}$=1.34 m/d and $K_{6/11\ \#11}$=0.62 m/d).

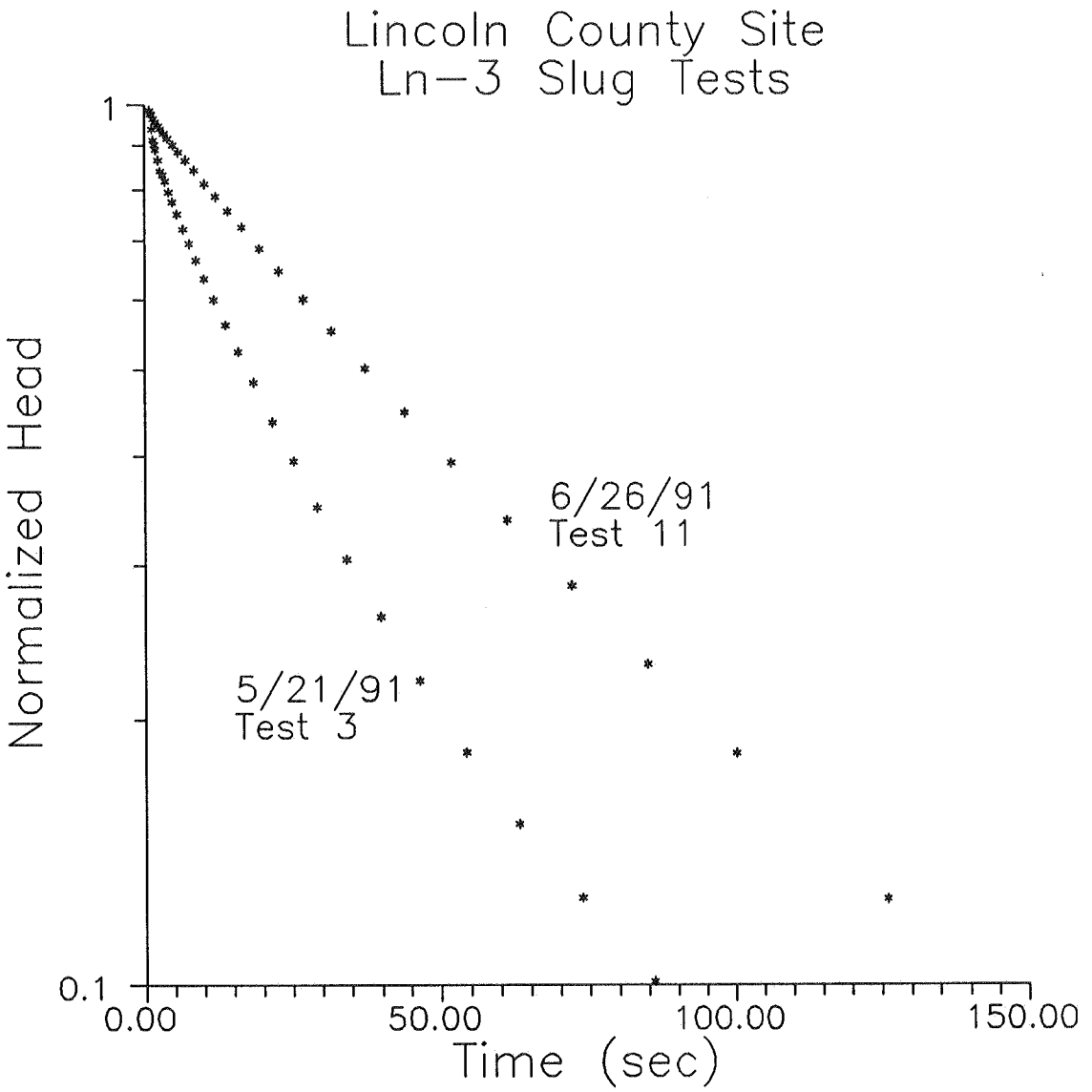

Figure 18 - Log normalized head ($H(t)/H_0$) versus time plot of 5/21/91 #3 and 6/26/91 #11 slug tests performed in well Ln-3 at Lincoln County site.

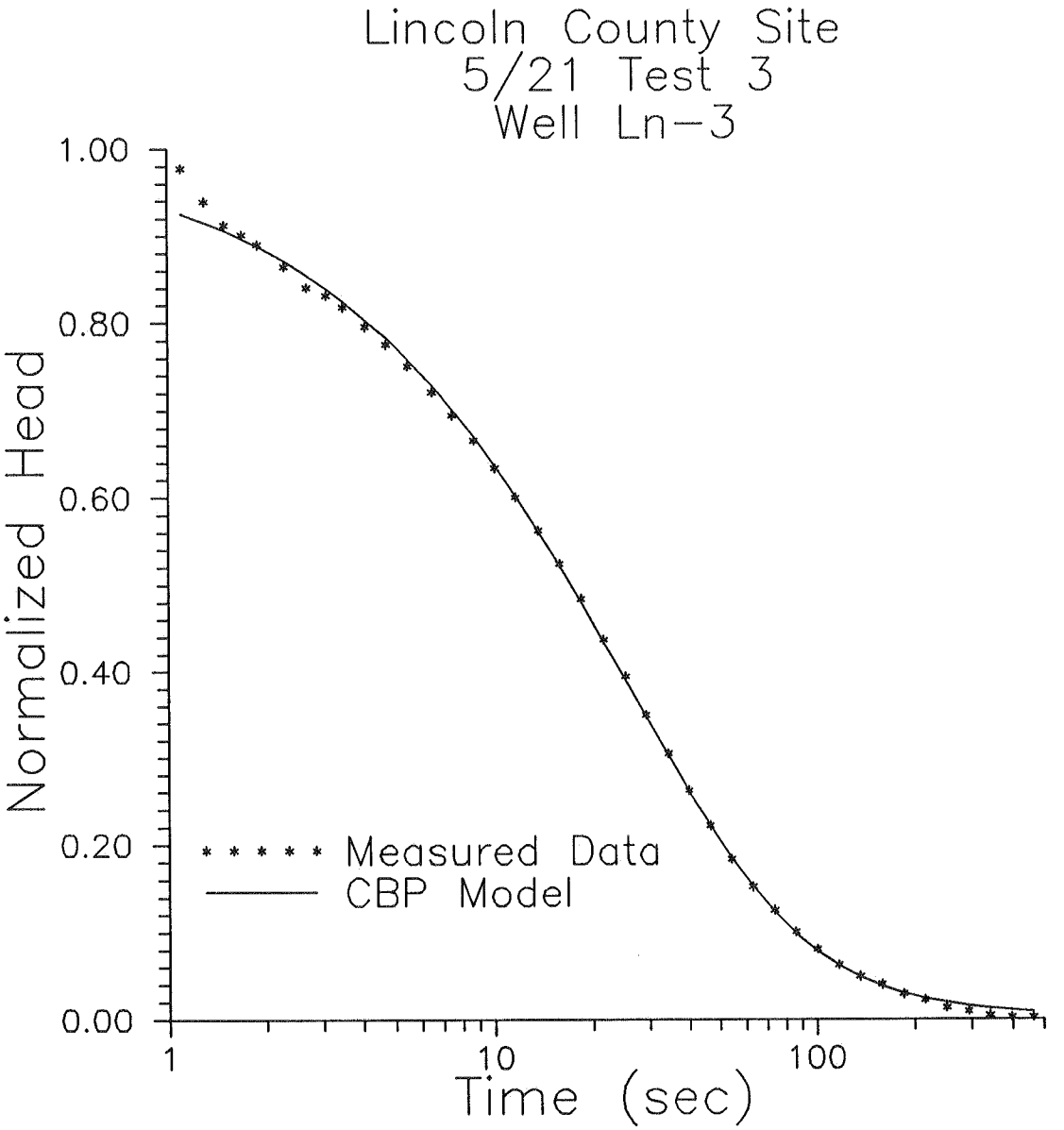

Figure 19 - Normalized head ($H(t)/H_0$) versus log time plot of 5/21/91 #3 slug test from well Ln-3 at Lincoln County site and the best-fit Cooper et al. model (K_{est}=1.01 m/day; no prior assumption concerning α).

F. DETECTION OF LOW-PERMEABILITY WELL SKINS USING SLUG TESTS

Introduction

The failure to recognize the existence of a low-permeability well skin is undoubtedly the largest source of error in hydraulic conductivity estimates obtained from slug tests. An underestimation in hydraulic conductivity of an order of magnitude or more can often be the result if a low-permeability skin is not recognized. In this section, a new approach for the identification of low-permeability well skins is proposed. This approach involves performing repeat slug tests in conjunction with a simple ratio method derived from the Hvorslev technique. The dimensionless storage parameter is changed between tests by modifying the effective radius of the well casing. The approach is based on the fundamental physics of slug-induced flow in the presence of a low-permeability skin. When used together with the procedures discussed in the previous section, the existence of both dynamic and static skins can readily be detected through repeat slug tests. Although the hydraulic conductivity of the formation may still be difficult to estimate, use of this method should enable the field practitioner to avoid inadvertently assigning properties reflective of a low-permeability skin to the formation. A field example will help demonstrate the potential of the approach.

Dependence of Slug-Test Responses on the Dimensionless Storage Parameter

The KGS Model (Hyder et al., 1994; Hyder and Butler, 1995; Liu and Butler, 1995) is currently the most general model for considering slug tests in confined or unconfined formations of moderate to low permeability. According to this model, in the absence of a well skin, the slug-induced head (H) in the test well can be written as

$$H/H_0 = f(\tau;\alpha,\beta,\psi,\varsigma) \qquad \text{(III.F.1)}$$

where

H_0 = magnitude of the initial slug-induced displacement (i.e. the size of the slug), [L];

$\tau = (tbK_r)/(r_c^2)$;

K_r = radial component of hydraulic conductivity, [L/T];

b = length of screened interval, [L];

r_c = radius of well casing, [L];
$\alpha = (2r_w^2 bS_s)/r_c^2$;
r_w = radius of well screen, [L];
S_s = specific storage, [1/L];
$\beta = B/b$;
B = formation thickness, [L];
$\psi = (A/a^2)^{.5}$;
$A = K_z/K_r$;
K_z = vertical component of hydraulic conductivity. [L/T];
$a = b/r_w$;
$\varsigma = d/b$;
d = depth of top of screen below top of formation, [L].

Once a well has been emplaced, most of the parameters of equation (III.F.1) may appear to be fixed quantities. However, certain of the well-construction parameters can be changed. For example, b (the screened interval) could be modified by using a packer to block off a certain portion of the screen or by perforating the casing. Although the radius of the well screen (r_w) can not be altered, the effective radius of the casing (r_c) can be readily changed by using a packer and standpipe arrangement (e.g., Butler and Healey, 1995). In this arrangement, the standpipe is attached to the central flow-through pipe of the packer, which can be opened or closed from the surface using a wireline. In an injection slug test performed with this equipment, the standpipe would extend from the packer (located below the static level in the well) to some distance above the expected H_0. Thus, all water level changes during the test would occur in the smaller-diameter standpipe. As shown by the definitions of the terms of equation (III.F.1), decreasing the casing radius speeds up the duration of the test (t) and increases the dimensionless storage parameter (α). Note that the ultimate result of continual decreases in casing radius is the shut-in slug test used for testing formations of very low permeability (Bredehoeft and Papadopulos, 1980; Neuzil, 1982).

In the work described here, repeat slug tests in which the casing radius (and hence α) is changed between tests will be the basis of a method for identification of low-permeability well skins. Moench and Hsieh (1985) speculated that performing repeat slug tests with different α might prove useful for estimating skin and formation properties. However, other than a series of tests described by Novakowski (1988) to assess if fracture width changed with depth of investigation, very little work has

apparently been done on varying α between slug tests. No previous work related to the approach proposed here could be found in the literature.

In order to understand the basis of the method proposed in this section, it is necessary to examine the dependence of slug test responses on α. It is widely recognized (e.g., Cooper et al., 1967) that slug test responses are not strongly dependent on α for the range of values found in most field applications (5.e-6 to 5.e-4). The Hvorslev (Hvorslev, 1951) and Bouwer and Rice (Bouwer and Rice, 1976) methods for analysis of slug-test response data are based on this insensitivity to α. As shown in Section III.E, these methods will often provide reasonable estimates of hydraulic conductivity for the range of α values commonly found in the field. Chirlin (1989) shows that a plot of the log of the deviation from static (henceforth designated as head) versus time for slug tests in fully penetrating wells ($\beta=1$ in (III.F.1)) should be approximately linear, as would be predicted by the Hvorslev method, when α is small. As α increases, the plots will display an increasingly pronounced concave upward curvature. A similar relationship will be seen in partially penetrating wells ($\beta>1$), although the vertical component of flow will suppress the concave upward curvature until higher α values. The lack of curvature of plotted response data is often considered as field verification of the appropriateness of the Hvorslev and Bouwer and Rice models. However, Hyder et al. (1994) and Hyder and Butler (1995) have recently shown that such linear plots can also be an indication of the existence of a low-permeability well skin.

Slug-Induced Flow in the Presence of a Low-Permeability Well Skin

The Hvorslev method for analysis of slug-test data is essentially based on two major assumptions concerning the slug-induced flow system. These assumptions are 1) there exists an effective radius beyond which the slug-induced disturbance has no effect on formation heads, and 2) the influence of specific storage on test responses is essentially negligible. When a slug test is performed at a well with a low-permeability skin, almost all of the head drop occurs across the skin. Heads in the formation are essentially unaffected by the test (e.g., Faust and Mercer, 1984). In addition, the specific storage of the skin has very little influence on the response data because the thickness of the skin is relatively small. Thus, the two major assumptions of the Hvorslev method actually appear to be more reasonable in the case of a low-permeability well skin than in the homogeneous case. This situation can be readily demonstrated through a series of simulations using the KGS Model. Figure III.F.1 shows the simulated responses of a pair of hypothetical slug tests performed in a fully

penetrating well. A straight line connecting the first and last points of each curve is included to better illustrate the degree of curvature. Note that the slug test with the larger α has a more pronounced concave upward curvature. In Figure III.F.2, analogous results are shown for the case of a low-permeability well skin, where the sk and fm subscripts refer to the skin and formation, respectively, and the dimensionless parameters employ the parameters of the formation. In this case, the high α response is still basically linear in form, even though α has increased over one and a half orders of magnitude. This approximate linearity of the log head versus time plot is a direct result of virtually all of the head drop occurring across the width of the skin (i.e. the assumptions of the Hvorslev model are being upheld). Further work has shown that as the skin-formation contrast increases, the high α plots will be virtually indistinguishable from a straight line. This difference in the dependence of the slug-induced responses on α for the homogeneous and low-permeability skin cases is the basis of the method proposed here for detecting the existence of a low-permeability skin.

Detecting the Existence of a Low-Permeability Well Skin

Equation (III.F.2) is the Hvorslev expression (case 8 of Hvorslev (1951)) for the radial component of hydraulic conductivity (K_{HV}) estimated from a slug test in a partially penetrating well:

$$K_{HV} = \frac{r_c^2 \ln[1/(2\psi) + [1+(1/2\psi)^2]^{0.5}]}{2bt_0} \qquad \text{(III.F.2)}$$

where

t_0 = basic time lag, the time at which a normalized head of 0.37 is reached.

Note that as the aspect ratio (b/r_w) gets large, equation (III.F.2) will reduce to the Hvorslev expression for a fully penetrating well (case 9) if the effective radius is set equal to the screen length in case 9 of Hvorslev (1951).

Assume that the increases in α shown in Figures III.F.1 and III.F.2 were effected by decreases in the casing radius. Since only the casing radius and t_0 would change between tests, the ratio of the right hand side of equation (III.F.2) for the high α case over that for the low α case can be written as

$$\frac{(r_c^2/t_0)_2}{(r_c^2/t_0)_1} \qquad \text{(III.F.3)}$$

where 1 and 2 designate the low α and high α cases, respectively. In the case of the simulations of Figure III.F.1, equation (III.F.3) equals 1.54. In the case of the simulations of Figure III.F.2, the ratio equals 1.12. This difference, which is a reflection of the increased curvature seen in the homogeneous case, is the basis of the method proposed here. Note that the change in α between 2.5e-5 and 1.6e-3 corresponds to using a 0.0159 m (0.625 inch) ID standpipe in a 0.127 m (5 inch) ID well.

The above example was purposefully designed to be rather conservative in nature. An α of 2.5e-5 would undoubtedly be near the lower end of the range for field conditions (e.g., all of the α of the field examples in Section III.E were larger). In addition, a relatively thin skin was used and the skin-formation contrast was only one order of magnitude. Figure III.F.3 is a plot of equation (III.F.3) (henceforth designated as the Hvorslev ratio) versus α, in which an α of 1.0e-4 is considered as the base case ("base case" is defined here as the denominator in equation (III.F.3)). As shown in Figure III.F.3, the difference between the Hvorslev ratios will increase with α and the contrast between the conductivity of the skin and the formation. Figure III.F.3 indicates that it should be possible to identify a low-permeability well skin that is an order of magnitude or more less conductive than the formation, even with relatively minor changes in α. Based on further simulations, it appears that this approach is viable for conductivity contrasts of a factor of two or greater in fully penetrating wells (Hvorslev ratio for a skin-formation contrast of a factor of two using the parameters of the above example would be 1.26).

Figure III.F.3 employed a skin with a radius twice that of the screen. As shown in Figure III.F.4, the Hvorslev ratios are dependent on the skin thickness. An interesting aspect of Figure III.F.4 is the pronounced upward rise seen in the $r_{skin}=10*r_w$ curve at very high α. This rise occurs because the effective radius of the slug test has become smaller than the outer radius of the skin. This well-known dependence of the effective radius of a slug test on α (e.g., Guyonnet et al., 1993) is the feature that Novakowski (1988) was trying to exploit in the series of repeat slug tests he describes.

The previous figures were developed for the case of a fully penetrating well.

Figure III.F.5 displays results for a partially penetrating well (ψ=0.1 corresponds to a b/r_w of 10 in an isotropic formation). The difference in Hvorslev ratios is clearly much smaller when there is a significant component of vertical flow. Thus, a relatively large change in α must be effected in order for the method to be viable in wells of small aspect ratios. In cases of very large ψ, one should only expect to be able to identify skins that are an order of magnitude or more less conductive than the formation. Note, however, that the difference between the Hvorslev ratios shown on Figure III.F.5 will increase as the aspect ratio increases or the anisotropy ratio (K_z/K_r) decreases. One additional point worth noting concerning this figure is the very small difference in Hvorslev ratios seen at small α values. This is a result of the earlier discussed insensitivity of slug-induced responses to α when ψ is large (significant component of vertical flow) and α is small. Hyder and Butler (1995) present example type curves for slug tests in partially penetrating wells that graphically illustrate this insensitivity to α.

Based on the theoretical results presented in the preceding paragraphs, the proposed approach appears quite promising. These results indicate that in almost all well-formation configurations of significance in hydrogeological applications, one should be able to recognize the existence of a skin that is an order of magnitude or more less permeable than the formation. However, the method clearly needs to be assessed in a field setting to see if the technique is viable in the presence of noisy data. The following subsection describes an initial field evaluation of the approach.

Field Evaluation at Trego County Monitoring Site

Butler and Healey (1995) describe a series of hydraulic tests that were performed by the Kansas Geological Survey at a Dakota aquifer monitoring well in Trego County, Kansas in July of 1994, and October-November of 1995. A constant-rate pumping test (total duration approx. 21.5 hours) and a series of slug tests were performed at this site. The hydraulic conductivity estimated from the recovery period of the pumping test was much larger than the values estimated from the slug tests. A series of repeat slug tests were performed at this site in an attempt to assess if this difference was due to the existence of a low-permeability skin. The standpipe and packer arrangement described earlier was used in these tests to change the diameter of the casing from the nominal casing diameter of 0.127 m (5 inches) to a diameter of 0.0508 m (2 inches). Figure III.F.6 displays the response data for three slug tests performed at this well. Test 2a was performed in the 0.127 m casing, while the other two tests were performed in the 0.0508 casing. Note that the small difference in t_0

values seen between the tests using the 0.0508 m casing is undoubtedly a product of dynamic-skin effects. Calculation of equation (III.F.3) for 11/16 test 4 over 11/16 test 2a produced a ratio of 1.04, while the ratio of 11/17 test 1 over 11/16 2a was 0.95. The average Hvorslev ratio from these tests was thus essentially one (0.995). If a S_s value of 8.50e-6 m^{-1} determined from tests elsewhere in the Dakota aquifer is employed, the α value for the 0.127 m casing test is 1.93e-4. Given that base value of α, the change in α effected here (factor of 6.25 increase), and the nominal ψ value for this well (equals 0.022 assuming isotropic conditions), an average Hvorslev ratio of 0.995 certainly points to the likelihood of a low-permeability well skin. However, the dynamic-skin effects were large enough to cast some uncertainty on this conclusion. Thus, a further series of test are planned using 0.0254 m (1 inch) and smaller standpipes. Note that the hydraulic conductivity range estimated from the analysis of the recovery data from the pumping test was 13.4-15.2 m/day, while that for these three slug tests was 0.066-0.072 m/day. This very large difference in conductivity estimates is just a further demonstration of the critical need for a technique to identify the existence of a low-conductivity skin in the absence of pumping-test data. The technique proposed here appears to fulfill that need.

Summary

In this section, a new method for the detection of low-permeability well skins was proposed. The method involves the performance of repeat slug tests with different dimensionless storage parameters (α). The approach is based on the fundamental physics of slug-induced flow in the presence of a low-conductivity well skin. The results of the work presented here indicate that the approach should be viable when the skin-formation conductivity contrast is greater than an order of magnitude, even in the presence of the noise inherent in field applications. Less dramatic contrasts can be identified when the vertical component of the slug-induced flow is small. This method should be useful for helping the field practitioner avoid inadvertently assigning a grossly inaccurate skin-biased conductivity estimate to the formation. A field example helped demonstrate the potential of the technique.

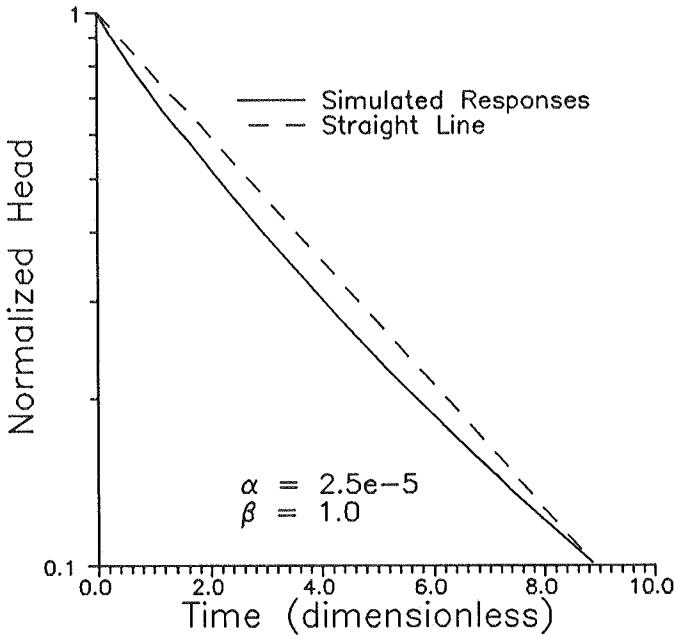

Figure III.F.1 - Plots of the logarithm of normalized head versus dimensionless time (τ) for simulations of slug tests in a homogeneous formation: a) Low α case;

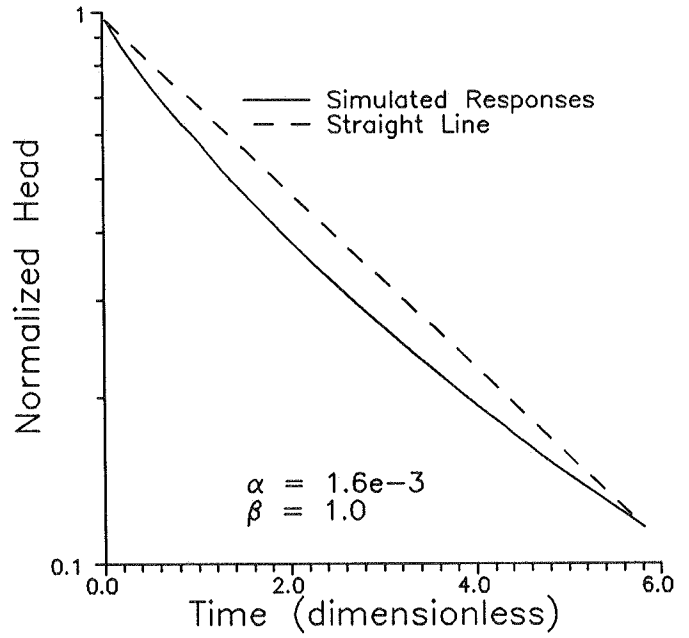

b) High α case ($\tau = (tbK_r)/r_c^2$, $\alpha = (2r_w^2bS_s)/r_c^2$, $\beta = B/b$; straight line joins first and last points of plotted data).

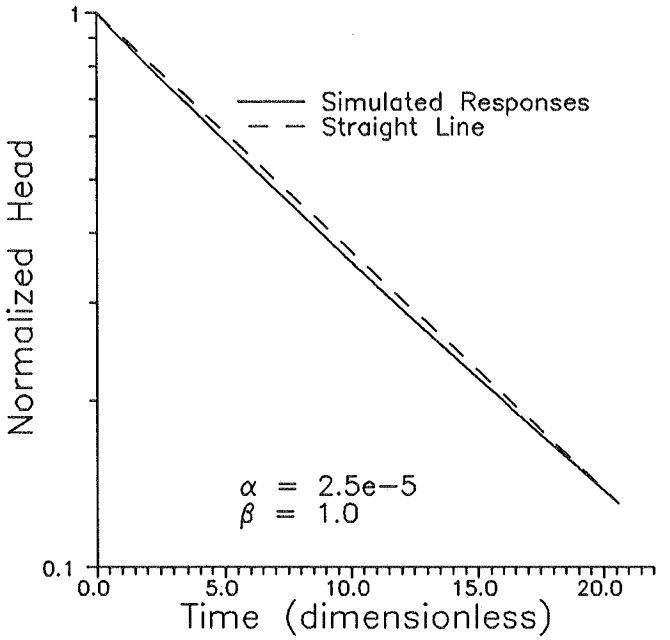

Figure III.F.2 - Plots of the logarithm of normalized head versus dimensionless time (τ) for simulations of slug tests in wells with low-permeability skins: a) Low α case;

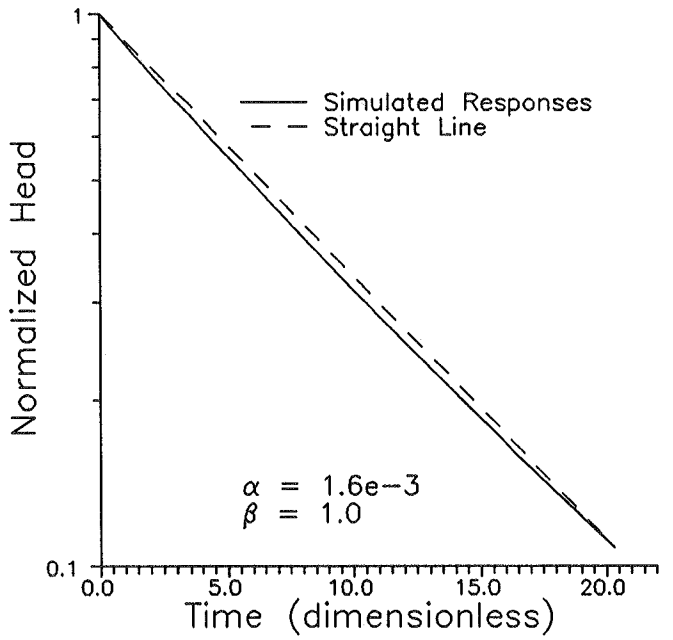

b) High α case ($\tau = (tbK_r)/r_c^2$, $\alpha = (2r_w^2bS_s)/r_c^2$, $\beta = B/b$, $K_{sk}/K_{fm} = 0.1$, $r_{sk} = 2*r_w$; straight line joins first and last points of plotted data).

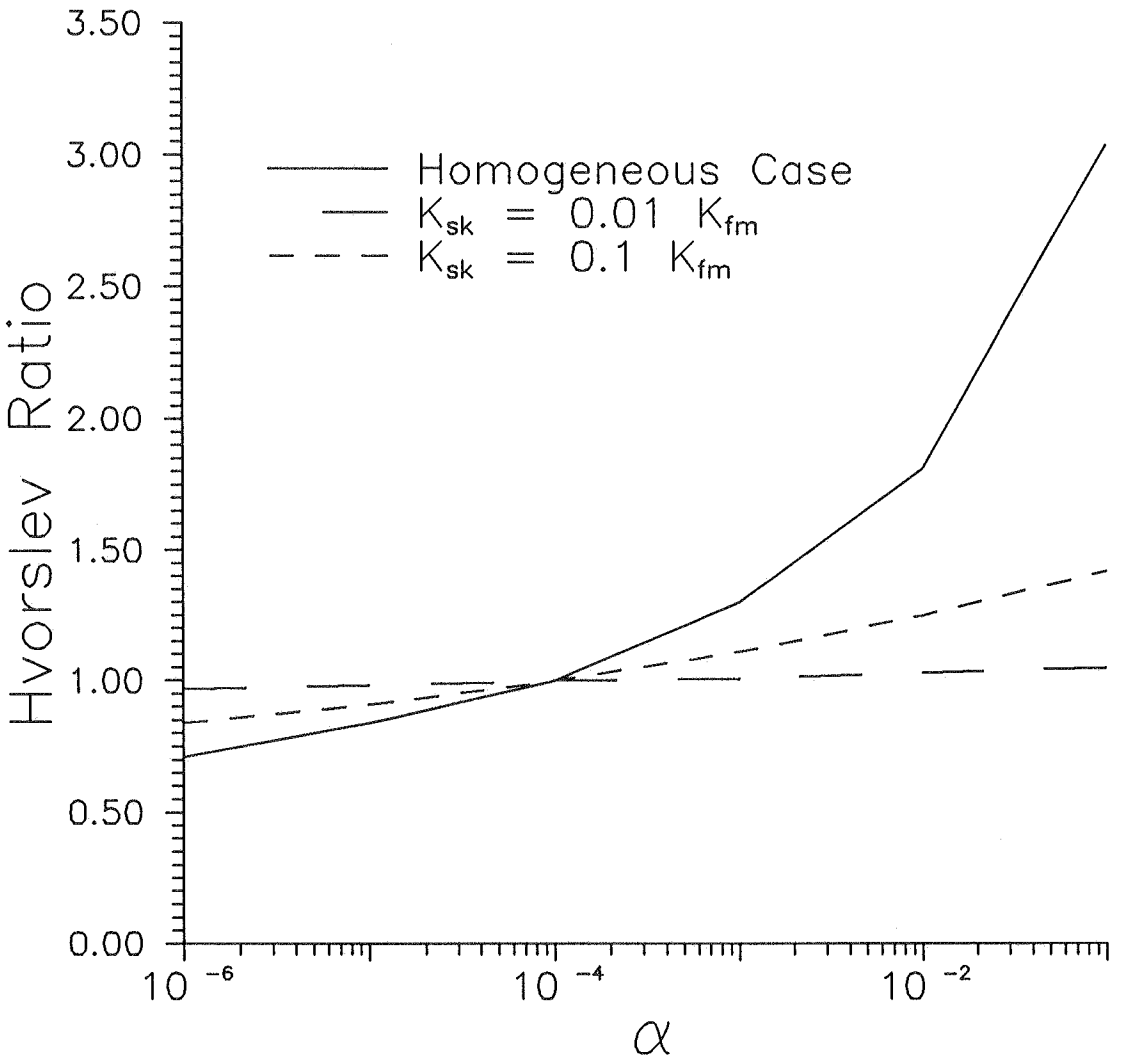

Figure III.F.3 - Plot of the Hvorslev ratio (equation (III.F.3)) versus the logarithm of α ($(2r_w^2bS_s)/r_c^2$) as a function of the conductivity contrast between the skin and the formation ($r_{sk} = 2*r_w$).

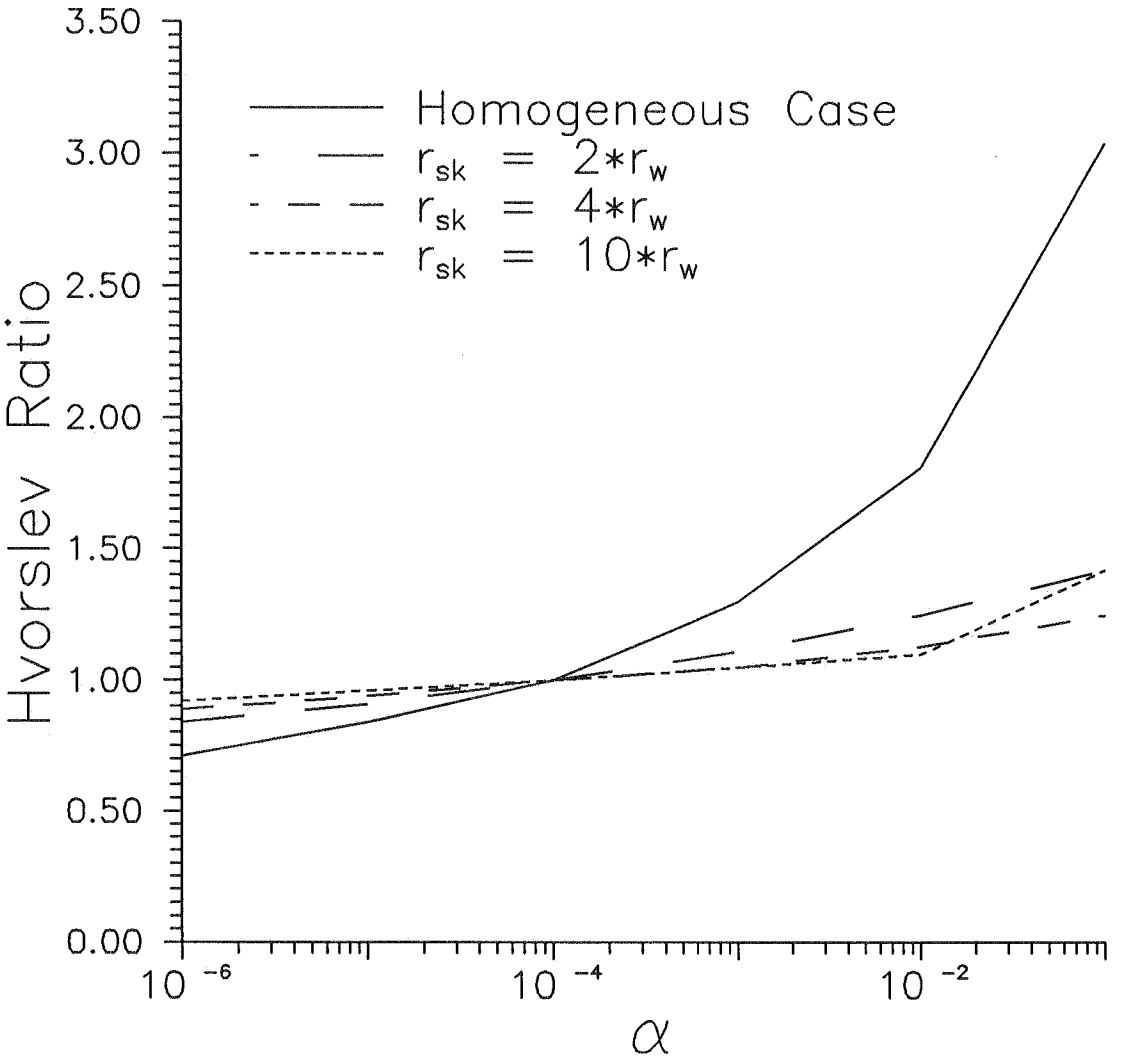

Figure III.F.4 - Plot of the Hvorslev ratio (equation (III.F.3)) versus the logarithm of α ($(2r_w^2bS_s)/r_c^2$) as a function of skin thickness ($K_{sk} = 0.1K_{fm}$)

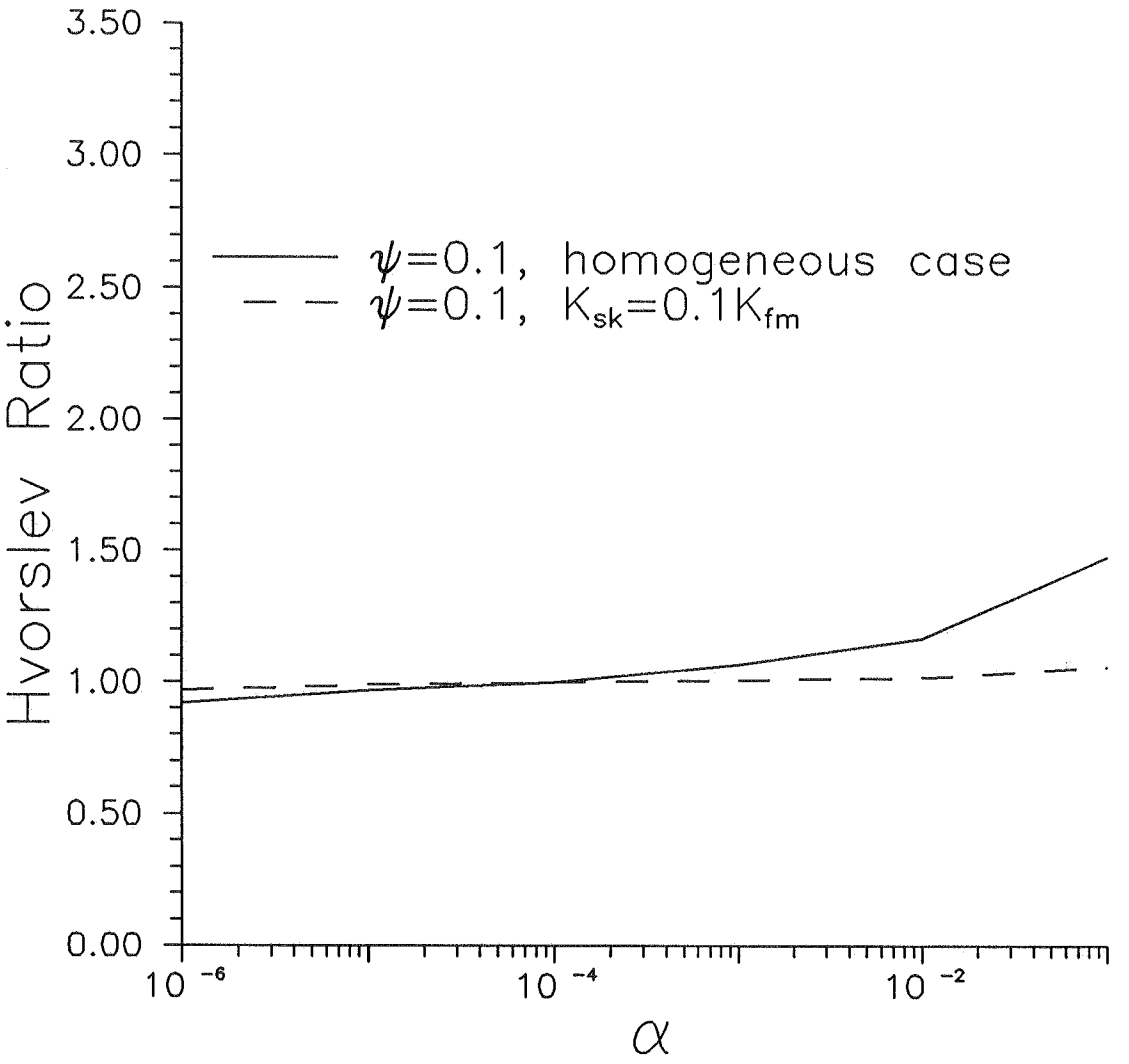

Figure III.F.5 - Plot of the Hvorslev ratio (equation (III.F.3)) versus the logarithm of α ($(2r_w^2bS_s)/r_c^2$) for the case of a partially penetrating well ($\psi = ((K_z/K_r)/(b/r_w)^2)^{.5}$).

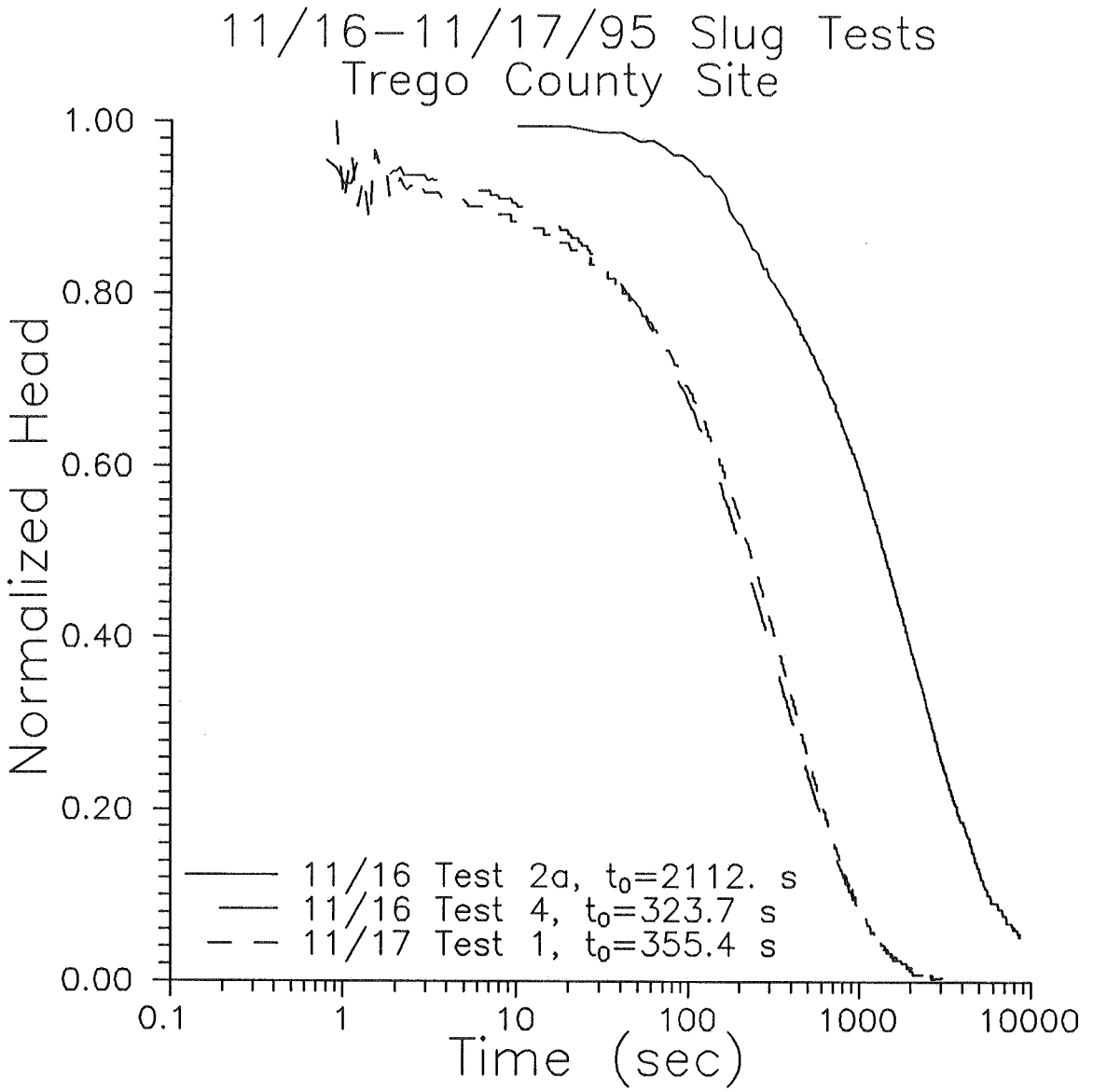

Figure III.F.6 - Normalized head versus the logarithm of time plot for Trego County slug tests (t_0=time at which a normalized head of 0.37 is reached).

IV. SITE CHARACTERIZATION ACTIVITIES

A. INTRODUCTION

The primary focus of the research of this project was on the use of well tests to describe spatial variations in hydraulic conductivity. The preceding portions of this report have described a variety of theoretical and field investigations directed at assessing the potential of various types of well tests to provide information about lateral and vertical variations in hydraulic conductivity. However, in addition to the focus on well tests, a considerable amount of the work of this project was directed at increasing our knowledge of the subsurface at GEMS. This effort involved drilling and sampling of the alluvium, and laboratory analysis of sampled cores. The goal of these characterization efforts was to gather as much detailed information about the subsurface at GEMS as possible, so that the quality of the estimates provided by the various well-testing approaches could be better evaluated. These characterization efforts are briefly summarized in this chapter. Note that since the characterization activities are still ongoing, the data interpretation phase of this work has not yet been initiated. The use of these data to assess the scale dependence of hydraulic properties, etc. will be the subject of future work.

B. DRILLING AND SAMPLING ACTIVITIES

Drilling and Sampling Procedures

Prior to the period covered by this report, twenty five wells had been installed at GEMS. Samples from the sand and gravel interval (10.7-21.3 meters below land surface) were taken at six of these wells using various techniques (McElwee et al., 1991). A modified Waterloo sampler (Zapico, 1987; Zapico et al., 1987) was employed with good success when drilling mud was used in the auger flights to control heaving sands and to help prevent the sediment from falling out the bottom of the sampler. The use of drilling muds, however, has disadvantages (potential to contaminate the formation and the cores) and recovery without sample loss is difficult since the recovery procedure is very sensitive to vibration and other mechanical forces. Without the use of drilling muds, the modified Waterloo sampler performed unsatisfactorily due to a large percentage of the sediment falling out the bottom of the sampler. In order to address this limitation, new sampler designs were developed and field tested in the first year of this project. The most promising design (dubbed "the KGS Bladder Sampler") did not require drilling mud, achieved a very high recovery percentage, and was not very sensitive to vibration and other

mechanical forces during recovery. In addition to the piston used in the Waterloo sampler, the new design incorporates an inflatable bladder, located in the drive shoe, which closes off the end of the sampler (McElwee et al., 1991). In the initial phase of the sampling, the rubber bladder lies deflated behind a plastic sample liner as the core enters the sampler. Near the end of the 1.52 meter sample drive, an extension at the upper end of the piston triggers a release mechanism and allows a 0.102 meter retraction of the plastic liner, resulting in the bladder being in direct contact with the sediment. The bladder is then inflated from the surface with nitrogen gas, closing off the bottom of the sampler and allowing recovery with minimal opportunity for sediment to fall out. After recovery, the samples are taken to the laboratory for storage until analyses for hydraulic conductivity, porosity, density, and particle-size fraction, which are described in Section IV.C, can be performed.

All except one of the monitoring wells at GEMS have been installed with hollow-stem auger techniques (Hackett, 1987). Auger flights with an inside diameter of 0.083 meters and an outside diameter of 0.168 meters were used for all but four of the augered wells. For those four wells, large diameter flights (inside diameter of 0.165 m, outside diameter of 0.254 m) were employed. Note that the one well that was not augered (GEMS 06) was drilled into the bedrock underlying the sand and gravel interval using mud-rotary techniques. Table IV.B.1 provides details concerning the GEMS wells. Note that many of the listed wells (e.g., the multilevel sampling wells) were installed as part of work not associated with this project.

As described in Section I.A (see Figure I.2), the near-surface stratigraphy at GEMS consists of approximately 10.6 meters of clay and silt overlying approximately 10.6 meters of sand and gravel. If samples from the clay and silt interval are desired, a split-spoon sampler with an overshoot mechanism for attachment inside the auger flights is used. The split-spoon samplers are 0.61 meters in length and must be retrieved after every 0.61 meters of drilling. Retrieval is done using a wire line on the drill rig. Although we have taken continuous samples through the clay and silt interval at four locations at GEMS, our primary interest is in the sand and gravel interval.

One of the biggest problems faced in obtaining relatively undisturbed samples from highly permeable saturated sands and gravel deposits, such as found at GEMS, is heaving sands or sandblows (Minning, 1982; Perry and Hart, 1985; Keely and Boateng, 1987; and Hackett, 1987). It is absolutely essential to maintain greater hydrostatic pressure inside the auger flights than in the formation when working in heaving sands. The water level inside the auger flights is maintained higher than the

ambient water level by adding water at critical times (i.e. any time when tools are moved within the open flights or the open flights themselves are moved). If a greater hydrostatic head is not maintained within the auger flights at these critical times, up to one or more meters of sediment may quickly enter the flights, making it impossible to obtain an undisturbed sample at that depth. Adding water to maintain a higher head in the flights may affect the chemistry and biota of an aquifer, so one must balance this concern with the need to control heaving sands. At GEMS, we simply pump water from a nearby well in the sand and gravel interval into the flights. There is no known contamination at GEMS, so we are adding water of a similar composition to the flights. This procedure seems appropriate for our purposes.

Samples are obtained from the sand and gravel interval using the KGS Bladder Sampler (McElwee et al., 1991). If samples are not taken in the overlying clay and silt interval, we first drill down to approximately 10.7 meters. The pilot bit is withdrawn via a wireline and the sampler emplaced at the bottom of the flights. The sampler is then driven 1.52 meters in advance of the flights. The sampler is retrieved using drill rods or a wireline, after which the pilot bit is reinserted and the augers advanced to the depth for the next sample. Note that due to the close fit of the pilot bit and the sampler in the interior of the flights, there is great potential to induce heaving sands during removal of the pilot bit and retrieval of the sampler. Special care must be taken to add water to the flights during these procedures.

If no samples are to be obtained during drilling, a knock-out plate is installed in the auger head in place of a pilot bit (Perry and Hart, 1985; Hackett, 1987). The plate is left in place until the completion depth is achieved. At that point, the plate is knocked out of the bottom of the flights using the casing string. The plate is then left in the formation below the well. Stainless steel, PVC, and aluminum knock-out plates have been used at GEMS. Note that water must be added to the flights when the plate is knocked out in order to prevent movement of sediment into the interior of the flights and possible binding of the casing string in the flights.

Results of Drilling and Sampling

Eighteen wells were drilled at GEMS as part of this project. When added to previously drilled wells and those that were drilled during this same time period for other projects, the total number of pumping, monitoring, and multilevel sampling wells at GEMS is now 68. Table IV.B.1 provides a summary of pertinent information about the GEMS wells, while Figure IV.B.1 is a site map showing the location of all the wells. The elevation data given in Table IV.B.1 were obtained through a

cooperative surveying exercise with the 1st Battalion of the 127th Field Artillery of the Kansas National Guard performed in March of 1992, supplemented by later work by KGS personnel. Note that a reference point was established at a central location on the site during the cooperative exercise. This reference point was used in the following surveys at the site. The elevation as well as the longitude and latitude of the reference point are given in Table IV.B.1. Most of the wells that were drilled during this period were installed to document the hydraulic properties at different levels in the sand and gravel interval. Two of the wells (GEMS 0-8 and 0-9) were also drilled to assess the effect of screen type on well-test results. GEMS 0-9 is screened with continuous wire-wrap PVC screen, while GEMS 0-8 employs standard slotted PVC screen. However, the assessment of the effect of screen type was not completed prior to the end of this project.

Detailed samples of the sand and gravel interval were taken at eight of the eighteen wells drilled as part of this project. In all cases, the sampling techniques outlined above were employed. Table IV.B.2 summarizes the sample recovery for all holes drilled in the reporting period, including two (TMO-1 and TME-8) that were sampled as part of work not associated with this project. As shown in Table IV.B.2, the average recovery was 75.3%. Note that ten percent of the total sample length (0.152 m) is lost for each sample as a result of the length and placement of the bladder in the drive shoe (denoted as "Bladder Loss" on Table IV.B.2). An additional 14.7% of the total sample length was lost on average for each sample. This additional loss was a result of a number of factors. In several instances, we had problems with large rock fragments blocking the sampler throat. Mechanical problems also plagued us throughout the project. Several times the retraction mechanism failed so that the bladder could not be inflated. In one instance, this resulted in the complete loss of the sample (sample #1 of well 7-1). Since the sampler takes a great deal of punishment while being driven by a jackhammer, it appears that we must expect some mechanical failures.

The samples of silt and clay obtained from the upper 10.7 meters at GEMS using the split-spoon sampler were examined visually and detailed written logs of the visible features were prepared. However, no additional work was done with these samples as part of this project.

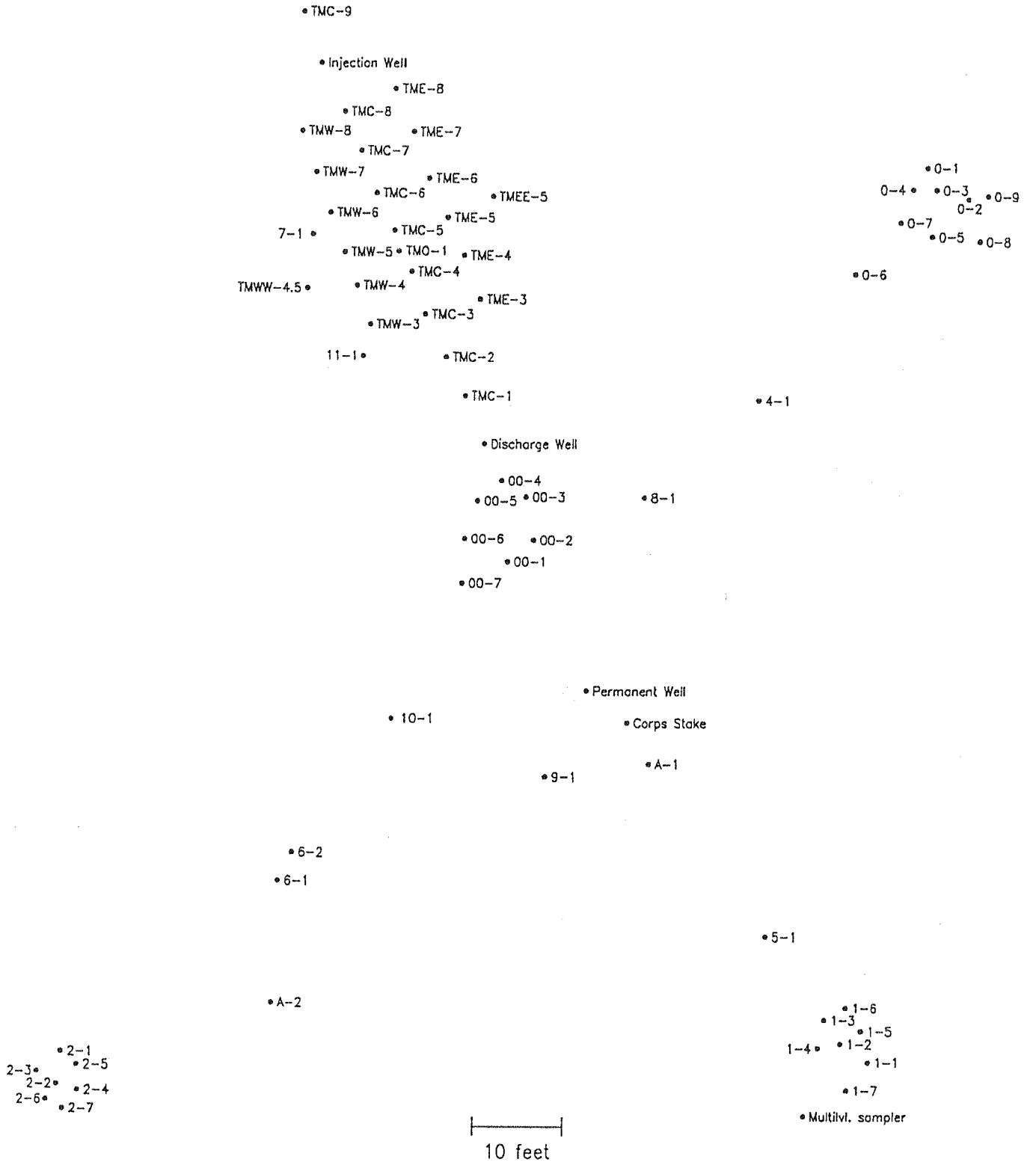

Figure IV.B.1 - GEMS well map.

Table IV.B.1

Well Data

Well Number	Elevation (m)	Depth (m/ft)	Screen Length (m/ft)
00-1	252.690	17.04/55.90	0.76/2.5
00-2	252.779	14.41/47.28	0.76/2.5
00-3	252.675	21.37/70.11	NA
00-4	252.660	11.18/36.68	NA
00-5	252.013	9.74/31.96	NA
00-6	252.753	12.91/42.36	NA
00-7	252.731	20.34/66.73	NA
0-1	252.811	21.74/71.32	9.14/30.0
0-2	252.762	14.08/46.19	0.70/2.3
0-3	252.845	11.00/36.09	0.74/2.4
0-4	252.772	7.94/26.05	0.76/2.5
0-5	252.799	19.84/65.09	0.70/2.3
*0-6**	252.854	24.66/80.90	1.52/5.0
0-7	252.801	16.57/54.63	0.70/2.3
*0-8#	253.178	18.52/60.76	0.76/2.5
*0-9#	253.116	17.29/56.74	0.76/2.5
1-1	252.805	14.26/46.78	0.76/2.5
1-2	252.724	11.22/36.81	0.61/2.0
1-3	252.808	8.55/28.05	0.65/2.1
1-4	252.813	6.15/20.18	1.45/4.75
1-5	252.802	20.33/66.70	9.14/30.0
1-6	252.916	17.06/55.97	0.73/2.4
1-7	252.725	21.42/70.28	9.14/30.0
2-1	252.807	11.92/39.11	0.57/1.9
2-2	252.804	14.72/48.29	0.56/1.8
2-3	252.803	8.53/27.98	0.63/2.1
2-4	252.812	6.04/19.82	1.41/4.6
2-5	252.807	21.42/70.28	9.14/30.0
2-6	252.761	20.24/66.40	9.14/30.0
2-7	252.741	17.17/56.33	0.79/2.6
4-1	252.740	21.58/70.80	9.14/30.0
5-1	252.818	21.54/70.67	9.14/30.0
6-1	252.747	20.34/66.73	0.77/2.5
6-2	252.765	21.55/70.70	11.6/38.0
7-1	252.480	17.74/58.20	9.14/30.0
8-1	252.701	17.44/57.22	NA
9-1	252.556	20.93/68.67	13.26/43.5
10-1	253.166	17.32/56.82	NA
11-1	252.453	19.63/64.40	13.72/45.0
A1	252.447	9.91/32.51	0.76/2.5
A2	252.775	7.86/25.79	0.61/2.0

+PW	NA	21.84/71.65	6.10/20.0
Multilvl. sampler	252.277	11.58/38.00	ps2
*Discharge well#	252.724	21.53/70.64	10.52/34.5
*Injection well#	252.873	21.67/71.09	10.36/34.0
TMC-1	252.584	11.58/38.00	ps2
TMC-2	252.608	16.15/53.00	ps1
TMC-3	252.682	11.58/38.00	ps2
TMC-4	252.803	16.15/53.00	ps1
TMC-5	252.711	11.58/38.00	ps2
TMC-6	252.614	16.15/53.00	ps1
TMC-7	253.016	11.58/38.00	ps2
TMC-8	252.759	16.15/53.00	ps1
TMC-9	252.663	11.58/38.00	ps2
TMO-1	252.686	20.33/66.71	###
TME-3	252.560	11.58/38.00	ps2
TME-4	252.673	11.58/38.00	ps2
TME-5	252.637	11.58/38.00	ps2
TME-6	252.639	11.58/38.00	ps2
TME-7	252.618	11.58/38.00	ps2
TME-8	252.480	11.58/38.00	ps2
TMEE-5	252.590	11.58/38.00	ps2
TMW-3	252.843	11.58/38.00	ps2
TMW-4	252.728	11.58/38.00	ps2
TMW-5	252.746	11.58/38.00	ps2
TMW-6	252.623	11.58/38.00	ps2
TMW-7	252.766	11.58/38.00	ps2
TMW-8	252.580	11.58/38.00	ps2
TMWW-4.5	252.535	11.58/38.00	ps2

KGS Reference Mark (Corps. Stake): Latitude-North 39°00' 55.628" ,
Longitude-West 95°12' 21.272" , Elevation 252.242 m

* - All well diameters are 0.051m (2 in.); except for wells PW (0.254 m/10 in.), Discharge (0.127m/5 in.), Injection (0.127 m/5 in.), 0-6 (0.127 m/5 in.), 0-8 (0.102 m/4 in.), and 0-9 (0.102 m/4 in.) which have the denoted diameters.
** - well drilled using mud rotary techique
# - well drilled with large diameter auger flights
- Well TMO-1 has 0.61 m (2.0 ft.) of screen at the bottom of the well and 0.61 m (2.0 ft.) of screen starting at 2.6 m (8.5 ft.) from the bottom of the casing and extending up.
+PW - High capacity pumping well with 0.254 m (10 in.) screen and casing diameter and 0.102 m (4 in.) drop pipe diameter.
NA - Information not currently available.
ps1 - Detailed sampler port spacing = 0.305 m (1.0 ft) between ports, except 0.610 m (2.0 ft) between ports 9 and 10
ps2 - Regular sampler port spacing = 0.610 m (2.0 ft) between ports.

Note: All multilevel sampler well depths were measured from top of casing to the first port.

Table IV.B. 2

Sample Recovery Analysis

Well Number	Sample Number	Sample Length (m/ft)	Head Space (m/ft)	% of Sample Length
Procedure: Hydraulic Jackhammer				
00-1	19	1.52/5.00	0.061/0.20	4.00
00-1	20	1.52/5.00	0.088/0.29	5.80
00-1	21	1.52/5.00	0.11/0.35	7.00
00-1	22	1.42/4.67	0.88/2.88	61.67
00-1	23	1.52/5.00	0.40/1.32	26.40
00-1	24	1.52/5.00	0.064/0.21	4.20
00-1	25	1.22/4.00	0.21/0.68	17.00
00-1 Totals		10.26/33.67	1.81/5.93	17.61
		Theoretical Recovery		82.39
		Bladder Loss		10.00
		Actual Recovery		72.39
Procedure: Hydraulic Hammer				
1-7	20	1.486/4.875	0.098/0.32	6.56
1-7	21	1.473/4.833	0.12/0.38	7.86
1-7	22	1.52/5.00	0.098/0.32	6.40
1-7	23	1.52/5.00	0.10/0.33	6.60
1-7	24	1.52/5.00	0.12/0.40	8.00
1-7	25	1.52/5.00	1.32/4.33	86.60
1-7	26	1.52/5.00	0.15/0.50	10.00
1-7	27	1.52/5.00	0.41/1.34	26.80
1-7 Totals		12.106/39.708	2.41/7.92	19.94
		Theoretical Recovery		80.06
		Bladder Loss		10.00
		Actual Recovery		70.06
Procedure: Electric Jackhammer				
8-1	20	1.31/4.30	0.14/0.46	10.70
8-1	21	1.52/5.00	0.18/0.60	12.00
8-1	22	1.54/5.05	0.16/0.53	10.50
8-1	23	1.52/5.00	0.11/0.36	7.20
8-1	24	1.54/5.05	0.25/0.81	16.04
8-1	25	1.52/5.00	0.16/0.52	10.40
8-1	26	1.52/5.00	0.30/0.98	19.60
8-1 Totals		10.49/34.40	1.30/4.26	12.38
		Theoretical Recovery		87.62
		Bladder Loss		10.00
		Actual Recovery		77.62

Procedure: Pneumatic Jackhammer				
10-1	19	1.52/5.00	0.064/0.21	4.20
10-1	20	1.54/5.05	0.052/0.17	3.37
10-1	21	Numbering Omission		
10-1	22	1.55/5.10	0.073/0.24	4.70
10-1	23	1.52/5.00	0.14/0.46	9.20
10-1	24	1.51/4.95	0.070/0.23	4.65
10-1	25	1.51/4.95	0.14/0.46	9.29
10-1	26	1.51/4.95	0.24/0.79	15.96
10-1 Totals		10.67/35.00	0.78/2.56	7.31
		Theoretical Recovery		92.69
		Bladder Loss		10.00
		Actual Recovery		82.69
Procedure: Pneumatic Jackhammer				
5-1	1	1.52/5.00	0.088/0.29	5.80
5-1	2	1.52/5.00	0.14/0.45	9.00
5-1	3	1.52/5.00	0.076/0.25	5.00
5-1	4	1.52/5.00	0.11/0.35	7.00
5-1	5	1.52/5.00	0.17/0.56	11.20
5-1	6	1.52/5.00	0.47/1.55	31.00
5-1	7	1.38/4.54	0.16/0.54	12.00
5-1 Totals		10.53/34.54	1.22/3.99	11.60
		Theoretical Recovery		88.40
		Bladder Loss		10.00
		Actual Recovery		78.40
Procedure: Pneumatic Jackhammer				
7-1	1*	1.52/5.00	1.37/4.50	90.00
7-1	2	1.52/5.00	0.16/0.53	10.60
7-1	3	1.52/5.00	0.24/0.78	15.60
7-1	4	1.52/5.00	0.31/1.02	20.40
7-1	5	1.52/5.00	0.23/0.75	15.00
7-1	6	1.52/5.00	0.30/1.00	20.00
7-1	7	0.91/3.00	0.016/0.54	18.00
7-1 Totals		10.06/33.00	2.77/9.10	27.60
		Theoretical Recovery		72.40
		Bladder Loss		10.00
		Actual Recovery		62.40

Procedure: Pneumatic Jackhammer				
9-1	1	1.52/5.00	0.11/0.35	7.00
9-1	2	1.52/5.00	0.082/0.27	5.40
9-1	3*	1.45/4.75	0.51/1.67	35.20
9-1	4	1.52/5.00	0.088/0.29	5.80
9-1	5*	1.47/4.83	0.15/0.49	10.10
9-1	6	1.52/5.00	0.23/0.76	15.20
9-1	7	1.31/4.29	0.41/1.34	31.20
9-1 Totals		10.33/33.87	1.58/5.17	15.30
		Theoretical Recovery		84.70
		Bladder Loss		10.00
		Actual Recovery		74.70
Procedure: Pneumatic Jackhammer				
11-1	1	1.52/5.00	0.58/1.90	38.00
11-1	2	1.52/5.00	0.13/0.44	8.80
11-1	3	1.52/5.00	0.12/0.41	8.20
11-1	4	1.52/5.00	0.23/0.77	15.40
11-1	5	1.52/5.00	0.21/0.69	13.80
11-1	6	1.52/5.00	0.55/1.81	36.20
11-1	7	1.02/3.35	0.19/0.62	18.50
11-1 Totals		10.17/33.35	2.02/6.64	19.90
		Theoretical Recovery		80.10
		Bladder Loss		10.00
		Actual Recovery		70.10
Procedure: Pneumatic Jackhammer				
TMO-1	1	1.52/5.00	0.29/0.95	19.00
TMO-1	2	1.52/5.00	0.043/0.14	2.80
TMO-1	3	1.52/5.00	0.034/0.11	2.20
TMO-1	4	1.52/5.00	0.18/0.58	11.60
TMO-1	5	1.52/5.00	0.085/0.28	5.60
TMO-1	6	1.52/5.00	0.076/0.25**	5.00
TMO-1	7	1.30/4.27	0.13/0.42	9.84
TMO-1 Totals		10.45/34.27	0.83/2.73	7.97
		Theoretical Recovery		92.03
		Bladder Loss		10.00
		Actual Recovery		82.03

Procedure: Pneumatic Jackhammer				
TME-8	1	1.48/4.85	0.39/1.29	26.60
TME-8	2	1.52/5.00	0.061/0.20	4.00
TME-8	3	No sample was retrieved from the sampler		
TME-8	4	1.52/5.00	0.091/0.30	6.00
TME-8	5	1.52/5.00	0.067/0.22	4.40
TME-8	6	1.52/5.00	0.00	0.00
TME-8	7	1.52/5.00	0.064/0.21	1.75
TME-8 Totals		9.10/29.85	0.61/2.00	6.70
		Theoretical Recovery		93.30
		Bladder Loss		10.00
		Actual Recovery		83.30
Project Totals		104.16/341.66	15.34/50.30	14.72
		Theoretical Recovery		85.28
		Bladder Loss***		10.00
		Actual Recovery		75.28

* Mechanical failure produced some anomalous results.

** Head space was measured in laboratory as opposed to the field.

*** Bladder Loss - 10% of the total possible recovery, 10.42 m (34.17 ft), is lost due to the bladder mounting dimensions.

C. LABORATORY ACTIVITIES

Introduction

The samples recovered from the drilling and sampling summarized in Section IV.B were taken to the laboratory for analysis. Samples were refrigerated while awaiting processing to minimize bacterial growth and evaporation. With the exception of the changes noted below, the procedures and methods used in analyzing the core samples were essentially the same as those described in Butler et al. (1991) and Jiang (1991).

Laboratory Improvements

A new apparatus was developed to more accurately and efficiently calibrate the pressure transducers used in the permeameter. The calibration apparatus consists of metal pipe into which pressure transducers can be inserted with an air-tight seal, a rubber bladder to increase the volume of gas within the system, and a high-accuracy pressure transducer (Druck PTX 620 pressure transmitter) to serve as a pressure standard. Nitrogen gas can be introduced into or released from the system in small amounts, simultaneously changing the pressure on both the pressure transducers and the pressure standard, while readings are recorded by a datalogger. The pressure transducers are then calibrated against the pressure standard. This system can be used to calibrate both the pressure transducers used in the permeameter (0-5 psig) and the pressure transducers used in the field for hydraulic testing (0-5 to 0-30 psig). Up to four pressure transducers can be calibrated at one time.

The constant-head permeameter used in this work was originally designed to process four cores at one time. The permeameter has now been expanded to process eight cores at once. Most parts of the permeameter that had been composed of opaque PVC have been replaced with clear PVC in order to more easily observe flow of water, transport of fine sediment, and entrapment of air bubbles within the system. The single filter that had been used in the permeameter recirculation tubing has now been replaced by a double-filter system. Water first flows through a 5 micron filter to remove most sediment particles and other debris, after which it passes through a 0.5 micron filter that should remove bacteria and virtually all sediment particles.

A temperature transmitter (Dwyer Series 650-2) has been installed next to the mercury thermometer in the permeameter. Water temperature is recorded by the datalogger at the same interval as water pressure in the outflow tubes of the permeameter. This enables a more accurate representation of the temporal variation in viscosity to be incorporated into the hydraulic conductivity calculations.

In order to more accurately determine the head drop across the cores, an

instrument incorporating a dial caliper has been constructed and mounted on the permeameter. Water levels in glass-topped manometer tubes, which measure head at the top of each core and at the constant head boundary, can be read to the nearest 0.025 mm (readings are generally reproducible to better than 0.13 mm). This device allows use of smaller head drops across the cores without increasing the percent error in the conductivity estimates.

Occasionally, a decrease in head at the constant head boundary occurs due to lack of flow from the upper reservoir. To reduce the frequency of this occurrence, a new reservoir was installed that drains from the bottom rather than relying on a siphon tube exiting from the reservoir top.

Laboratory Procedures and Methods

X-rays are taken of each core sample to aid in the identification of sedimentological features (e.g., changes in grain size, sedimentary structures, etc.). An aluminum filter is employed to improve resolution at the edges of the core (Baker and Friedman, 1969). Using the X-rays as a guide, the sample is cut into segments that are as homogeneous as possible within the 0.1-0.2 meter limit on segment size imposed by the permeameter setup. To inhibit organic growth, the core segments are wrapped in plastic and aluminum foil, and refrigerated until they are placed in the permeameter.

In order to keep the Reynolds number small and reduce the possibility of non-Darcian flow, the head drop over the cores is kept as small as possible. This also decreases the entrainment of fine material as water moves through the core. Typically, the head drop is initially set at approximately 0.013 meters and increased only if no flow occurs after 12 to 24 hours. With this small head drop, it takes a minimum of 36 hours to process a core segment, with some segments requiring four to five days.

During the drying process that precedes particle density analysis and dry sieving, clay-sized particles tend to coat larger grains and form sand-sized aggregates. This will cause the weight percentages of the larger grain sizes to be overestimated at the expense of the fines. To more accurately determine the weight percent of fine material in the core, the samples are wet-sieved with a 53 micron sieve after the particle density analysis. The weight percent of fine material is determined by comparing the dry weight of the sample before and after wet sieving. The coarse fraction is then dry-sieved to complete the grain size analysis.

No photographs are taken of the sediment before sieving.

Water Chemistry Investigations

We have observed that the laboratory-determined hydraulic conductivity estimates follow a characteristic pattern: the conductivity estimate increases (as the core nears saturation), reaches a maximum, and then decreases as the residence time of the sample in the permeameter increases. An example of this phenomenon for one typical core segment is illustrated in Figure IV.C.1. Possible explanations for the decrease in conductivity at large times include biological growth, movement of fines, and mineral deposition. Employing a biocide and as low a flow rate through the core as practical should reduce the influence of the first two factors. Calcite deposits have been observed on the plastic tubing, thermometer, and temperature transmitter of the permeameter, so a geochemical-equilibrium model, PHREEQE (Parkhurst et al., 1980), was run to determine the nature and amount of mineral material that might be deposited during the permeameter experiments. As discussed in a later subsection, the results of the simulation indicated that the decrease in hydraulic conductivity with time could be a result of the deposition of calcite in pore throats. However, another possible explanation would be the expansion and/or dispersion of clays, which would also produce a clogging of pore throats. In an attempt to identify the primary mechanism responsible for the observed decreases in conductivity with time, a series of experiments were conducted using a single core in the permeameter. The chemistry of the water prior to passage through the core and after passage through the core was carefully monitored with the assistance of the Analytical Services Section of the Kansas Geological Survey.

The water used in the permeameter was obtained from wells at GEMS that are screened close to or over the same interval from which the core was taken. At the same time water was collected for use in the permeameter experiments, samples were taken in the field for analysis by the Analytical Services Section. The collected water was then transported to the laboratory where it was allowed to sit for two weeks in order to equilibrate with laboratory temperatures and pressures. Additional samples were taken during this period in order to assess changes occurring as the water equilibrated with laboratory conditions. Once the water was placed in the permeameter, samples were taken several times a day from the water that had passed through the core (henceforth designated as outflow-tube water) and once a day from the permeameter water that had not passed through the core (henceforth designated as permeameter water). A subset of these samples was chosen for major cation analysis by the Analytical Services Section using observed changes in hydraulic conductivity as the selection criterion. Note that the permeameter setup is normally run in a recirculating mode, i.e. the water that passes through the cores is circulated back through the apparatus. For these experiments,

however, no recirculation was allowed. This enabled any chemistry changes occurring in the water passing through a core to be readily identified and not be masked by mixing.

In addition to the major cation analyses performed by the Analytical Services Section, the pH and dissolved oxygen of the permeameter and outflow-tube waters were monitored in the laboratory. The pH was determined using a CARDY Twin pH meter (Horiba Instruments). Measurement of the pH of the outflow-tube water was done several times a day, while measurement of the pH of the permeameter water was done at least once a day. Dissolved oxygen (DO) was measured using a K-7512 CHEMets colorimetric kit (CHEMetrics). DO was determined for outflow-tube water once a day and once every 3 to 4 days for the permeameter water.

Sediment samples from the cores used in these experiments were collected for x-ray analysis of clay mineralogy both before and after being processed in the permeameter.

Results and Discussion

Core Analyses

Values for original and repacked hydraulic conductivity, original and repacked porosity, the mean grain size (in phi units), and the percent fines (<53 microns) were estimated for each core segment (approximately 450 core samples were analyzed). Figures IV.C.2 - IV.C.8 present plots of these quantities versus depth for GEMS 00-1. The relationships displayed on these plots are fairly typical of those observed at all of the wells sampled at GEMS. Table IV.C.1 summarizes the results of the laboratory core analyses for all holes sampled during the period of this project. Note that this table includes results from two wells (TMO and TME-8) that were sampled as part of work not associated with this project.

As shown on Figure IV.C.4 and Table IV.C.1, the repacked hydraulic conductivity was greater than the original conductivity estimate for most samples. This is most likely due to the repacking process eliminating thin layers of fine material that may be exerting a strong influence on the original conductivity estimates. The redistribution of this fine material during the repacking process results in the repacked cores generally being more homogeneous than the original cores. In some cases, it is possible that the repacked cores could be less homogeneous than the original cores. Layers can be created within the core if a poorly sorted sediment is not sufficiently mixed while being repacked into the sample tube. For example, a one-centimeter layer of fine material was noted at the top of the repacked sample 00-1, 24, 7 (depth 20.37-

20.56 m). In the later portions of the project, a sediment sample splitter was used to produce numerous small, homogeneous samples for repacking in an attempt to eliminate this problem. This approach, however, did not appear to make a significant difference in the analysis results.

The porosity of the repacked samples tended to be slightly higher than that of the original cores. Possible reasons for this difference could be an inability to repack the cores to exactly the same volume as the original cores, and loss of sediment during the repacking process. In most cases, however, the difference was quite small.

PHREEQE Simulation of Water Chemistry

A geochemical-equilibrium model, PHREEQE (Parkhurst et al., 1980), was used to investigate the nature and amount of material that might be deposited while a sample was in the permeameter. The water in the permeameter is taken from the same site and interval from which the cores are taken to ensure as much as possible that the water will be in chemical equilibrium with the cores during the permeameter experiments. However, the water does experience some changes before it is used in the permeameter. The changes include increases in temperature, decreases in partial pressure of PCO2, and effects arising from addition of the biocide Thymol. These changes may cause the water to precipitate mineral material in order to regain equilibrium. Chemical analyses of water samples from GEMS are available from the fall of 1990 and the summer of 1991. Two of these samples are from the same depth from which water for the permeameter is collected. Both samples have similar chemical characteristics.

The PHREEQE simulation was performed by first creating a solution matching the temperature, pH and chemical composition of the two GEMS water samples. Alkalinity was input as HCO3-, aqueous nitrogen gas was removed from the data base, and the pe was set at 9.0. The pe and pH were allowed to be determined by the reaction. The most abundant constituents of the coarse fraction in the cores are quartz and K-feldspar, so the saturation indices of quartz and microcline were adjusted to match the silica and potassium contents of the water samples. This resulted in the solution being slightly oversaturated with respect to quartz and undersaturated with respect to microcline. The solution was then equilibrated with laboratory temperatures (22 degrees C) and the surface partial pressure of PCO2 (log PCO2 = -3.5). Thymol was added as a reaction to the computer simulated solution, and the solution was equilibrated with calcite to determine the amount of calcium carbonate that might be deposited.

The changes in alkalinity, pH, and pe that take place in the water according to the PHREEQE simulation are shown in Figure IV.C.9. The changes in the saturation index (log IAP/KT) of calcite are shown in Figure IV.C.10. The simulation shows that when well water is equilibrated with surface temperatures and pressures, calcite should precipitate. Calculations indicate that 38 liters of GEMS well water (approximately the amount used in the permeameter at one time) precipitate 3.56 cm^3 of calcite. What is not presently known is the kinetics of the reaction. PHREEQE assumes all reactions reach equilibrium instantaneously. It is unclear how much of the calcite precipitates during the time the water is left to equilibrate with laboratory conditions (two weeks minimum) and how much is deposited in the cores and on the permeameter. Observation of the gradual buildup of a calcite film on permeameter tubing indicates that some deposition is occurring throughout the period during which a single 38-liter supply of water is being used in the permeameter. It is likely that a similar film is being deposited in the cores themselves.

Insight into the impact of the deposition of 3.56 cm^3 of calcite on the conductivity estimates can be obtained by calculating the volume of the pore space of the cores used in the permeameter. Using values representative of the cores at GEMS (core volume = 47.5 cm^3, porosity = 30%), the pore volume of a typical core at GEMS is calculated to be 14.25 cm^3. Assuming that approximately 32 cores are processed per each 38 liters of water employed in the permeameter, the total pore volume of the processed cores is 456 cm^3. If the deposited calcite can be considered to be equally distributed over the 32 cores, the total amount of deposition amounts to 0.8% of the pore volume. Given that a very small amount of deposition in the pore throats can have a considerable impact on the permeability of the core, it appears that calcite deposition could be responsible for the observed decreases with time. Note that the observed deposition of calcite in the permeameter tubing is ignored in the above calculations because of the much greater surface area of the cores. Clearly, further work needs to be done on the kinetics of this reaction before the role of calcite deposition can be clarified. In an attempt to get a better idea of the importance of calcite deposition, the series of single-core permeameter experiments described earlier were performed. The results of those experiments are described in the following subsection.

Chemistry Analyses

The pH of GEMS water measured in the field is approximately 7. Monitoring of the pH of water collected for use in the permeameter did not reveal any trend while the water equilibrated to laboratory conditions over a 19 day period. After the water

was introduced into the permeameter, the pH rose fairly rapidly to approximately 8 and fluctuated between 8 and 9 (with no apparent trend in time) while circulating through the permeameter (Figure IV.C.11). There was no significant change in pH after the water had passed through the cores, the measured differences are within the limit of accuracy of the pH meter. The rise in pH when the water started circulating through the permeameter was thought to be most likely due to the loss of CO_2. Therefore, CO_2 gas was bubbled through the upper reservoir in an attempt to maintain the pH at a level comparable to that of the water at GEMS. This procedure has proven to be quite successful in maintaining the permeameter water at a pH close to 7.

Dissolved oxygen (DO) measurements indicate that the oxygen content of the water increases after the water is placed in the permeameter. Before the water is placed in the permeameter, it has a DO content of 1 to 2 ppm (very little change occurs over the 19-day equilibration period). After the water has been placed in the permeameter, the DO content increases to 5 to 8 ppm. There is no significant change in DO content after the water has passed through a core.

Major cation analyses of the water in the permeameter and outflow-tube for the three cores employed in these experiments indicate that the calcium content of the water generally decreases with time (Figure IV.C.12), further demonstrating that precipitation of calcite is occurring within the permeameter apparatus.

The first core placed in the apparatus (GEMS 9-1, sample #1, segment #1) shows a consistently lower calcium content in the outflow-tube water as compared to that in the permeameter (the accuracy of the chemical analysis is better than 1 ppm for calcium). This indicates that calcite is being precipitated in the core and perhaps contributing to a decrease in hydraulic conductivity. The pH rose at the beginning of the period that this core was in the permeameter and the calcium content of the permeameter water remained fairly high.

GEMS 11-1, sample #5, segment #3 was the next core placed in the permeameter. During the period of time that water was flowing through this core the calcium content of the water decreased. No conclusions concerning the relative calcium content of the outflow tube and permeameter water can be made. Only three analyses of the permeameter water were done, with one having a higher calcium content than the outflow-tube water, one having a lower calcium content, and a third sample (marked by a star) that is probably not representative of the system because circulation had been very slow for some time.

The third core placed in the permeameter for this experiment was GEMS 11-1, sample #3, segment #3. The outflow-tube water from this core had a calcium content

consistently higher than that of the permeameter water, suggesting that calcite was being dissolved out of a portion of the core. However, the hydraulic conductivity of this core decreased with time, which indicates that deposition of calcite may not be the controlling mechanism in reducing hydraulic conductivity during this time period.

X-ray analyses of the clays have determined that the clays are composed primarily of smectite, with some kaolinite and some illite (which is fairly crystalline, bordering on mica). There is no change in the composition of the clays while they are in the permeameter, but there was some deposition of calcite on the clays.

During preparation of the clays for x-ray analysis, it was noted that the clays are easily flocculated and dispersed, and that thymol, which had been used in the system as a biocide, caused the clays to flocculate. This tendency to readily flocculate and disperse could result in the clogging of pore throats and decreases in hydraulic conductivity. Fogler and Vaidya (1993) suggested that if the hydraulic conductivity of a core was reduced due to fines blocking the pore throats, reversing the flow direction through the core should flush out the clogged pore throats and produce an increase in hydraulic conductivity. GEMS 7-1, sample #4, segment #3, which experienced a decrease in hydraulic conductivity, was turned upside down in the permeameter. However, no increase in conductivity was observed.

Since thymol appeared to be causing the clays to flocculate, it was replaced by a different biocide, dichlorophene. This appears to have reduced, but not eliminated, the decreases in hydraulic conductivity with time. Whether this is due to more effective biocidal action in the core (though it appears to be less effective in the permeameter tubing), or due to the fact that the dichlorophene is not reacting with the clays is unclear at this time.

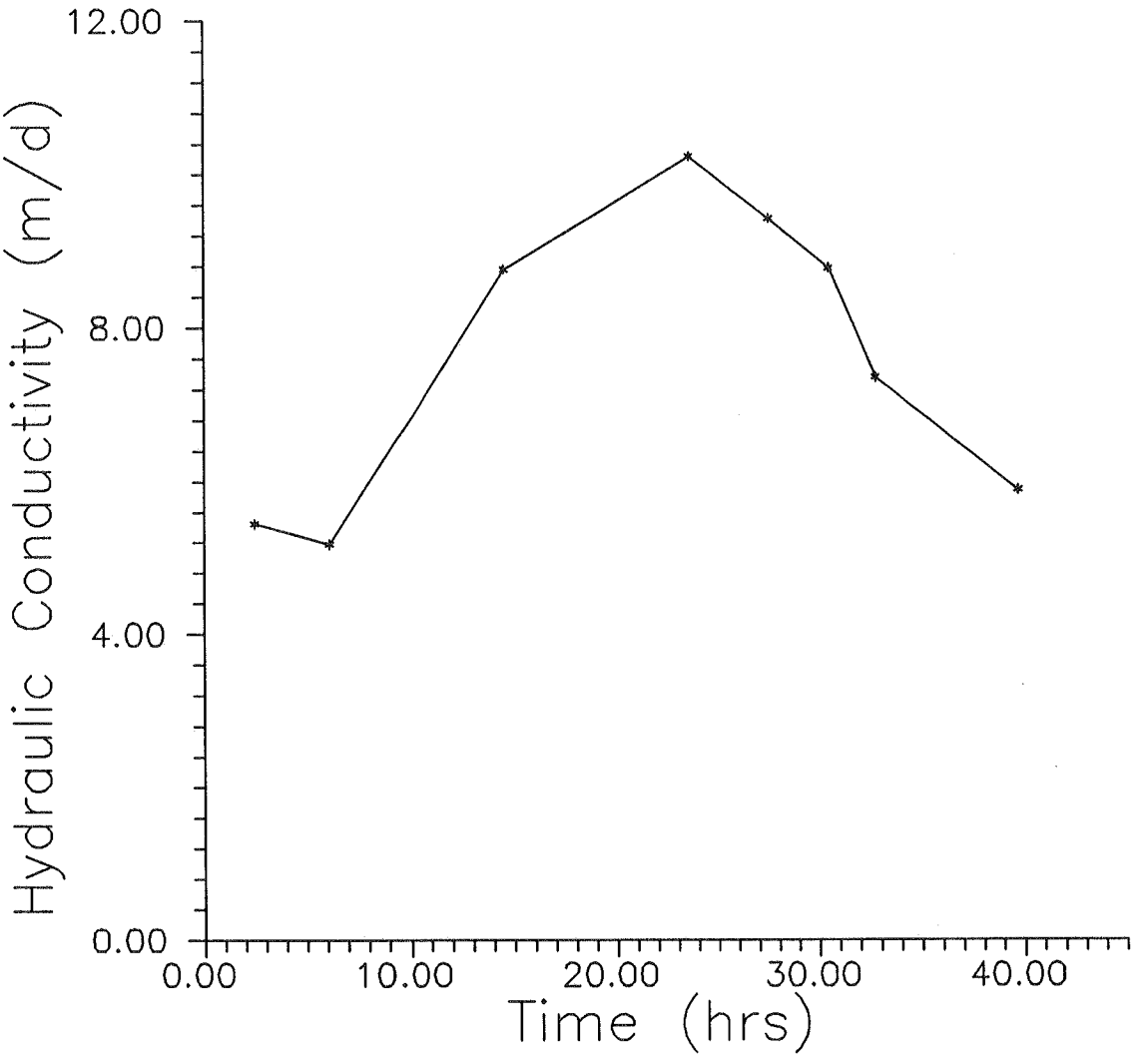

Figure IV.C.1 - Hydraulic conductivity versus time plot for sample 24 of core segment 5 of GEMS well 00-1.

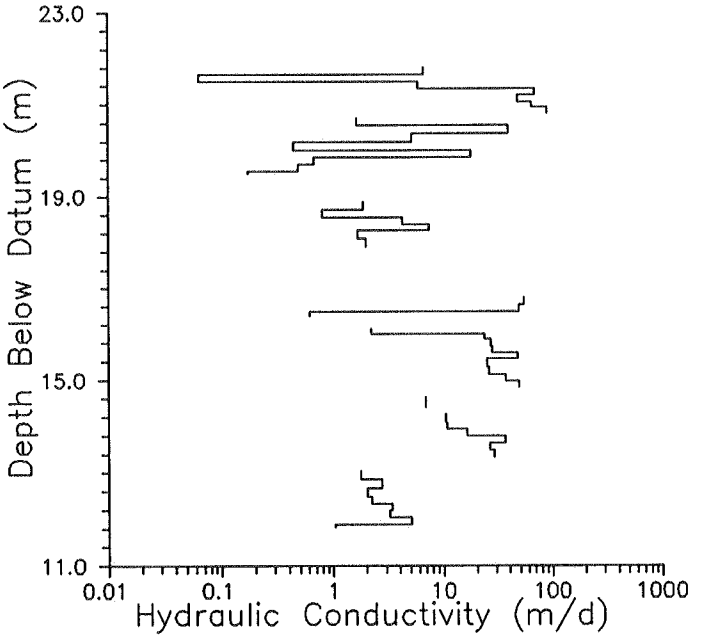

Figure IV.C.2 - Original hydraulic conductivity vs. depth for GEMS well 00-1.

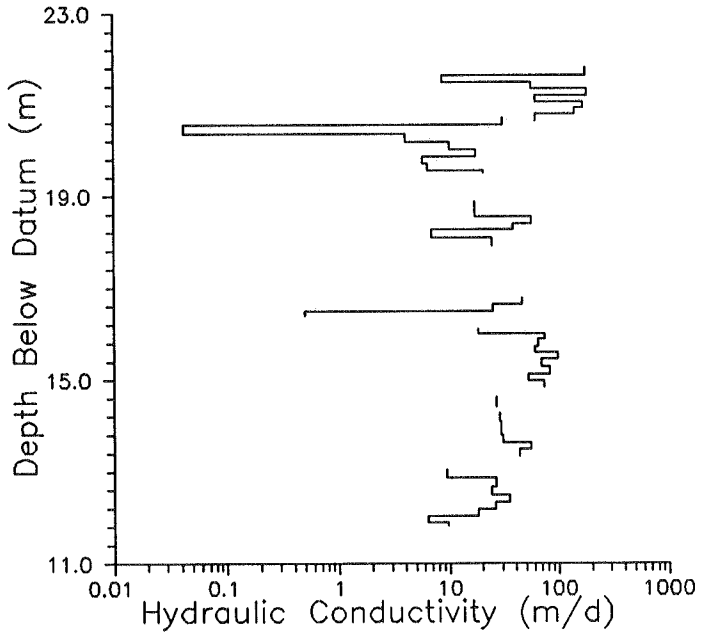

Figure IV.C.3 - Repacked hydraulic conductivity vs. depth for GEMS well 00-1.

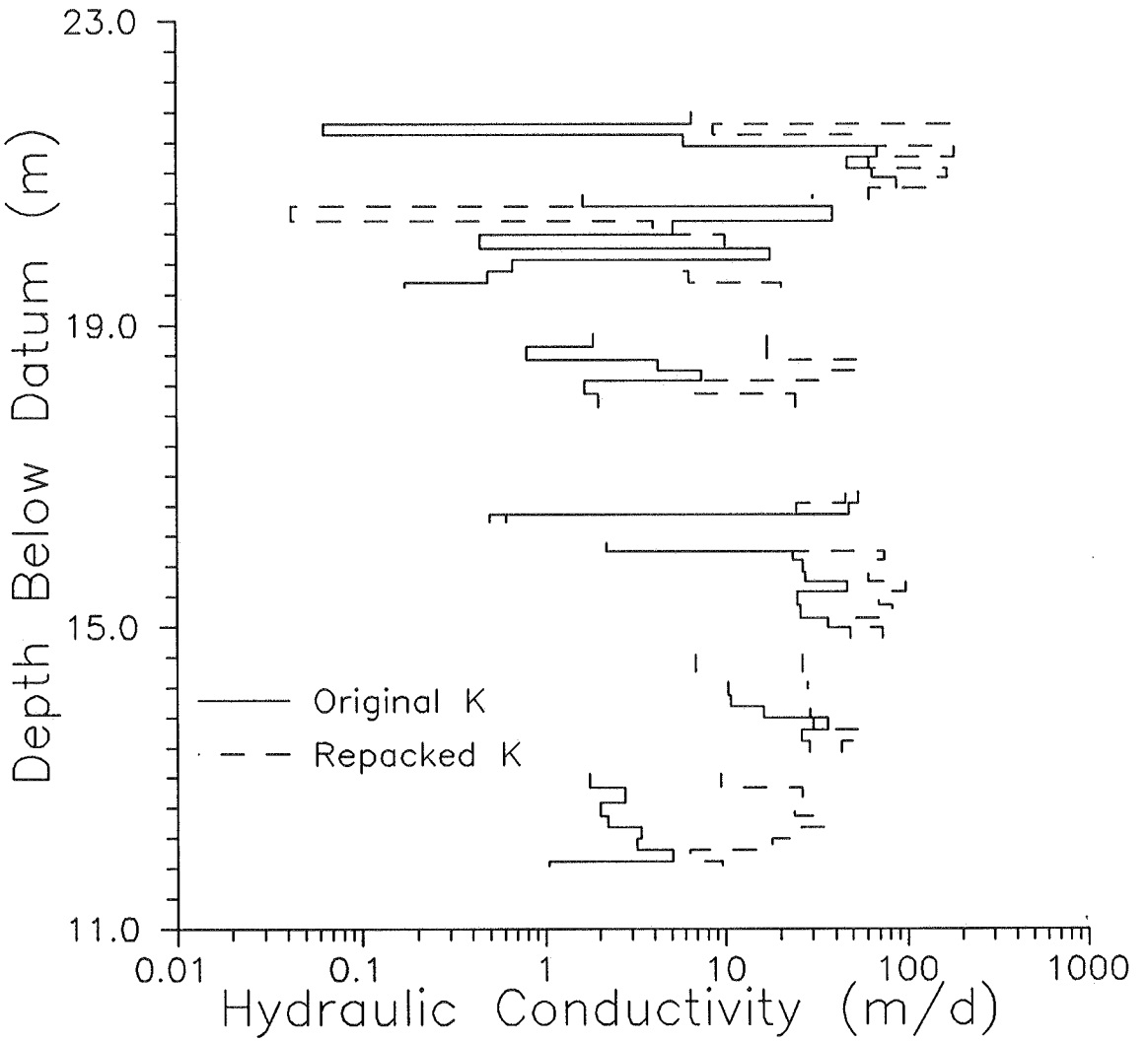

Figure IV.C.4 - Original and repacked conductivity vs. depth for GEMS well 00-1.

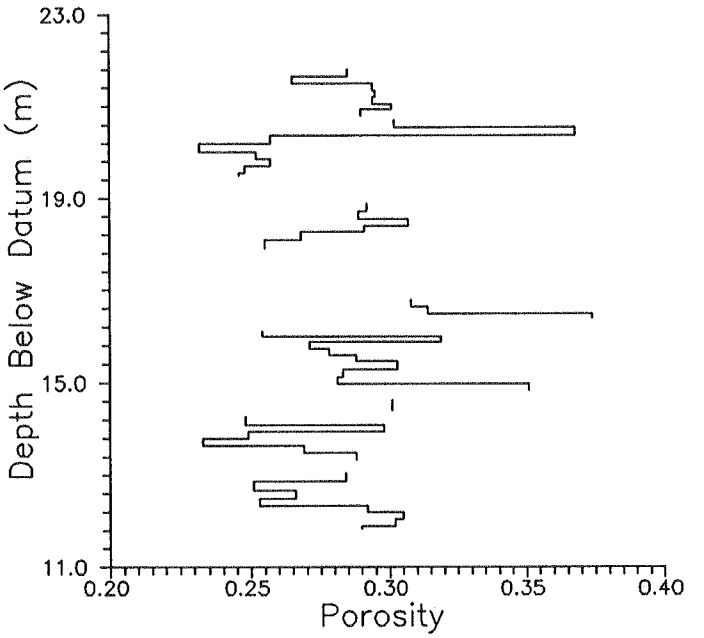

Figure IV.C.5 - Original porosity vs. depth for GEMS well 00-1.

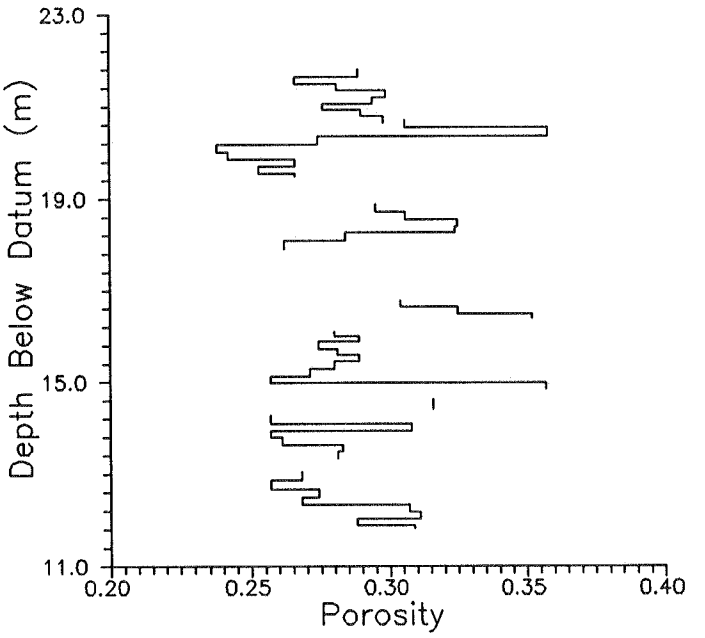

Figure IV.C.6 - Repacked porosity vs. depth for GEMS well 00-1.

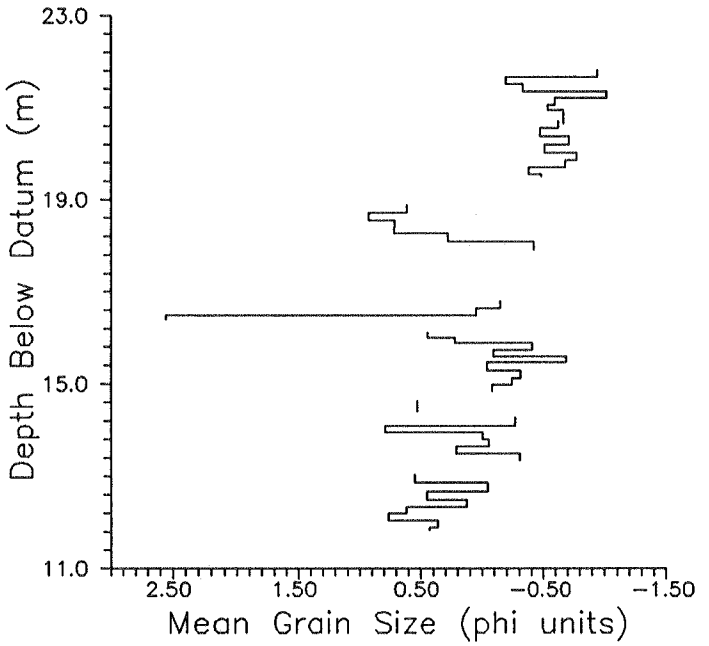

Figure IV.C.7 - Mean grain size (in phi units) vs. depth for GEMS well 00-1.

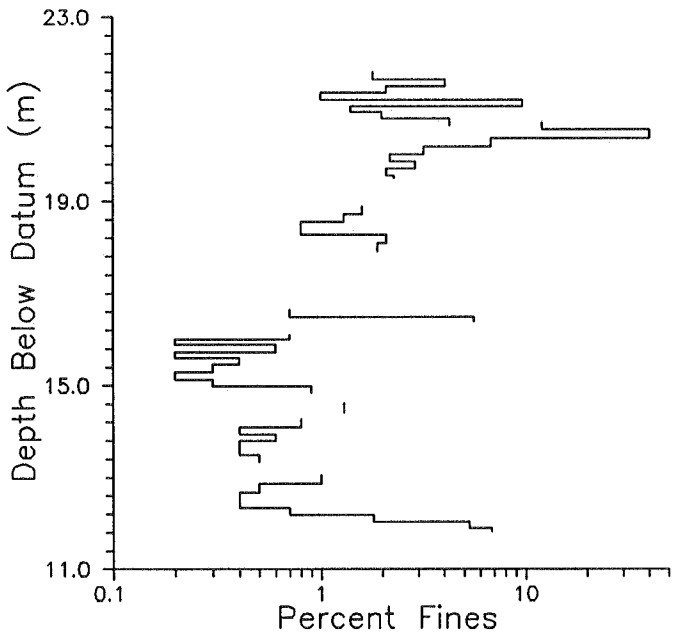

Figure IV.C.8 - Percent fines (<.053 mm) vs. depth for GEMS well 00-1.

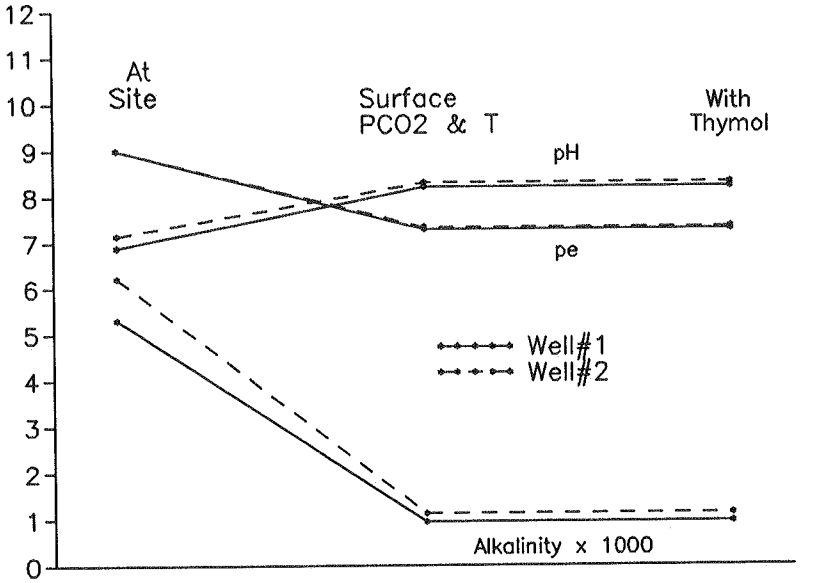

Figure IV.C.9 - Changes in alkalinity, pH, and pe.

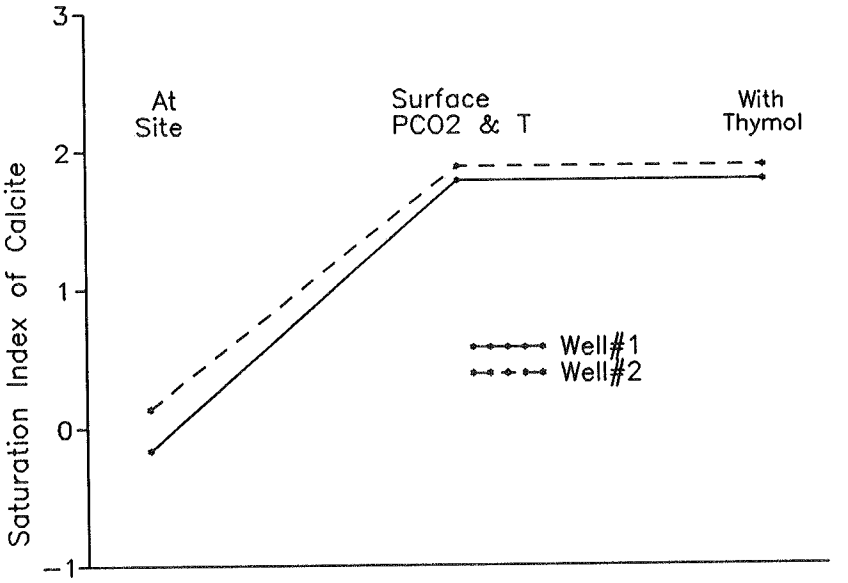

Figure IV.C.10 - Changes in the saturation index (SI) of calcite (SI = log ion activity product/equilibrium constant).

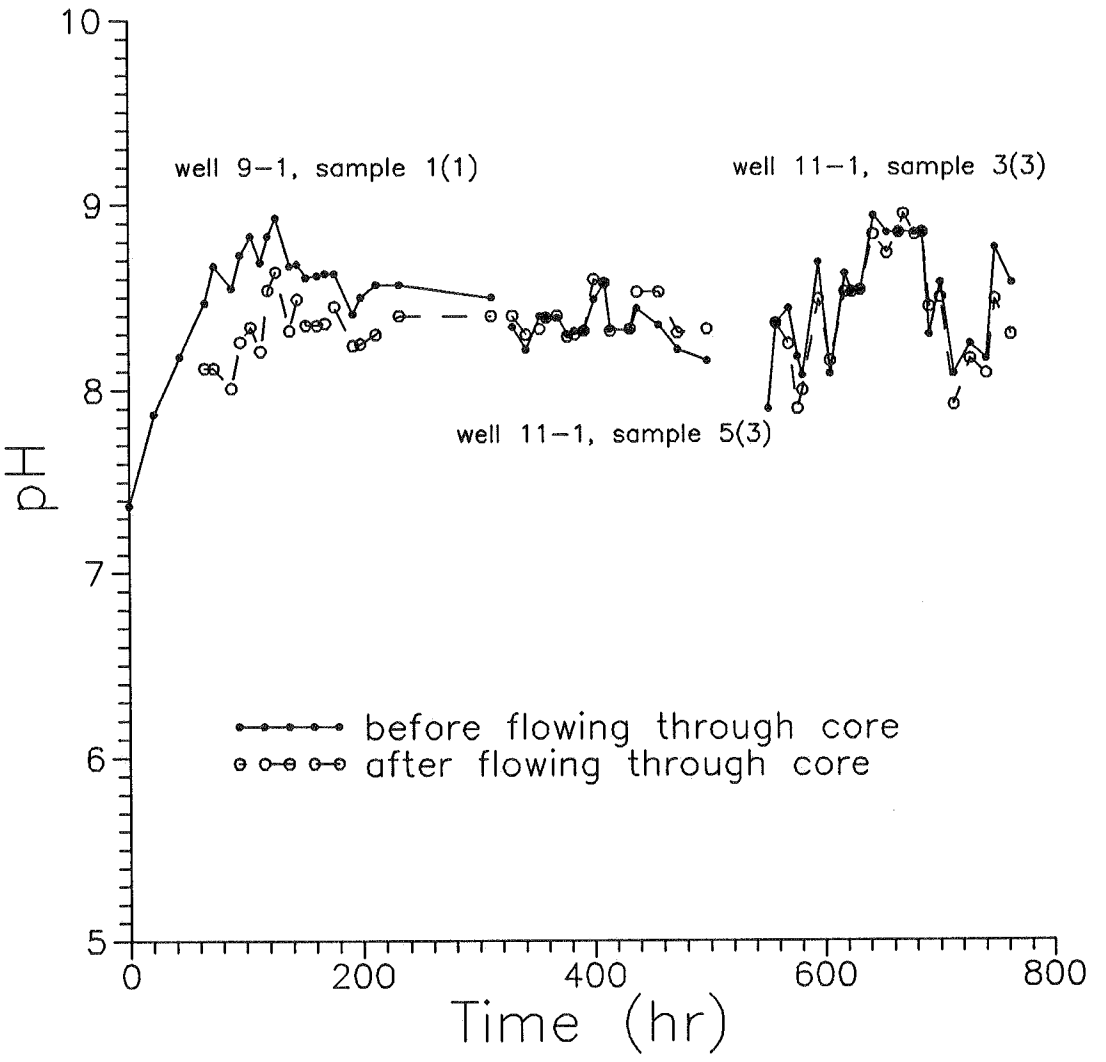

Figure IV.C.11 - pH of water vs. time.

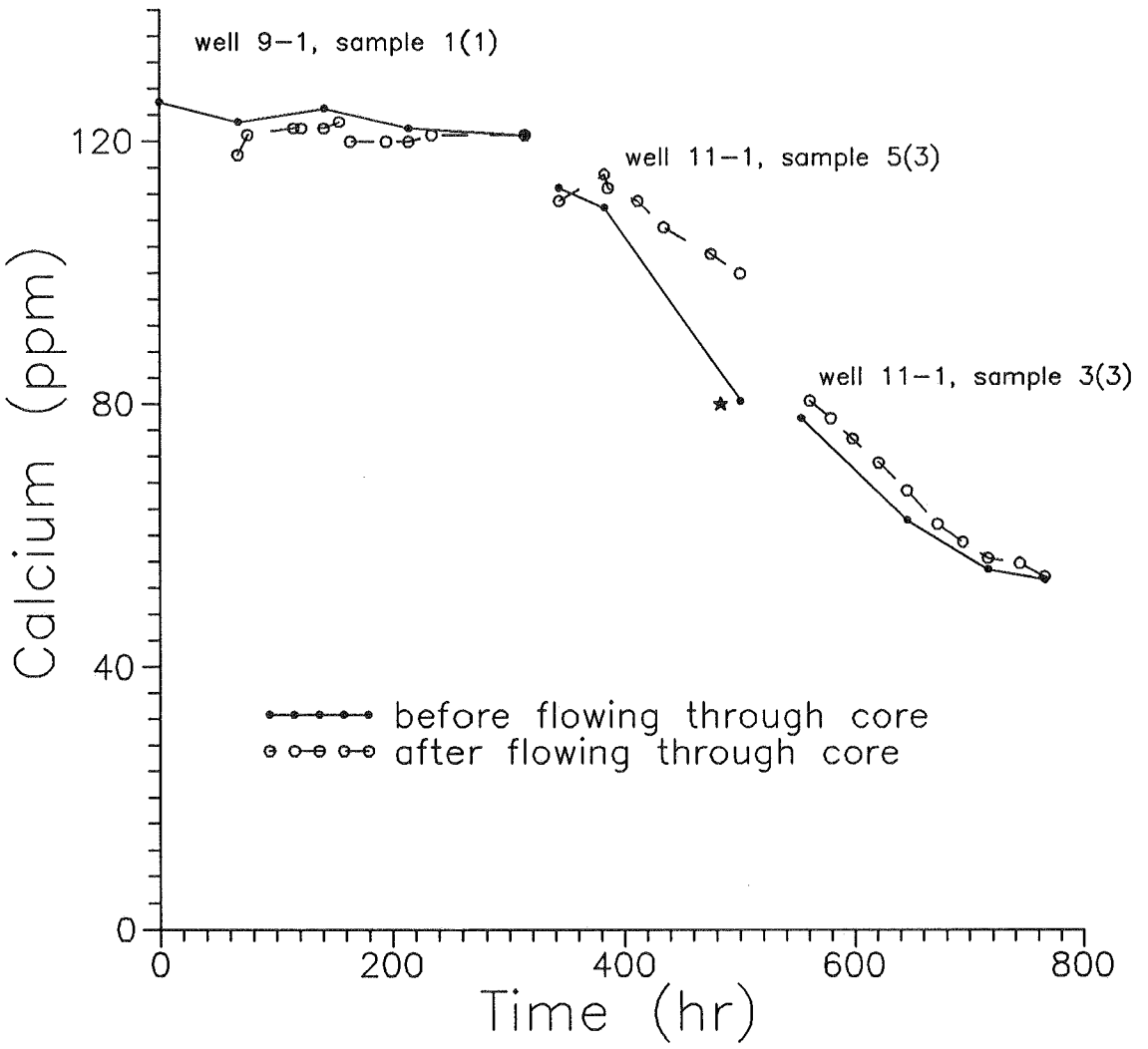

Figure IV.C.12 - Calcium content of water vs. time.

Table IV.C.1 - Results of Laboratory Analysis of Core Samples

Well No.	No. of Cores	Variable[1]	Mean	Std. Dev.	Min.	Max.
GEMS 00-1	49[2]					
		K	20.16	24.26	0.06	94.28
		repacked K	44.82	44.65	0.04	185.43
		n	28.4	3.1	23.2	37.4
		repacked n	28.8	2.7	23.8	35.8
		% fines	2.9	6.1	0.2	40.6
		mean grain size	-0.02	0.65	-1.02	2.55
GEMS 1-7	54					
		K	16.43	20.47	0.83	129.03
		repacked K	58.26	38.11	0.39	171.28
		n	28.2	2.0	23.1	33.1
		repacked n	28.6	2.1	23.2	32.5
		% fines	2.1	3.7	0.01	20.3
		mean grain size	-0.05	0.69	-1.19	2.24
GEMS 5-1	55[3]					
		K	16.88	15.41	0.12	65.32

		repacked K	44.01	36.59	4.97	159.61
		n	26.8	2.3	20.6	32.7
		repacked n	27.5	2.4	22.2	36.2
		% fines	1.9	1.9	0.1	8.6
		mean grain size	0.19	0.76	-1.05	2.44
GEMS 7-1	35					
		K	32.38	48.85	0.28	261.78
		repacked K	39.91	36.94	0.18	153.65
		n	25.8	3.4	19.8	36.4
		repacked n	26.5	3.3	20.2	36.0
		% fines	3.3	4.1	0.4	20.28
		mean grain size	0.02	0.45	-0.73	0.98
GEMS 8-1	52[4]					
		K	33.19	34.83	0.08	207.71
		repacked K	79.45	66.35	2.06	279.27
		n	29.7	4.6	23.0	47.8
		repacked n	30.0	2.9	25.0	40.3
		% fines	1.78	2.01	0.22	8.83
		mean grain size	-0.08	0.69	-1.01	2.45

GEMS 9-1	47[5]					
		K	27.19	32.59	0.19	134.73
		repacked K	49.19	43.36	0.16	233.27
		n	26.4	2.8	21.3	36.3
		repacked n	27.6	3.0	21.5	37.2
		% fines	2.7	5.9	0.2	33.43
		mean grain size	0.19	0.69	-1.05	2.07
GEMS 10-1	51					
		K	19.55	23.29	0.13	123.44
		repacked K	35.36	35.36	0.32	225.18
		n	27.94	2.07	23.42	32.35
		repacked n	28.45	2.29	22.63	33.38
		% fines	2.47	2.98	0.46	11.01
		mean grain size	0.13	0.52	-0.88	1.34
GEMS 11-1	29[6]					
		K	29.6	32.51	0.41	118.57
		repacked K	63.93	45.26	1.20	166.72
		n	26.4	2.7	22.2	33.0

		repacked n	26.8	3.7	21.2	31.7
		% fines	NA	NA	NA	NA
		mean grain size	NA	NA	NA	NA
GEMS TMO-1	57[7]					
		K	45.31	41.46	0.04	166.79
		repacked K	41.73	34.94	0.25	179.98
		n	28.02	2.60	18.88	35.54
		repacked n	28.56	3.23	22.45	37.98
		% fines	2.24	2.73	0.01	15.34
		mean grain size	0.05	0.54	-0.81	1.39
GEMS TME-8	30					
		K	83.26	74.02	5.85	327.9
		repacked K	44.41	44.59	1.48	205.08
		n	29.73	3.09	25.12	37.76
		repacked n	29.94	3.02	25.26	37.78
		% fines	2.21	1.61	0.42	6.12
		mean grain size	0.32	0.62	-0.98	1.50

1 - K and repacked K have units of m/d,
n and repacked n are dimensionless,
% fines is dimensionless,

mean grain size has units of phi ($-\log_2$ particle diameter);

2 - K and repacked K determined for 50 samples;

3 - grain size data only determined for 53 samples;

4 - grain size data only determined for 50 samples,
lengths of sample 24, segments 5-7, and sample 26, segments 5-7 may be incorrect;

5 - grain size data only determined for 45 samples,
porosity only determined for 46 samples;

6 - numerous problems with data from this well,
NA = not available;

7 - grain size data only determined for 54 samples;

V. SUMMARY OF PROJECT RESEARCH

The major focus of this project was on the use of well tests to describe spatial variations in hydraulic conductivity. Both theoretical and field investigations were carried out in an attempt to better understand the utility of well tests in heterogeneous formations. In this chapter, research of this project is summarized and the major findings of the work are briefly discussed

The theoretical component of this research was directed at developing a better understanding of the kind of information that can be obtained from various types of well tests performed in heterogeneous units. Since traditional modeling techniques are of limited effectiveness for the analysis of data from tests in heterogeneous formations, a new numerical model, which is continuous in time and employs an approximate representation of flow in the well bore, was developed. This model was then used in a detailed study of slug tests in layered aquifers. The results of this study helped to 1) define the manner in which layer properties are vertically averaged during a slug test, and 2) delineate conditions under which multilevel slug tests can provide valuable information about vertical variations in hydraulic conductivity within a unit. The best conditions for multilevel slug tests were shown to be units with low frequency vertical variations in hydraulic conductivity in which test intervals considerably shorter than the thickness of the average layer are employed. Even in such conditions, however, well skins of both lower and higher permeability than the undamaged formation can dramatically decrease the effectiveness of the approach. Careful well construction and development procedures were stressed as ways of decreasing the impact of such skins.

Sensitivity analysis is a formalism that allows relationships between model responses and parameters to be examined in considerable detail. In this work, the principles of sensitivity analysis were used to investigate the type of information that can be obtained from slug tests with observation wells. This analysis showed that the use of observation wells in slug tests can considerably improve the reliability of the estimated storage coefficient as a result of a significant decrease in parameter correlation when observation wells are employed.

When slug tests are performed in wells surrounded by a finite-radius zone (well skin) of permeability differing from that of the formation, the parameters estimated from test responses are a function of both the skin and formation properties. Although the form of the effective parameter obtained when a uniform-aquifer model is applied to data from a well with a skin has been clarified, it clearly will be very difficult to translate the effective parameter estimate into components characterizing skin and aquifer

properties, respectively. The general conclusion of this work is that it will be quite difficult to estimate formation parameters using data from a slug test performed at a well with a low-permeability skin.

Since many of the wells at GEMS are screened for only a portion of the sand and gravel interval, the partially penetrating nature of the wells must be considered when slug-test data from these wells are analyzed. One popular approach for the analysis of slug-test data from partially penetrating wells is the method of Nguyen and Pinder. A theoretical evaluation of this method revealed that an error was made in the analytical solution upon which the approach is based. Field and numerical examples demonstrate that the ramifications of this error are of considerable practical significance.

One of the goals of this project was to assess the potential of hydraulic tomography, i.e. the utilization of data from multiple well tests in a tomographic inversion procedure. An initial investigation of hydraulic tomography in a planar steady-state flow field was performed as part of this work. The tomographic method is based on the concept that the head drop between any two points on a streamline is given by a line integral of the flux along the streamline multiplied by the hydraulic resistivity (inverse of hydraulic conductivity). Streamline trajectories and flux integrals are computed from a finite difference solution for stream function values based on an estimate of the resistivity distribution. Computing flux integrals along a number of streamlines with known heads at each end results in a system of linear equations that can be solved for an updated set of resistivities. Stream function values and flux integrals are recomputed and the process is repeated until the resistivity estimates converge. Numerical examples indicate that the approach has potential in layered systems of considerable lateral continuity. Further work, however, is clearly needed to fully assess the viability of the approach.

The field component of this study of well tests in heterogeneous formations concentrated on slug tests. A prototype multilevel slug-test system, built at the KGS, was tested at GEMS. The results of the multilevel tests indicated that slug tests in the sand and gravel section at GEMS are being affected by mechanisms not accounted for in the conventional theory on which the standard methods for slug-test data analysis are based. The existence of these mechanisms was reflected by a concave downward curvature on log head versus arithmetic time plots, a dependence of slug-test responses on the magnitude of the induced slug (H_0), and systematic deviations between plots of the test data and the best-fit conventional models. A series of experiments were carried out at GEMS in order to clarify the mechanisms producing the observed behavior. Although these experiments are still ongoing, friction within the well screen and non-Darcian flow

within the formation are considered the most likely mechanisms producing the observed behavior. A new general nonlinear slug-test model was developed in an attempt to include mechanisms not accounted for in the conventional theory. This model allows the effects of nonlinearities, inertia, turbulence, radially nonuniform velocity distributions, viscous work within the well casing, and changing casing radii to be assessed. Efforts to use an approximate three-parameter form of this model to analyze GEMS slug-test data appear successful, as the model reproduces the key features of the GEMS data. Although this model appears to incorporate the majority of the relevant mechanisms controlling slug-test responses, it may be difficult to use on a routine basis. In an effort to obtain a tool for routine field analyses, we have developed an approximate approach called the Projection Method. This approach is based on the idea that the nonlinear effects should become insignificant as the initial head (i.e. size of the slug) goes to zero. Preliminary theoretical and field analyses of this approach appear quite promising.

The original proposal presented pulse testing as a promising well-testing methodology for use in hydrogeologic investigations. A program of multiwell slug tests (slug tests with observation wells) was initiated at GEMS as part of the pulse-test research of this project. The results of this program of field testing and a complementary theoretical analysis demonstrated that the assumption of a fully screened well can introduce a very large amount of error into parameter estimates determined from response data at observation wells. A new analytical model, which allows partial penetration at both the stressed and observation wells, was developed. Application of this model to data from GEMS yielded parameters that were in keeping with the values obtained from the laboratory analysis of cores.

The slug test has the potential to provide very useful information about the hydraulic properties of a formation. In order for the potential of this technique to be fully realized, however, considerable care must be given to all phases of test design, performance, and analysis. A series of practical guidelines were proposed here that should allow the quality of parameter estimates obtained from a program of slug tests to be improved. Three very important points arising from these guidelines cannot be overemphasized: 1) it is critical that a series of slug tests at a given well be designed so as to assess whether conventional theory is applicable (i.e. is there a dependence on initial head or mechanism of test initiation, is there a well skin that is developing during the course of testing, etc.); 2) the analysis of the response data must be done using the most appropriate model for the test configuration and with considerable care; and 3) inattention to details of well construction and development can produce a situation in which it is virtually impossible to use slug tests to obtain parameter estimates that are

representative of formation properties.

The failure to recognize the existence of a low-permeability well skin is undoubtedly the largest source of error in hydraulic conductivity estimates obtained from slug tests. An underestimation in hydraulic conductivity of an order of magnitude or more will often be the result if a low-permeability skin is not recognized. A new approach for the identification of low-permeability well skins was proposed as part of this work. This approach, which exploits some basic features of the physics of slug-induced flow in the presence of a low-permeability skin, involves performing repeat slug tests in conjunction with a simple ratio method derived from the Hvorslev technique. The dimensionless storage parameter is changed between tests by modifying the effective radius of the well casing. Results indicate that the approach should work well when the skin-formation K contrast is greater than an order of magnitude, even in the presence of the noise inherent in field applications. Less dramatic contrasts can be identified when the vertical component of the slug-induced flow is small. Although the hydraulic conductivity of the formation may still be difficult to estimate, use of this method should enable the field practitioner to avoid inadvertently assigning properties reflective of a low-permeability skin to the formation.

In addition to the research on well tests in heterogeneous formations, a significant amount of the work of this project was focussed on increasing our knowledge of the sand and gravel interval at GEMS. This work included the drilling of additional wells using hollow-stem auger techniques, obtaining relatively undisturbed samples of the unconsolidated alluvium using the KGS bladder sampler, and the laboratory analysis of the core samples. The ultimate goal of these characterization efforts was the development of a detailed picture of the subsurface at GEMS that will enable us to better assess the results of the hydraulic tests performed at the site. The use of the data collected as part of these characterization efforts to assess the scale dependence of hydraulic properties will be the subject of future work.

VI. REFERENCES

Anderson, M.P., and Woessner, W.W., 1992, Applied Groundwater Modeling, Academic Press, Inc., San Diego, 381 pp.

Baker, S.R., and Friedman, G.M., 1969, A non-destructive core analysis technique using x-rays, Jour. Sed. Petrology, v. 39, no. 4, 1371-1383.

Barker, J.A., 1982, Laplace transform solutions for solute transport in fissured aquifers, Adv. Water Resources, v. 5, 98-104.

Barker, J.A., and Black, J.H., 1983, Slug tests in fissured aquifers, Water Resour. Res., v. 19, no. 6, 1558-1564.

Bear, J., 1972, Dynamics of Fluids in Porous Media, American Elsevier, New York, 764 pp.

Beauheim, R.L., 1994, Practical considerations in well testing of low-permeability media (abstract), EOS, v. 75, no. 16, 151-152.

Beck, J.V., and Arnold, K.J., 1977, Parameter Estimation in Engineering and Science, John Wiley, New York, 501 pp.

Black, J.H., 1985, The interpretation of slug tests in fissured rocks, Quart. Jour. Eng. Geol., v. 18, 161-171.

Bliss, J.C., and Rushton, K.R., 1984, The reliability of packer tests for estimating the hydraulic conductivity of aquifers, Quart. Jour. Eng. Geol., v. 17, 81-91.

Bohling, G.C., and McElwee, C.D., 1992, SUPRPUMP: An interactive program for well test analysis and design, Ground Water, v. 30, no. 2, 262-268.

Bouwer, H., 1989, The Bouwer and Rice slug test - an update, Ground Water, v. 27, no. 3, 304-309.

Bouwer, H., and Rice, R.C., 1976, A slug test for determining hydraulic conductivity of unconfined aquifers with completely or partially penetrating wells, Water Resour. Res., v. 12, no. 3, 423-428.

Braester, C., and Thunvik, R., 1984, Determination of formation permeability by double-packer tests, J. of Hydrology, v. 72, 375-389.

Bredehoeft, J.D., and Papadopulos, I.S., 1980, A method for determining the hydraulic properties of tight formations, Water Resour. Res., v. 16, no. 1, 233-238.

Brother, M.R., and Christians, G.L., 1993, In situ slug test analysis: A comparison of three popular methods for unconfined aquifers, Proc. of the 7th National Outdoor Action Conf., NGWA, Ground Water Management, v. 15, 597-607.

Butler, J.J., Jr., 1986, Pumping Tests in Nonuniform Aquifers: A deterministic and stochastic analysis (Ph.D. dissertation), Stanford Univ., Stanford, CA, 220 pp.

Butler, J.J., Jr., 1990, The role of pumping tests in site characterization: Some theoretical considerations, Ground Water, v. 28, no. 3, 394-402.

Butler, J.J., Jr., 1996, Slug tests: Some practical considerations, Kansas Geological Survey Open-File Rept. 94-16.

Butler, J.J., Jr., and Healey, J.M., 1995, Analysis of 1994-95 hydraulic tests at Trego County monitoring site, Kansas Geological Survey Open-File Rept. 95-66, 30 pp.

Butler, J.J., Jr., and Hyder, Z., 1994, An assessment of the Nguyen and Pinder method for slug test analysis, Ground Water Monitoring and Remediation, v. 14, no. 4, 124-131.

Butler, J.J., Jr., and Liu, W.Z., 1993, Pumping tests in nonuniform aquifers: The radially asymmetric case, Water Resour. Res., v. 29, no. 2, 259-269.

Butler, J.J., Jr., and Liu, W.Z., 1994, Analysis of 1991-1992 slug tests in the Dakota aquifer of central and western Kansas, Kansas Geological Survey Open-File Rept. 93-1c.

Butler, J.J., Jr., and McElwee, C.D., 1990, Variable-rate pumping tests for nonuniform aquifers, Water Resour. Res., v. 26, no. 2, 291-306.

Butler, J.J., Jr., and McElwee, C.D., 1992, Well-testing methodologies for characterizing heterogeneities in alluvial-aquifer systems: First year report, Kansas Geol. Survey Open-File Rept. 92-53, 152 pp.

Butler, J.J., Jr., Liu, W.Z., and Young, D.P., 1993, Analysis of October 1993 slug tests in Stafford, Pratt, and Reno counties, south-central Kansas, Kansas Geological Survey Open-File Rept. 93-52, 70 pp.

Butler, J.J., Jr., McElwee, C.D., and Hyder, Z., 1993, Slug tests in unconfined aquifers, Kansas Water Resources Research Inst. Contribution No. 303, 67 pp.

Butler, J.J., Jr., McElwee, C.D., and Hyder, Z., 1994, Slug tests in unconfined aquifers - Phase two, Kansas Water Resources Research Inst. Contribution No. 310, Manhattan, Ks., 109 pp.

Butler, J.J., Jr., Bohling, G.C., Hyder, Z., and McElwee, C.D., 1994, The use of slug tests to describe vertical variations in hydraulic conductivity, J. of Hydrology, v. 156, 137-162.

Butler, J.J., Jr., McElwee, C.D., Bohling, G.C., and Healey, J.M., 1990, Hydrogeologic characterization of hazardous waste sites, Kansas Water Resources Research Inst. Contribution No. 283, 114 pp.

Butler, J.J., Jr., McElwee, C.D., Bohling, G.C., and Healey, J.M., 1991, Hydrogeologic characterization of hazardous waste sites, Kansas Water Resources Research Inst. Contribution No. 289, 129 pp.

Campbell, M.D., Starrett, M.S., Fowler, J.D., and Klein, J.J., 1990, Slug tests and hydraulic conductivity, Proc. of the Petroleum Hydrocarbons and Organic Chemicals in Ground Water: Prevention, Detection, and Restoration Conf., NWWA, Ground Water Management, v. 4, 85-99.

Carrera, J., and Neuman, S.P., 1986, Estimation of aquifer parameters under transient and steady state conditions: 2. Uniqueness, stability, and solution algorithms, Water Resour. Res., v. 22, no. 2, 211-227.

Chen, C., 1985, Analytical and approximate solutions to radial dispersion from an injection well to a geological unit with simultaneous diffusion into adjacent strata, Water Resour. Res., v. 22, no. 4, 1069-1076.

Chen, C., 1986, Solutions to radionuclide transport from an injection well into a single fissure in a porous formation, Water Resour. Res., v. 22, no. 4, 508-518.

Chen, H.T., and Chen, C.K., 1988, Hybrid Laplace transform/finite element method for two-dimensional heat conduction, J. Thermophys., v. 2, no. 1, 31-36.

Chirlin, G.R., 1989, A critique of the Hvorslev method for slug test analysis: The fully penetrating well, Ground Water Monitoring Review, v. 9, no. 2, 130-138.

Chirlin, G.R., 1990, The slug test: the first four decades, Ground Water Management, v. 1, 365-381.

Churchill, R.V., 1972, Operational Mathematics, McGraw Hill, New York, 481 pp.

Cooper, H.H., Bredehoeft, J.D., and Papadopulos, I.S., 1967, Response of a finite-diameter well to an instantaneous charge of water, Water Resour. Res., v. 3, no. 1, 263-269.

Cordes, C., and Kinzelbach, W., 1992, Continuous groundwater velocity fields and path lines in linear, bilinear, and trilinear finite elements, Water Resour. Res., v. 28, no. 11, 2903-2911.

Crump, K.S., 1976, Numerical inversion of Laplace transforms using a Fourier series approximation, J. Assoc. Comput. Mach, v. 23, no. 1, 89-96.

Dagan, G., 1978, A note on packer, slug, and recovery tests in unconfined aquifers, Water Resour. Res., v. 14, no. 5, 929-934.

Dagan, G., 1986, Statistical theory of groundwater flow and transport: pore to laboratory, laboratory to formation, and formation to regional scale, Water Resour. Res., v. 22, no. 9, 120S-134S.

Dahl, S. and Jones, J., 1993, Evaluation of slug test data under unconfined conditions with exposed screens, and low permeability filter pack, Proc. of the 7th National Outdoor Action Conf, NGWA, Ground Water Management, v. 15, 609-623.

Dax, A., 1987, A note on the analysis of slug tests, J. of Hydrology, v. 91, 153-177.

De Hoog, F.R., Knight, J.H., and Stokes, A.N., 1982, An improved method for numerical inversion of Laplace transforms, SIAM J. Sci. Stat. Comput., v. 3, no. 3, 357-366.

Demir, Z., and Narasimhan, T.N., 1994, Towards an improved interpretation of Hvorslev tests, ASCE J. of Hydraulics, v. 120, no. 4, 477-494.

Desbarats, A.J., 1991, Spatial averaging of transmissivity, in Proceedings of the 5th Canadian/American Conference on Hydrogeology: Parameter Identification and Estimation for Aquifer and Reservoir Characterization, edited by S. Bachu, 139-154, National Water Well Association, Dublin, Ohio.

Desbarats, A.J., 1992a, Spatial averaging of transmissivity in heterogeneous fields with flow toward a well, Water Resour. Res., 28(3), 757-767.

Desbarats, A.J., 1992b, Spatial averaging of hydraulic conductivity in three-dimensional heterogeneous porous media, Math. Geol., 24(3), 249-267.

Deutsch, C.V., and Journel, A.G., 1992, GSLIB: Geostatistical Software Library and User's Guide, Oxford University Press, New York, 340 pp.

Dougherty, D.E., and Babu, D.K., 1984, Flow to a partially penetrating well in a double-porosity reservoir, Water Resour. Res., v. 20, no. 8, 1116-1122.

Dubner, H., and Abate, J., 1968, Numerical inversion of Laplace transforms by relating them to the finite Fourier cosine transform, J. Assoc. Comp. Mach., v. 15, no. 1, 115-123.

Ehlig-Economides, C.A., and Joseph, J.A., 1987, A new test for determination of individual layer properties in a multilayered reservoir, SPE Formation Eval., v. 2, no. 3, 261-283.

Eskinazi, S., 1967, Vector Mechanics of Fluids and Magnetofluids, Academic Press, New York.

Faust, C.R., and Mercer, J.W., 1984, Evaluation of slug tests in wells containing a finite-thickness skin, Water Resour. Res., v. 20, no. 4, 504-506.

Ferris, J.G., and Knowles, D.B., 1954, The slug test for estimating transmissivity, U.S. Geological Survey Ground Water Note 26.

Fogler, H.S., and Vaidya, R.N., 1993, Effects of pH on fines migration and permeability reduction, in Manipulation of Groundwater Colloids for Environmental Restoration, J. F. McCarthy and F. J. Wobber (eds.), 123-128.

Freeze, R.A., and Cherry, J.A., 1979, Groundwater, Prentice-Hall, Inc., Englewood Cliffs, N.J., 604 pp.

Freyberg, D.L., 1986, A natural gradient experiment on solute transport in a sand

aquifer, 2, Spatial moments and the advection and dispersion of nonreactive tracers, Water Resour. Res., v. 22, no. 13, 2031-2046.

Frind, E.O., and Matanga, G.B., 1985, The dual formulation of flow for contaminant transport modeling, 1, Review of theory and accuracy aspects, Water Resour. Res., v. 21, no. 2, 159-169.

Frind, E.O., and Pinder, G.F., 1973, Galerkin solution of the inverse problem for aquifer transmissivity, Water Resour. Res., v. 9, no. 5, 1397-1410.

Gelhar, L.W., 1986, Stochastic subsurface hydrology from theory to applications, Water Resour. Res., v. 22, no. 9, 135S-145S.

Guppy, K.H., Cinco-Ley, H., Ramey, H.J., Jr., and Samaniego, F.V., 1982, Non-Darcy flow in wells with finite-conductivity vertical fractures, Soc. of Pet. Eng. J., v. 22, no. 10, 681-698.

Gurtin, M.E., 1965, Variational principles for initial value problems, Q. App. Math., v. 22, 252-256.

Guyonnet, D., Mishra, S., and McCord, J., 1993, Evaluating the volume of porous medium investigated during a slug test, Ground Water, v. 31, no. 4, 627-633.

Haberman, R., 1987, Elementary Applied Partial Differential Equations, Prentice-Hall, Inc., Englewood Cliffs, N.J., 547 pp.

Hackett, G., 1987, Drilling and constructing monitoring wells with hollow-stem augers, Part 1: Drilling considerations, Ground Water Monitoring Review, v. 7, no. 4, 51-62.

Hansen, A.G., 1967, Fluid Mechanics, John Wiley and Sons, Inc., New York.

Hantush, M.S., 1964, Hydraulics of wells, in: V.T. Chow, ed., Advances in Hydrosciences, Academic Press, New York, v. 1, 281-432.

Harvey, C.F., 1992, Interpreting Parameter Estimates Obtained From Slug Tests in Heterogeneous Aquifers (M.S. thesis), Stanford Univ., Stanford, Ca., 99 pp.

Hayashi, K., Ito, T., and Abe, H., 1987, A new method for the determination of in situ hydraulic properties by pressure pulse tests and application to the Higashi Hachimantai geothermal field, J. Geophys. Res., v. 92, no. B9, 9168-9174.

Herzog, B.L., 1994, Slug tests for determining hydraulic conductivity of natural geologic deposits, In: D.E. Daniel and S.J. Trautwein (Editors), Hydraulic Conductivity and Waste Contaminant Transport in Soils, ASTM STP 1142, American Society for Testing and Materials, Philadelphia, 95-110.

Hess, K.M., Wolf, S.H., and Celia, M.A., 1992, Large-scale natural gradient tracer test in sand and gravel, Cape Cod, Massachusetts, 3. Hydraulic conductivity variability and calculated macrodispersivities, Water Resour. Res., v. 28, no. 8, 2011-2027.

Hinsby, K., Bjerg, P.L., Andersen, L.J., Skov, B., and Clausen, E.V., 1992, A mini slug test method for determination of a local hydraulic conductivity of an unconfined sandy aquifer, J. of Hydrology, v. 136, 87-106.

Hufschmied, P., 1986, Estimation of three-dimensional anisotropic hydraulic conductivity field by means of single well pumping tests combined with flowmeter measurements, Hydrogeologie, 163-174.

Hvorslev, M.J., 1951, Time lag and soil permeability in ground-water observations, Bull no. 36, Waterways Exper. Sta., Corps of Engrs., U.S. Army, 50 pp.

Hyder, Z., and Butler, J.J., Jr., 1995, Slug tests in unconfined formations: An assessment of the Bouwer and Rice technique, Ground Water, v. 33, no. 1, 16-22.

Hyder, Z., Butler, J.J., Jr., McElwee, C.D., and Liu, W.Z., 1994, Slug tests in partially penetrating wells, Water Resour. Res., v. 30, no. 11, 2945-2957.

Javandel, M.S., and Witherspoon, P.A., 1968, Application of the finite element method to transient flow in porous media, Soc. Pet. Eng. J., v. 8, 241-252.

Jiang, X., 1991, A Field and Laboratory Study of Scale Dependence of Hydraulic Conductivity (M.S. thesis), Univ. of Ks, Lawrence, Ks, 149 pp.

Kabala, Z.J., Pinder, G.F., and Milly, P.C.D., 1985, Analysis of well-aquifer response to a slug test, Water Resour. Res., v. 21, no.9, 1433-1436.

Karasaki, K., 1986, Well Test Analysis in Fractured Media (Ph.D. dissertation), Univ. of Ca., Berkeley, 239 pp.

Karasaki, K., Long, J.C.S., and Witherspoon, P.A., 1988, Analytical models of slug tests, Water Resour. Res., v. 24, no. 1, 115-126.

Keely, J.F., and Boateng K., 1987, Monitoring well installation, purging and sampling techniques, Part 1: Conceptualizations, Ground Water, v. 25, no. 3, 300-313.

Kipp, K.L., Jr., 1985, Type curve analysis of inertial effects in the response of a well to a slug test, Water Resour. Res., v. 21, no. 9, 1397-1408.

Kreyszig, E., 1983, Advanced Engineering Mathematics, John Wiley and Sons, New York.

Kruseman, G.P., and de Ridder, N.A., 1989, Analysis and Evaluation of Pumping Test Data - ILRI publication 47, ILRI, The Netherlands, 377 pp.

Levy, B.S., and Pannell, L., 1991, Evaluation of a pressure system for estimating in-situ hydraulic conductivity, Proc. of the 5th National Outdoor Action Conf., NWWA, 131-146.

Li, S.G., Ruan, F., and McLaughlin, D., 1992, A space-time accurate method for solving solute transport problems, Water Resour. Res., v. 28, no. 9, 2297-2306.

Liu, W.Z., and Butler, J.J., Jr., 1991, A time-continuous finite difference approach for

flow and transport simulations, Kansas Geol. Survey, Open File Report 91-20, 19 pp.

Liu, W.Z., and Butler, J.J., Jr., 1995, The KGS Model for slug tests in partially penetrating wells, Kansas Geological Survey Computer Series Rept. 95-1.

McDonald, M.G., and Harbaugh, A.W., 1984, A modular three-dimensional finite-difference ground-water flow model, USGS Open-File Report 83-875.

McElwee, C.D., 1982, A one-dimensional study of the groundwater inverse problem using sensitivity analysis, Kansas Geol. Survey Open-File Rept. 82-12, 68 pp.

McElwee, C.D., 1982, Sensitivity analysis and the ground-water inverse problem, Ground Water, v. 20, no. 6, 723-735.

McElwee, C.D., 1987, Sensitivity analysis of ground-water models, in: Bear, J., and Corapcioglu, M.Y., ed., Proc. of the 1985 NATO Advanced Study Inst. on Fundamentals of Transport Phenomena in Porous Media: Martinus Nijhoff Publishers, Dordrecht, The Netherlands, 751-817.

McElwee, C.D., and Butler, J.J., Jr., 1989, Slug testing in highly permeable aquifers (abstract), GSA 1989 Annual Mtg. Abstract with Program, p. A193.

McElwee, C.D., and Butler, J.J., Jr., 1993, Characterization of heterogeneities controlling transport and fate of pollutants in unconsolidated sand and gravel aquifers: Second year report, Kansas Geological Survey Open-File Rept. 93-21, 221 pp.

McElwee, C.D. and Butler, J.J., Jr., 1994, Characterization of Heterogeneities Controlling Transport and Fate of Pollutants in Unconsolidated Sand and Gravel Aquifers: Third Year Report, Project Report to Air Force Office of Scientific Research, University Research Initiative, Research Initiation Program, U.S. Dept. of Defense, 237 pp.

McElwee, C.D., Bohling, G.C., and Butler, J.J., Jr., 1995a, Sensitivity analysis of slug tests, Part 1. The slugged well, J. of Hydrology, v. 164, 53-67.

McElwee, C.D., Butler, J.J., Jr., and Bohling, G.C., 1992, Nonlinear analysis of slug tests in highly-permeable aquifers using a Hvorslev-type approach, EOS, v. 73, no. 43, p. 164.

McElwee, C.D., Butler, J.J., Jr., and Healey, J.M., 1991, A new sampling system for obtaining relatively undisturbed samples of unconsolidated coarse sand and gravel, Ground Water Monitoring Review, v. 11, no. 3, 182-191.

McElwee, C.D., Butler, J.J., Jr., Bohling, G.C., and Liu, W.Z., 1991, The use of observation wells with slug tests, Kansas Geological Survey Open-File Report 91-63, 32 pp. (see also McElwee, et al., 1995b).

McElwee, C.D., Butler, J.J., Jr., Bohling, G.C., and Liu, W.Z., 1995b, Sensitivity

analysis of slug tests, II. Observation wells, J. of Hydrology, v. 164, 69-87.

McElwee, C.D., Butler, J.J., Jr., Liu, W.Z., and Bohling, G.C., 1990, Effects of partial penetration, anisotropy, boundaries and well skin on slug tests (abstract), EOS, v. 71, no. 17, p. 505 (see also Hyder et al., 1994).

McLane, G.A., Harrity, D.A., and Thomsen, K.O., 1990, A pneumatic method for conducting rising and falling head tests in highly permeable aquifers, Proc. of 1990 NWWA Outdoor Action Conf.

Melville, J.G., Molz, F.J., Guven, O., and Widdowson, M.A., 1991, Multilevel slug tests with comparisons to tracer data, Ground Water, v. 29, no. 6, 897-907.

Minning, R.C., 1982, Monitoring well design and installation, Proc. of the Second National Symposium on Aquifer Restoration and Ground Water Monitoring, NWWA, Columbus, Ohio, 194-197.

Moench, A.F., 1984,. Double porosity models for a fissured groundwater reservoir with fracture skin, Water Resour. Res., v. 10, no. 7, 831-846.

Moench, A.F., and Hsieh, P.A., 1985, Analysis of slug test data in a well with finite-thickness skin, In: Memoirs of the 17th Intern. Cong. on the Hydrogeology of Rocks of Low Permeability, v. 17, 17-29.

Moench, A.F., and Ogata, A., 1984, Analysis of constant discharge wells by numerical inversion of Laplace transform solutions, in: Rosenshein, J., and Bennett, G.D., ed., Groundwater Hydraulics, AGU Water Resour. Monogr. 9, AGU, Washington, DC., 146-170.

Moltyaner, G.L., and Killey, R.W.D., 1988, Twin Lake tracer tests: Longitudinal dispersion, Water Resour. Res., v. 24, no. 10, 1613-1627.

Molz, F.J., Guven, O., and Melville, J.G., 1989a, Characterization of the hydrogeologic properties of aquifers: The next step, in: Proc. of the Conf. on New Field Techniques for Quantifying the Physical and Chemical Properties of Heterogeneous Aquifers, NWWA, 407-418.

Molz, F.J., Morin, R.H., Hess, A.E., Melville, J.G., and Guven, O., 1989b, The impeller meter for measuring aquifer permeability variations: Evaluation and comparison with other tests, Water Resour. Res., v. 25, no. 7, 1677-1686.

Moridis, G.J., and Reddell, D.L., 1991, The Laplace transform finite difference method for simulation of flow through porous media, Water Resour. Res., v. 27, no. 8, 1873-1884.

Morin, R.H., Hess, A.E., and Paillet, F.L., 1988, Determining the distribution of hydraulic conductivity in a fractured limestone aquifer by simultaneous injection and geophysical logging, Ground Water, v. 26, no. 5, 587-595.

National Ground Water Association, 1993, Analysis and design of aquifer tests - including slug tests and fracture flow, 1994 Catalog of Ground Water and Environmental Education, 17-18.

Nelson, R.W., 1960, In-place measurement of permeability in heterogeneous media, 1, Theory of a proposed method, J. Geophys. Res., v. 65, no. 6, 1753-1758.

Nelson, R.W., 1961, In-place measurement of permeability in heterogeneous media, 2, Experimental and computational considerations, J. Geophys. Res., v. 66, no. 8, 2469-2478.

Nelson, R.W., 1968, In-place determination of permeability distribution for heterogeneous porous media through analysis of energy dissipation, Soc. Pet. Eng. J., v. 8, no. 1, 33-42.

Neuman, S.P., 1973, Calibration of distributed parameter groundwater flow models viewed as a multiple-objective decision process under uncertainty, Water Resour. Res., v. 9, no. 4, 1006-1021.

Neuman, S.P., 1980, A statistical approach to the inverse problem of aquifer hydrology, 3, Improved solution method and added perspective, Water Resour. Res., v. 16, no. 2, 331-346.

Neuzil, C.E., 1982, On conducting the modified "slug" test in tight formations, Water Resour. Res., v. 18, no. 2, 439-441.

Nichols, E.M., 1985, Determination of the Hydraulic Parameters of Salt Marsh Peat Using In-Situ Well Tests (M.S. thesis), Mass. Inst. Tech., 109 pp.

Nguyen, V., and Pinder, G.F., 1984, Direct calculation of aquifer parameters in slug test analysis, in: Rosenshein, J., and Bennett, G.D., eds., Groundwater Hydraulics, AGU Water Resour. Monogr. No. 9, 222-239.

Novakowski, K.S., 1988, Comparison of fracture aperture widths determined from hydraulic measurements and tracer experiments, Proc. of the Fourth Canadian/American Conf. on Hydrogeology.

Novakowski, K.S., 1989, A composite analytical model for analysis of pumping tests affected by well bore storage and finite thickness skin, Water Resour. Res., v. 25, no. 9, 1937-1946.

Novakowski, K.S., 1989a, Analysis of pulse interference tests, Water Resour. Res., v. 25, no. 11, 2377-2387.

Orient, J.P., Nazar, A., and Rice, R.C., 1987, Vacuum and pressure test methods for estimating hydraulic conductivity, Ground Water Monitoring Review, v. 7, no. 1, 49-50.

Osborne, P.S., 1993, Suggested operating procedures for aquifer pumping tests,

EPA/540/S-93/503, U.S. EPA, Office of Research and Development, 23 pp.

Palmer, C.D., and Johnson, R.L., 1989, Determination of physical transport parameters, in: Transport and Fate of Contaminants in the Subsurface, Environmental Protection Agency, EPA/625/4-89/019, 29-40.

Palmer, C.D., and Paul, D.G., 1987, Problems in the interpretation of slug test data from fine-grained tills, Proc. of the NWWA FOCUS Conf. on Northwestern Ground Water Issues, NWWA, 99-123.

Papadopulos, I.S., 1966, Nonsteady flow to multiaquifer wells, J. Geophys. Research, v. 71, no. 20, 4791-4797.

Papadopulos, I.S., and Cooper, H.H., Jr., 1967, Drawdown in a well of large diameter, Water Resour. Res., v. 3, no. 1, 241-244.

Parkhurst, D.L., Thorstenson, D.C., and Plummer, L.N., 1980, PHREEQE--A computer program for geochemical calculations, U.S. Geological Survey Water-Resources Investigations Rept. 80-96, 195 pp.

Parmakian, J., 1963, Waterhammer Analysis, Dover Pub., New York, 161 pp.

Perry, C.A., and Hart, R.J., 1985, Installation of observation wells on hazardous waste sites in Kansas using a hollow-stem auger, Ground Water Monitoring Review, v. 5, no. 4, 70-73.

Peterson, J.E., Paulsson, B.N.P., and McEvilly, T.V., 1985, Application of algebraic reconstruction techniques to crosshole seismic data, Geophysics, v. 50, no. 10, 1566-1580.

Pollock, D.W., 1988, Semianalytical computation of path lines for finite-difference models, Ground Water, v. 26, no. 6, 743-750.

Prijambodo, R., Raghavan, R., and Reynolds, A.C., 1985, Well test analysis for wells producing layered reservoirs with crossflow, Soc. Pet. Eng. J., v. 25, 380-396.

Raghavan, R., 1989, Behavior of wells completed in multiple producing zones, SPE Formation Evaluation, v. 4, no. 2, 219-230.

Ramey, H.J., Jr., Agarwal, R.G., and Martin, I., 1975, Analysis of "slug test" or DST flow period data, Jour. Can. Pet. Technol., v. 14, 53-67.

Rehfeldt, K.R., Hufschmied, P., Gelhar, L.W., and Schaefer, M.E., 1989, Measuring hydraulic conductivity with the borehole flowmeter, Rept. EN-6511, Electric Power Res. Inst., Palo Alto, Ca.

Rushton, K.R., and Chan, Y.K., 1977, Numerical pumping test analysis in unconfined aquifers, J. Irrigation and Drainage Div., v. 103, no. IR1, 1-12.

Russell, D.G., and Prats, M., 1962, Performance of layered reservoirs with crossflow-single-compressible-fluid case, Soc. of Pet. Eng. J., v. 2, no. 12,

53-67.

Sageev, A., 1986, Slug test analysis, Water Resour. Res, v. 22, no. 8, 1323-1333.

Scott, D.M., 1992, Evaluation of flow net analysis for aquifer identification, Ground Water, v. 30, no. 5, 755-764.

Settari, A., and Aziz, K., 1974, A computer model for two-phase coning simulation, Soc. of Pet. Eng. J., v. 14, no. 3, 221-236.

Springer, R.K., and Gelhar, L.W., 1991, Characterization of large-scale aquifer heterogeneity in glacial outwash by analysis of slug tests with oscillatory responses, Cape Cod, Massachusetts, U.S. Geological Survey Water Resour. Inv. Rept. 91-4034, 36-40.

Stehfest, H., 1970, Numerical inversion of Laplace transforms, Commun. ACM., v. 13, no. 1, 47-49.

Stone, D.B. and Clarke, G.K.C., 1993, Estimation of subglacial hydraulic properties from induced changes in basal water pressure: A theoretical framework for borehole response tests, J. of Glaciology, v. 39, no. 132, 327-340.

Streltsova, T.D., 1988, Well Testing in Heterogeneous Formations, John Wiley and Sons, Inc., New York, 413 pp.

Sudicky, E.A., 1989, The Laplace transform Galerkin technique: A time-continuous finite element theory and application to mass transport in groundwater, Water Resour. Res., v. 25, no. 8, 1833-1846.

Sudicky, E.A., and McLaren, R.G., 1992, The Laplace transform Galerkin technique for large-scale simulation of mass transport in discretely fractured porous media, Water Resour. Res., v. 28, no. 2, 499-514.

Talbot, A., 1979, The accurate numerical inversion of Laplace transforms, J. Inst. Math. Appl., v. 23, 97-120.

Taylor, K., and Molz, F., 1990, Determination of hydraulic conductivity and porosity logs in wells with a disturbed annulus, J. of Contaminant Hydrology, v. 5, 317-332.

Taylor, K., Wheatcraft, S., Hess, J., Hayworth, J., and Molz, F., 1990, Evaluation of methods for determining the vertical distribution of hydraulic conductivity, Ground Water, v. 28, no. 1, 937-945.

Theis, C.V., 1935, The relation between the lowering of the piezometric surface and the rate and duration of discharge of a well using ground-water storage, Trans. AGU, 16th Ann. Mtg., pt. 2, 519-524.

Tongpenyai, Y., and Raghavan, R., 1981, The effect of wellbore storage and skin on interference test data, J. Pet. Tech., v. 33, no. 1, 151-160.

Van der Kamp, G., 1976, Determining aquifer transmissivity by means of well response

tests: The underdamped case, Water Resour. Res., v. 12, no. 1, 71-77.

Van Dyke, N.V.R., Rhodes, J.R., Richardson, D.W., and McTigue, W.H., 1993, Evaluating confined aquifer properties using the pneumatic displacement method and the repeated pressure pulse technique, in Proc. of the Seventh National Outdoor Action Conf., NGWA, Ground Water Management, v. 15, 405-419.

Vennard, J.K., and Street, R.L., 1975, Elementary Fluid Mechanics, Wiley and Sons, New York, 740 pp.

Von Rosenberg, D.U., 1969, Methods for the Numerical Solution of Partial Differential Equations, Elsevier, 125 pp.

Walter, G.R., and Thompson, G.M., 1982, A repeated pulse technique for determining the hydraulic properties of tight formations, Ground Water, v. 20., no. 2, 186-192.

Wang, H. F., and Anderson, M.P., 1982, Introduction to Groundwater Modeling: Finite Difference and Finite Element Methods, W. H. Freeman and Company, New York, 237 pp.

Widdowson, M.A., Molz, F.J., and Melville, J.G., 1990, An analysis technique for multilevel and partially penetrating slug test data, Ground Water, v. 28, no. 6, 937-945.

Yeh, W. W-G., 1986, Review of parameter identification procedures in groundwater hydrology: The inverse problem, Water Resour. Res., v. 22, no. 2, 95-108.

Yu, Y.H., and Lloyd, J.W., 1992, A multi-layered radial flow model interpretation of drill stem test data, J. of Hydrology, v. 136, 73-86.

Zapico, M.M., 1987, Aquifer Evaluation Procedures - Core Acquisition and an Assessment of Slug Tests (M.S. thesis), University of Waterloo.

Zapico, M., Vales, S., and Cherry, J., 1987, A wireline piston core barrel for sampling cohesionless sand and gravel below the water table, Ground Water Monitoring Review, v. 7, no. 3, 74-82.

Zlotnik, V., 1994, Interpretation of slug and packer tests in anisotropic aquifers, Ground Water, v. 32, no. 5, 761-767.

VII. APPENDIX A - NUMERICAL LAPLACE TRANSFORMS

This appendix begins by briefly discussing three commonly used numerical methods for the back transformation of Laplace-space functions into real space. The Crump (1976) method is the focus of the remainder of the appendix and the algorithm of De Hoog et al. (1982) is introduced as an approach for accelerating the convergence of the summation series employed in the Crump method.

The inversion step, i.e. the back transformation of the Laplace-space function into real space, is probably the most difficult step of a problem involving the Laplace transformation. Many methods for the numerical inversion of Laplace-space solutions have been employed in the groundwater literature. The most commonly used methods are those of Stehfest (1970), Crump (1976), and Talbot (1979). The numerical inversion scheme of Stehfest produces a solution for one specific time. At least 10 or more Laplace solutions (i.e. 10 p_k values) are usually required for the inversion in order to obtain a solution of acceptable accuracy. The maximum number of Laplace solutions (K) that can be used in the Stehfest algorithm is related to the largest number the computer can manipulate. Generally, K should be assigned a value as large as possible for a given machine in order to minimize the error of the inversion. Once the value of K is selected, the accuracy of the inversion is fixed.

The Talbot inversion algorithm also produces a solution for one specific time. In this case, however, there is no limit on the value of K and thus on the accuracy of the inversion. Computations are terminated when a summation series converges to a prespecified criterion by comparing inversion results obtained using two successive p_k values.

The Crump method differs from both of the preceding methods in that a single set of p_k solutions can be employed to perform the inversion for a range of times. The accuracy of the inversion in this case is determined by both the number of terms in the summation and the values of summation-series parameters.

Previous work (e.g., Barker, 1982; Moench and Ogata, 1984; Moench, 1984; Chen, 1985; Kipp, 1985; Chen, 1986) has shown that all three of the above methods can be used in groundwater flow and transport applications with high accuracy. The selection of an inversion method should therefore be based on the specific requirements of the problem being addressed. If solutions are required at only a few

points in time, then the Talbot or Stehfest algorithms are the most appropriate approaches. If, as is often the case in well-test applications, there are a large number of points in time, the method of Crump (1976) is the most efficient approach. Although 3DFDTC enables the user to select either the Stehfest or Crump algorithms, the algorithm of Crump will undoubtedly be the most commonly used approach for well testing applications and thus is the focus of the remainder of this discussion.

Crump (1976) found that a series transformation may be incorporated into equation (II.A.12) to speed up the rate of convergence and, at the same time, reduce the truncation error. This approach, known as the epsilon algorithm, produces, without exception, much faster series convergence than a conventional summation. The number of Laplace-space solutions required in the summation series is reduced from hundreds to tens. The epsilon algorithm involves the approximation of the summation series of (II.A.12) by a sequence of partial sums that are calculated using a recursive equation. De Hoog et al. (1982) present a quotient difference algorithm that dramatically improves on the speed of convergence of the epsilon algorithm. Liu and Butler (1991) provide a detailed description of the De Hoog algorithm, a summary of which is given here.

In the De Hoog algorithm, the summation series inside the brackets of (II.A.12) is rewritten as the real value of the following equation,

$$S_{2N} = \sum_{k=0}^{2N} a_k z^k \qquad \text{(A.1)}$$

where

$$z = e^{\frac{i\pi t}{Tmax}};$$

$$a_k = \overline{s_j}(p_k)$$

This summation can be approximated by

$$S_{2N} \approx v(z, 2N) = d_0/(1 + d_1 z/(1 + \cdots + d_{2N} z)) \qquad \text{(A.2)}$$

where d_j, ···, j=1, 2N are called the continued fraction coefficients and are defined as $d_0 = a_0$, $d_{2n-1} = -q_n^{(0)}$, $d_{2n} = -e_n^{(0)}$, $n = 1, \cdots\cdots, N$. The initial $e_r^{(i)}$ and $q_r^{(i)}$

terms are defined as:

$e_0^{(i)}=0$, for $i=0, 1, \cdots, 2N$, and $q_1^{(i)}=a_{i+1}/a_i$, for $i=0, 1, \cdots, 2N-1$.

An array of q and e coefficients can be formed using the following relationships

$$\text{for } r=1,\cdots,2N,\ e_r^{(i)}=q_r^{(i+1)}-q_r^{(i)}+e_{r-1}^{(i+1)},\ i=0,\cdots,2N-2r \quad \textbf{(A.3)}$$

$$\text{and for } r=2,\cdots,N,\ q_r^{(i)}=q_{r-1}^{(i+1)}e_{r-1}^{(i+1)}/e_{r-1}^{(i)},\ i=0,\cdots,2N-2r-1 \quad \textbf{(A.4)}$$

This array can be written out as

$$\begin{array}{ccccccc}
 & & q_1^{(0)} & & & & \\
 & e_0^{(1)} & & e_1^{(0)} & & & \\
 & & q_1^{(1)} & & q_2^{(0)} & & \\
 e_0^{(2)} & & & e_1^{(1)} & & e_2^{(0)} & \\
 & & q_1^{(2)} & & q_2^{(1)} & & \\
 & e_0^{(3)} & & e_1^{(2)} & & & \\
 & & q_1^{(3)} & & & & \\
 e_0^{(4)} & & & & & &
\end{array} \quad \textbf{(A.5)}$$

The following recursive equations can then be used to calculate the terms required in the approximate summation of (A.2):

$$\begin{aligned} A_n &= A_{n-1} + d_n z A_{n-2} \\ B_n &= B_{n-1} + d_n z B_{n-2} \end{aligned} \qquad n = 1, 2, \cdots, 2N \qquad \textbf{(A.6)}$$

with $A_{-1} = 0$, $B_{-1} = 1$, $A_0 = d_0$ and $B_0 = 1$.

Using these recursive equations, (A.2) can now be written as $S_{2n} \approx v(z,2N) = A_{2N}/B_{2N}$. Equation (II.A.12) thus becomes:

$$h_j(t) \approx \frac{1}{Tmax} e^{p_0 t} S_{2N} = \frac{1}{Tmax} e^{p_0 t} RE\left[\frac{A_{2N}}{B_{2N}}\right] \qquad \text{(A.7)}$$

Liu and Butler (1991) show that use of (A.7) instead of the epsilon algorithm approach can reduce the number of terms required in the summation by a factor of two or more. Note that as described by Liu and Butler (1991), careful selection of the Tmax parameter is required in order to realize the maximum computational reductions. Those authors provide recommendations on the selection of Tmax and other summation parameters.

VIII - APPENDIX B - SENSITIVITY ANALYSIS

Introduction

Sensitivity analysis (McElwee, 1987) is a formalism that allows relationships between model responses and model parameters to be examined in considerable detail. In this appendix, a brief summary of the first-order sensitivity approach as applied to the modeling of groundwater flow in response to a stress at a central well is given.

Sensitivity Coefficients

Assuming three parameters of interest, the first-order Taylor expansion for hydraulic head is

$$H^* \cong H^m + U_{P_1}^m \Delta P_1^m + U_{P_2}^m \Delta P_2^m + U_{P_3}^m \Delta P_3^m \qquad \text{(B.1)}$$

where

P_i = model parameters such as transmissivity (T), storage (S), initial head (H_0), etc.;

H^* = vector of heads based on the true parameters P_i^* ;

H^m = vector of heads based on current parameter estimates P_i^m ;

$U_{P_i}^m = \dfrac{\partial H^m}{\partial P_i^m}$ = sensitivity coefficient;

ΔP_i^m = unknown perturbation in the parameter estimates;

m = iteration index.

Note that equation (B.1) is a linear approximation of a nonlinear process as a result of the neglection of the higher order terms in the expansion.

Normalized Sensitivities

The multiplication of a sensitivity coefficient by the parameter of interest is defined as a normalized sensitivity coefficient (McElwee, 1987) and is denoted by U'_{P_i} . When investigating the head response in a slug test, the normalized sensitivity to relative head (u'_{P_i}) is often used. This quantity is defined as

$$u'_{P_i} = P_i \frac{\partial (H/H_0)}{\partial P_i} = P_i \frac{\partial h}{\partial P_i} \qquad \textbf{(B.2)}$$

where

h = relative head = H/H_0.

An examination of the spatial and temporal dependence of the normalized sensitivity will often yield considerable insight into the physical processes occurring during a well test.

Parameter Estimation

Sensitivity coefficients can be employed in an unweighted least squares inversing routine to estimate model parameters. McElwee (1982, 1987) describes the technique in considerable detail. The approach is an iterative procedure involving the minimization of an error functional in the form of the sum over all measurement points of the squared differences between the observed and calculated heads:

$$E = \sum_n [HO_n - HC_n]^2 \qquad \textbf{(B.3)}$$

where

$HO_n = H^* + \epsilon$ = observed head at index point n;

HC_n = calculated head at index point n;

ϵ = measurement error;

n = spatial and temporal location of measurement.

The righthand side of equation (B.1) is substituted for HC_n in equation (B.3) and the functional minimized with respect to the parameters. This produces a system of equations with the unknown being a vector of parameter changes:

$$[A]\,\Delta P = R \qquad \textbf{(B.4)}$$

where

[A] = the sensitivity summation matrix;

ΔP = vector of parameter changes, $\Delta P^{+} = (\Delta P_1, \Delta P_2, \Delta P_3)$;

R = residual vector.

The new parameter estimates are then found using

$$P_i^{m+1} = P_i^m + \Delta P_i^m \tag{B.5}$$

Since the outlined procedure employs a linear approximation of a nonlinear process, a number of iterations are generally required to obtain convergence to within a predefined criterion.

Sensitivity Summation Matrix

The sensitivity summation or sensitivity design matrix ([A] of equation (B.4)) is a summation over time and space of products of any two sensitivity coefficients:

$$a_{ij} = [A]_{ij} = \sum_n U_i(n)\, U_j(n) \tag{B.6}$$

where

i,j = P_1, P_2, P_3.

The diagonal elements of the matrix are simple summations of the squares of the sensitivity coefficients with respect to the same parameter. In general, the solution to equation (B.4) is well behaved if the diagonal elements are large and nearly equal and the off-diagonal elements are small. This will be the case when sensitivity coefficients are large and poorly correlated.

Sensitivity Correlation Matrix

The sensitivity summation matrix can be transformed into a "pseudo" sensitivity correlation matrix whose elements are defined as

$$c_{ij} = [C]_{ij} = \frac{a_{ij}}{\sqrt{a_{ii}a_{jj}}} \qquad \textbf{(B.7)}$$

where

c_{ij} = a "pseudo" correlation between sensitivity coefficients for parameters P_i and P_j, $|c_{ij}| \leq 1$.

The elements of this matrix quantify the degree of correlation between sensitivity coefficients characterizing different parameters. By definition, the diagonal elements of the matrix will be one. If any of the off-diagonal terms are exactly one, the inverse of [A] in equation (B.4) does not exist and the parameter estimation problem cannot be solved. In practice, anytime the off-diagonal elements of the sensitivity correlation matrix get above 0.9 the [A] matrix becomes ill-conditioned rather rapidly and the parameter estimates become more unreliable.

Parameter Covariance Matrix

Equation (B.4) shows that the inverse of the [A] matrix is employed to calculate the vector of parameter changes. The inverse of [A] is also employed to estimate the approximate covariance of the estimated parameters:

$$cov(P) = [B] = [A]^{-1}s^2 \qquad \textbf{(B.8)}$$

where

[B] = covariance matrix;

$s^2 = \sum_n [HO_n - HC_n]^2/(N-M)$;

N = total number of measurements;

M = total number of parameters.

The estimated standard error of parameter P_i is given by the $\sqrt{b_{ii}}$ element of the covariance matrix. Note that the form of the parameter covariance matrix is based on some simplifying assumptions about the measurement error. These assumptions include that the measurement error is additive, has a zero mean and constant variance, and is uncorrelated with the measurement error at another location.

Equations (B.7) and (B.8) indicate that correlation between sensitivity coefficients will affect the reliability of parameter estimates. Butler and McElwee (1990) present a demonstration of the design of well testing procedures to reduce the correlation between sensitivity coefficients and therefore increase the reliability of parameter estimates. Section II.C of this report describes a sensitivity analysis of slug tests in which observation wells other than the stressed well are employed to improve the reliability of parameter estimates.